# IONIC AND MOLECULAR DIFFUSION IN CEMENTITIOUS MATERIALS

by

SHU WEN YU

Doctor of Philosophy

THE UNIVERSITY OF ASTON IN BIRMINGHAM

March 1990

THE UNIVERSITY OF ASTON IN BIRMINGHAM
"IONIC AND MOLECULAR DIFFUSION IN CEMENTITIOUS MATERIALS"
SHU WEN YU Doctor of Philosophy 1990

SUMMARY

The work described in this thesis is an attempt to provide improved understanding of the effects of several factors affecting diffusion in hydrated cement pastes and to aid the prediction of ionic diffusion processes in cement-based materials.

Effect of pore structure on diffusion was examined by means of comparative diffusion studies of quaternary ammonium ions with different ionic radii. Diffusivities of these ions in hydrated pastes of ordinary portland cement with or without addition of fly ash were determined by a quasi-steady state technique. The restriction of the pore geometry on diffusion was evaluated from the change of diffusivity in response to the change of ionic radius. The pastes were prepared at three water-cement ratios, 0.35, 0.50 and 0.65.

Attempts were made to study the effect of surface charge or the electrochemical double layer at the pore/solution interface on ionic diffusion. An approach was to evaluate the zeta potentials of hydrated cement pastes through streaming potential measurements. Another approach was the comparative studies of the diffusion kinetics of chloride and dissolved oxygen in hydrated pastes of ordinary portland cement with addition of 0 and 20% fly ash. An electrochemical technique for the determination of oxygen diffusivity was also developed.

Non-steady state diffusion of sodium, potassium, chloride and hydroxyl ions in hydrated ordinary portland cement paste of water-cement ratio 0.5 was studied with the aid of computer-modelling. The kinetics of both diffusion and ionic binding were considered for the characterization of the concentration profiles by Fick's first and second laws. The effect of the electrostatic interactions between ions on the overall diffusion rates was also considered. A general model concerning the prediction of ionic diffusion processes in cement-based materials has been proposed.

KEY WORDS: cements, diffusion, pore solution, pore structure, surface charge.

ACKNOWLEDGMENTS

I am deeply indebted to Dr. C.L. Page, my supervisor, for the guidance, advice and all the help he has given throughout the period of this research.

I should like particularly to thank Dr. G. Sergi for his kind permission to use the diffusion data in his Ph.D. thesis entitled "Corrosion of Steel in Concrete: Cement Matrix Variables". All of the experimental data used in chapter 6 of the present work are from his thesis.

I should also like to thank Mr. C.J. Thompson for his excellent technical assistance.

I wish to thank the Department of Civil Engineering for the financial support during the last one and half years of my study.

Finally, To my wife, Yan, goes more appreciation than I can ever adequately express.

## LIST OF CONTENTS

## LIST OF FIGURES

## LIST OF TABLES

**Tables in appendices**

**App. No.**

## LIST OF APPENDICES

## ABBREVIATIONS AND FREQUENTLY USED SYMBOLS

### ABBREVIATIONS

Cement compounds nomenclature:

$Al_2O_3$=A; CaO=C; $SiO_2$=S

| | |
|---|---|
| BFS: | blast-furnace slag |
| PFA: | pulverized fly ash |
| OPC: | ordinary portland cement |
| w/c: | water:cement (ratio) |

### SYMBOLS

| | |
|---|---|
| A | diffusion area, $cm^2$ |
| $A_e$ | surface area of electrode, $cm^2$ |
| C | concentration expressed as a function of x and t, mol/l |
| $C_2$ | concentration in the compartment 2 of the diffusion cell, mol/l |
| $C_i$ | initial concentration in a diffusion sample, mol/l |
| $C_s$ | concentration at the surface of a diffusion sample, mol/l |
| $C_t(x,t)$ | first derivative of C with respect to t |
| $C_x(x,t)$ | first derivative of C with respect to x |
| $C_{xx}(x,t)$ | second derivative of C with respect to x |
| D | diffusivity calculated from the flux per unit area of bulk solution or the pore solution, $cm^2/sec$ |
| $D_O$ | absolute diffusivity, $cm^2/sec$ |
| $D_e$ | effective diffusivity, $cm^2/sec$ |

| | |
|---|---|
| $D_i$ | intrinsic diffusivity calculated from the flux per unit area of the bulk cement paste, $cm^2/sec$ |
| E | electrical potential, volts |
| $E_x(x,t)$ | first derivative of E with respect to X |
| $E_s$ | the streaming potential, mv |
| e | protonic charge |
| F | Faraday number, 96486.8 coulombs |
| f | viscosity, poise |
| I | current, mA |
| $I_o$ | current at t=0, mA |
| $I_d$ | current equivalence of the total flux, mA |
| $I_e$ | current recorded at the end of polarization, mA |
| J | flux, mmol $cm^{-2}$ $sec^{-1}$ |
| $J_x(x,t)$ | first derivative of J with respect to x |
| $K_1, K_2$ | constants for chloride binding |
| k | Boltzmann's constant |
| L | thickness of the disc sample, cm |
| l | diffusion layer thickness at the solution/ electrode interface, cm |
| n | number of electron transferred per molecule |
| Q | charge passed, coulombs |
| $Q_t$ | accumulative charge, coulombs |
| R | gas constant |
| r | radius of a hydrated ion |
| S | adsorbed ionic amount expressed as a function of x and t, mmol per gram cement |
| $S_t(x,t)$ | first derivative of S with respect to t |

| | |
|---|---|
| s | adsorbed ionic amount expressed as a function of concentration, mmol per gram cement |
| T | absolute temperature, K° |
| t | time, seconds |
| $t_d$ | total diffusion time, seconds |
| u | absolute mobility, cm $sec^{-1}$ $dyn^{-1}$ |
| V | volume of the compartment 2 of the diffusion cell, $cm^3$ |
| W | content of the pore solution in which diffusion occurs, on weight of cement. |
| Wb | bound water content on weight of cement. |
| We | evaporable water content on weight of cement or of oven-dried paste. |
| Wn | non-evaporable water, on weight of cement. |
| x | distance or diffusion depth, cm. |
| z | valence number. |
| $\epsilon$ | volume or area of the pore solution in which diffusion occurs, on volume or area of the bulk cement paste. |

# CHAPTER 1 INTRODUCTION

It is widely known that chloride can induce corrosion of embedded steel in concrete[1,2]. When there is a chloride source of substantial quantity in the surroundings, it seems to be only a matter of time for sufficient chloride to reach the steel to initiate corrosion. Studies of the kinetics of chloride diffusion in hydrated cement pastes and concrete are thus of practical interest.

Furthermore, cement-based materials have many potential applications in the field of radioactive waste encapsulation and disposal[3-5]. Studies of the diffusion of relevant ionic species are thus essential to enable predictions regarding the long-term stability of encapsulated radio-nuclides in cemented wastes to be made.

The research to be described in this thesis was concerned with the elucidation of some kinetic and phenomenological aspects of ionic and molecular diffusion in hydrated cement pastes. The aim was to provide improved understanding of the important factors that control diffusion rates in cement-based materials and to aid the prediction of diffusion processes in concrete structures.

Diffusion in dilute aqueous electrolytes is a relatively established field closely related to the topic of this research, so it will be first reviewed in this chapter to illustrate the basic laws of diffusion. The scope of the

present study and the structure of the thesis will then be described.

## 1.1 Diffusion in Aqueous Electrolytes

Diffusion or the mass transport caused by a concentration gradient is a common physical process involved in many systems. It was Fick who first put diffusion on a quantitative basis[6,7]. With the hypothesis that diffusion could be described on the same mathematical basis as Fourier's law of heat flow or Ohm's law of electrical conduction, Fick developed the fundamental law of diffusion[6-8]:

$$J=-DC_x(x,t) \qquad \ldots\ldots (1.1)$$

which is commonly called Fick's first law for one-dimensional diffusion. Here J is the flux, and C is the concentration expressed as a function of the distance (x) and time (t). The quantity, D, is the diffusivity or diffusion coefficient, which is an important parameter characterizing the diffusion process.

Fick's first law has been found to be adequate to describe diffusion in many binary systems[6]. It explicitly refers the concentration gradient to be the driving force of diffusion. However, a concentration gradient does not necessarily mean that diffusion will occur. It has been known[9] that diffusion would not occur at small concentration gradients in a binary liquid mixture at the consolute point at which the two liquid phases are

completely miscible and no gradient of free energy exists. Therefore, the gradient of free energy has been more commonly considered as the generalized driving force for a transport process[10].

Sometimes diffusion in aqueous electrolytes is accompanied by electro-migration, so the gradient of the electro-chemical potential can be regarded as the driving force for the combined transport[10-13]. In a very dilute aqueous electrolyte at a constant temperature T, diffusion and electro-migration are simply related by the Nernst-Planck equation[6,10-12]:

$$J=-ukT[C_x(x,t)+zeCE_x(x,t)/(kT)] \quad \ldots\ldots (1.2)$$

where E is the electrical potential, and u is the absolute mobility defined as the limiting velocity attained under unit force. In the absence of concentration gradients, the absolute mobility is thus related to the conductivity, and can be calculated[14] from the equivalent conductivity ($\lambda$ in $cm^2\ ohm^{-1}\ equiv.^{-1}$)

$$u=6.466\times10^6\lambda/|z| \quad \ldots\ldots (1.3)$$

As the motion of a neutral species will normally not be affected by an electrical field, the diffusivity determined from Fick's first law, here denoted as $D_O$, is therefore correlated to the absolute mobility, which is shown by the Nernst-Einstein equation[14]:

$$D_O=kTu \quad \ldots\ldots (1.4)$$

This equation can be obtained by combining Fick's first

law with the Nernst-Planck equation. When this equation is used for an ion, the $D_0$ obtained is sometimes called the absolute diffusivity[15]. However, for the reasons shown below, the absolute ionic diffusivity is, in most cases, not that determined from Fick's first law.

The absolute ionic diffusivity at infinite dilutions can be calculated based on equations 1.3 and 1.4 from the limiting equivalent conductivity given in the literature such as Ref.[14]. The calculated limiting diffusivities at 25°C for some ions are shown in table 1.1. As suggested by table 1.1, most anions tend to move faster than cations. For an electrolyte containing two ions of different absolute mobilities or diffusivities, the anion, however, must diffuse at the same rate or Fickian diffusivity as the cation does because of the requirement of electroneutrality. As a result of the difference in their mobilities, an internal electrical field must be automatically created to attain the charge balance[6,7,10-13].

Therefore, the ionic diffusivity calculated from the flux and the concentration gradient according to Fick's first law is not the absolute diffusivity which should be calculated from the electrical field in addition to the flux and the concentration gradient. The diffusion rates are thus affected by the electrostatic interactions between the ions present in the electrolyte.

Theoretically, the Nernst-Planck equation is applicable to

the diffusion in mixed dilute electrolytes, but the mathematics involved is often very complex[10,12] (see subsection 6.1.2, chapter 6). Diffusion in concentrated electrolytes, which is closer to that in hydrated cement pastes, is much more complex than in dilute solutions. However, Cussler[6] was able to show experimentally that the electrostatic field described above accounts for most of the effect of ionic interactions on diffusion in concentrated electrolytes.

Ions in electrolytes are associated with certain water molecules, so they are hydrated. Normally, the sizes of hydrated ions can not be calculated from simple molecular

**Table 1.1** Ionic radii and absolute diffusivities in infinitely diluted solutions (25°C)

| IONS | $r_s$ (Å) | r (Å) | $D_o$ ($\times 10^{-6}$) |
|---|---|---|---|
| $N(CH_3)_4^+$ | 2.05 | 3.47 | 11.96 |
| $N(C_2H_5)_4^+$ | 2.82 | 4.00 | 8.69 |
| $N(C_3H_7)_4^+$ | 3.93 | 4.52 | 6.23 |
| $N(C_4H_9)_4^+$ | 4.73 | 4.94 | 5.18 |
| $N(C_5H_{11})_4^+$ | 5.27 | 5.29 | 4.65 |
| $Na^+$ | 1.83 | 3.3 | 13.3 |
| $K^+$ | 1.25 | | 19.6 |
| $Cl^-$ | | | 20.3 |
| $OH^-$ | | | 53.0 |

models. Nevertheless, the Stokes-Einstein formula offers a starting point for the estimation of ionic radius[14]:

$$D_0 = kT/(6\pi f r_s) \quad \ldots\ldots (1.5)$$

where f is the viscosity of water, and $r_s$ is the Stokes' law radius in centimetres. However, this equation generally tends to underestimate the sizes of most of the common ions[16].

Robinson and Stokes[14] estimated the radii of $(C_4H_9)_4N^+$ and $(C_5H_{11})_4N^+$ ions from certain molecular models, and found there was good agreement with those calculated by the Stokes-Einstein formula. They then calculated the radii of all of the smaller quaternary ammonium ions from similar molecular models. This enabled them to construct a calibration curve by relating the Stokes' law radii to the sizes of the quaternary ammonium ions listed in table 1.1. The radii of some other hydrated ions of symmetrical shape can thus be approximated from this curve, provided their sizes are close to those of the quaternary ammonium ions. Their results are also shown in table 1.1.

The Stokes-Einstein formula (equation 1.5) suggests that viscosity of the solution has a definite effect on diffusion rate. Robinson and Stokes[14] compared the product of the viscosity and the limiting equivalent conductivity at different temperatures for various ions. They found that the product is almost constant for ions of large size. The products have similar variation with temperature for some monatomic ions; however, this

variation is only of the order of 30% over the temperature range 0 to 100 °C. As they pointed out, this suggests that viscous forces account for most of the resistance to the motion of ions in water, though there are evidently some other effects operative as well.

### 1.2 Scope of Study and Plan of Presentation

The steady-state diffusion technique which will be described in chapter 3 is a common method employed to study ionic diffusion in hydrated cement pastes and mortars. Kondo et al[17] used this technique to study the diffusion of various ions in OPC paste made at w/c 0.4 and cured for 28 days in saturated lime water. By putting the solution shown in table 1.2 in one compartment of the diffusion cell and deionised water in the other compartment, the authors determined the intrinsic diffusivities for a number of ions at 25°C. Their results are shown in table 1.2. It can been seen from the table that all the ions diffuse significantly slower in the cement paste than in bulk solutions. The cations diffuse a few times slower than the accompanying anions.

Addition of PFA and particularly BFS to OPC results in a considerable decrease of the diffusivity[18-21]. Typical values of chloride diffusivity in various types of cement paste were given by Page et al[22]. The authors[23] also studied chloride diffusion in hydrated pastes of alite and

alite blended with $C_3A$, and their results are shown in table 1.3. It was found that adding $C_3A$ to alite decreases the chloride diffusivity.

Page et al[22] determined the intrinsic diffusivity of chloride ions for OPC paste of three w/c ratios (0.4, 0.5, 0.6) over a temperature range 7 to 45 °C. For each w/c ratio they obtained a linear relationship between the reciprocal of the absolute temperature and the logarithm of the diffusivity, enabling the calculation of the activation energy for diffusion (see table 1.4). Goto and Roy[24] used OPC paste of w/c ratio 0.4 and quartzite for their diffusion experiments. Diffusivities of both $Cl^-$ and $Na^+$ ions were obtained over a wider range of temperature. The activation energies for sodium and chloride diffusion in the OPC paste (see also table 1.4) were found to be significantly greater than those (about 20 kJ/mol) found for the bulk solutions[25] and quartzite.

Based on the Arrhenius-type dependence of diffusivity on temperature, Page et al[23,26] subsequently suggested that ionic diffusion in hydrated cement pastes is a single-step dominated rate process. However, the mechanisms of the diffusion have not yet been understood. Pore structure[27,28] and surface charge[28-32] have been considered to be important in determining ionic diffusion rates.

The initial objectives of the present work were to understand more of the diffusion kinetics. The thesis is

**Table 1.2** Intrinsic diffusivities in 0.4 w/c OPC paste[17]

| L | Solutions | $D_i$ ($\times 10^{-8}$ $cm^2/sec$) | | | |
|---|---|---|---|---|---|
| | | $Cl^-$ | $Li^+$ | $Na^+$ | $K^+$ |
| 0.3 | 0.5M LiCl | 8.13 | 1.70 | | |
| | 0.5M NaCl | 6.25 | | 1.70 | |
| | 0.5M KCl | 6.73 | | | 2.95 |
| 0.2 | 0.5M LiCl | 7.81 | 1.44 | | |
| | 0.5M NaCl | 6.94 | | 1.89 | |
| | 0.5M KCl | 7.35 | | | 3.78 |
| 0.3 | Mixture of 0.5M LiCl 0.5M NaCl 0.5M KCl | 7.72 | 1.45 | 2.22 | 3.30 |

**Table 1.3** Chloride diffusivities in various pastes at 25°C ($\times 10^{-8}$ $cm^2/sec$, Ref. 22 and 23)

| | |
|---|---|
| 0.5 w/c OPC | 4.47 |
| 0.5 w/c OPC/30%PFA | 1.47 |
| 0.5 w/c OPC/65%BFS | 0.41 |
| 0.5 w/c SRPC | 10.00 |
| 0.6 w/s alite | 6.67 |
| 0.6 w/s alite/12%$C_3A$ | 3.80 |

**Table 1.4** Activation energies for sodium and chloride diffusion in hydrated OPC paste[22,24] (kJ/mol)

| w/c | $Cl^-$ | $Na^+$ |
|---|---|---|
| 0.4 | 41.8 | |
| 0.5 | 44.6 | |
| 0.6 | 32.0 | |
| 0.4 | 50.2 | 83.6 |

divided into seven chapters. Following this introductory chapter, chapter 2 describes the experimental techniques employed. The next three chapters deal with the mechanisms of diffusion. The effect of pore structure is considered in chapter 3, while that of surface interaction is covered in chapter 4. Oxygen diffusion was studied and is compared with chloride diffusion in chapter 5. Chapter 6 is concerned with the modelling and prediction of ionic diffusion in hydrated OPC pastes. The last chapter contains general conclusions and suggestions for further work.

Diffusion in cementitious systems occurs through a network of tortuous and interconnected pore channels. It is therefore quite intuitive that the diffusion rate should depend on the pore structure of the cement-matrix. However, it appears that the pore size distributions determined from mercury intrusion porosimetry for hydrated OPC/PFA pastes are coarser than those for OPC pastes of the same w/c

ratio[22], which could not explain the experimental finding that ions diffuse slower in PFA blended pastes. However, it has been suggested[33] that the pores in the PFA pastes are relatively discontinuous, and that the discontinuity tends to be destroyed by the sample pre-treatment such as drying which is required for the use of the conventional pore-structure analysis techniques such as capillary condensation and mercury intrusion.

To examine the effects of pore structure on diffusion, it is therefore necessary either that existing methods of obtaining pore size distribution be made more reliable, or that alternative techniques should be developed. This present investigation followed the latter approach. An attempt to probe the effects of pore structure on diffusion was made by means of comparative diffusion studies of quaternary ammonium ions. Since this homologous series of ions have unit charge and different ionic sizes, the "molecular sieve" influence of pore size restrictions on diffusion can be conceived from the changing pattern of the diffusion rates in response to the size of the diffusing species. This is presented in chapter 3.

As stated earlier, the activation energy for diffusion at infinite dilution is basically a manifestation of the temperature dependence of water viscosity. It seems, however, that the viscosity of the pore solution may not be the only important factor responsible for the low ionic

diffusion rates found in hydrated cement pastes. The obvious difference in the activation energies for sodium and chloride diffusion in OPC paste, as found by Goto and Roy[24], can hardly be explained in terms of the effect of the pore solution viscosity. In contrast with OPC paste, slag cement paste appears to give similar activation energies for sodium and chloride diffusion, and the activation energies obtained are very close to those found for diffusion in dilute bulk solutions[34]. Although the viscosity of the pore solution is likely to vary with the type of pores, its temperature dependence, on average, might be expected not to vary very much with the type of mature paste of similar w/c ratios.

Some other factors besides the pore structure of the cement-matrix and the viscosity of the pore solution may also be expected to affect ionic diffusion rates. Page et al[23] suggested that some form of interaction between the diffusing ions and the C-S-H gel may be important. Goto and Roy[24] considered that diffusing cations may interact more strongly with the cement-matrix than with quartzite. The difference in diffusion behaviours between cations and anions, i.e. much faster diffusion of the anions as shown in table 1.2, has been attributed by several authors[24, 29-32] to the effect of the electrochemical double layer at the pore/solution interfaces. The cement hydrate surfaces were regarded as positively charged by Takagi et al[29], who accordingly explained that the electro-

statically repelled cations would encounter more difficulty in entering the micropores and would thus diffuse slower than the anions.

Although there have been some studies[35-37] on the electrochemical properties of hydrating cements, few studies on those of mature pastes have been made. Preliminary measurements of zeta potential were therefore made in this work to study the equilibrium double layer of hydrated cement surfaces. This was intended to provide a basis from which the development of the non-equilibrium double layer during diffusion may be better understood, allowing the effects of the surface charge and associated factors to be estimated. The results are reported in chapter 4.

Molecular diffusion in hydrated cement pastes differs from ionic diffusion in that the double layer can have less direct (electrostatic) effect on the transport of neutral molecules, although collisions between the diffusing species and the pore walls are always likely to occur in micropores. By comparing the diffusion kinetics of ions with those of neutral molecules such as oxygen, it may thus be possible to distinguish the effects of pore structure to some extent from those of the double layer. Diffusion of dissolved oxygen in both OPC and OPC/20%PFA pastes was studied and is compared with that of chloride in chapter 5.

Non-steady state diffusion is a major form of ionic transport for some marine structures constantly in contact with sea water[38]. Characterization of chloride and hydroxyl ion diffusion in water-saturated hydrated cement pastes can provide a basis for the assessment of chloride-induced reinforcement corrosion in such marine structures. In order to predict the ionic concentration profiles, both the diffusion kinetics and the chemical interactions between the diffusing ions and the cement-matrix should be considered. Although diffusion in cement-based materials is a multi-component process and can be expected to be very complex, there is a need to develop a practical and systematic model. Such work was initiated at Aston University by Page and Sergi[39] whose approach was extended in this work. Diffusion of sodium, potassium, chloride and hydroxyl ions is considered in chapter 6 with the aid of computer-modelling.

# CHAPTER 2 MATERIALS AND EXPERIMENTAL TECHNIQUE

This chapter outlines the major experimental techniques employed in the subsequent chapters. Some of the techniques such as pore-solution expression and ionic concentration analysis have been previously used in the field of cement chemistry. The other techniques such as streaming potential and oxygen diffusion measurements were designed or developed specifically for this work.

## 2.1 Cements

OPC and PFA of the chemical analyses shown in table 2.1 were used to prepare neat cement pastes. They were passed through a 150 μm sieve before use. The detailed procedures of preparing specimens are given mainly in subsection 3.3.1, chapter 3.

## 2.2 Expression of Pore Solution

The development by Longuet et al[40] of a method of removing capillary pore solutions by pressure has allowed detailed study of the pore-liquid phase chemistry of hydrated cements. The device illustrated in figure 2.1 was employed to extract the pore solution for the work described in subsection 3.3.2, chapter 3. A slowly increasing pressure was applied to the cement pastes by means of the piston, reaching a maximum of 310 MPa. A PTFE disc was inserted between the specimen and the piston to

**Table 2.1** Oxide compositions of the OPC and PFA

(% by weight)

| Oxide | OPC | PFA |
|---|---|---|
| CaO | 64.5 | 2.7 |
| $SiO_2$ | 20.0 | 48.1 |
| $Al_2O_3$ | 5.3 | 31.2 |
| $Fe_2O_3$ | 3.4 | 5.6 |
| $SO_3$ | 3.0 | 0.3 |
| $Na_2O$ | 0.10 | 0.25 |
| $K_2O$ | 0.78 | 1.10 |
| I.R | 0.27 | 0.50 |
| L.O.T | 0.90 | 6.89 |

seal the whole diameter of the die body, preventing the liquid squeezed out from escaping other than through the fluid drain via a circular groove on the platen. The extracted solution was then drawn into a syringe through a PTFE-lined drain hole and stored in sealed plastic vials to prevent unnecessary exposure to air.

After each run, the separate parts of the press were thoroughly cleaned with water and acetone, and the connecting surfaces were sprayed with PTFE non-stick spray for lubrication and protection ready for the next specimen. The rate of increase of the applied pressure was the same for all the specimens, as it is suggested[41] that this may affect the results.

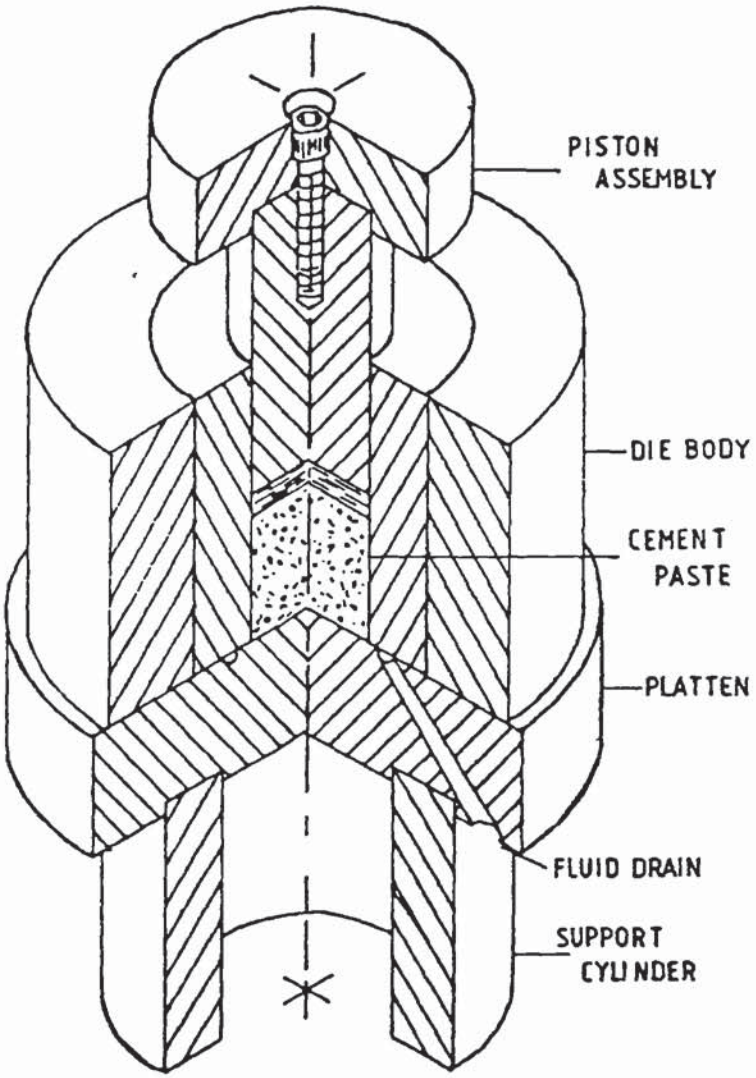


Figure 2.1 The pore-expression device

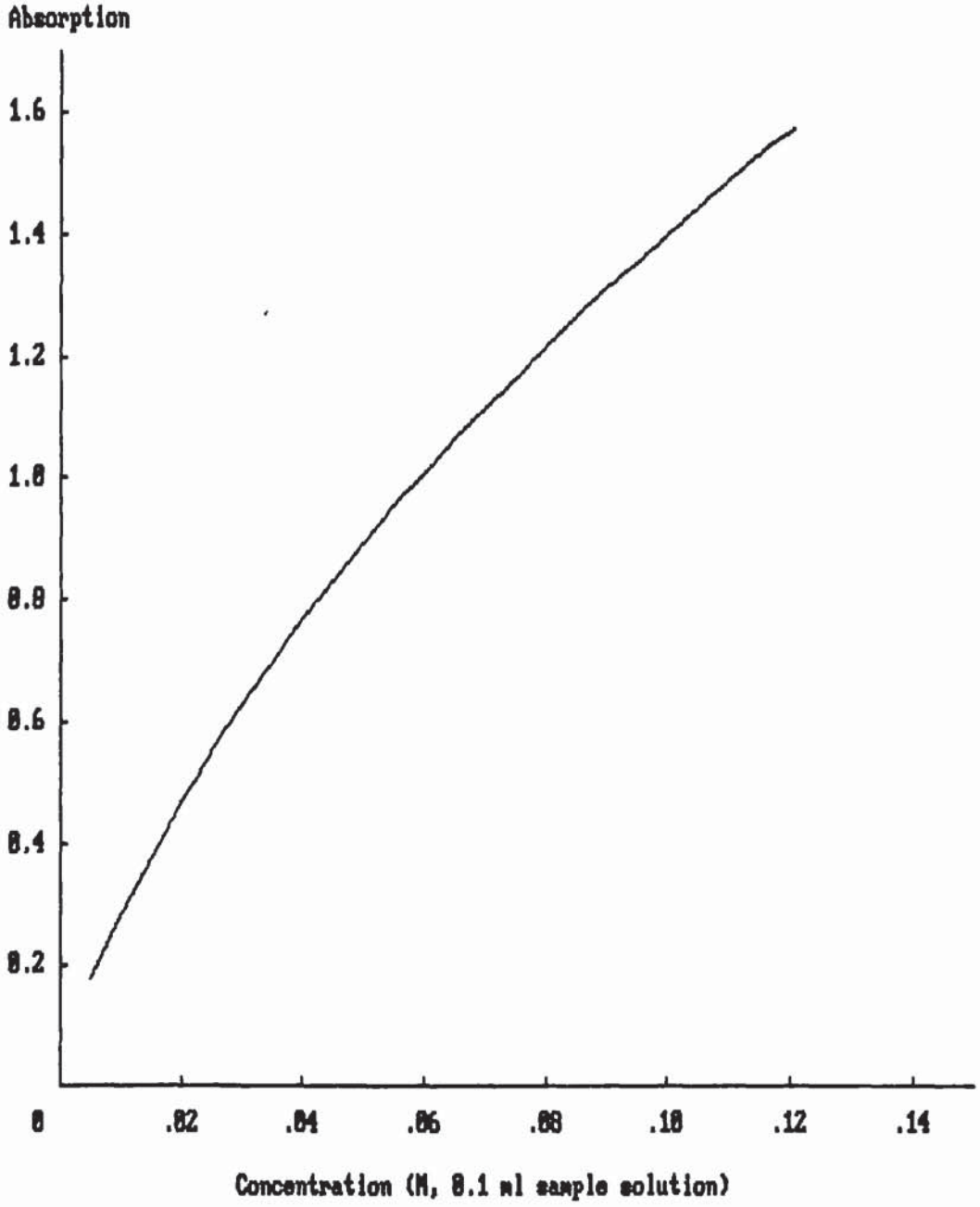


Figure 2.2 Calibration curve for chloride ion

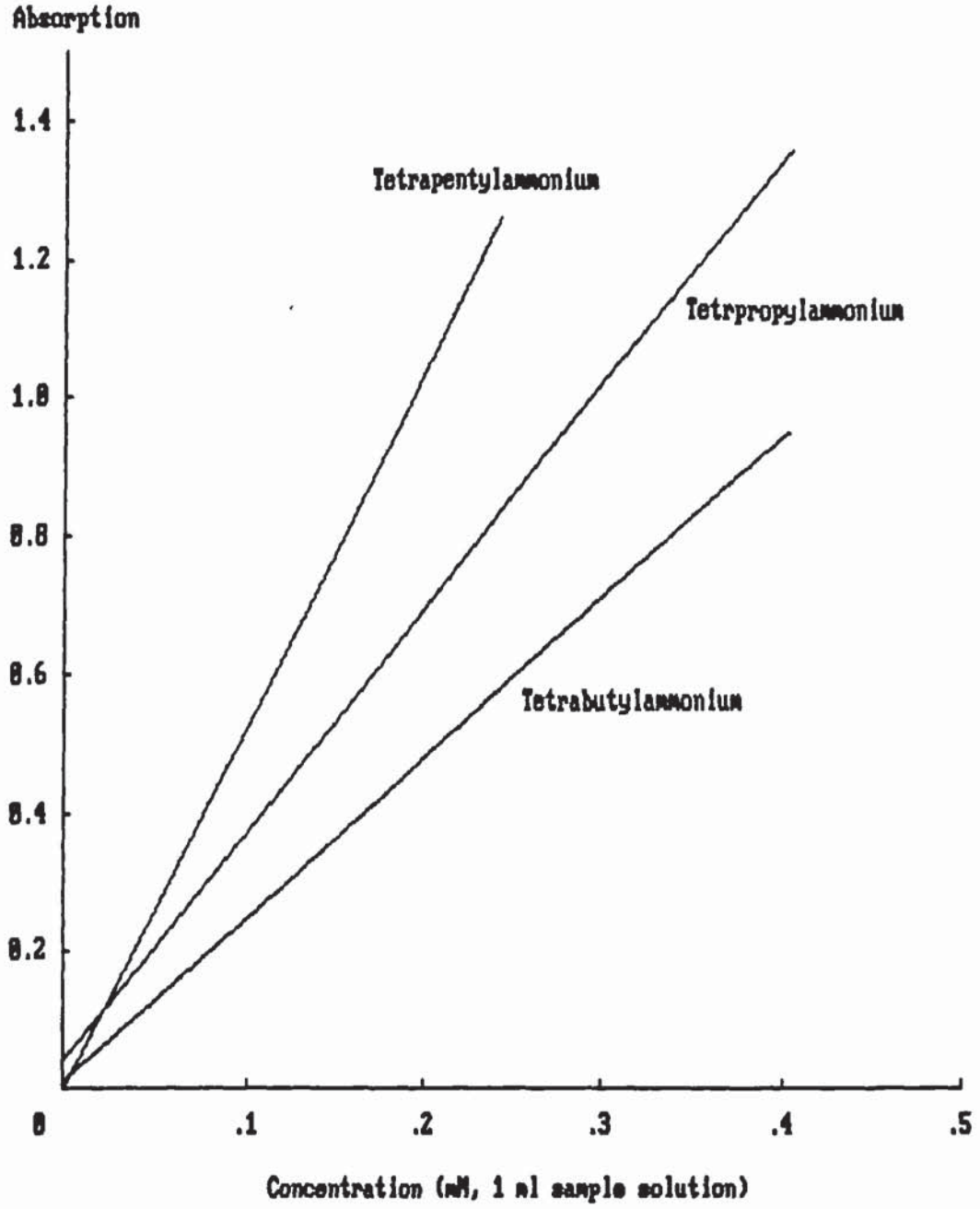


Figure 2.3 Calibration curves for $(C_3H_7)_4N^+$, $(C_4H_9)_4N^+$ and $(C_5H_{11})_4N^+$ ions

## 2.3 Analyses of Ionic Concentration

The present work used a Beckman Model 24 spectrophotometer to determine the concentrations of chloride and quaternary ammonium ions. The sample solution was added to certain reagents and buffer solutions to form a coloured complex. The light absorption of the coloured solution was then measured against a blank solution by the spectrophotometer at specific wavelengths. Ionic concentrations were determined from the calibration curves constructed by plotting the absorption against known concentrations of standard solutions. Fresh calibration curves were made at an interval of a few months, and some examples are given in figures 2.2 and 2.3.

### 2.3.1 Chloride

Chloride concentrations were determined by the following procedures. Each 0.1 or 0.2 ml aliquot of the sample solution was made up to 10 ml with deionised water in a glass flask. To these were added 2 ml 0.25 M ammonium ferric sulphate in 9 M nitric acid and 2 ml ethanol saturated with mercuric thiocyanate. Chloride causes the thiocyanate ion to be displaced which then forms a highly coloured complex with the ferric ion, which is shown by[42]

$$2Cl^- + Hg(SCN)_2 + 2Fe^{3+} \longrightarrow HgCl_2 + 2Fe(SCN)^{2+}$$

The coloured solution obtained was lightly shaken, left undisturbed for twenty minutes, and then poured into the

test cell. The light absorption at the optimum wavelength of 460 nm was measured by the spectrophotometer against deionised water contained in the blank cell.

### 2.3.2 $(C_4H_9)_4N^+$ and $(C_5H_{11})_4N^+$

Methyl orange reacts with tetrabutylammonium, $(C_4H_9)_4N^+$, and tetrapentylammonium, $(C_5H_{11})_4N^+$, to form a coloured complex which is soluble in chloroform but not in water. The concentrations of the two ions were determined by a colori-metric method adapted from that of Crompton[43].

The sample solution contained in a glass vessel was diluted with deionised water to 20 ml. To these were added 5 ml chloroform, 1 ml solution of methyl orange (reagent) prepared at 0.1% by weight, and 2 ml buffer solution mixed from 0.25 M citric acid and 0.1 M disodium hydrogen orthophosphate solutions in equal proportions. After shaking vigorously for thirty seconds the solution was allowed to stand undisturbed for twenty minutes so that the coloured chloroform could settle as a lower layer.

The chloroform layer was drawn into a 5ml pipette, and transferred into the test cell through a small funnel containing a plug of glass wool to absorb any residual water but not chloroform. The spectrophotometric reading at the optimum wavelength of 415 nm was obtained by placing the test cell and the blank cell containing only chloroform into the spectrophotometer.

### 2.3.3 $(C_2H_5)_4N^+$ and $(C_3H_7)_4N^+$

The principle[43,44] and procedures of the method used for the two ions were similar to those described above. The sample solution was diluted to 18 ml, and to this were added 4 ml of water-saturated bromo cresol green solution (the reagent) and 2 ml of the buffer solution mentioned above. The rest of the measurement procedures were the same as those described in the above subsection.

$(C_3H_7)_4N^+$ concentration could have been determined by the method described in the above subsection, but it was found that the method described in this subsection was better in terms of the sensitivity. The sensitivity for $(C_2H_5)_4N^+$ was not as good as for the other three quaternary ammonium ions, so a relatively larger volume of the sample $(C_2H_5)_4N^+$ solution was required.

## 2.4 Evaporable, Non-evaporable and Bound water

The water in hydrated cement pastes was classified by Powers[45] as follows:

(1). Water which is chemically combined into the hydrate compounds. It is in the form of either hydroxyl ions or water of crystallisation.

(2). Adsorbed water which is held by surface forces on the gel particles. The gel-pore water belongs to this type.

(3). Free water which is present in the pores, generally

the capillaries, beyond the range of the surface forces.

Although there is a great deal of interest in the nature of the chemical and physical states of the water in hydrated cement pastes[46], the types of the water are defined somewhat arbitrarily in practice. This is mainly because, unlike crystalline hydrates, cement hydrates on drying lose weight continuously with temperature or water-vapour pressure so that the states of the water can not be clearly distinguished.

The water lost at 105°C by hydrated cement pastes, namely the evaporable water as described by Powers[45], was determined in this work. The non-evaporable water content was determined as the weight lost over the temperature range from 105 to 950 °C. A sample of initial weight, $W_0$ (about 20 grammes), was heated in an oven at 105°C until a constant weight, $W_{105}$, was obtained. When the age was less than two weeks, the sample was broken into small particles and immersed in alcohol overnight before heating. The oven-dried sample was then placed in a platinum crucible and heated to 950°C for thirty minutes to give a final weight $W_{950}$.

The amount of the unhydrated cement contained in the sample, Wc in grammes, was first calculated:

$$Wc = W_{950}/(1-L.O.I) \quad \ldots\ldots (2.1)$$

where L.O.I is the loss-on-ignition[47] per gramme unhydrated cement. The evaporable water content, We, can

thus be expressed based on either the weight of the unhydrated cement as

$$We=(W_0-W_{105})/Wc \quad \ldots\ldots (2.2)$$

or weight of the oven-dried paste,

$$We=(W_0-W_{105})/W_{105} \quad \ldots\ldots (2.3)$$

The non-evaporable water content, Wn, expressed on weight of the unhydrated cement was

$$Wn=(W_{105}-W_{950})/Wc - L.O.I \quad \ldots\ldots (2.4)$$

The bound water considered in this work is that defined by Taylor[46], which includes the interlayer water in C-S-H and AFm phases, the crystal water in ettringite and the adsorbed water. It can be practically determined[46] as the water retained when a sample was placed over saturated LiCl solution which gives a value of relative humidity of about 11% at room temperature. The sample was first broken into small particles. When its age was less than two weeks, the sample was immersed into alcohol overnight. It was then placed on a filter paper of known weight, and positioned in a sealed desiccator containing saturated LiCl solution at the bottom. It was observed that a steady sample weight ($W_{11}$), obtained as the difference in the total weight and the weight of the filter paper, could be achieved in one week. The bound water content (Wb) expressed on weight of the unhydrated cement was calculated from

$$Wb=(W_{11}-W_{950})/Wc - L.O.I \quad \ldots\ldots (2.5)$$

## 2.5 Measurement of the Streaming Potential

### 2.5.1 The streaming potential

When two phases are placed in contact, a difference in potential normally develops between them. The separation of charge that occurs at the interface between the two phases is called an electrochemical or electrical double layer, because it consists, ideally, of two regions of opposite charge[48]. The structure of the double layer will be reviewed in subsection 4.1.1, chapter 4.

When liquid is forced through a capillary, the charge in the mobile part of the double layer is carried towards one end. This constitutes a streaming current of ionic flow. The accumulation of charges thus sets up an electrical field. The field causes a current flow in the opposite direction through the bulk of the liquid and when this latter conduction current is equal to the streaming current, a steady state is achieved. The resulting electrostatic potential difference between the ends of the capillary is termed the streaming potential[48].

The zeta potential can be practically calculated for aqueous electrolytes at 20°C from[48]

$$\text{Zeta} = 1.055*10^{5} d(E_s/P) \quad (\text{mv}) \qquad \ldots\ldots (2.6)$$

where P is the pressure in cmHg, d is the conductivity in $\text{ohm}^{-1}\text{cm}^{-1}$, and $E_s$ is the streaming potential.

Overbeek[49] showed that the above equation can be applied

to porous plugs provided all or almost all of the current is transported by the bulk (i.e. little surface conductance). The surface conductance becomes pronounced when dilute solution is used, requiring some procedures for the correction of the calculated values[50,51]. The liquid flow must be linear and laminar. Pressure below 1 atmosphere, normally 5-20 cmHg, is applied through the plug to produce the required flow of the solution[48].

### 2.5.2 The asymmetry potential

If two identical electrodes are placed at the ends of the porous plug, the steady-state potential difference measured between the electrodes is the streaming potential. However, when any two electrodes are placed in an electrolyte, they normally give a potential difference which is called the asymmetry potential[48]. The streaming potential should therefore be obtained by subtracting the asymmetry potential from the total potential measured.

Difficulties in calculating the streaming potential can arise from the fact that the asymmetry potential between two electrodes tends to change with time or pressure[52]. Hunter and Alexander[53] proposed a simple "back-off" method to determine the streaming potential, and found that accordingly determined streaming potentials are accurate enough for most purposes. As depicted in figure 2.4, the streaming potential can be taken as the potential drop after streaming has been stopped[54].

### 2.5.3 The apparatus

The apparatus for the measurement of the streaming potential must thus supply a constant stream of the solution to the plug and should permit easy replacement of both the streaming solution and the plug while retaining a fixed geometry for the plug packing when an experiment is in progress.

By reference to a number of typical measurement systems in the literature[54-59], it was decided to construct the system as shown in fig 2.5. The electrodes were made of perforated platinised titanium with 0.75-1 mm holes. The potential developed was read from a digital multimeter or a potential recorder. The two 3-way taps allowed the flow to be directed in either direction and pressure to be read from the manometer. The resistance of the plug could be measured by a conductivity bridge.

### 2.5.4 Testing of the apparatus

Silica gel (for use as a laboratory adsorbent) was used first to test the apparatus. The gel was crushed in a mortar and sieved. The particles of 300 to 1000 μm were stored in 1 litre deionised water for one day. The solution after being saturated with the gel was used as the streaming solution. The prepared particles were packed into the sample cell with the help of pressurized nitrogen so as to form a firmly compacted diaphragm. The measurement system was established by transferring the

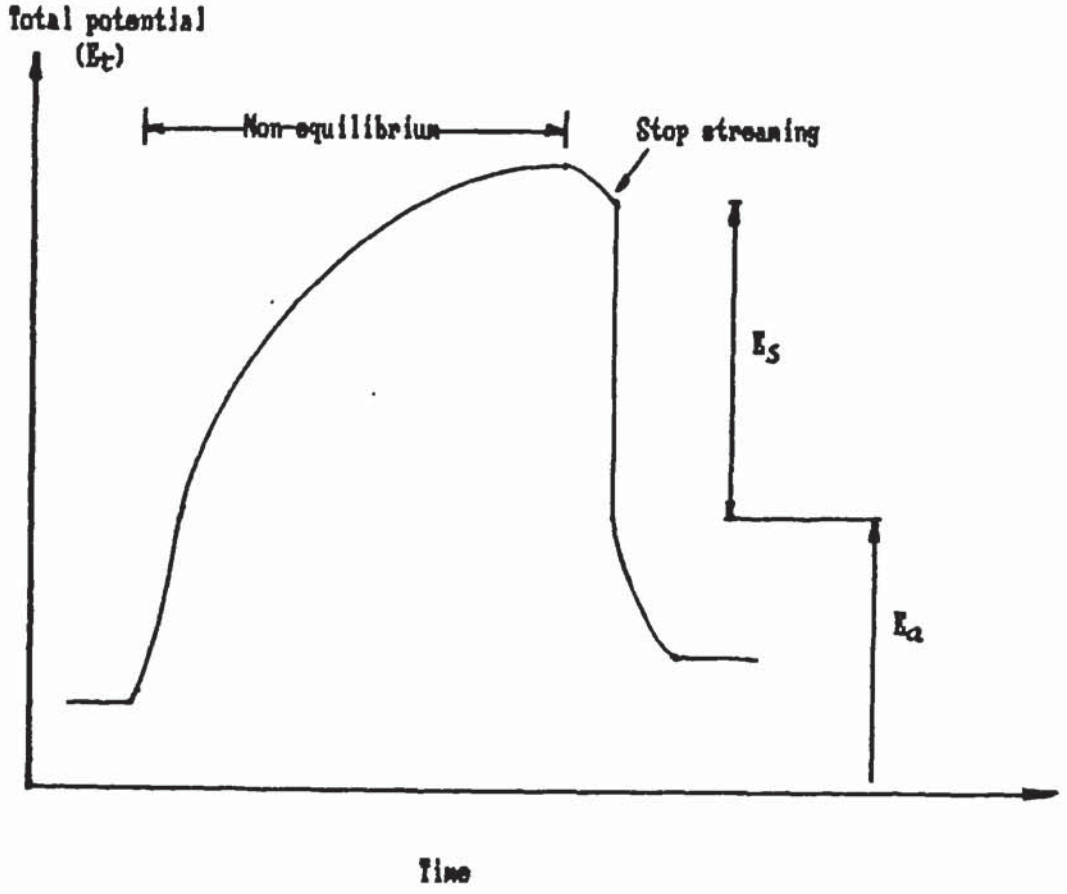


Figure 2.4 Calculation of the streaming potential

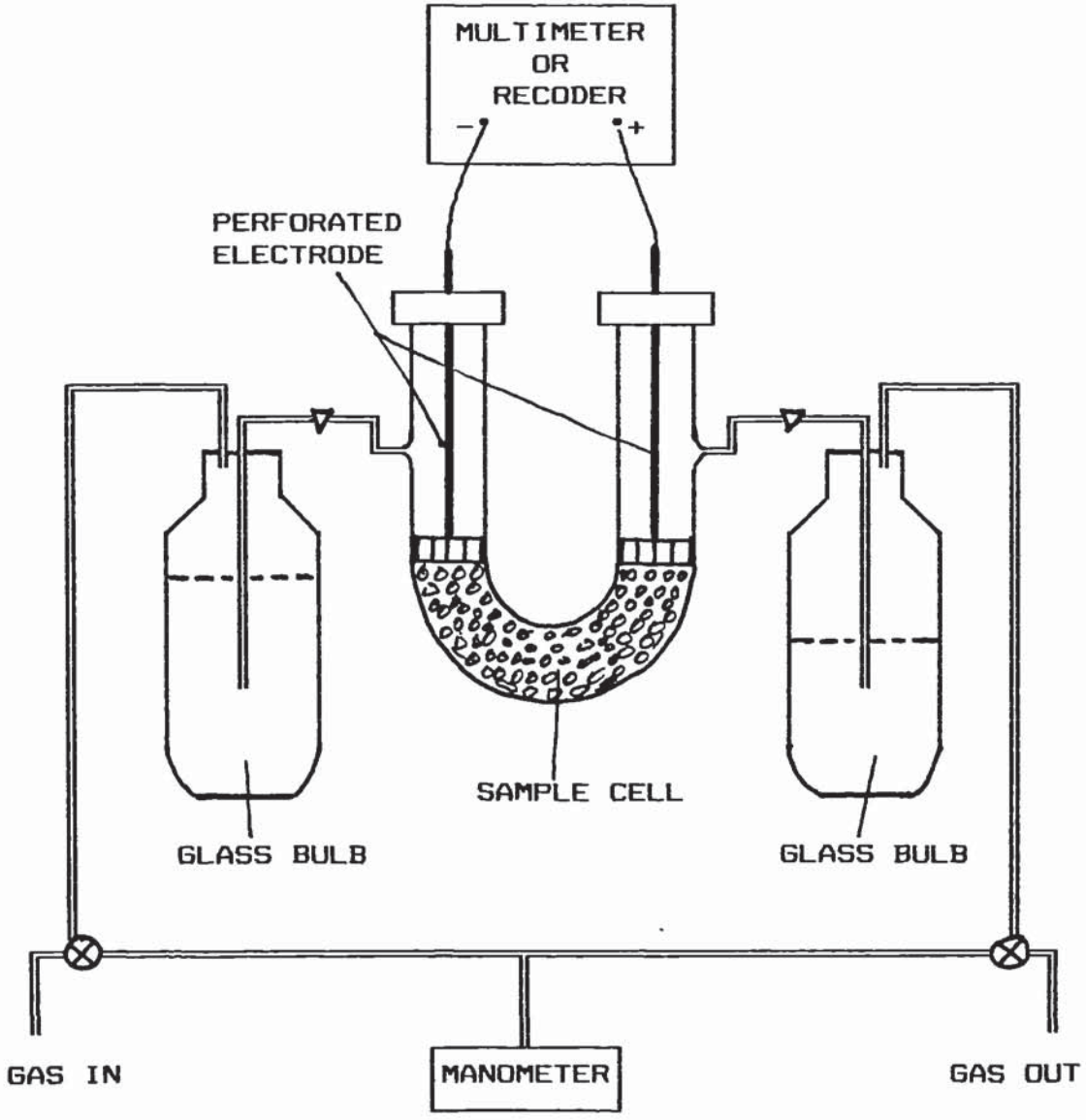


Figure 2.5 Apparatus for streaming potential measurement

solution into the two bulbs. The samples in the cell were finally flushed several times to eliminate any air bubbles from the cell and left for half an hour to achieve a reasonable initial equilibrium.

The 2-way tap on the left was closed, and the left bulb was pressurized by nitrogen gas to about 40 to 50 cmHg. Then the tap was opened to allow the liquid to flow through the plug, resulting in a continuous increase of potential. After the potential had changed in the reverse direction, one of the 2-way taps was closed and the potential was recorded with time. The potential-time curve was similar to that illustrated in figure 2.4. The pressure actually applied was calculated from the reading of the manometer and the liquid levels in the two bulbs. With regard to the electrical circuit arrangement of the multimeter shown in figure 2.5, this curve suggests that positive charge in the mobile part of the double layer was flowing towards the right, so the immobile part of the double layer was negatively charged relative to the bulk solution and the streaming potential was negative.

The starting pressure for the next flow was the previous pressure at which streaming was stopped. Another two runs of measurement were carried out at half hour intervals. The data in table 2.2 show that the asymmetry potential of the system varied regularly, slightly decreasing with successive streaming experiments, but increasing greatly with time. The streaming potential was calculated by

Hunter's "back-off" method. It can be seen from table 2.2 that the calculated values of $E_s/P$ did not show much scatter, indicating that the apparatus was working and that the method for the determination of streaming potential was applicable.

To estimate the measurable range of the streaming potential, alumina was used because of its high recorded values of zeta potential in concentrated solution (-60 to -80 mv in solutions of pH 11 to 12[58]). After being first cleaned with dilute nitric acid and then washed with deionised water[59], very fine alumina (<150 μm) was placed in 1 litre 0.01M NaOH solution. A sheet of very thin filter paper was used to cover the electrode surface to help form a plug with minimised resistance to the flow of the solution. The results are shown in table 2.3. The zeta potential of alumina is more negative than -60mv as the conductivity is above 0.001 $ohm^{-1}cm^{-1}$ which can be estimated from equation 4.5 (see chapter 4). It can thus be concluded that a streaming potential of approximately 3 mv could be quite accurately determined for the system.

## 2.6 Diffusion Measurements

Experimental work on ionic diffusion is presented in chapters 3 and 5. Details including the technique and experimental procedures are given in subsections 3.2.1 and 3.3.1, chapter 3. The technique developed for the

determination of oxygen diffusivity is described in chapter 5.

**Table 2.2** Streaming potentials of Silica gel in water

| $E_t$ (mv) | $E_a$ (mv) | $E_s$ (mv) | P(cmHg) | $E_s/P$ |
|---|---|---|---|---|
| Left ====> Right streaming | | | | |
| -85.1 | -64.0 | -21.1 | 21.0 | 1.01 |
| -83.6 | -64.5 | -19.1 | 18.2 | 1.04 |
| -81.2 | -65.6 | -15.6 | 14.4 | 1.08 |
| -79.0 | -66.2 | -12.8 | 11.4 | 1.12 |
| -77.7 | -66.7 | -10.3 | 9.6 | 1.07 |
| -76.4 | -67.9 | -8.48 | 7.8 | 1.08 |
| Left ====> Right streaming | | | | |
| -65.3 | -34.4 | -30.9 | 31.9 | 0.97 |
| -64.0 | -38.0 | -26.0 | 25.8 | 1.00 |
| -61.5 | -41.2 | -20.3 | 19.4 | 1.04 |
| -60.0 | -44.2 | -15.8 | 14.8 | 1.07 |
| -58.0 | -46.3 | -11.7 | 11.0 | 1.06 |
| Right ====> Left streaming | | | | |
| 5.0 | -22.1 | -27.1 | 27.2 | 1.00 |
| 2.0 | -19.6 | -21.6 | 21.2 | 1.02 |
| 0.0 | -17.0 | -17.0 | 16.2 | 1.06 |
| -1.0 | -15.3 | -14.3 | 13.2 | 1.08 |
| -2.4 | -13.3 | -10.9 | 10.0 | 1.09 |

Table 2.3 Streaming potentials of alumina in 0.01 M NaOH

| $E_s$(mv) | P (cmHg) | $E_s$/P |
|---|---|---|
| -3.4 | 5.6 | 0.61 |
| -4.6 | 7.7 | 0.60 |
| -6.4 | 10.0 | 0.64 |
| -8.1 | 13.8 | 0.59 |
| -9.4 | 16.4 | 0.57 |
| -10.6 | 19.0 | 0.56 |
| -13.6 | 24.2 | 0.56 |
| -14.3 | 25.0 | 0.58 |

# CHAPTER 3 DIFFUSION OF QUATERNARY AMMONIUM IONS

## 3.1 Introduction

As already mentioned in Chapter 1, pore structure is one of the most important factors that influences ionic and molecular diffusion rates in hydrated cement pastes. There are four aspects of pore structure to be considered; porosity or pore volume, pore size distribution, pore geometry and the inter-connection of the pores. Although there are a number of techniques, which help to determine the quantitative or qualitative nature of the pore structure, the information obtained is insufficient to explain fully the effects of pore structure on diffusion.

Among the conventional experimental techniques, capillary condensation and mercury intrusion porosimetry are the most widely used methods to give quantitative information on the pore size distribution in hydrated cement pastes. However, both methods involve drying the samples to remove the original water, which may alter the actual pore structure. This alteration may be expected to be more significant for young and blended cement pastes, especially so for their small pores[33,60]. As a consequence, it is difficult to make a satisfactory comparison of the relationship between pore structures and diffusivities of different types of cement paste.

Furthermore, there are some controversies concerning the

applicability of the two methods with regard to the basic equations and assumptions involved in the quantitative calculation of the pore size distribution[61]. In a critical comparison, Diamond[62] found some discrepancies between the results of the two types of measurement for hydrated OPC cement pastes. The capillary condensation data yielded a mean pore diameter between 50 and 100 A. The mercury intrusion data indicated considerably coarser size distributions with mean diameters of the order of several hundred Angstroms.

To promote improved understanding of the pore structure effect, some new techniques have to be developed directly related to the diffusion process. An approach that has been devised in the present work involves study of the diffusion of quaternary ammonium ions which are strongly hydrated in water. This homologous series of ions has a unit positive charge and a symmetrical tetrahedral geometry. By varying the carbon chain length, different ionic sizes can be obtained. As the diffusing ions get larger, one would expect a decrease in diffusion rate, as entry to more pores is restricted. These quaternary ammonium ions can be considered here as a "probe" to investigate the pore structure. The diffusion path can thus be conceptually separated if diffusion rates of such ions correspond, to some degree, to the change of ionic sizes.

Diffusivities of four quaternary ammonium ions in hydrated

OPC and PFA pastes of w/c ratios 0.35, 0.50 and 0.65 were obtained by the steady-state technique which is to be described in the next subsection. To aid the interpretation of the diffusivities obtained with regard to the effect of pore structure on diffusion, two forms of experiment, designated the type 1 and type 2, were used to estimate the volume proportion of the pores that can not be entered by these relatively large quaternary ammonium ions. The sizes of the ions investigated have been given in table 1.1.

In the type 1 experiment, a certain amount of the $(C_3H_7)_4N^+$ ions was introduced into 0.65 w/c OPC paste during mixing. The $(C_3H_7)_4N^+$ has an ionic radius 4.52 Å, which is greater than the molecular radius of nitrogen (2.03 Å). As it has been considered that nitrogen could enter fewer of the pores in hydrated cement pastes than water molecules could (see subsection 3.3.2), it is possible that the $(C_3H_7)_4N^+$ ions would be excluded from some pores during cement hydration. The $(C_3H_7)_4N^+$ concentrations in the pore solution were determined at different lengths of the hydration time. The geometrical restriction of the pore structure to diffusion of $(C_3H_7)_4N^+$ ions could thus be estimated from calculations based on the mass balance.

If an oven-dried cement paste sample is placed in a solution containing $(C_3H_7)_4N^+$ ions, it is possible that

some pores in the sample can be entered by the water molecules but not by the relatively large $(C_3H_7)_4N^+$ ions. This could result in an increase of the $(C_3H_7)_4N^+$ concentration in the external solution after the transport has been completed. The type 2 experiment was based on this idea and used to estimate the volume of pores that can not be practically passed through by the $(C_3H_7)_4N^+$ ions.

## 3.2 Literature Review

### 3.2.1 Steady-state diffusion

Diffusion at a steady state, more exactly at a quasi-steady state, can be easily achieved through the experimental arrangement shown in figure 3.1. A thin test disc, generally of hydrated cement paste or mortar, is fixed between the two half cells containing solutions of unequal concentrations of the ion investigated. At the steady state, the flux (J) per unit bulk section area of the test disc is a constant at any distance (x) within the disc,

$$J=-\epsilon D(dC/dx)=-D_i(dC/dx) \qquad \ldots\ldots (3.1)$$

where $\epsilon$ has a similar meaning to the porosity of a water-saturated paste; more specifically, it is the volume fraction of the pore solution in which the diffusion occurs.

When $\epsilon$ is constant within the disc, the concentration

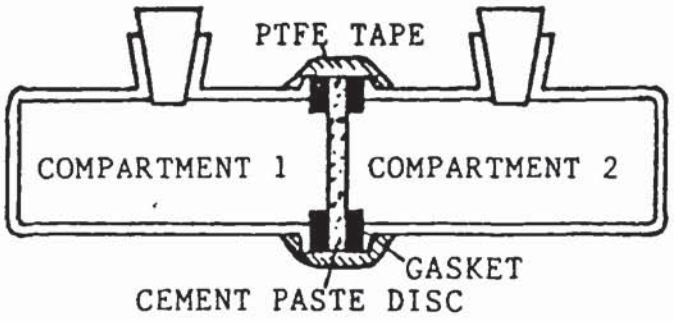


Figure 3.1 The ionic diffusion cell

gradient (dC/dx) should be a constant and can be obtained by dividing the concentration difference between the two solutions by the disc thickness, which enables the determination of the intrinsic diffusivity ($D_i$) from the flux observed experimentally. This technique has been widely employed to study ionic diffusion in hydrated cement pastes because of its speed and simplicity[15,63]. Typical diffusivities of some simple ions for certain hydrated cement pastes have been shown in tables 1.2 and 1.3.

Atkinson and Nickerson[4] considered several factors that may affect the applicability of the "thin-disc" technique, including the osmotic flow and temperature variation. The possible osmotic flow was eliminated by filling the half cell with 1M KI and KCl respectively, since the two salt solutions have approximately the same osmotic coefficients. By comparing the diffusivities obtained with those reported in the literature, the authors essentially supported the results obtained by other workers. However, they used a temperature cycle, rising from 20 to 60 °C, cooling down to 10°C and then back to 20°C, which induced some irreversible effects that tended to increase the diffusivity. They concluded that the temperature had at least two effects; one was the temperature-induced changes in the pore structure and the other, the basic temperature dependence of the diffusion mechanism. Nevertheless, the temperature range used in their experiments is excessive,

particularly with regard to to their relatively young specimens (cured for four weeks).

The fact that anions normally diffuse faster than cations, as indicated in table 1.2, suggests that certain ions rather than the ions investigated can be involved in the co- or counter-diffusion, as the charge balances regarding both the concentration and the flux must be maintained. This was considered by Sergi[64] who carried out experiments involving the diffusion of NaOH. It was found that sodium and hydroxyl ions diffused in OPC paste at the same rates, suggesting that the hydroxyl ion is the main species responsible for the counter-diffusion in the systems employed, for example, by Kondo et al[17] (see table 1.2). By adding PFA and BFS to the OPC, Sergi observed that the hydroxyl diffusivity was also decreased.

### 3.2.2 Models of pore structure in hydrated cement pastes

The classical model of the pore structure in hydrated portland cement was given by Powers[45]. In this model, gel pores are visualized as the spaces between gel particles of which the solid-to-solid distance is on average about 18 A, contributing a minimum porosity of 28% to the cement gel. Any spaces not filled by cement gel are called capillary cavities. However, Diamond and Dolch[65] questioned the existence of such a separated class of gel pores in hydrated cement pastes. They showed that for a

mature paste, the pore volume intruded by mercury below about 60 A in diameter, is not only less than that predicted by a log-normal distribution plot, which suggests that all the pores intruded belong to a single pore size distribution, but is almost negligible in absolute terms.

Feldman and Sereda[66] proposed a quite different model from the above Powers-Brunauer representation. The C-S-H is also considered to be of layered structure. However, according to this view, these layers may come together randomly to create interlayer spaces. Assuming that the interlayer spaces are bounded by two parallel plates, Feldman and Sereda estimated that the average separation between the plates is 3.3 A. This model is consistent with an internal system composed of layers separated by, on the average, one water molecule, so the interlayer water is regarded as part of the solid structure. Most of this water is not removed from the structure on drying until relative humidities of below 10% are reached. The volume of the interlayer spaces, as calculated by Feldman et al[67] based on the data obtained from capillary condensation methods, is approximately the volume of the pores that can be passed through by water which has a molecular radius of 1.63 A, but not by nitrogen which has a molecular radius of 2.03 A. However, it is still an open question[68,69] why such a small difference in their molecular sizes could result in a big difference in the

specific surface areas of the cement gel determined from their adsorption isotherms.

Based on adsorption studies on hydrated $C_3S$ paste after the removal of calcium hydroxide, Daimon et al[70] modified the Feldman-Sereda model. Adsorption measurements indicated the existence of two kinds of pores: a wider inter-gel-particle pore which can be seen even in the inner C-S-H by SEM, and a smaller intra-gel pore existing within the gel particles which cannot be observed by SEM. The intra-gel pores are further classified into an inter-crystalline pore similar to the micropores reported by Brunauer et al[71], and intra-crystalline pores corresponding to the interlayer spaces in the Feldman-Sereda model. Daimon et al also suggested that some relatively large pores in dense pastes are accessible to water only through interlayer spaces.

### 3.2.3 Effects of pore structure on diffusion

The interconnectivity of pores has been considered to be an important underlying parameter for water permeability and ionic diffusion rates. Powers et al[72,73] carried out permeability measurements with mature OPC paste varying in w/c ratio. The obvious effects of w/c ratio are to change the total porosity and pore size distribution. The authors[73] showed clearly that permeability is related to capillary porosity; gel pores control the permeability for pastes of w/c ratios below 0.4 as the capillary spaces are

only interconnected by the gel pores. When capillary porosity is relatively high, the capillaries are a continuous interconnected network through the gel. This is the case for a mature paste if the w/c ratio is above 0.5, so capillary porosity determines permeability.

Page et al[22] showed similar effects of the pore structure on diffusion, as indicated by the considerable decrease of the activation energy for chloride diffusion as w/c ratio changes from 0.4 and 0.5 to 0.6 (see table 1.4). Parrott et al[74] found a sharp change of the diffusion behaviour in hydrated alite cement at the porosity 0.35 for pores greater than 500 Å wide, and concluded that open channels are blocked by relatively small quantities of hydration products. Kumar et al[27,75] showed by statistical analysis that chloride diffusivity is related to fractional porosity and modal pore radius.

There are some difficulties in interpreting the variations of diffusivity with type of cement paste in terms of the experimentally measured porosity and pore size distribution. Goto et al[28-30] determined the diffusivities of $Cl^-$, $I^-$ and $Na^+$ in pastes of various w/c ratios and curing temperatures, including ordinary portland, blast furnace slag and sulphate resisting cement pastes. They suggested that the diffusivities are correlated with the volume of pores of radius below 20 Å. This correlation is independent of types of paste, though no clear explanation was given.

Feldman[76] examined the pore structure damage in blended cement pastes caused by mercury intrusion. He found that pores of slag and fly-ash pastes were relatively discontinuous, despite large values for porosity and pore-size distribution. During mercury intrusion, these discontinuous and thin-walled pores were disrupted at high pressure and intruded. The presence of calcium hydroxide in hydrated OPC pastes has been used to explain the relative continuity of pore structure compared to those of blends[77].

Marsh and Day[78] compared the porosity data obtained from mercury intrusion and helium pycnometry. The results for the OPC pastes showed close agreement, whereas those for the blended cement pastes of low porosities did not. This was considered as an indication of the discontinuities in pore systems of blended cement pastes since helium pycnometry is a relatively gentle technique which would, presumably preserve more of the original pore structure.

## 3.3 Experimental and Results

### 3.3.1 Diffusion

#### 3.3.1.1 Specimen preparation

OPC and PFA were first mechanically mixed with deionised water for ten minutes in the required proportions to

produce mixtures of 0%, 20% or 40% PFA content at w/c ratio 0.35, 0.5 or 0.65. They were then poured into cylindrical PVC containers of dimensions, 45 mm in diameter and 75 mm in height, and compacted by vibration for ten minutes.

On at least two occasions the foamy layer that had accumulated on the surface during the vibration was removed and replaced by fresh paste. A polythene sheet was then placed on the top of each container to prevent any entrapment of air by the cap which was subsequently fitted on top.

In order to minimize segregation and to enable the production of uniform cement pastes, the cylinders were rotated top to bottom at a speed of 8 rpm overnight and stored in a curing room controlled at 22°C for two weeks. The pastes were then demoulded and finally immersed in saturated lime water for four months in the curing room.

3.3.1.2 Experimental set-up

The number of ions in the quaternary ammonium series that can be easily used in the diffusion measurements is limited by their solubilities which decrease with increase in size of the carbon chain. The $(CH_3)_4N^+$ ion could have been used in this investigation but was eliminated because its concentration could not be measured by the same methods as described in section 2.3, chapter 2. When the carbon chain is bigger than that of $(C_6H_{13})_4NBr$ the

solubility was found experimentally to be smaller than 0.03 M. Hence, diffusion measurements were carried out by the thin-disc steady state diffusion technique with the series of quaternary ammonium bromides including:

(1) tetraethylammonium bromide, $(C_2H_5)_4NBr$

(2) tetrapropylammonium bromide, $(C_3H_7)_4NBr$

(3) tetrabutylammonium bromide, $(C_4H_9)_4NBr$

(4) tetrapentylammonium bromide, $(C_5H_{11})_4NBr$

The molar concentration used in the high concentration side of the diffusion cell was 0.1 which is slightly below the solubility of $(C_5H_{11})_4NBr$.

Discs, approximately 1.3 or 2.3 mm in thickness, were obtained by cutting the cylindrical paste using a diamond saw. They were ground on both sides by hand on 400 grade emery paper, prior to mounting into the glass diffusion cell as shown in figure 3.1. Each disc was mounted between the ground flanges of two half cells, sealed with lightly greased rubber gaskets, placed between the disc and the flanges. The flange joint was well wrapped with PTFE tape to ensure isolation of the cell contents. A layer of PVC insulation tape was wound around to add strength, and the seal completed with a final layer of PTFE tape.

The high concentration side (compartment 1) of each cell was filled with a solution of saturated calcium hydroxide, containing 0.1 M quaternary ammonium bromide. The low concentration side (compartment 2) was filled with a known

volume (about 80 ml) of saturated calcium hydroxide solution. The cells were finally put into a water-bath of controlled temperature, 25°C.

3.3.1.3 Results

The concentrations of the quaternary ammonium ions in the compartment 2 were analyzed using the colorimetric methods described in section 2.3 (chapter 2), at a time interval, generally about 10 to 20 days. An example of the concentration increasing with time is presented in figure 3.2.

The intrinsic diffusivity ($D_i$) was calculated as explained in subsection 3.2.1 from:

$$D_i = VL/(0.1A)(dC_2/dt) \quad \ldots\ldots (3.2)$$

where 0.1 is the molar concentration in the compartment 1, V is the volume of compartment 2, L is the thickness of the disc, and A is the diffusion area (about 10 $cm^2$) which was measured from the marks left by the grease on the gasket after the experiment was completed. The quantity, $dC_2/dt$ in M $sec^{-1}$, is the slope determined from the concentration-time curve as shown in figure 3.2. The diffusivities obtained are listed in appendix 1. The average diffusivities are shown in tables 3.1 and 3.2 for the OPC and PFA pastes respectively.

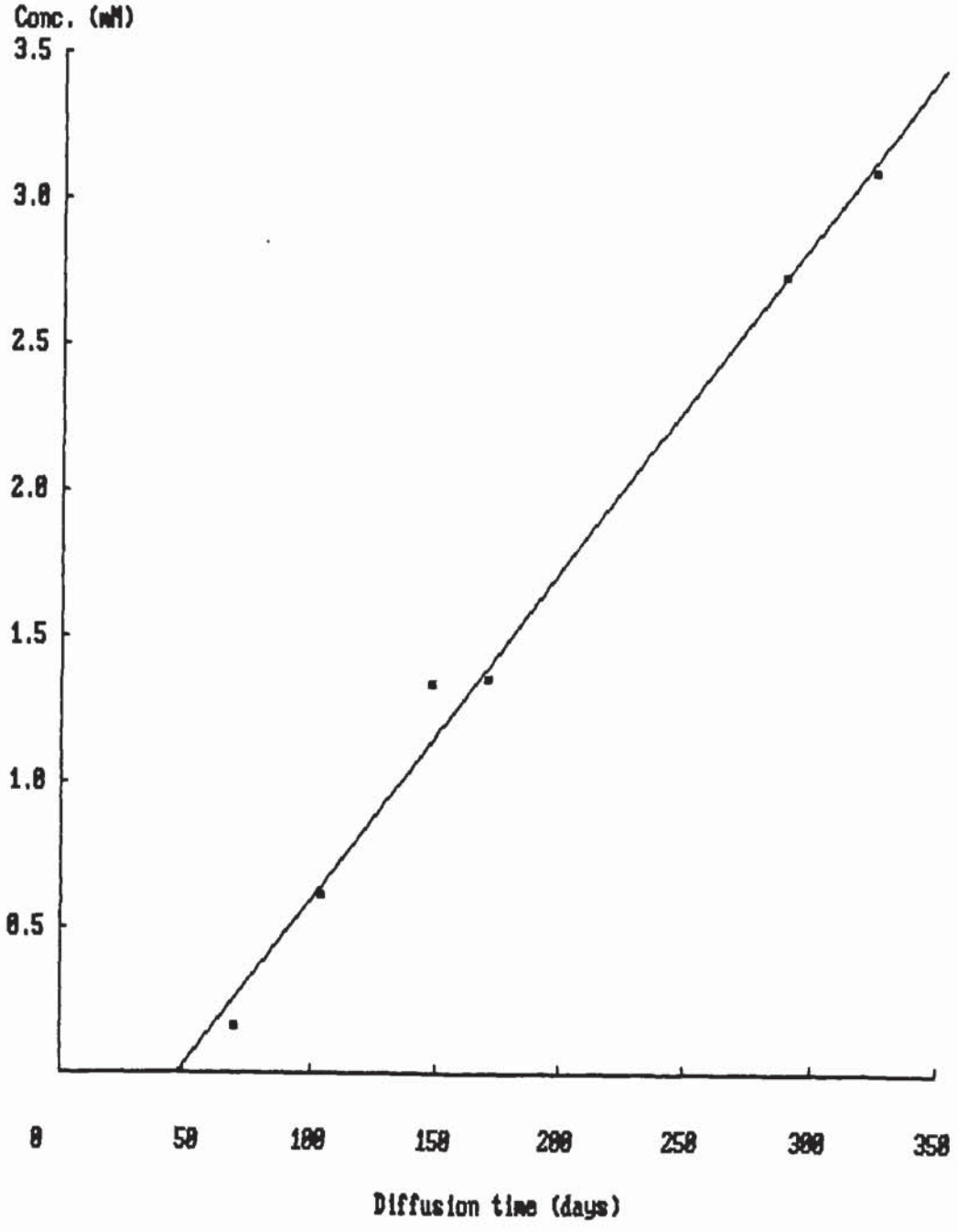


Figure 3.2 Rise of $(C_3H_7)_4N^+$ concentration in the compartment 2 of the diffusion cell

**Table 3.1** Average diffusivities of quaternary ammonium ions in hydrated OPC pastes ($x10^{-10}$ $cm^2/sec$)

| IONS | w/c | | |
|---|---|---|---|
| | 0.35 | 0.50 | 0.65 |
| $(C_2H_5)_4N^+$ | 26.6 | 24.3 | 848 |
| $(C_3H_7)_4N^+$ | —— | 15.4 | 426 |
| $(C_4H_9)_4N^+$ | 5.8 | 11.3 | 305 |
| $(C_5H_{11})_4N^+$ | 1.2 | 1.0 | 465 |

**Table 3.2** Average diffusivities of quaternary ammonium ions in hydrated OPC/PFA pastes ($x10^{-10}$ $cm^2/sec$)

| IONS | w/c ¦ PFA mix-portion | | | |
|---|---|---|---|---|
| | 0.35 ¦ 40% | 0.50 ¦ 40% | 0.65 ¦ 40% | 0.65 ¦ 20% |
| $(C_2H_5)_4N^+$ | | 14.6 | 494 | 724 |
| $(C_3H_7)_4N^+$ | 6.3 | 7.9 | 398 | 483 |
| $(C_4H_9)_4N^+$ | 2.4 | 5.2 | 274 | 296 |
| $(C_5H_{11})_4N^+$ | 0.7 | 2.1 | 212 | 192 |

### 3.3.2 Type 1 Experiment

#### 3.3.2.1 Experimental procedures

$(C_3H_7)_4NOH$ was introduced during mixing of OPC slurry at the concentration of 0.4, 0.8, 1.2 or 1.6 mM and cement-solution ratio of 0.65. The slurry was mixed mechanically for twenty minutes. It was then cast into PVC moulds and vibrated for four minutes as described in paragraph 3.3.1.1. The specimens prepared were capped, and PTFE tape was wound around the joints between the mould and the caps to avoid any loss of water during the storage in the curing room.

Having been cured for a certain period of time, two-thirds of each paste cylinder was broken off, and the pore solution was extracted using the pore-press technique described in section 2.2, chapter 2. The concentration of $(C_3H_7)_4N^+$ ions in the extracted solution was determined. The remaining one-third of the cylinder was used for determination of the contents of the bound, evaporable and non-evaporable water as described in section 2.4, chapter 2.

#### 3.3.2.2 Results

For a simple explanation for the calculation of the results, assume:

(1). $C_0$ is the $(C_3H_7)_4N^+$ concentration (mM) in the solution used for the mixing.

(2). Wt is the content of the total water in the paste, and Wt=We+Wn, where We and Wn are the evaporable and non-evaporable water contents respectively.

(3). Cp is the concentration (mM) of the $(C_3H_7)_4N^+$ ions in the extracted pore-solution.

(4). The content of the water which dissolved or hydrated the $(C_3H_7)_4N^+$ ions is Wp, and assume that only this form of water was squeezed out by the pore-press device employed.

(5). The $(C_3H_7)_4N^+$ ions were distributed uniformly in the water represented by Wp.

Because one gramme cement contained $WtC_0$ mmol $(C_3H_7)_4N^+$ ion, there should be a mass balance as expressed by

$$WtC_0=WpCp \qquad \ldots\ldots (3.3)$$

Therefore, the content (Wpx) of the water that cannot accommodate this ion can be expressed based on weight of the unhydrated cement as

$$Wpx=Wt-Wp=(1-C_0/Cp)Wt \qquad \ldots\ldots (3.4)$$

The Wpx obtained can be compared with the non-evaporable or bound water, and the water contents are listed in table 3.3.

As can been seen from the mass balance equation 3.3, if the evaporable water is assumed to have been squeezed out by the pore solution technique, the $(C_3H_7)_4N^+$ concentration (Cp) in the extracted pore solution should have been $WtC_0/We$, and thus the Wpx obtained should have been the non-evaporable water. Table 3.3 shows that the

Table 3.3 Water contents determined from the type one experiment (% on weight of cement)

| AGE (days) | Wpx | Wn | Wb |
|---|---|---|---|
| 1 | 21.7 | | |
| | 18.6 | | |
| | 20.2 | | |
| (average) | 20.2 | | |
| 4 | 24.0 | 14.1 | 18.7 |
| | 24.3 | 13.9 | 20.1 |
| | 25.3 | ——— | 18.7 |
| (average) | 24.5 | 14.0 | 19.2 |
| 7 | 24.8 | 15.1 | 24.3 |
| | 25.0 | 14.9 | 25.6 |
| | 27.3 | 15.0 | 24.0 |
| | 25.9 | 14.9 | 23.8 |
| (average) | 25.8 | 15.0 | 24.4 |
| 14 | 25.7 | 16.1 | 23.8 |
| | 25.9 | 15.0 | 20.5 |
| | 30.4 | 15.6 | 22.9 |
| | 31.9 | 15.7 | 23.4 |
| (average) | 28.5 | 15.6 | 22.7 |
| 30 | 27.1 | 16.9 | 24.6 |
| | 30.3 | 17.1 | 24.4 |
| | 34.5 | 18.1 | 25.6 |
| | 34.3 | 17.4 | 25.6 |
| (average) | 31.6 | 17.4 | 25.1 |
| 65 | 32.5 | 18.5 | 27.9 |
| | 34.7 | 18.9 | 28.2 |
| (average) | 33.6 | 18.7 | 28.1 |

values of the Wpx obtained are always greater than the non-evaporable and bound water contents. It is therefore obvious that the Cp is also the minimum weight content of the water that cannot be extracted from the pore-press technique. Furthermore, if some water that did not contain the $(C_3H_7)_4N^+$ ions due to the geometrical restriction mentioned in the introduction section was extracted during the pore-pressing, the Cp calculated would thus underestimate the restriction effect to the diffusion of $(C_3H_7)_4N^+$ ions. This is because the water that hydrated the $(C_3H_7)_4N^+$ ions was diluted.

### 3.3.3 Type 2 Experiment

#### 3.3.1.1 Calculations

As mentioned in the introduction section, this experiment was intended to estimate the volume of the pores that the $(C_3H_7)_4N^+$ ions can not pass through during the diffusion process. To explain this experiment which is to be described in the next paragraph, the calculation of the results will be first considered.

If $W_{105}$ gramme oven-dried paste is placed into $V_0$ ml solution of $(C_3H_7)_4N^+$ concentration $C_0$ mM, transport of both the water and the $(C_3H_7)_4N^+$ ions will occur from the bulk solution into the paste. As the $(C_3H_7)_4N^+$ ions cannot enter some pores that can be entered by water, the $(C_3H_7)_4N^+$ concentration in the bulk solution would

increase to a value Cp (mM) after the transport is completed.

With similar assumptions as were made for the type 1 experiment, the mass balance can be expressed as

$$C_0V_0=(V_0-WeW_{105})Cp + WpW_{105}Cp \quad \ldots\ldots (3.5)$$

where Wp is the content of the water contained in the pores that can be entered by the $(C_3H_7)_4N^+$ ions, and Wp and We is expressed based on weight of the oven-dried paste. So the Wp is

$$Wp=[C_0V_0-(V_0-WeW_{105})Cp]/(W_{105}Cp) \quad \ldots\ldots (3.6)$$

and the content (Wpy) of the water contained in the pores that can not be entered by the $(C_3H_7)_4N^+$ ions is

$$Wpy= We-Wp \quad \ldots\ldots (3.7)$$

Furthermore, a surface-dried sample can be used for this experiment. If a sample of water-saturated paste is placed into the bulk solution, the mass balance equation is

$$C_0V_0=V_0Cp+WpW_{105}Cp \quad \ldots\ldots (3.8)$$

where $W_{105}$ is the weight of this sample at 105°C, so

$$Wp=(C_0V_0-V_0Cp)/(W_{105}Cp) \quad \ldots\ldots (3.9)$$

3.3.3.2 Experimental procedures and results

The OPC paste specimens of w/c ratio 0.35, prepared as for diffusion experiments and cured for four months, were first cut into thin discs (<1 mm). The discs (about 20 grammes), either oven-dried or surface-dried, were weighed. They were then quickly broken into very small pieces and immersed in a tube containing a weighed 0.8 mM

$(C_3H_7)_4NOH$ solution saturated with calcium hydroxide. Each tube was tightly closed to prevent any possible evaporation of the solution.

About four months later, each solution was filtered on a dried paper of known weight. The filter paper and contents were dried at 105 °C, and the weight of the broken disc particles was calculated. The filtrate was analyzed to determine the $(C_3H_7)_4N^+$ concentration. The values of Wp and Wpy obtained using one oven-dried and three surface-dried samples are shown in table 3.4. The contents of the evaporable water are also included in this table.

**Tabel 3.4** Water contents determined from the type two experiment

(% on weight of the oven-dried paste)

| SAMPLE | We | Wp | Wpy |
|---|---|---|---|
| pre-oven dried | 19.6 | 4.6 | 15.0 |
| pre-surface dried | 20.1 | 4.3 | 15.8 |
| | 19.2 | 2.6 | 16.6 |
| | 19.4 | 4.1 | 15.3 |
| (Average) | 19.6 | 3.9 | 15.7 |

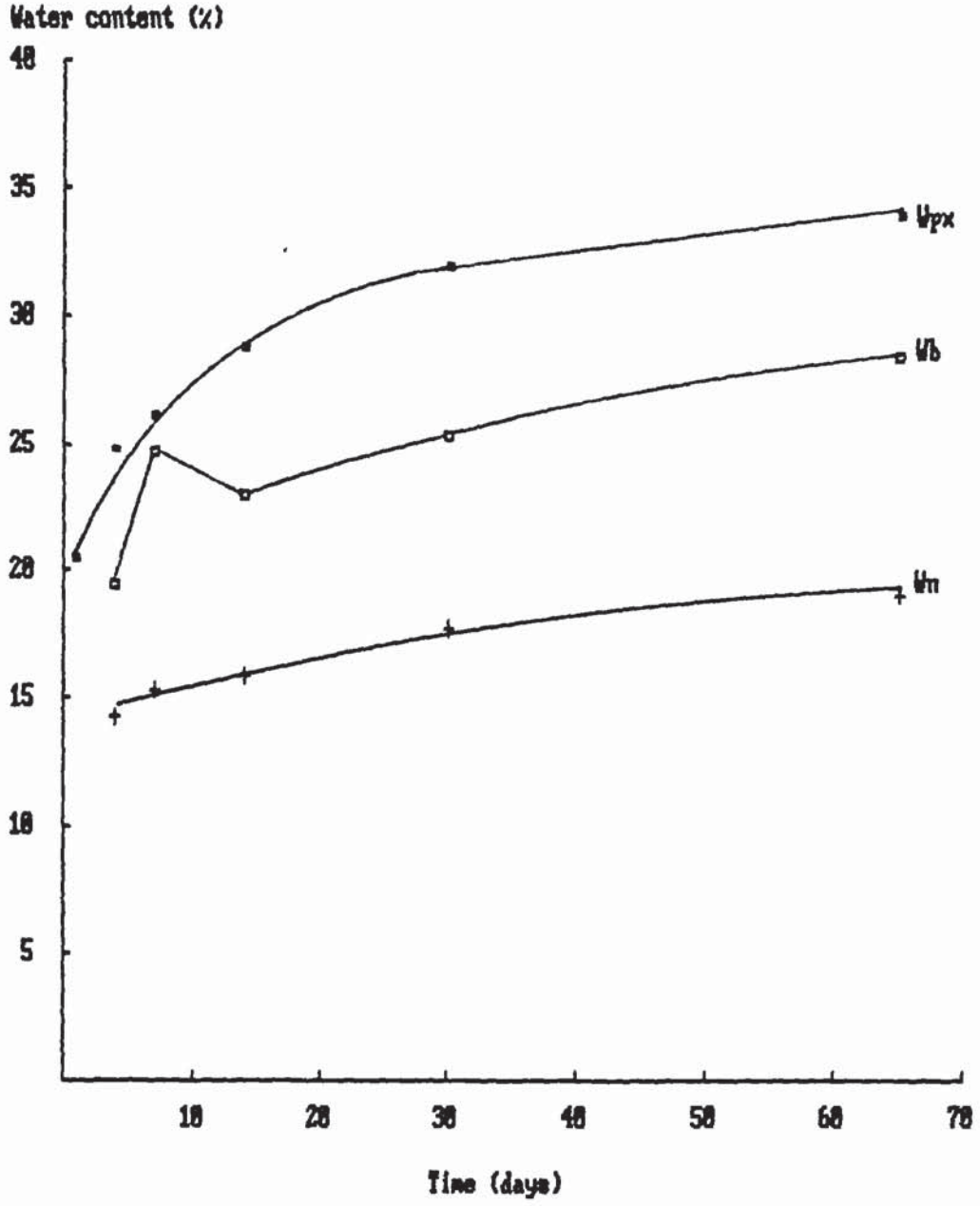


Figure 3.3 Change of water contents with hydration time

## 3.4 Discussion

### 3.4.1 Geometrical restriction to $(C_3H_7)_4N^+$ diffusion

Figure 3.3 shows the time variation of the three types of water content (Wn, Wb and Wpx) determined from type 1 experiment. As expected from the process of cement hydration, the non-evaporable and bound water contents were found to increase with time. The water content denoted as Wpx is considered here as a measure of the degree to which the structure of the cement-matrix cannot accommodate the relatively large $(C_3H_7)_4N^+$ ions. It can been seen from figure 3.3 that this water content is always greater than both the bound and non-evaporable water contents. Because the non-evaporable water has been considered in the literature[14] to be only one part of the chemically combined water, the comparison between the Wpx and the bound water would therefore be more meaningful with regard to the discussion on the geometrical restriction of the pore structure to diffusion of the $(C_3H_7)_4N^+$ ions.

Taylor[46] considered the types of water in hydrated cement pastes based on the pore-structure model proposed by Daimon et al (see subsection 3.2.2). According to Taylor's calculations, the water (Wb) retained at relative humidity 11% is the total of the interlayer water in C-S-H and AFm phases, crystal water in ettringite and adsorbed water. This water was described by the author as the bound

water, as it is either chemically combined into the cement hydrate phases or held to these phases by strong surface forces. Quantitatively speaking, the bound water is also nearly the same as the content of the interlayer water in the Feldman-Sereda model.

With regard to the high w/c ratio (0.65) used for the type 1 experiment, it is reasonable to assume that micropores and interlayer spaces in the paste were water-saturated. As mentioned in subsection 3.2.2, the interlayer pores are considered to be impermeable to nitrogen molecules. The $(C_3H_7)_4N^+$ ions have an ionic radius 4.52 Å, so they are bigger than the nitrogen molecules of (molecular) radius 2.03 Å. It is therefore obvious that the Wpx obtained from the type 1 experiment should be at least equal to the bound water. It is evident from figure 3.3 that about 5% difference between the Wpx and the bound water existed for the specimens hydrated for 1 to 2 months. It can be thus concluded that $(C_3H_7)_4N^+$ ions can not pass through some pores bigger than the interlayer spaces represented by the Feldman-Sereda model, or probably the gel pores by the Powers' model. However, it is difficult to conclude anything further about the capillary pore sizes through which the $(C_3H_7)_4N^+$ ions can pass.

The results shown in table 3.4 obtained from the type 2 experiment tend to show that for the 0.35 w/c OPC paste, certain pores, which contain approximately 80% of the

evaporable water, can be a pathway to water transport but not to $(C_3H_7)_4N^+$ diffusion. However, the calculation used for the type 2 experiment is not as reliable as that for the type 1 experiment, though the type 2 experiment is more related to the actual diffusion process. In the calculation concerning the type 2 experiment, it was assumed that concentration gradient of the $(C_3H_7)_4N^+$ ions in the pore solution was negligible after the specimens had been exposed to the bulk solution for four months. Since table 4.1 from the diffusion experiment indicates that all the quaternary ammonium ions diffused very slowly in the 0.35 w/c OPC paste, the assumption made may be quite unrealistic, despite the fact that considerably greater exposure surface and quite small particles were employed in the type 2 experiment. Nevertheless, the results obtained from the type 2 experiment are still valid in indicating that a relatively large portion of the pores effectively restrict the diffusion of $(C_3H_7)_4N^+$ ions.

Table 1.1 in chapter 1 shows that all the quaternary ammonium ions used in the diffusion experiment are bigger than nitrogen molecules. Diffusion of these ammonium ions would thus not occur through the gel pores by Powers' model. The diffusion flux measured experimentally was therefore contributed by the diffusion through the capillary pores. However, as the gel pores may interconnect the capillaries, particularly in dense pastes

as suggested by Powers et al[45,73], they may control the diffusion rate in terms of the degree of this interconnectivity.

### 3.4.2 Diffusion in the OPC paste

Table 3.2 shows that the diffusivities of the quaternary ammonium ions decreased with increase of ionic radius for the OPC pastes of w/c ratios 0.35 and 0.5. However, for the OPC paste of w/c ratio 0.65, the diffusivity first decreased from $(C_2H_5)_4N^+$, $(C_3H_7)_4N^+$ to $(C_4H_9)_4N^+$, but $(C_5H_{11})_4N^+$ ions diffused evidently faster than $(C_4H_9)_4N^+$.

The diffusivities of the quaternary ammonium ions at infinite dilutions have been given in table 1.1. Because the diffusivities of the quaternary ammonium ions in free solutions also decrease with the ionic radius, the diffusibility[4], defined as the ratio of the diffusivity in hydrated cement pastes to that in infinitely diluted aqueous solutions, can be considered as a relative measure of the restriction of the cement pastes to the diffusion of different ions. The greater the diffusibility is, the less restriction the paste offers. The diffusibilities calculated for the OPC pastes are shown in table 3.5.

The diffusibilities for the OPC pastes of w/c ratios 0.35 and 0.50 are plotted in figure 3.4 against the ionic radii, while those for the paste of w/c ratio 0.65 are shown in figure 3.5. It can be seen from figure 3.4 that the diffusibility decreased with ionic radius for the

**Table 3.5** Diffusibilities of quaternary ammonium ions in hydrated OPC pastes ($x10^{-4}$)

| IONS | w/c | | |
|---|---|---|---|
| | 0.35 | 0.50 | 0.65 |
| $(C_2H_5)_4N^+$ | 3.06 | 2.80 | 95 |
| $(C_3H_7)_4N^+$ | —— | 2.47 | 68 |
| $(C_4H_9)_4N^+$ | 1.11 | 2.16 | 59 |
| $(C_5H_{11})_4N^+$ | 0.26 | 0.21 | 100 |

**Table 3.6** Diffusibilities of quaternary ammonium ions in hydrated OPC/PFA pastes ($x10^{-4}$)

| IONS | w/c : PFA mix-portion | | | |
|---|---|---|---|---|
| | 0.35 : 40% | 0.50 : 40% | 0.65 : 40% | 0.65 : 20% |
| $(C_2H_5)_4N^+$ | | 1.68 | 57 | 83 |
| $(C_3H_7)_4N^+$ | 1.01 | 1.26 | 64 | 78 |
| $(C_4H_9)_4N^+$ | 0.46 | 0.99 | 53 | 57 |
| $(C_5H_{11})_4N^+$ | 0.15 | 0.45 | 46 | 41 |

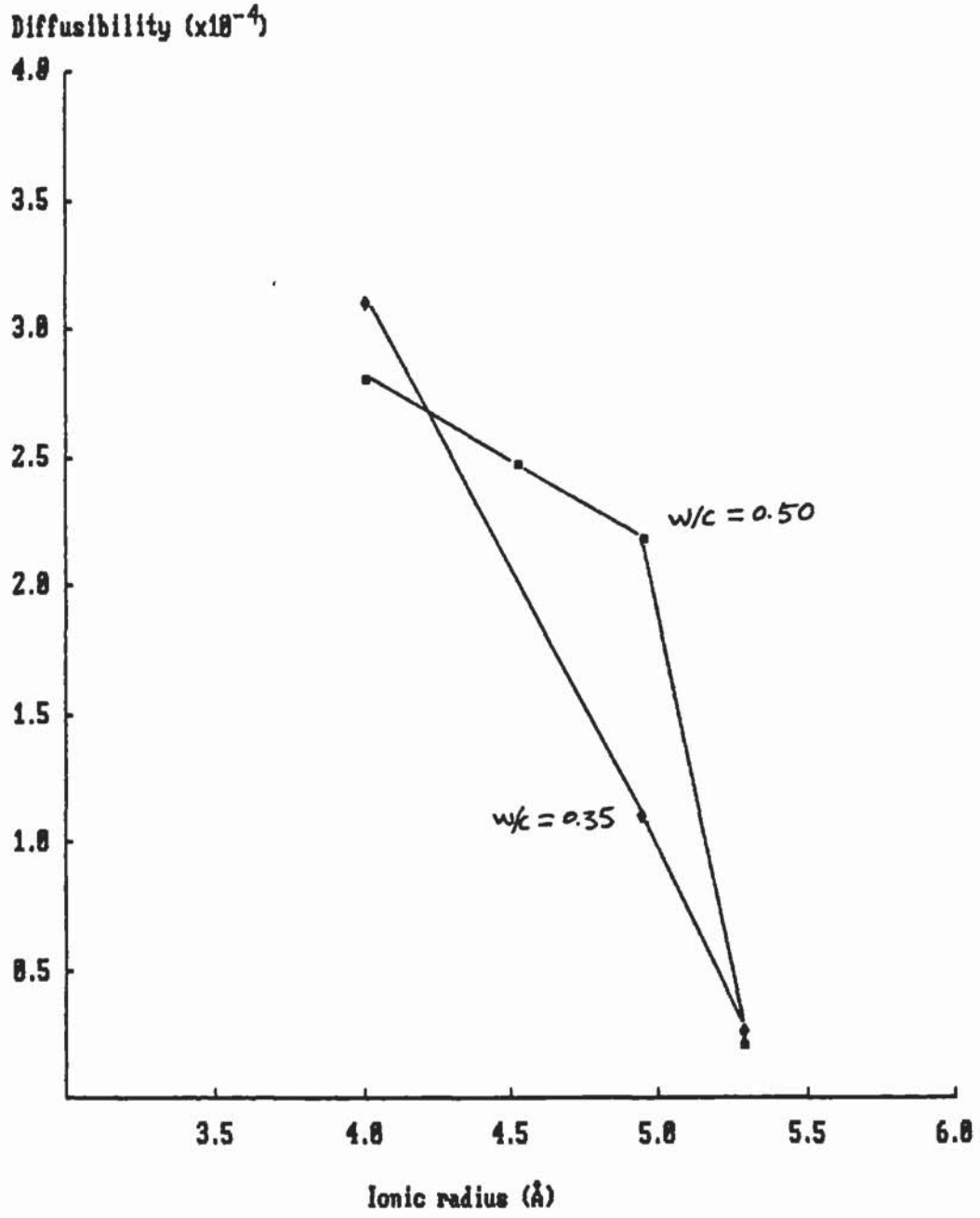


Figure 3.4 Variation of diffusibility with ionic radius for the OPC pastes of w/c ratios 0.35 and 0.50

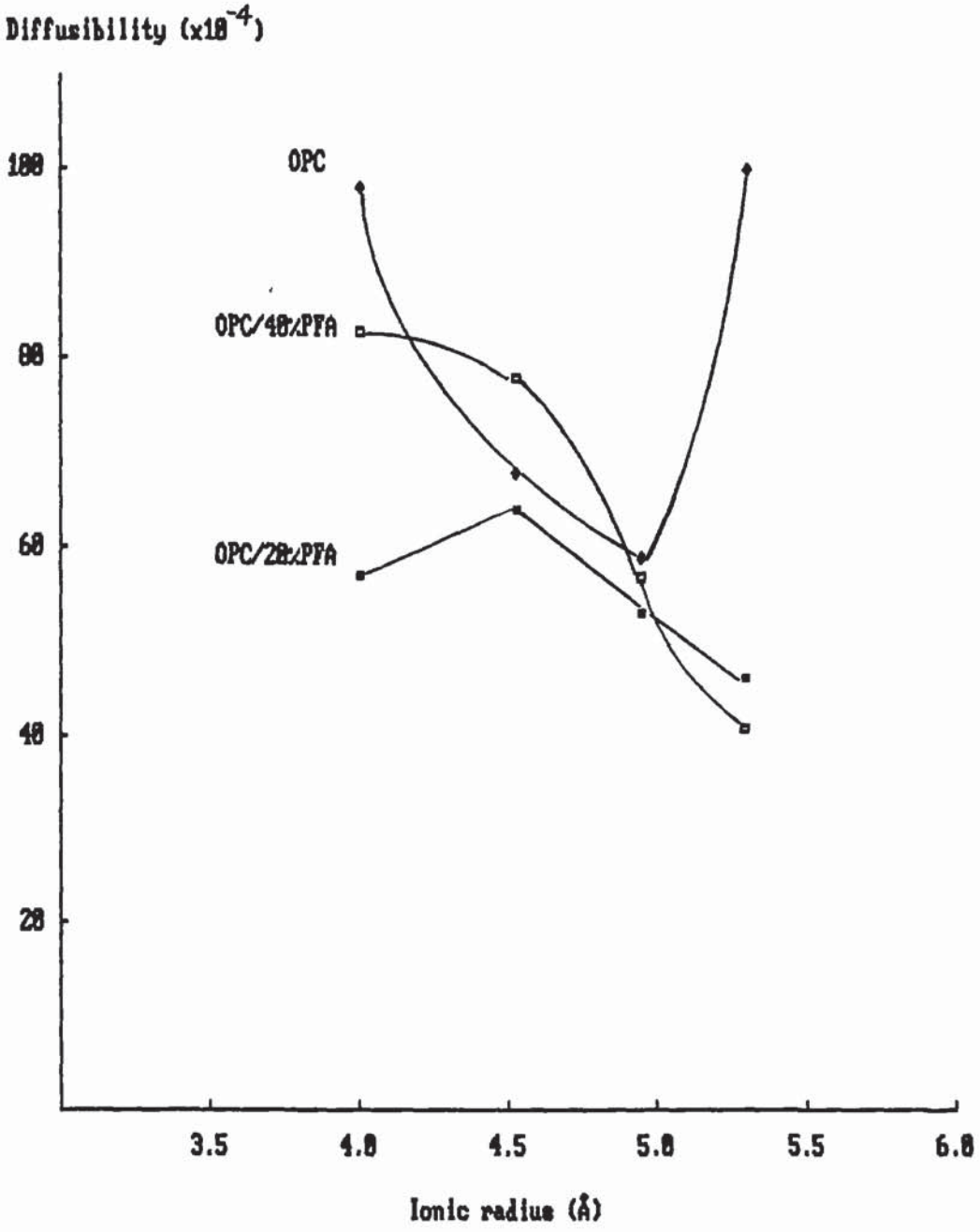


Figure 3.5 Variation of diffusibility with ionic radius for the OPC pastes of w/c ratios 0.65

dense pastes. However, as shown in figure 3.5 for the coarser OPC paste, they did not vary regularly with the ionic radius, and it appears that $(C_2H_5)_4N^+$ and $(C_5H_{11})_4N^+$ ions had almost the same diffusibilities.

It was mentioned in section 1.2 of chapter 1 that the geometrical restriction of the pore structure, and the interactions between the diffusing ion and the surfaces of the cement phases may determine the diffusion rate. As the size of the quaternary ammonium ion gets larger, on one hand, the diffusion rate may decrease, as the ion can enter a smaller proportion of the continuous capillary pores. The effective diffusion area would thus decrease with increase of ionic radius. Furthermore, because it is possible that the macropores can be interconnected by micropores, the tortuosity of the diffusion paths would increase with increase of ionic size. Therefore, the geometrical restriction of the pore structure to diffusion tends to increase with the increase of ionic radius.

On the other hand, a larger quaternary ammonium ion also has a smaller charge to volume ratio or charge density. It will be shown in chapter 4 that surfaces of the hydrated cement pastes are normally negatively charged relative to the pore solution. Therefore, the electrostatic attractions between the quaternary ammonium ions and the cement surfaces would become weaker as the ionic sizes get larger, provided that the ions do not react specifically or chemically with the surface. This could also suggest

that the collisions between the ions and the surface would become less frequent as the diffusing ions get larger. Consequently, the diffusibilities of the quaternary ammonium ions can increase with the increase of ionic sizes if the effect of the surface interactions is important, despite the fact that decreasing or steady diffusibilities should be expected from a purely geometrical consideration of the effect of the pore structure.

With regard to the irregular response of the diffusibility to the change of ionic radius for the OPC paste of w/c ratio 0.65, the decrease of diffusibility with the increase of ionic radius from 4 to 4.65 A could be ascribed to the effect of pore structure. The approximately 70% increase of the diffusibility from about 0.006 to 0.01 as the ionic radius changes from 4.65 to 5.29 A may reveal the existence of the surface charge effect described earlier. This would imply that the interactions of the $(C_5H_{11})_4N^+$ ions with the cement surfaces of the 0.65 w/c OPC paste are weaker than those of the other quaternary ammonium ions.

Furthermore, the surface charge effect on ionic diffusion should be expected to be insignificant for a large diffusion channel, say a few times wider than the double-layer thickness or than the distance of an individual jump of the random ionic motions (see section 4.3, chapter 4).

This is because the surface forces in such a big channel can have relatively little effect on the motions of the ion. From the approximately 70% increase in the diffusibility from 0.006 for $(C_4H_9)_4N^+$ to 0.01 for $(C_5H_{11})_4N^+$, it may be concluded that some micropores, in which the surface charge effect can be operative for the $(C_4H_9)_4N^+$ ions, can contribute to the diffusion even in the paste of coarse pore structure.

The pattern of variation of the diffusibility with ionic radius for the OPC paste of w/c ratio 0.5 indicates that the diffusibility decreased, but not greatly among $(C_2H_5)_4N^+$, $(C_3H_7)_4N^+$ and $(C_4H_9)_4N^+$ ions. Figure 3.4 shows that the diffusibility for $(C_5H_{11})_4N^+$ ions is significantly smaller than those found for the other quaternary ammonium ions. There is thus a relatively sudden increase of the restriction of the paste to diffusion when the ionic radius is somewhere between 4.9 and 5.3 Å. This sudden increase of restriction was not exhibited by the 0.35 w/c paste. However, the denser paste showed that the diffusibility decreased more steeply with the increase of ionic radius within 4 and 4.9 Å. This may be explained by the difference in the pore structures of the two pastes in terms of the continuous capillary pores.

As gel pores are practically not accessible to all the quaternary ammonium ions studied, it was the continuous capillary pores that contributed to the diffusion. The sharp decrease of the diffusibility in the 0.5 w/c OPC

paste for the ions of radius somewhere between 4.9 and 5.3 A seems to suggest that most of the pores contributing to the diffusion of the quaternary ammonium ions smaller than $(C_5H_{11})_4N^+$ effectively restrict the $(C_5H_{11})_4N^+$ diffusion. These pores appear to be able to behave as a "molecular sieve", since only a small difference (about 0.35 A) between the sizes of $(C_5H_{11})_4N^+$ and $(C_4H_9)_4N^+$ ions resulted in about 10 times difference in the diffusibilities or the relative diffusion rates. This is in contrast with the "molecular sieve" behaviour found for the interlayer spaces, as it is known that a similar difference in the sizes between water and nitrogen molecules can yield a big difference in the specific surface areas determined from the adsorption isotherms[69].

However, this relatively sharp drop of diffusibility could not be explained purely by the difference in the effective diffusion areas between the $(C_5H_{11})_4N^+$ and the smaller quaternary ammonium ions. The change in the tortuosity of their diffusion pathways may be also important. The pores contributing to the diffusion of $(C_5H_{11})_4N^+$ ions may be highly tortuous, probably because they are interconnected by most of the continuous capillary pores contributing to the diffusion flux of the smaller quaternary ammonium ions.

Although the 0.35 w/c OPC paste did not show a sudden

change of diffusibility with ionic radius, the restriction to the diffusion also increased considerably with ionic radius. The $(C_5H_{11})_4N^+$ ions diffused about 5 times slower than the $(C_4H_9)_4N^+$ in terms of the diffusibility. The continuous capillary pores can be expected to be smaller or more tortuous in the 0.35 w/c OPC paste than in the 0.5 OPC w/c paste. As suggested by the continuous drop of the diffusibility with ionic radius (see figure 3.4), the continuous capillary pores in the 0.35 w/c OPC paste appear to be much finer or more tortuous, but their volumes may increase more steadily with their sizes compared with those in the 0.50 w/c paste which showed a sudden change of the diffusibility with ionic radius.

As suggested by the diffusibilities shown in table 3.5 and the diffusivities shown in table 3.1, the w/c ratio has a strong influence on ionic diffusion rates. For the pastes of w/c ratios 0.35 and 0.5, the diffusibilities are approximately within 1 and $4x10^{-4}$ for the ions smaller than $(C_4H_9)_4N^+$ and are about $0.25x10^{-4}$ for the $(C_5H_{11})_4N^+$ ions. In contrast, the diffusibilities for the coarser paste are of the order of $10^{-2}$. The effect of w/c ratio on the diffusibility is in qualitative agreement with that on water permeability found by Powers et al[73]. As described in subsection 4.2.2, this was explained for the water permeability by Powers et al who postulated that most of the capillary pores in the dense pastes of w/c below 0.5 are interconnected by gel pores, and the capillaries in

coarser pastes are less tortuous and bigger.

### 3.4.3 Diffusion in the PFA paste

The diffusivities and diffusibilities of the quaternary ammonium ions in the PFA pastes are shown in table 3.2 and 3.6 respectively. The diffusibilities are plotted in figures 3.5 and 3.6 against the ionic radii. It can be seen from the two figures that the diffusibilities for one particular PFA paste decreased, in general, with the increase of ionic radius. The w/c ratio was also found to have a marked effect on the diffusibilities in the PFA pastes. As w/c ratio changed from 0.65 to 0.50, it can be seen from table 3.6 that there was a sharp decrease of the diffusibilities, approximately 100 times. Further reducing the w/c ratio only resulted in less than three times decrease of the diffusibilities for each ion. Increasing the w/c ratio can increase the continuity and the volume of the capillary pores in the coarser paste, which has been explained earlier.

It has been suggested in the previous subsection that the increase in the diffusibility from $(C_4H_9)_4N^+$ to $(C_5H_{11})_4N^+$ for the 0.65 w/c OPC paste is probably associated with the surface charge effect on ionic diffusion. However, there is no obvious increase of the diffusibility with ionic radius for the 20% and 40% PFA pastes of w/c ratio 0.65. As shown in figure 3.5, the diffusibilities are almost constant for the 40% paste, while they decrease with the

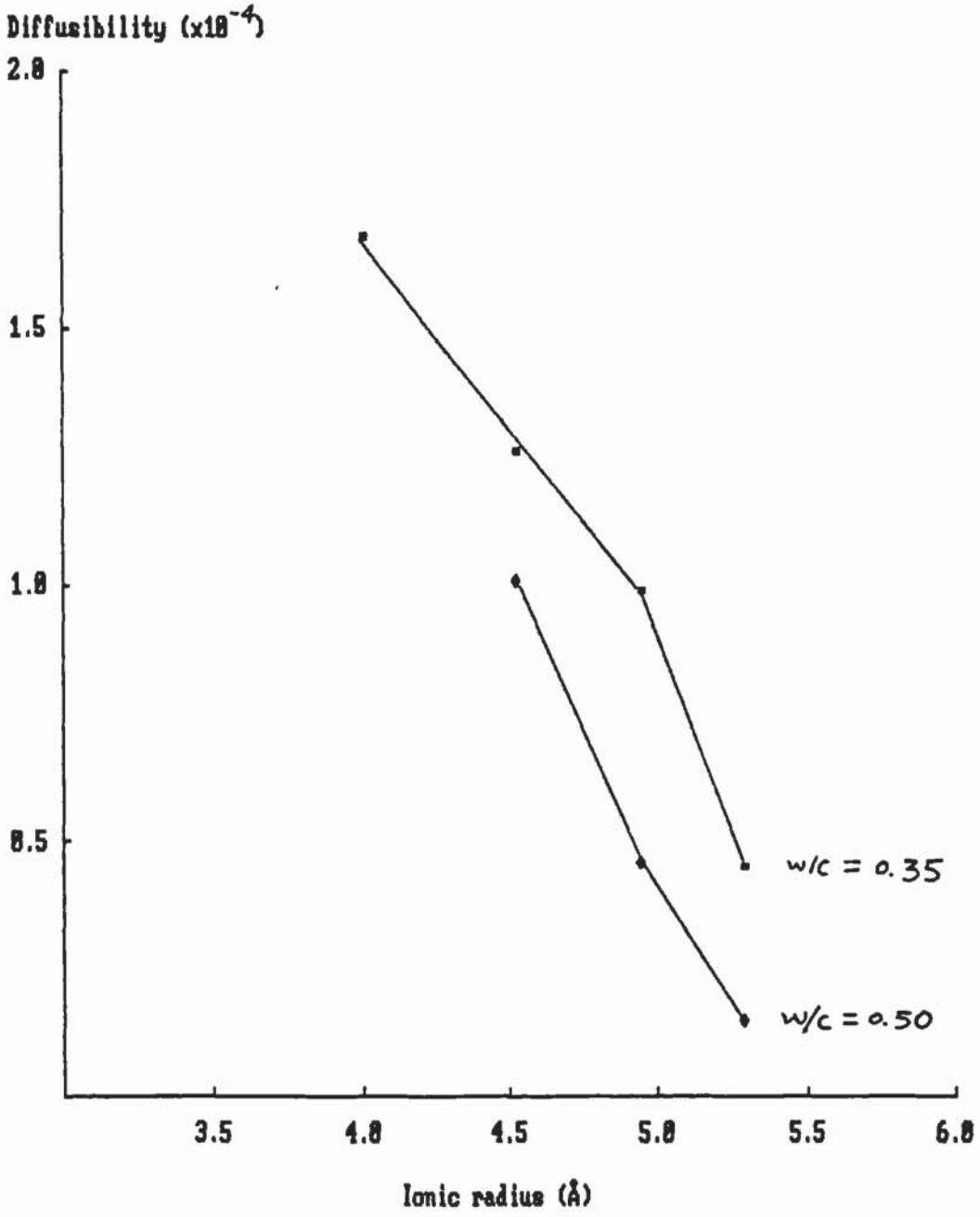


Figure 3.6 Variation of diffusibility with ionic radius for the OPC/40%PFA pastes of w/c ratios 0.35 AND 0.50

increase of ionic radius for the 20% paste. Therefore, it is difficult to distinguish, based on the results obtained, the pore structure effect from that of the surface charge on the diffusion of the quaternary ammonium ions in the PFA paste.

It can be seen from tables 3.5 and 3.6 that a particular quaternary ammonium ion appears to diffuse twice as slowly in the 40% PFA paste as in the OPC paste of the same w/c ratio. As shown in figure 3.6, the diffusibilities in the dense PFA pastes also decrease considerably with the increase of ionic sizes. The restriction of the PFA paste to diffusion thus increases as the sizes of the diffusing ions increase. However, in contrast with the responses of the diffusibility to the ionic radius for the dense OPC pastes of the same w/c ratio, the diffusibilities in the dense PFA pastes seem to be less strongly influenced by the ionic radius, which can be seen from tables 3.5 and 3.6. The difference in the diffusion behaviours between the dense OPC and PFA pastes may suggest that their pore structures are somewhat different.

The reaction of the active components in PFA with the calcium hydroxide liberated from the primary hydration of OPC has been considered[32,33,80] to be able to produce more divided pores in the C-S-H phases. The continuous capillary pores responsible for the diffusion of the quaternary ammonium ions, especially of the ions smaller than $(C_5H_{11})_4N^+$, would thus be either finer or more

tortuous in the 40%PFA paste than those in the OPC pastes of similar w/c ratios. This may explain why the diffusion is normally slower in the PFA paste. However, it was mentioned before that the diffusibilities decrease generally more regularly with the ionic radius in the dense 40%PFA pastes than in the OPC pastes of the same w/c ratio. Therefore, as the sizes of the diffusing ions get larger, the tortuosity for the dense PFA pastes seems to increase less sharply in the OPC pastes of comparable w/c ratio.

## 3.5 Conclusions

(1). The quaternary ammonium ions cannot pass through the interlayer or gel pores, so it is the continuous capillaries that contribute to the diffusion of these ions.

(2). It was found that w/c ratio has a marked effect on the diffusibilities of the quaternary ammonium ions for both OPC and OPC/40%PFA pastes. The diffusibilities decreased very sharply as w/c ratio decreased from 0.65 to 0.5, whereas comparably much smaller reductions of the diffusibilities were observed as w/c ratio decreased further.

(3). The relative diffusion rate or the diffusibility in dense OPC and OPC/40%PFA pastes decreases considerably with increase of the ionic sizes of the quaternary

ammonium ions, indicating that pore structure is an important factor in determining the diffusion rates.

(4). The $(C_5H_{11})_4N^+$ ions diffused faster in the 0.65 w/c OPC paste than $(C_4H_9)_4N^+$ ions, suggesting that the effect of surface charge may also be important in determining ionic diffusion rates in OPC pastes

(5). There was a relatively sudden drop of the diffusibility in the 0.5 w/c OPC paste as the ionic radius increased from 4.92 to 5.3 A, indicating that the continuous capillary pores contributing to the diffusion of the quaternary ammonium ions smaller than $(C_5H_{11})_4N^+$ may interconnect most of the macropores.

(6). The capillary pore structures in the OPC/40% PFA pastes appears to be finer or more tortuous than those in the OPC paste of the same w/c ratio. However, the diffusibilities of quaternary ammonium ions in the dense OPC pastes increased more sharply with the increase of ionic radius than those in the OPC/40%PFA pastes of the same w/c ratio.

# CHAPTER 4 EFFECT OF SURFACE CHARGE ON IONIC DIFFUSION

## 4.1 Introduction and Literature Review

### 4.1.1 The Double Layer

The classical model concerning the structure of the electro-chemical double layer at a solid-liquid interface, namely the flat plate model, is that usually attributed to Helmholtz in which both layers of charge are regarded as fixed in parallel planes to form a molecular condenser[48,49]. The potential (E) at a distance (x) from the surface can be derived from the Poisson-Boltzmann equation for a surface potential ($E_0$) below 25 mv[48]:

$$E(x)=E_0\exp(-Kx) \qquad \ldots\ldots (4.1)$$

The Debye-Huckel parameter, K in $cm^{-1}$, is very important in that it moderates the decay of potential with distance from the surface. It can be calculated for aqueous solution at 25°C from[48]

$$K=3.288\Sigma(z^2C_0/2)^{1/2} \quad (nm^{-1}) \qquad \ldots\ldots (4.2)$$

where $C_0$'s are the bulk concentrations of the ions, and z's are the valence numbers. Its reciprocal, 1/K, is referred to as the thickness of the double layer which decreases with ionic concentrations and will be considered in section 4.3 to estimate the effect of the surface charge on ionic diffusion in hydrated cement pastes. Generally speaking, the electrical field extends from the surface to a distance of the order of 2/K[81]. The

potential distribution from equation 4.1 is schematically shown in figure 4.1(a) for a negatively charged surface.

For a given surface potential, E, the spatial distribution of any ion in the diffuse layer can be derived by setting the Nernst-Planck equation 1.2 (see chapter 1) to be zero,

$$J=-uRT(dC/dx + zeC/(kT)dE/dx) = 0 \quad \ldots\ldots (4.3)$$

so[82]

$$C(x)=C_0\exp(-zeE/kT) \quad \ldots\ldots(4.4)$$

If the surface potential is very small, the exponential in equation 4.4 can be expanded and combined with equation 4.1 for a simpler description of the concentration distribution which is shown in figure 4.1(b) for a 1-1 symmetrical electrolyte. It can be seen from figure 4.1(b) that the co-ion is repelled from the surface and the counter-ion is attracted to the surface.

There have been a number of modern theories[48,49,82] giving more complete pictures of the double layer structure, but they are not reviewed in this work which is concerned mainly with the zeta potential. In almost all the theories, the zeta potential is considered as the potential at the so-called shear plane. The liquid phase at distances between the surface and the shear plane is normally considered to be immobile, while at the distances beyond the shear plane, tangential flow of the liquid can be induced. Zeta potential can thus be determined from the electrokinetic phenomena that are involved with relative motions between the solid and liquid phases. These

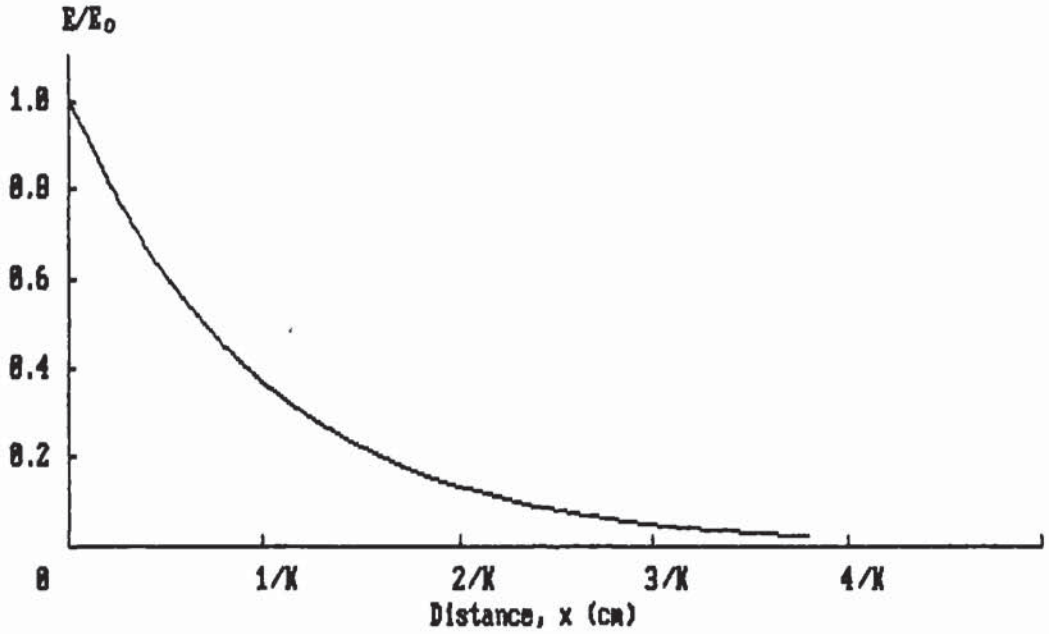


(a) Potential distribution

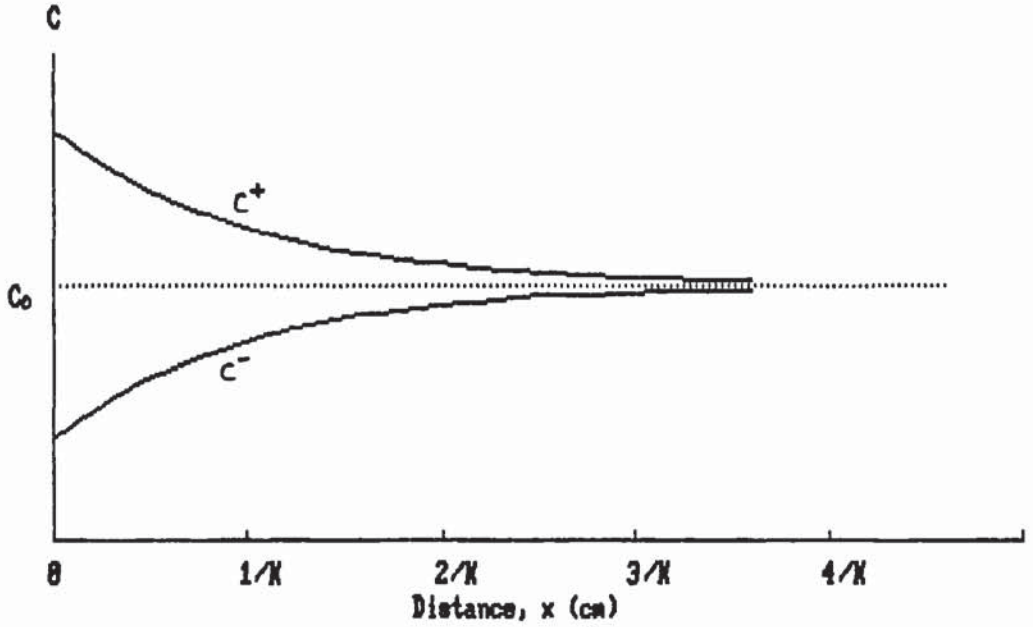


(b) Concentration distribution

Figure 4.1 Potential and concentration distributions at a negatively charged surface

phenomena include electro-osmosis, electrophoresis, sedimentation potential and the streaming potential which was explained in section 2.5, chapter 1.

### 4.1.2 Zeta potentials of cement hydrates

Nagele et al[83] measured zeta potentials of four types of hydrating commercial OPC by electrophoresis. They found that the zeta potentials were positive and initially quite high but decreased to near zero within one hour. By controlling the pH of the solution below 12 in the later work reported by Nagele[84-86], the zeta potentials of OPC (see figure 4.2) and slag cements were found to be between 0 and 20 mv after hydration for about 2 hours. The author claimed that the zeta values of the hydrating colloids were stable after about two hours. However, it was also pointed out by the author[84] that because the double layer during hydration is at non-equilibrium state, the sign of the zeta potential would depend on the ions migrating at the interface.

Stein[87] studied the electrochemical properties of $C_3S$ hydrates in solutions of various calcium concentrations (the results obtained using electrophoresis technique are shown in figure 4.3). Calcium ion was shown to be a potential determining ion for $C_3S$ hydrates, as it can reverse the sign of the zeta potential. In general, hydroxyl ion is the main potential determining ion for silicate and aluminate materials[81]. This was proved by

Spierings et al[88] who studied $C_3A$ hydrated for ten days in a variety of solutions. As the NaOH concentration increased from 0.01 to 0.1 M, the zeta potential became more negative from -17 to -30 mv. When the concentration of $NaNO_3$ or $KNO_3$ in the solution was increased, the zeta values became less negative. This indicates that sodium ion may not be strongly adsorbed on to the surface. The zeta potential was 10.7 mv in saturated calcium hydroxide solution.

### 4.1.3 Initial objectives

It has been shown in figure 4.1 that an electrical field or a local separation of charge exists in the double layer of an equilibrium solid/electrolyte interface. The double layer existing at the interface between the cement hydrate surfaces and the pore-solution has been considered in the literature to be important in affecting mechanisms of ionic diffusion.

Takagi et al[29] and Goto et al[30] speculated that the surfaces of hydrated cement paste were positively charged because of the adsorption of calcium ions. Their suggested kinetic description of the surface charge effect on ionic diffusion is that the surface would attract anions towards it and enable the anions to enter into the micropores more easily than the cations which are electrostatically repelled from the surface.

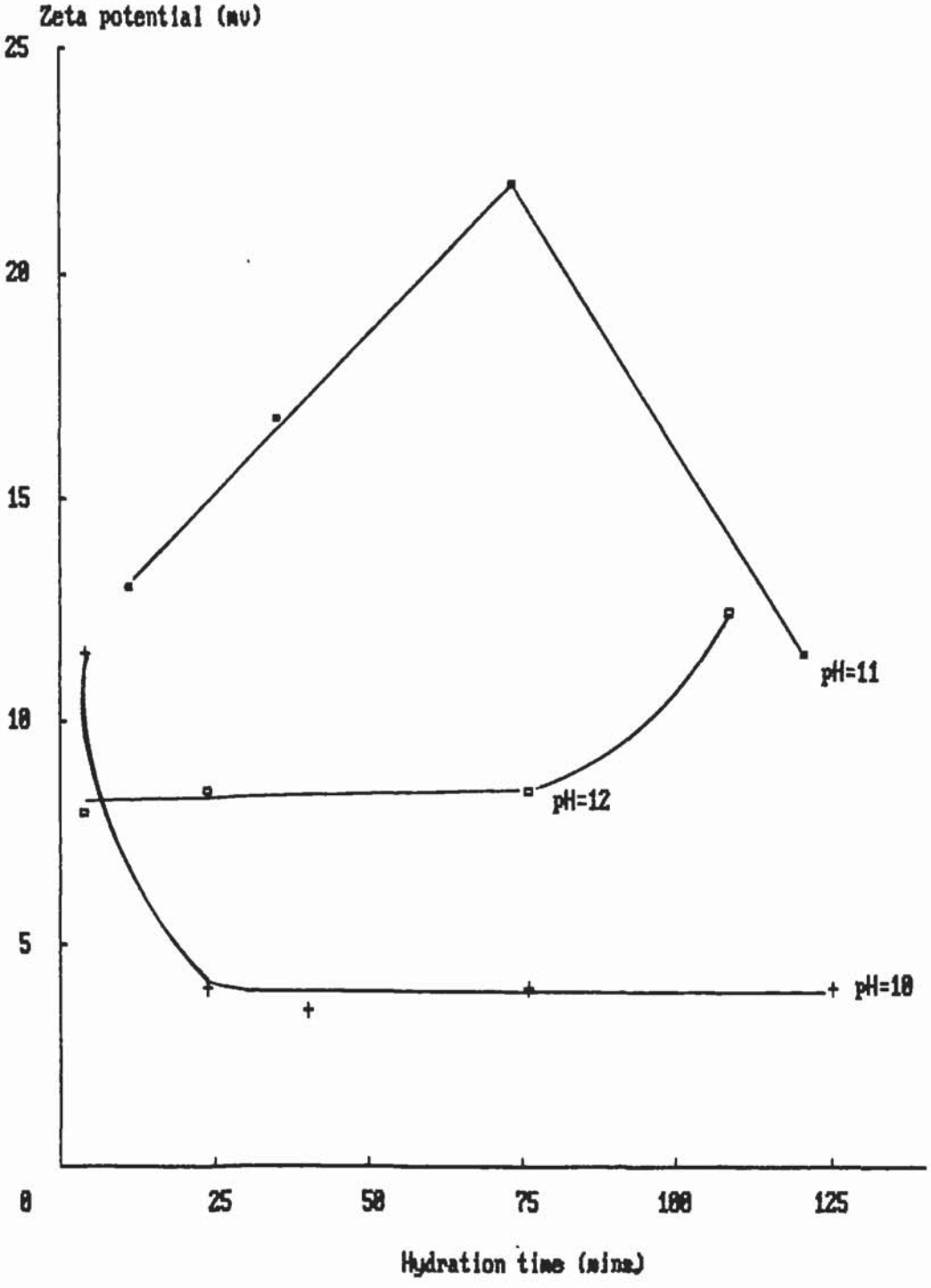


Figure 4.2 Zeta potentials of hydrating OPC cement in solutions of various intial pH values (Ref. 86)

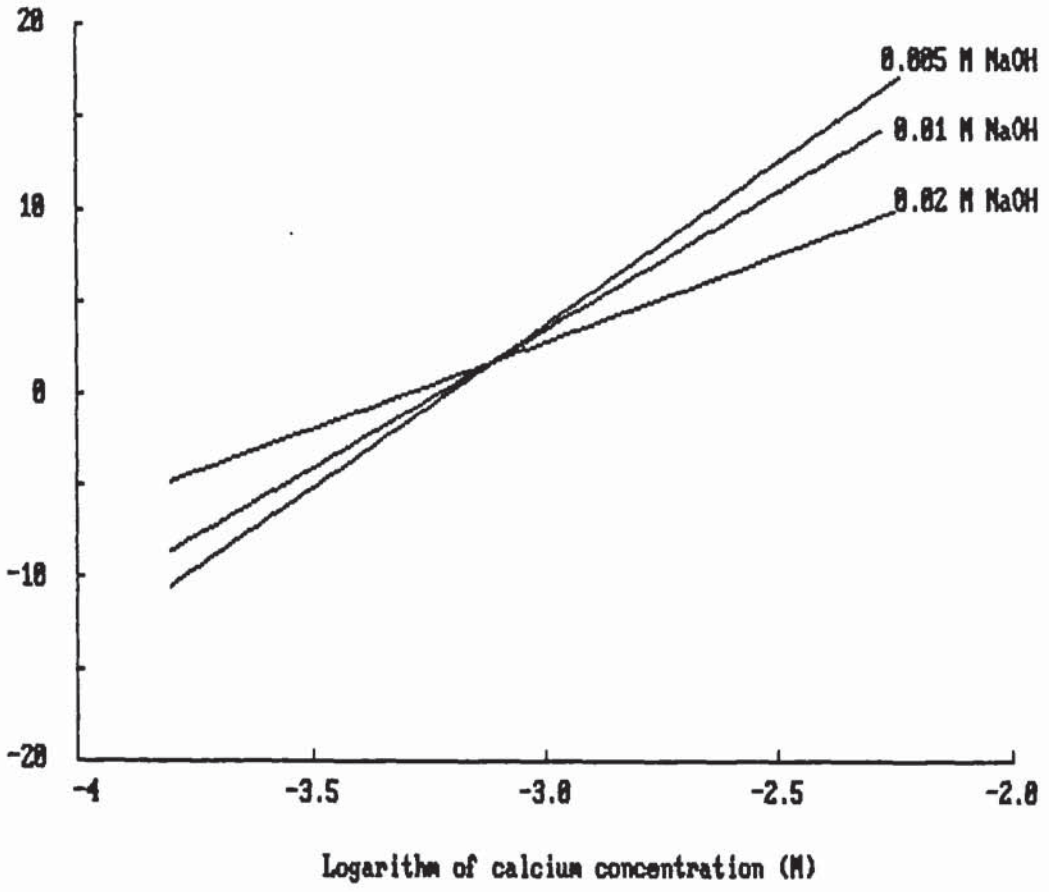


Figure 4.3 Zeta potentials of $C_3S$ hydrates in solutions of various calcium concentrations (Ref.87)

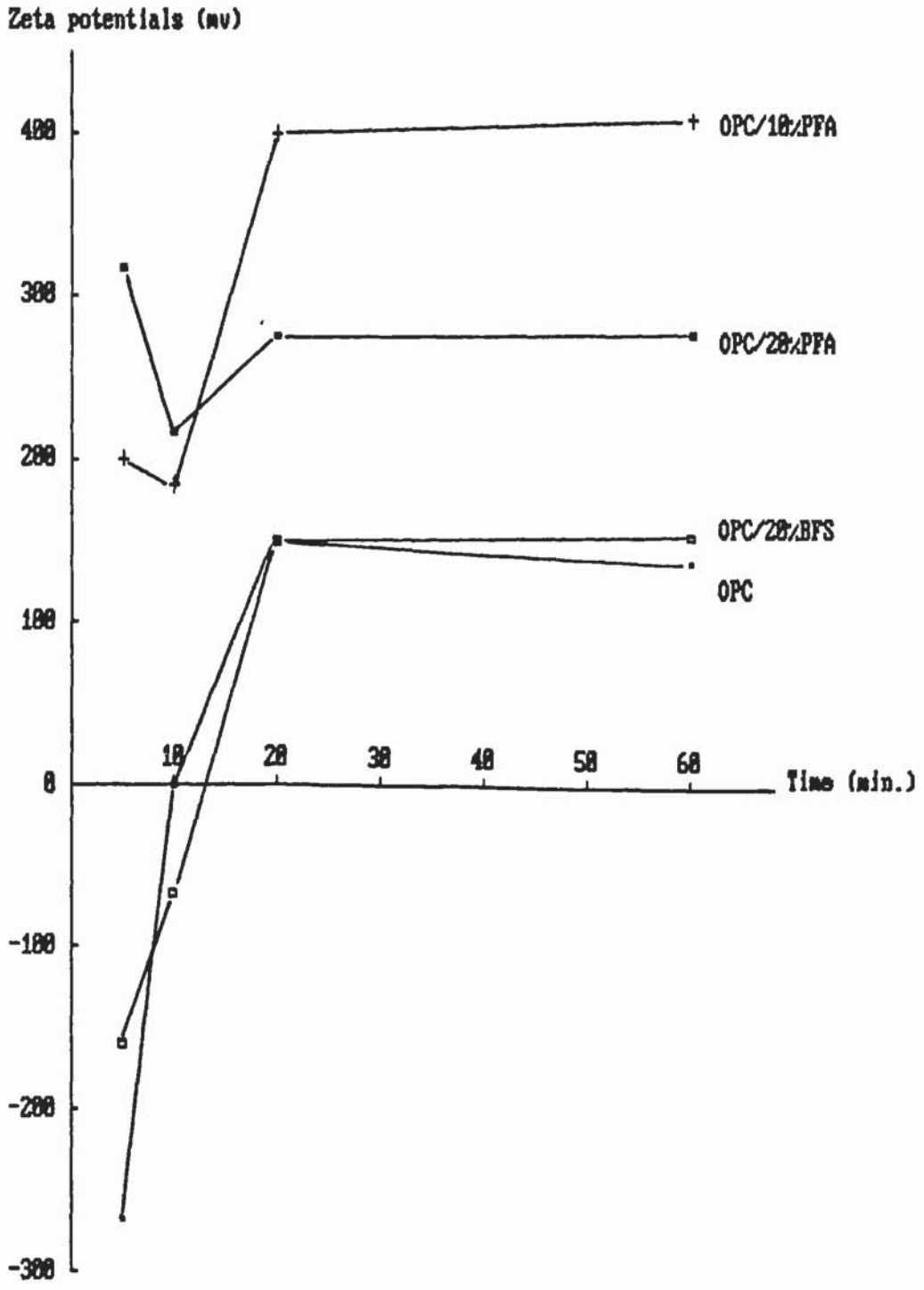


Figure 4.4 Zeta potentials of mature pastes in 1M NaOH solution (Ref. 31)

According to Wittman and Hollenz[89], the surfaces of hydrated cement pastes were, however, negatively charged relative to the pore solution. The authors considered Coehn's rule[90] which states that a substance having a higher dielectric constant is positively charged when in contact with another substance having a lower dielectric constant. It is known that an adsorbed water film has a higher dielectric constant than cement hydrates[89].

The effect of surface charge on diffusion was also considered by Uchikawa et al[31]. The authors determined the zeta potentials of hydrated OPC, PFA and BFS cement pastes in 1M NaOH solution by the streaming potential technique, but experimental details were not given. The zeta potentials varying from 100 to 400 mv were reported and are shown in figure 4.4. The blended pastes were shown to be more positively charged than the OPC pastes. The authors suggested that sodium ion may be easily adsorbed on to the C-S-H gel in the blended pastes decreasing its mobility. Higher zeta potentials for the blended cement pastes were also considered by the authors to explain why these pastes have greater resistance to ionic diffusion than the OPC paste.

Almost all of the reported measurements[35-37,83-86] of zeta potential concerned with cement have been conducted to study the early stage of cement hydration. The surfaces of mature cement pastes might be electrochemically quite different from those of the hydrating cements or cement

minerals, which can be seen by comparing their reported zeta potentials as follows:

(1). Compared with the magnitudes of the zeta potentials reported by Nagele[83-86] for hydrating cements and Stein[87] and Spierings et al[88] for cement hydrates, those reported by Uchikawa et al[31] for hydrated cement pastes are extremely high.

(2). The results from Stein and Spierings et al show that $C_3S$ and $C_3A$ hydrates are negatively charged in solutions of high pH values, whereas Uchikawa et al indicated that the hydrated cement pastes in equilibrium with 1M NaOH solution were positively charged.

(3). The surface charge can be very high for some solids in contact with concentrated electrolytes, but the zeta potentials have been found to be generally very small[90]. This is because, as the ionic concentration increases, the double-layer thickness decreases and the potential at the interface drops faster with the distance in the region between the surface and the shear plane.

With regard to the possible important effects of the double layer on ionic diffusion, it is necessary to know some electrochemical properties of hydrated cement surfaces. Furthermore, if the big difference in the diffusivities of cations and anions is qualitatively determined, as suggested by Takagi et al[29] and Uchikawa et al[31], by the sign of the zeta potential for a normal

diffusion system of hydrated cement paste, this difference could be changed or even reversed when the sign of the zeta potential is deliberately altered by different choices of experimental conditions of diffusion.

The streaming potential technique which measures the average properties of many particles was used to determine zeta potentials in the present work. This technique has been described in section 2.5, chapter 2.

## 4.2 Experimental and Results

As explained in subsection 4.1.2, the net charges in the region between the shear plane and infinity can be forced to move together with the solution. When the solution is moving through a porous plug, a potential difference between the ends of the plug, called the streaming potential, can be developed and measured by inserting two identical electrodes between the ends. The zeta potential is related to the streaming potential ($E_S$) and the driving pressure (P in cmHg) by[48]

$$\text{Zeta} = 1.055 * 10^5 d(E_S/P) \quad \text{(mv)} \qquad \ldots\ldots(4.5)$$

for aqueous solutions at 20°C, where d in $\text{ohm}^{-1}\text{cm}^{-1}$ is the conductivity of the streaming solution.

To show the effect of ionic concentrations on the accuracy of the streaming potential technique, the conductivity can be estimated for most salt solutions of concentration $C_O$ (M) by the expression[48]:

$$d=0.14C_0 \quad (ohm^{-1}cm^{-1}) \qquad \ldots\ldots (4.6)$$

Equations 4.5-6 indicate that for a certain value of the zeta potential, the $E_s/P$ measured should decrease with concentration. If the zeta potential is assumed to be 100 mv, the $E_s$ for a 0.01M solution will vary within 3 and 20 mv for a pressure of 5 to 30 cmHg, but $E_s$ for a 0.1M solution will be only 2 mv at a pressure value of 30 cmHg. It is therefore necessary to use a streaming solution of low concentration in order to obtain an accurate determination of the zeta potential. Because cement pastes are not stable in solutions of low pH value, either $Ca(OH)_2$ or NaOH solution was used.

OPC and OPC/30%PFA pastes made at 0.5 w/c ratio and cured for 1 to 3 months were used for the measurements of the streaming potential as described in chapter 2. The sample particles of about 600 to 1000 μm were collected by sieving the material after crushing in a mortar.

An OPC sample was used for the preliminary measurement. It was first washed with 0.005 M NaOH solution, then packed into the sample cell as described in section 2.5, chapter 2. The measurement system was established by filling the cell and the glass bulbs with fresh 0.005 M NaOH solution and allowing half an hour to achieve a reasonable initial equilibrium.

The solution was then allowed to flow from left to right through the sample by applying pressure with nitrogen gas,

resulting in a small but continuous increase of the total potential measured (see figure 2.5 for the arrangement of the test system). After the potential had just started to decrease, the flow was stopped. The potential developed over the period of flow was recorded, and an example is shown schematically in figure 4.5. The potential variation with time when the solution was flowing from right to left is also shown in this figure.

As mentioned in chapter 2, when the streaming potential developed is high enough so that it can be distinguished from the asymmetry potential between the two electrodes, it is approximately the sudden drop or increase of the total potential measured when the streaming was stopped. Figure 4.5 indicates that this drop was too small to be accurately determined. This also shows that the zeta potential could not be accurately determined by this streaming potential technique.

Although the streaming potential could not be accurately quantified, its development during the flow corresponds systematically to the behaviour that would be expected for a negatively charged surface. The sign of the total potentials developed was recorded according to the electrical circuit shown in figure 2.5. When the solution was forced to flow from left to right, net positive charge must be carried together with the solution so that the potential developed, due to the establishment of

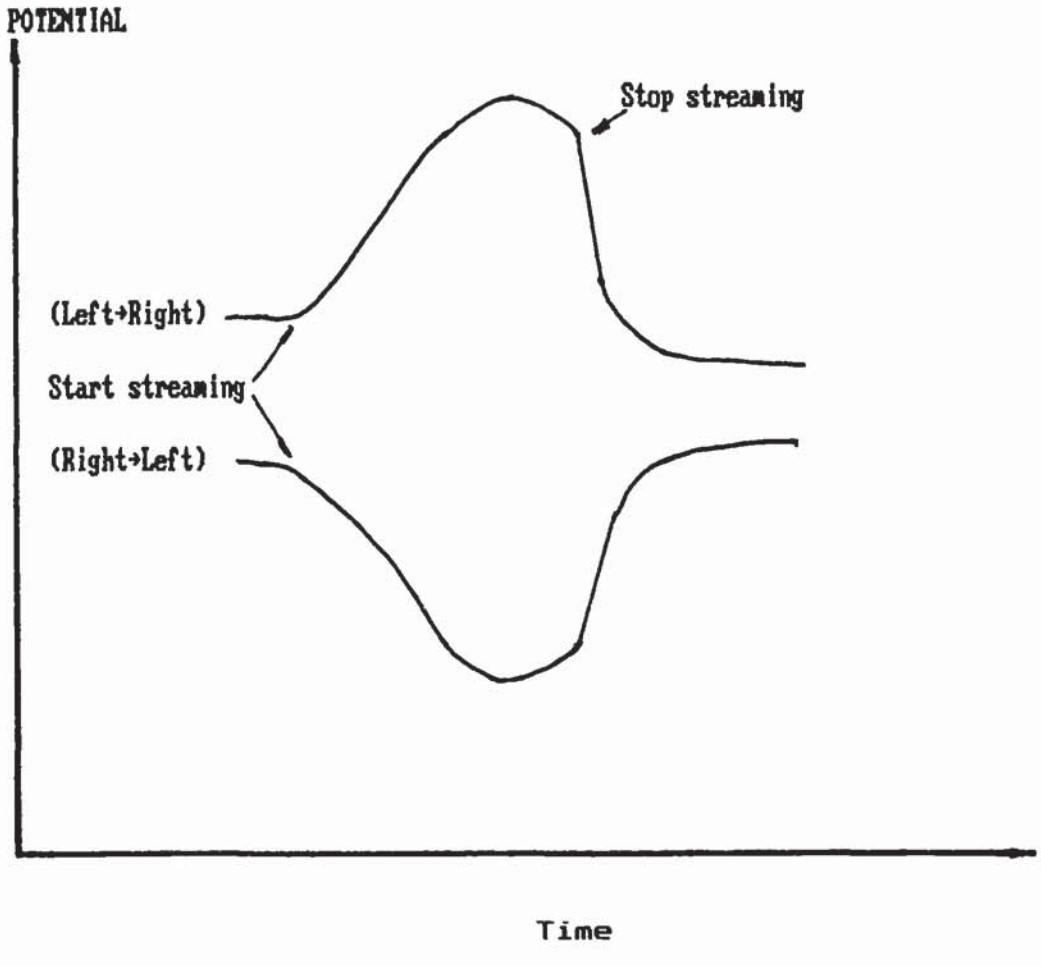


Figure 4.5 Development of the total potential with time

equilibrium, increased to be more positive. After the steady state had been established, the streaming potential decreased as the pressure applied dropped continuously. There was also faster drop of the total potential just after the flow had been stopped. The residual potential was the asymmetry potential. The behaviour for a negatively charged surface could also be seen when the solution was carried from the reverse direction. This negative sign of the zeta potential was confirmed by repeated measurements.

Further measurements were then made with the OPC and 30%PFA pastes in various solutions. The results obtained confirmed the above conclusions and are summarized as follows: the OPC and PFA pastes in 0.005 to 0.05 M NaOH or KCl solution showed a negatively charged immobile part of the interface; On addition of $Ca(OH)_2$ suspensions to these solution, the zeta potential became positive. In saturated $Ca(OH)_2$, zeta potentials were found to be positive.

### 4.3 Discussion

It has been shown experimentally that the zeta potentials of hydrated OPC and OPC/PFA pastes were too small to be accurately determined by the streaming potential technique. The signs of the zeta potentials were found to be dependent on calcium or hydroxyl concentrations, which is in reasonable qualitative agreement with the results obtained by Stein[87] and Spierings et al[88] for hydrated

$C_3S$ and $C_3A$. Therefore, It would be quite difficult to interpret the differences in the diffusion behaviour of different types of cement paste in terms of their small values of zeta potential.

The distributions of ions in an equilibrium double layer are described by equation 4.4 on the basis that no net flow of any ion occurs at the interface. For a hydrated cement paste subject to diffusion ionic flow occurs at the pore/solution interface, so the ionic distributions in the double layer may be quantitatively quite different from those in an equilibrium double layer. However, In order to estimate the possible effects of the double layer on ionic diffusion in different pores, the thickness of the double layer, which is defined in equation 4.3 for an equilibrium interface, will be first considered. It has been shown in subsection 4.1.1 that the charge separation due to the surface charge would not occur at the distances, approximately twice the value of the double layer thickness, away from the surface. Parallel-sided pores containing NaOH solution will be assumed for the calculation. As the double layer thickness depends mainly on the ionic concentrations, the NaOH concentration will also be assumed.

Assuming a pore contains 0.032 M NaOH solution, it can be calculated from equation 4.2 that the thickness of the double layer, 1/K, would be 18 A. The separation of charge

would presumably extend to a distance about 18x2=36 A from the pore wall. If the pore is narrower than 72 A (=2x36) in width, the double layer would thus not be fully developed. However, for a pore containing 1M NaOH solution, the double layer thickness calculated is only 3.3 A, suggesting that the charge separation at the interface is limited within a relatively very short distance. In most cases, the pore solutions in hydrated cement pastes are fairly concentrated (>0.2 M), so values of the double layer thickness would be very small, despite the fact that the ionic sizes are not considered in the flat-plate model of the double layer[49,93].

The above calculation shows that in hydrated cement pastes there is some proportion of micropores which do not permit a fully developed double layer at low ionic concentration; for instance, the double layer of pores of solid-solid distance below 72 A would be suppressed or overlapped if in contact with a 0.03M NaOH solution. For the interlayer space of average solid-solid distance 3.3 A, a double layer would obviously be meaningless. The concept of a normal diffuse layer in a concentrated solution or in gel pores cannot therefore be justified as far as the mechanism of diffusion is concerned, because the calculated "double layer thickness" is comparable with an individual Brownian jump distance.

Measurements of ionic diffusivity in hydrated cement pastes have been made using solutions of various $Ca^{2+}$ and

$OH^-$ concentrations[17-23]. Despite the fact that the zeta potentials of hydrated cement pastes can be either positive or negative, depending on the concentration of $Ca^{2+}$ and $OH^-$, as shown experimentally in section 4.3, cations have been found to diffuse generally slower than anions. It thus appears that the double layer effect on ionic diffusion in hydrated cement pastes is different from that suggested by Takagi et al[29] who assumed the surfaces of cement-matrix to be always positively charged.

The effect of the surface charge would not be expected to be significant for macropores containing concentrated solutions, as the double-layer thickness is very small. A possibly important factor for the effect of the interface on ionic diffusion is the surface charge of micropores and the gel pores. Because these pores are not only small but highly inter-connected, their double layers are normally overlapped or not fully developed. The silicate or aluminate groups are normally not hydrated, so the ionization of cations would result in a negatively charged surface[48,81,91]. A positive zeta potential of a surface is caused by a relatively strong chemical affinity of the surface to cations. However, the cations are normally considered[48] to be at the so-called Outer Helmholtz Plane (OHP) which is very close to the shear plane mentioned in subsection 4.1.1. Therefore, the surfaces of micro and gel pores may be considered to be, as a whole, always negatively charged, despite there being some

positive sites on the surface. With regard to charge distributions of cations and anions at the interfaces, the cations would be much more compressed near the surface to attain an overall electroneutrality within the pores[92, 93]. This could cause retarded diffusion of cations compared with anions.

Ionic diffusion is a result of the random molecular motion directed by the dissipation of entropy, so diffusion is a discontinuous process microscopically. For micro and gel pores, the jump distance of individual random movement is comparable with the size of pores, so there is some proportion of time during which ions will have hopped on to the surface. The diffusion process can be viewed as a sequence of jumps possessing a certain jump frequency and jump distance, which are related to the diffusivity[94].

Therefore, one effect of the surface charge on diffusion is associated with the collision between the pore walls and the diffusing ions. A longer resident time on the walls would lead to slower diffusion. This may be the main reason why the $(C_5H_{11})_4N^+$ ion was found, in the work presented in the previous chapter, to diffuse faster than the $(C_4H_9)_4N^+$ ion in the hydrated 0.65 w/c OPC paste. As the $(C_5H_{11})_4N^+$ ion diffuses slower in bulk solution than $(C_4H_9)_4N^+$, it would thus tend to do so in hydrated cement pastes. However, the $(C_5H_{11})_4N^+$ has a smaller charge density, so it would be less easily attracted

electrostatically to the pore surfaces of the paste, resulting in less frequent collisions with the surfaces.

Nevertheless, some ions could have stronger interaction with the cement hydrate surfaces than the others, depending on the electrostatic, chemical, or ionic size differences. These factors may vary for cations and anions, but it is hard to say whether the effect will be greater for cations than anions, since there is evidence that chloride ion may have a strong chemical affinity for the cement surfaces (see subsection 6.2.2, chapter 6).

Since the effect of surface charge on diffusion is present mainly in gel and micro pores, its nature would be highly dependent on the interconnection, size and shape of these pores. It is therefore hard to distinguish the surface charge effect from the pore structure effect. The differences in the diffusion behaviour for different types of cement paste cannot therefore be simply inferred from the electrochemical surface properties obtained from experimental studies which may reveal only the properties for macropores walls.

## 4.5 Conclusions

(1). The streaming potential technique could not give accurate determinations of the zeta potentials of hydrated cement pastes

(2). Hydrated PFA and OPC cement pastes are characterized

by negatively charged surfaces unless they are in solutions of high calcium concentration.

(3). The surface charge effect may be important for ionic diffusion in gel and micro pores.

# CHAPTER 5 DIFFUSION OF DISSOLVED OXYGEN

## 5.1 Introduction

It has been shown in chapter 3 that the diffusibilities for quaternary ammonium ions varied irregularly with the ionic radius for the OPC paste of w/c ratio 0.65. This reveals that the interaction between diffusing ions and micropore walls may play a part in determining ionic diffusion rates. However, it has also been concluded in chapter 4 that direct study of the electrochemical characteristics of the hydrated cement surface by measurement of zeta potentials can provide only limited information regarding the effect of the surface interaction on ionic diffusion. The degree to which this interaction affects ionic diffusion therefore has to be assessed from other approaches.

In comparison with diffusion of chloride, diffusion of oxygen would be considerably less affected by the surface charge or the double layer at the pore/solution interface. The pore structure of the hydrated cement paste and the viscosity of the pore solution are the main factors expected to determine the diffusion rates of dissolved oxygen. Since oxygen and chloride have very close values of diffusivity in water, for example, $2.1 \times 10^{-5}$ (from Ref.7) and $2.03 \times 10^{-5}$ $cm^2$ respectively at 25°C, they should have similar sizes, and accordingly they may diffuse through similar pores in hydrated cement pastes. By

comparing their diffusion kinetics in hydrated cement systems, the effect of surface interaction on ionic diffusion can be better understood and evaluated. Furthermore, useful information about the viscosity and its dependence on temperature can be obtained if the activation energies for oxygen diffusion are determined. By taking account of the viscosity effect, the differences in the pore structures of different hydrated pastes can be therefore estimated indirectly from their different effects on the kinetics of oxygen diffusion.

Diffusion of both oxygen and chloride in OPC and OPC/20%PFA pastes of w/c ratios 0.35, 0.5 and 0.6 was studied in this work. Chloride diffusivity was determined by the steady-state diffusion technique described in chapter 3. The present work used a diffusion cell, which also served as an electrochemical cell, to consume and measure potentio-statically the amount of oxygen diffused at steady state at 25°C, enabling the determination of oxygen diffusivity. This cell is a modified one that was initially developed by Page and Lambert[95].

It was found throughout this work that the electrochemical technique employed can give very accurate determinations of oxygen diffusivity, provided some specific conditions are achieved with regard to the efficiency of oxygen consumption. Difficulties were encountered in the preliminary work due to inadequate considerations of the

low efficiency of oxygen reduction, and this preliminary work is also presented in this chapter as it is useful for further improvements of the technique. The design of the diffusion cell used to obtain the oxygen diffusivities was based on the theory initially proposed by Lingane[96,97] whose approaches are reviewed in subsection 5.2.2.

## 5.2 Literature Review

### 5.2.1 Oxygen reduction at platinum in alkaline solutions

From steady-state polarization studies on platinum cathodes in alkaline solutions, the overvoltage-current curve contains, in general, a Tafel region with a slope of about 0.05 volts per decade[98]. The exchange current density is between $10^{-9}$ and $10^{-10}$ A/cm$^2$. Platinum is considered as the best catalyst among the noble metals for the cathodic reduction of oxygen. Nevertheless, when this exchange rate is compared with, e.g. $10^{-3}$ A/cm$^2$ for the hydrogen discharge reaction, platinum is still a poor catalyst for oxygen reduction[98].

The overall reaction of oxygen reduction in alkaline solution is[98]:

$$O_2 + 2H_2O + 4e^- \longrightarrow 4OH^-$$

with the standard potential -400 mv Vs NHE. Oxygen is considered to be reduced at a platinum cathode along a series of complex parallel-consecutive steps. The

consecutive steps were considered by Hoare[98] to be as follows:

$$(O_2)_{ads} \xrightarrow{e^-} (O_2^-)_{ads} \xrightarrow{H_2O} (HO_2)_{ads} + OH^- \xrightarrow{e^-} (HO_2^-)_{ads} \Longrightarrow \tfrac{1}{2}O_2 + OH^-$$

Because it was found that the overvoltage depended on the oxygen partial pressure, and that the potential at which oxygen reduction began was virtually unaffected by pH, it appeared that the first step might be rate-determining.

Laitinen and Kolthoff[99,100] studied the current-potential behaviour at a stationary platinum micro-electrode in 0.01M NaOH + 0.01M KCl and 0.1M KCl solutions saturated with air. A diffusion current was observed, as indicated in figure 5.1 by the steady current obtained when the potential was within -0.6 and -1.0 volts Vs AgCl. The authors also found that rotating the electrode could greatly increase the diffusion current; for instance, the diffusion current was increased in 0.1M KCl solution from 3 μA at the stationary electrode to 61 μA at the rotating electrode.

### 5.2.2 Current decay controlled by diffusion at the electrode/solution interface

#### 5.2.2.1 Current-concentration relationship

If an electrochemically active substance is to be consumed at a constant potential with respect to a reference electrode, the criterion for a virtually complete

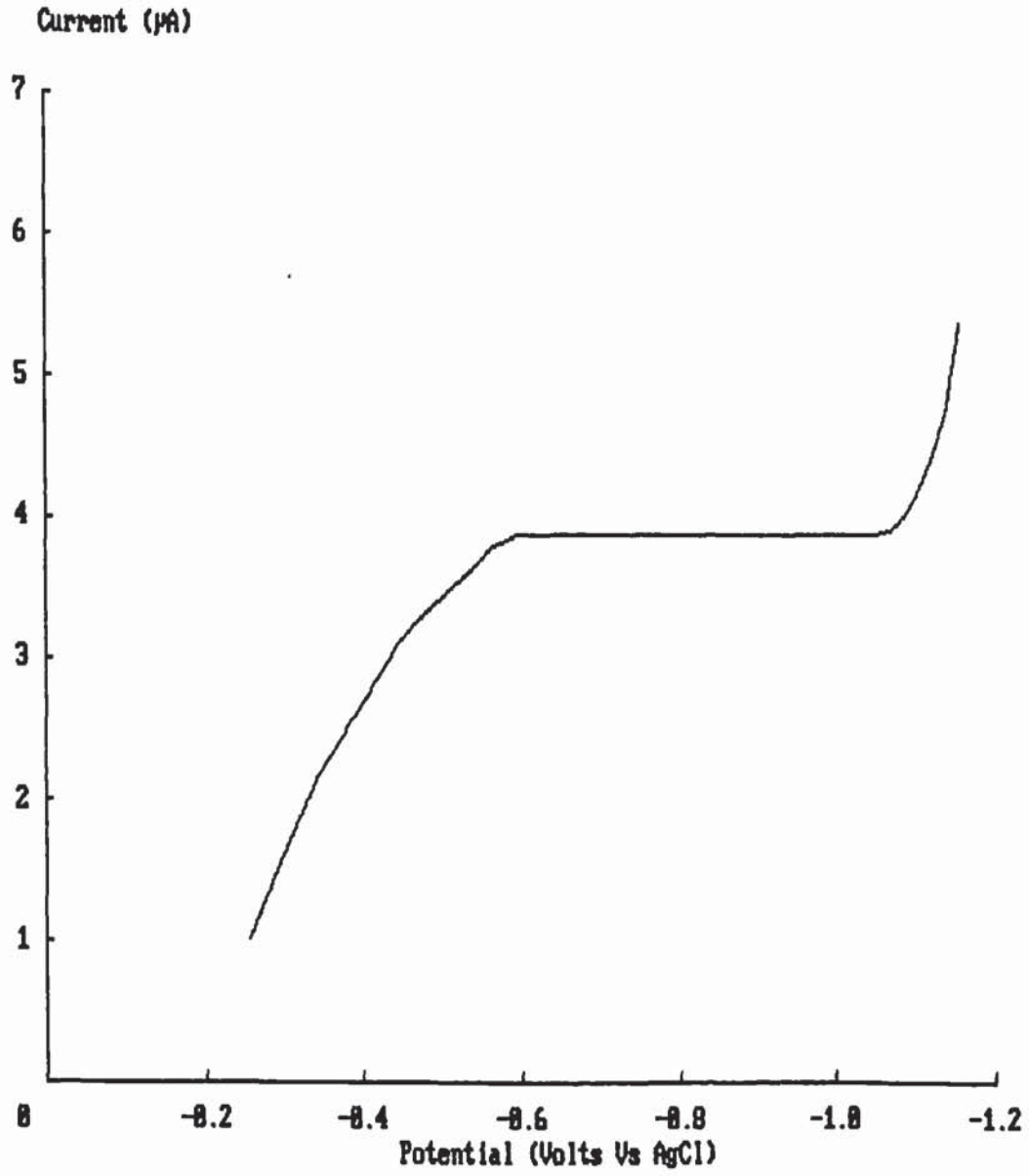


Figure 5.1 I-E curve for the reduction of oxygen at a stationary Pt-wire electrode in an air-saturated solution of 0.01 M NaOH and 0.01 M KCl (Ref. 99)

consumption is the decay of current from a high value initially to a value close to zero. Lingane[96] considered such a system where the rate of the electrode process is limited by the diffusion and electro-migration of the reacting species from the bulk solution to the electrode surface. Suppose the current-controlling factor is the rate of diffusion through the depleted layer of the solution in contact with the electrode, and the concentration of the reacting species near the electrode is practically zero. The instantaneous current (I) was derived from Fick's first law and Faraday's law as:

$$I=nFDA_eC_2/l \qquad \ldots\ldots (5.1)$$

where n is the number of electron transferred per molecule of the reacting substance, F is the Faraday number, D and $C_2$ are respectively the diffusivity and concentration of this substance in the solution, $A_e$ is the effective surface area of the electrode, and l is the thickness of the diffusion layer. This equation is based on the assumption that the substance which diffuses through the diffusion layer to the electrode surface is immediately consumed.

5.2.2.2 Current-time relationship

If the diffusion-layer thickness, l, is a constant during flow of current, the current from equation 5.1 should be proportional to the concentration. The current decay during a potentiostatic polarization, resulting from the gradual consumption of a single reactant having an initial

concentration $C_O$ (M) in a solution of fixed volume (V) was first derived from current-concentration equation 5.1 by Lingane[96,97]:

$$I=I_O\exp[-DA_e t/(Vl)] \quad \ldots\ldots (5.2)$$

for a constant value of 1, where t is the polarization time in seconds, and $I_O$ is the initial current (at t=0) correlated to the initial concentration $C_O$ by equation 5.1. Equation 5.2 has been found to be satisfactory for describing the current decay for the cathodic deposition of $Cu^{2+}$ (see Ref. 101) and for the anodic oxidation of $Fe^{2+}$ (see Ref. 102)

5.2.2.3 Degree of consumption

The extent to which this electro-active species has been consumed at a certain polarization time can be explicitly expressed by the ratio of the consumed quantity (Q) to its initial quantity (Qo)[96,97]:

$$Q/Qo=1-\exp[-DA_e t/(Vl)] \quad \ldots\ldots (5.3)$$

where Q can be obtained by integrating equation 5.2 over time and it has the same units as Qo, here the charge passed in coulombs.

The practical value of equations 5.1 to 5.3 is, as stressed by Lingane[97], that they provide a logical basis for the optimum design of cells and the choice of experimental conditions to achieve rapid depletion of the reacting species. The efficiency equation 5.3 also indicates that the efficiency can be exponentially

improved by increasing the ratio of the electrode area to the solution volume.

5.2.2.4 Thickness of the diffusion layer

Any experimental condition affecting the diffusion layer and the diffusion coefficient would change the efficiency. Temperature, for instance, is one of the factors able to affect both the diffusivity and diffusion layer thickness; as it increases, the diffusivity also increases, while furthermore, the viscosity of water decreases, resulting in a decrease of the diffusion layer thickness. For a water/ solid or water/electrode interface, the thickness of the diffusion layer at room temperature has been found to be of the order of magnitude 0.001 and 0.01 cm under turbulent flow and natural convection respectively[103]. The time average thickness, l, as a function of the speed of stirring U (rpm) is given by the empirical equation[103]

$$l=aU^{-b} \quad 0.5<b<1 \qquad \ldots\ldots (5.4)$$

for a turbulent flow around a rotating electrode surface, where a and b are constants. Nernst and Merriam[104] determined b to be 0.6, and their data (cited by Vetter[103]) are shown in figure 5.2.

Studies show that if the electrolyte is not stirred, no constant thickness of the diffusion layer can be obtained with any experimental arrangement[103]. The thickness depends on a number of factors, such as electrolyte

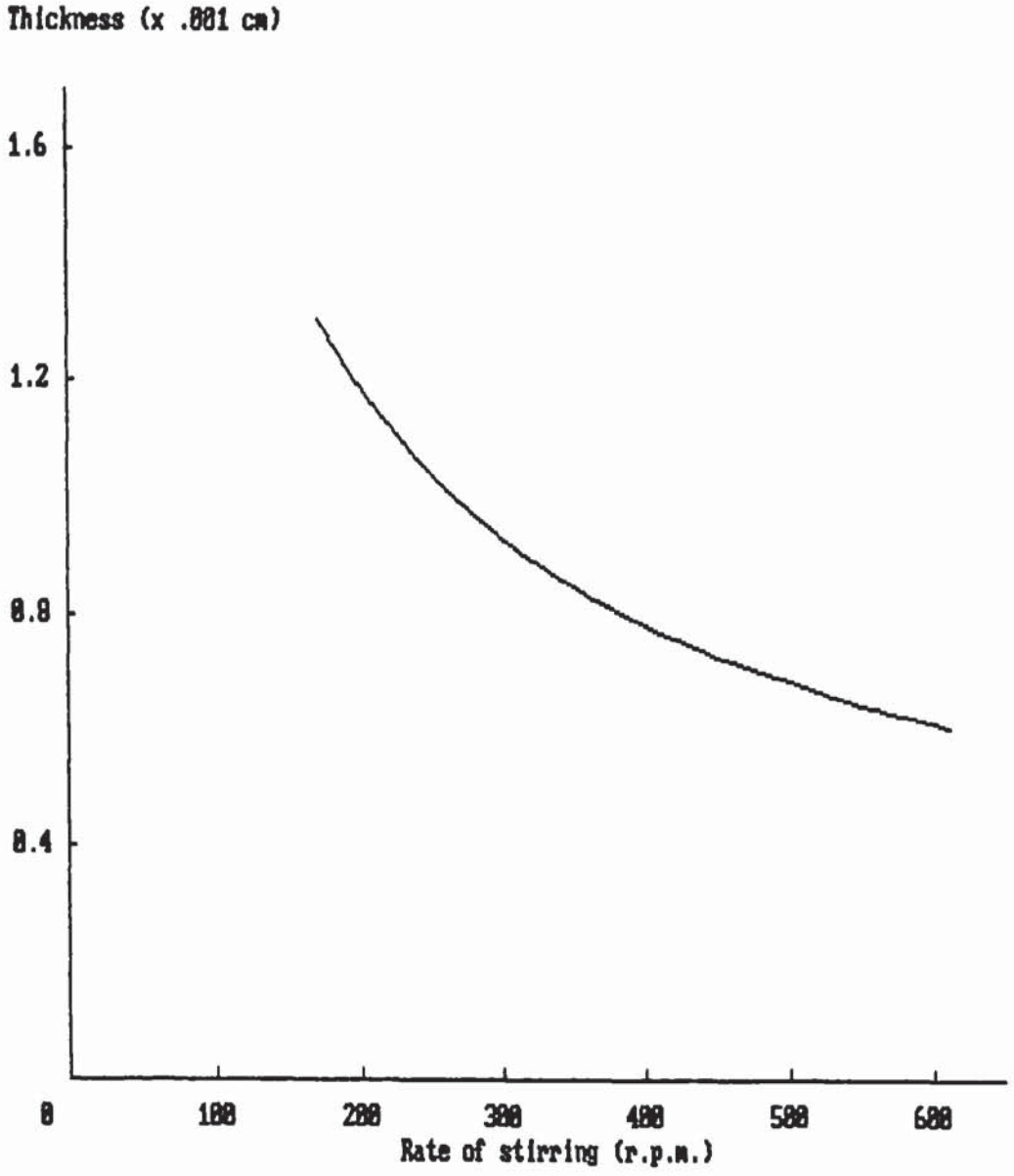


Figure 5.2 Diffusion-layer thickness as a function of the rate of stirring according to Nernst-Merriam (Ref. 104)

composition, current density, diffusivity, electrode reaction, and geometry of the electrode. Laitinen and Kolthoff[99] estimated a diffusion layer thickness of about 0.025 cm.

### 5.2.3 Potentiostatic measurement of oxygen diffusivity

Gold[105], platinum[106] and steel[106] cathodes have been used in studies of oxygen diffusion in water-saturated cement paste, mortar and concrete. Oxygen diffusivity can be determined potentiostatically from the flux and diffused amount during steady state diffusion. Two types of test system have been designed for experimental measurements. The first type is an electrochemical cell composed of two compartments joined together by a specimen. One compartment is filled with a solution of known oxygen concentration, usually air or oxygen saturated $Ca(OH)_2$ solution. The other compartment contains an initially $O_2$-free solution and a cathode. The diffusion from the high concentration side to the low concentration side is monitored electrochemically. This test system is similar to the one described in chapter 3 for ionic diffusion as far as the establishment of the diffusion process is concerned. The alternative approach for determining oxygen diffusivities employs a cathode buried in the test sample. This second type of system may be considered to be more realistic if the effect of oxygen transport on reinforcement corrosion is to be examined.

With the first type of test system the cathode is polarized at a potential such that the reduction of oxygen is the only significant cathodic reaction to take place. If diffusion of oxygen is at steady-state, it is possible to obtain a stable flux current $I_d$. Since at this flux current, the diffused amount is the same as that being consumed, the total flux $J_O$ (mmol/sec) is

$$J_O = I_d/nF \qquad \ldots\ldots (5.5)$$

and the flux current is related to the intrinsic diffusivity by Fick's first law

$$I_d = nFD_iA(dC/dx) \qquad \ldots\ldots (5.6)$$

where $D_i$ is the oxygen diffusivity, A is the diffusion area, and dC/dx is the gradient of oxygen concentration. By this method Gjorv et al[106] obtained diffusivities within the range $10^{-6}$ to $10^{-5}$ $cm^2$/sec for some mortar and concrete specimens. One disadvantage of this method is, as mentioned by the authors, that prolonged polarization for up to 4 weeks was required to achieve such a stable current.

Previous work[95] at Aston University used an electrochemical cell, similar to the ionic diffusion cell described in chapter 3, to measure the accumulated amount of diffused oxygen instead of the steady-state diffusion current. The important features of the cell design were the use of a large cathode (ca. 10 $cm^2$) and the incorporation of a stirring system, so that the accumulated

oxygen in the cathode compartment could be reduced reasonably effectively. This test cell was the basis for the design of a modified and improved version which is to be presented in the next section.

The second type of test system was employed by Gjorv et al[106] and Newton[105] to determine the quantity of accumulated oxygen around the buried cathode during an interruption of steady-state diffusion. After the cathode had been polarized long enough for a stable current to be achieved, the electrical circuit was opened to allow oxygen to build up around the cathode. The circuit was then closed again after a pre-determined time period (<60 second[106]). The charge passed or the accumulated oxygen was integrated from the current decay curve. It was reported[106] that it took about 2 minutes for the cathodic current to return to the steady state.

## 5.3 Experimental and Results

### 5.3.1 Design of the oxygen diffusion cell

#### 5.3.1.1 Theoretical considerations

It has been mentioned earlier that the type of diffusion cell considered in this work was basically that shown in figure 5.3. The cell was to be composed of an anode compartment, a cathode compartment and a stirring system. Both compartments contained saturated $Ca(OH)_2$ solutions. The anode compartment was always saturated with oxygen

during diffusion, while the oxygen diffused through the cement paste disc within a certain period of time, say 1 to 4 days, was to be consumed potentiostatically in the cathode compartment. In order to be able to determine, with reasonably good accuracy, the amount of oxygen diffused, it is thus essential that the consumption of oxygen could be completed within a time period which is much shorter than the interval of diffusion time, say 1 to 2 hours.

Figure 5.1 from Laitinen and Kolthoff[99] suggests that with a stationary platinum cathode the transport of oxygen from the bulk solution to the cathode is liable to dominate its reduction rate if the potential is held at an appropriately low value. Laitinen and Kolthoff[100] were also able to show that this could be true for a rotating platinum micro-electrode in 0.1M KCl solution. Since oxygen is a neutral species, diffusion driven by the concentration gradient could be reasonably assumed to be its only transport process in the depleted layer at the solution/ cathode interface. If such experimental conditions are imposed on the test system depicted in figure 5.3 that the rate of the oxygen reduction is ultimately limited by the diffusion of oxygen in the cathode-compartment solution to the cathode surface, this should be the most favorable situation for a rapid consumption of the oxygen diffused through the test sample.

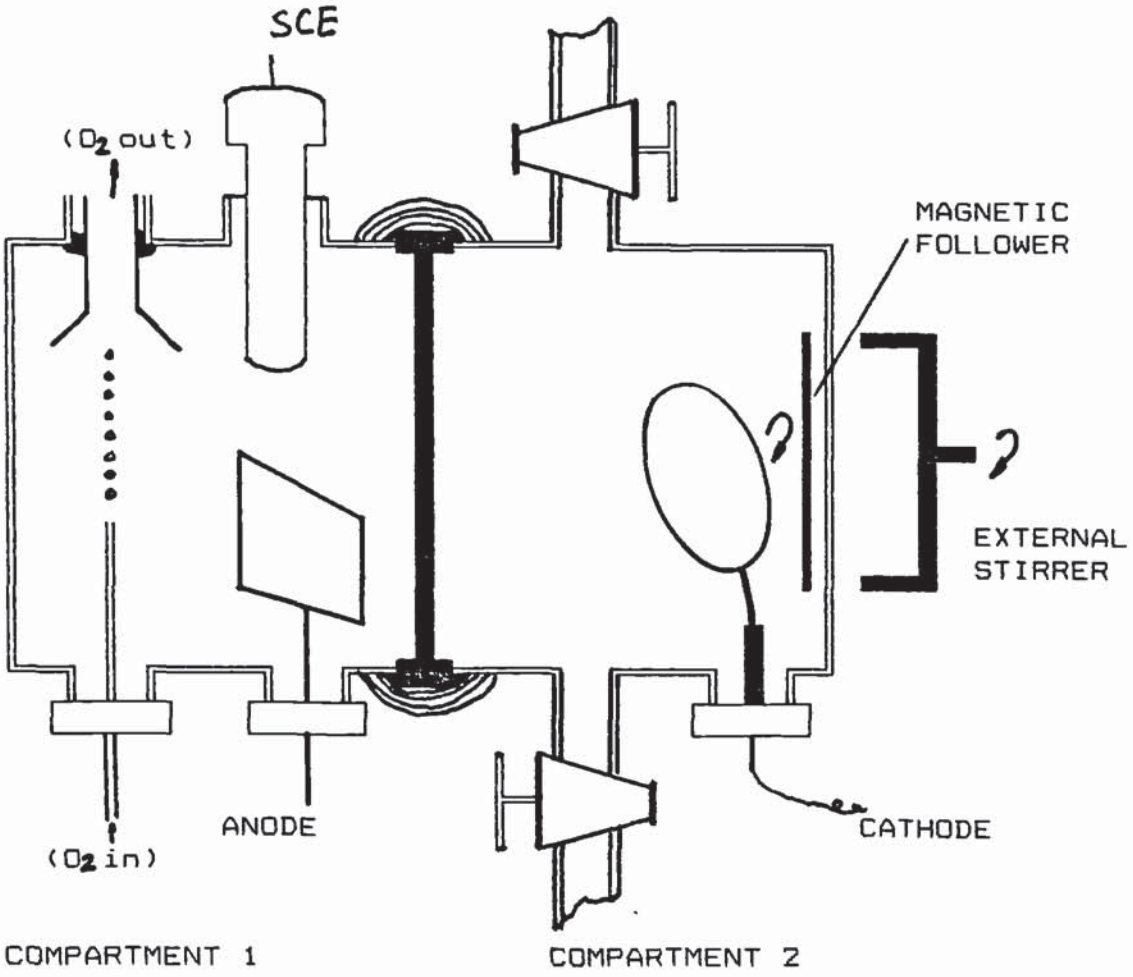


Figure 5.3 The oxygen diffusion cell

In order to be able to consume the diffused oxygen, it is important to use a cathode of large external surface area. However, it would be useful to estimate at first the cathode size required for a workable diffusion cell on the basis given by Lingane[96,97]. With regard to the diffusion cell concerned in this work, assume:

(1). The rate of consumption of the oxygen in the cathode compartment is controlled by the diffusion at the cathode/ solution interface.

(2) The diffusion layer has a constant thickness.

(3) The concentration on the cathode surface is zero.

(4) When the cathodic polarization is in process, the amount of oxygen diffusing through the test sample per second is negligible compared with that left in the cathode compartment.

Therefore, the instantaneous current achieved for an oxygen concentration $C_2$ (M) in the cathode compartment is given by equation 5.1 which is rewritten as follows for the purpose of defining the terms,

$$I=nFC_2K=nFC_2(DA_e/l) \qquad \ldots\ldots (5.7)$$

where n=4, $A_e$ is the effective surface area of the cathode, D is the oxygen diffusivity in the depleted layer of thickness l, and K is a constant in appropriate units.

The efficiency equation for the oxygen consumption would be the same as equation 5.3, and also rewritten as,

$$Q/Qo=1-\exp[-DA_et/(Vl)]=1-\exp(-Kt/V) \qquad \ldots\ldots (5.8)$$

where Q in coulombs is the amount of oxygen consumed at time t, and Qo in coulombs is the initial amount of oxygen in the cathode compartment of volume V.

The time of cathodic polarization required to achieve a certain degree of oxygen consumption at 25°C in water is tabulated in table 5.1(a) for two choices of the "cell constants" with l=0.001 cm estimated from figure 5.2 and with $D=2.1\times10^{-5}$ $cm^2/sec$. The calculations are based on the efficiency equation 5.8. The approximate "cell constants" shown in the second column correspond to the cell used in the preliminary work, and in the third column are for the cell used in later work.

Table 5.1(b) gives the currents expected from the current-concentration equation 5.7, Is and Ia (mA), in oxygen and air saturated water with the solubilities of $1.23\times10^{-3}$ M (from Ref. 107) and $2.5\times10^{-4}$M (from Ref. 42) respectively. As the assumptions made for the above calculations may be quite unrealistic for oxygen reduction, these two values of current can be used to check whether or not the estimation of the efficiency is appropriate for a diffusion cell. This is because the efficiency (Q/Qo) defined earlier can be derived, without any further assumption, from the current-concentration relationship shown by equation 5.8.

**Table 5.1(a)** Calculated Polarization Time required to achieve certain degrees of oxygen consumption, Q/Qo

| Q/Qo | Cell 1: $A_e$=5 $cm^2$ V=130 ml | Cell 2: $A_e$=20 $cm^2$ V=35 ml |
|---|---|---|
| 0.60 | 18.9 | 1.3 |
| 0.80 | 33.2 | 2.2 |
| 0.90 | 47.5 | 3.2 |
| 0.95 | 61.8 | 4.2 |

**Table 5.1(b)** Calculated currents for air- and oxygen-saturated solutions

| CURRENT (mA) | Cell 1 | Cell 2 |
|---|---|---|
| Is | 52 | 207 |
| Ia | 11 | 42 |

5.3.1.2 Preliminary work

The glass diffusion cell used in the preliminary work is illustrated in figure 5.3. The cell was a simplified version of that employed in the previous study[95]. The compartment 1 contained a platinised titanium anode (ca. 5 $cm^2$) and a reference electrode (SCE). A platinum wire was fixed into the compartment 2 to serve as the cathode. To minimize the loss of solution due to the bubbling of gases, a funnel was placed in each compartment to direct the gas stream. A magnetic bar follower, coupled with an external magnetic stirrer, was added to the cathode compartment, enabling the stirring of the solution during an electrochemical measurement.

To set up an experiment, a disc of hydrated cement paste was mounted between the two compartments, as described in subsection 3.3.1.2, chapter 3 for ionic diffusion. The two compartments were filled with saturated calcium hydroxide solution, and the cell was then placed in a water-bath controlled at 25°C. Prior to starting the experiment, a potentiodynamic scan at 1 mv/sec was performed whilst stirring the solution. An example of the potential-current behaviour (E-I curve) is given in figure 5.4. The potentiostat to which the three cell electrodes were connected was the Model 350 Corrosion Measurement System from Princeton Applied Research.

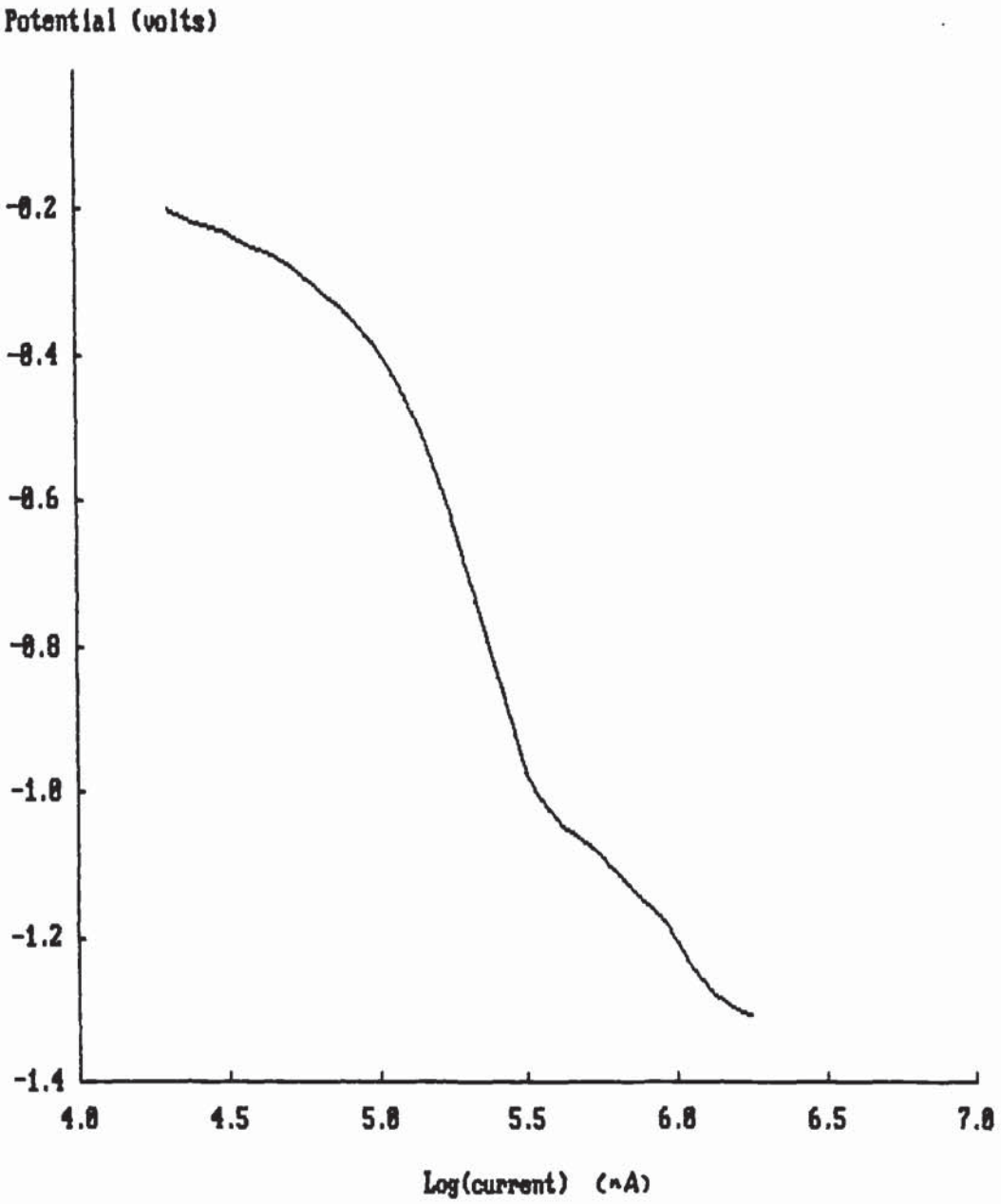


Figure 5.4 Potential-current curve at Pt electrode in air saturated $Ca(OH)_2$ solution

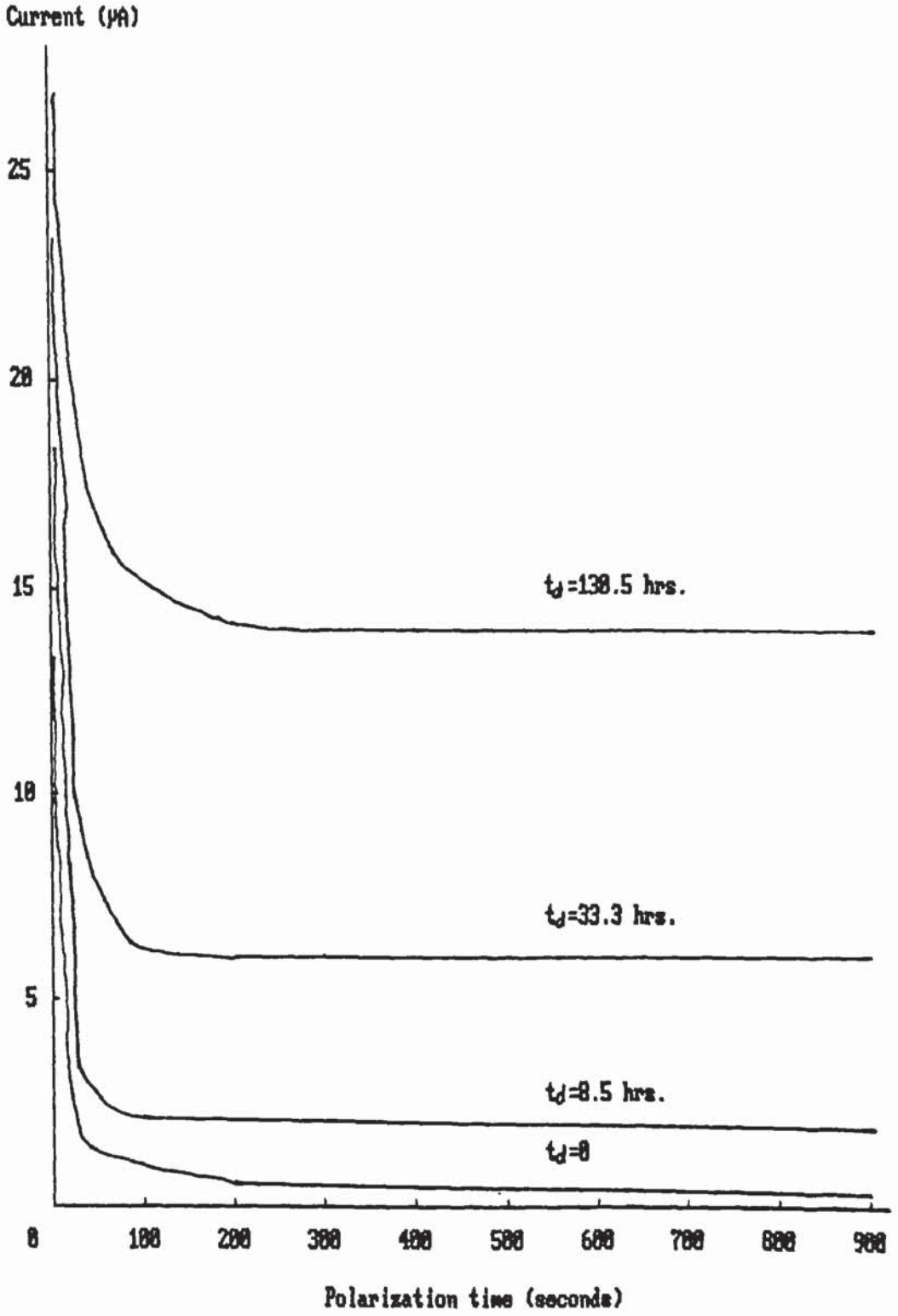


Figure 5.5 Current decay recorded in the preliminary work (sample: 0.65 w/c OPC; L=0.28 cm)

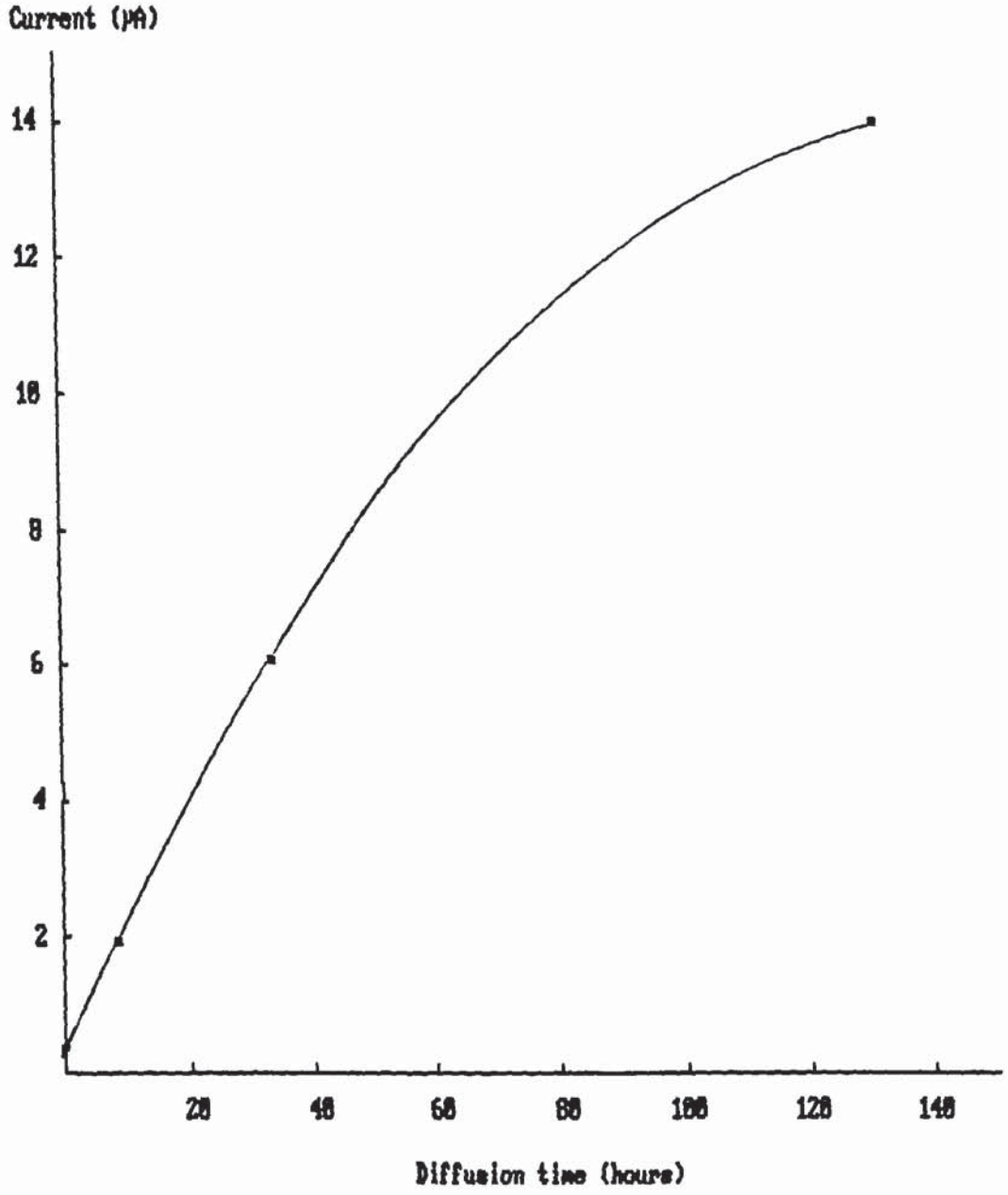


Figure 5.6 Increase of the end current with increase of the diffusion time (preliminary work)

The anode and cathode compartments were finally saturated with oxygen and "white spot grade" ($O_2$-free) nitrogen respectively by bubbling the gases through for 2 to 4 days. Steady-state diffusion of oxygen in the test sample would be expected to take place. The nitrogen was then stopped but the oxygen stream was maintained.

The first run of cathodic polarization was carried out immediately after the nitrogen stream had been stopped. This was considered necessary to obtain an initial state of almost zero concentration of oxygen in the cathode compartment. The cathode was polarized at -0.400 volt Vs SCE for 900 to 2000 seconds after the stirrer had been started, and the current and the charge passed were recorded. The potential, -0.400 volt, was chosen since the only significant cathodic reaction at this potential is the reduction of oxygen[95]. The currents recorded at the end of polarization were generally between 0.15 and 0.5 μA. Diffusion of oxygen through the test sample was then allowed to occur for certain periods of time. The cathodic polarization was then undertaken, intending to consume all the oxygen that had diffused.

One example of the current-time curves at certain diffusion time periods, $t_d$, relative to the time ($t_d$=0) when the nitrogen stream was stopped, is shown in figure 5.5 for a disc (2.8 mm in thickness) of 0.65 w/c OPC paste. The potential was held for 900 seconds for this particular example. The current-time behaviour from

repeated experiments is summarised as follows:

(1).The decay of current with time of polarization (except for the one at $t_d$=0) was very slow, and current remained almost constant from 10 minutes to a few hours. Obvious drop of the current could be observed only during the first approximately 300 seconds.

(2). For the first run of cathodic polarization carried out just after the nitrogen stream had been stopped, the current decreased at first to be below 0.5 μA; however, if the potential was maintained for a few hours, there was gradual increase of the current.

(3). The current recorded at the end of polarization, $I_e$, increased with length of diffusion time, $t_d$, which is shown in figure 5.6.

These indicate that the oxygen diffused could not be consumed efficiently using this diffusion cell.

It is probable that diffusion of oxygen near the cathode surface was controlling the rate of the reduction reaction, as suggested by figure 5.4. Although the current increased as the applied potential became more negative, the potential-current curve in the potential range from -0.4 to -1 volt is much steeper compared with the curve that would be expected when the electrode process is controlled by activation (with Tafel slope of about 0.05 volt per decade). However, the efficiency of oxygen reduction, estimated in table 5.1 on the assumption that the electrode process is under diffusion-control, appears

to deviate far away from what was actually obtained. This may not be surprising as the current obtained in air saturated $Ca(OH)_2$ solution within the potential ranging from -0.4 to -1 volt is at least 30 times smaller than the Ia calculated from equation 5.3 with the assumed diffusion-layer thickness l=0.001 cm (table 5.1).

It is likely that when the stirring speed is not fast enough, stirring the solution is less effective as a means of reducing the diffusion layer thickness, l, than rotating the electrode (when 600 to 2000 rpm rotation speeds of the electrode are commonly used[98]). This was perhaps the main reason for small current obtained in air-saturated solution, and accordingly for the ineffectiveness in consuming the diffused oxygen.

As already explained, an exponential decay of the current with time (equation 5.4) can be expected only when the current is proportional to the oxygen concentration. For a steady-state diffusion of oxygen in the test sample, the concentration in the cathode compartment should rise linearly with the diffusion time. The current shown in figure 5.5 is very small, so the amount of oxygen consumed cathodically is negligible compared with the total amount in the cathode compartment. Therefore, a linear relationship between the end current and the diffusion time is an indication of the linear relationship between the concentration and the instantaneous current. It can be

seen from figure 5.6 that the current did not increase linearly with concentration for the diffusion cell used.

However, in order to estimate the approximate time required to achieve a reasonably complete consumption of the diffused oxygen, and to aid the design of a better diffusion cell, the current-concentration equation 5.7 was used to obtain an approximate value of the parameter, K, so the efficiency equation 5.8 can be used.

The current obtained at -0.4 volt at the assumed oxygen concentration $2.5 \times 10^{-4}$ M is about 0.1 mA (see figure 5.4), so the value of K is estimated, from equation 5.7, to be $0.1/(4F \times 2.5 \times 10^{-4}) = 0.001$, and the exponential factor K/V in equation 5.8 is $7.69 \times 10^{-6}$ $sec^{-1}$. It was calculated from equation 5.5 that to consume 50% and 90% of the oxygen in the cathode compartment, cathodic polarization for 1 and 3.5 days would have been required respectively.

Since the oxygen concentration in the cathode compartment should be expected to increase linearly with the diffusion time at a steady-state diffusion, figure 5.6 indicates that the current at low concentration, and thus the actual efficiency of oxygen consumption, would be underestimated if the K-value is estimated from the current obtained at higher concentrations. Nevertheless, the effectiveness in reducing oxygen had to be increased considerably. With regard to the discussions in paragraph 5.3.1.1, a cathode compartment with a very large ratio of electrode surface

area to compartment volume, like that shown in the third column of table 5.1, must be employed.

The possibility of leakage was also considered, as leakage tends to create great uncertainty and confusion. After the nitrogen stream had been stopped, there was a gradually slow increase of the current if the potential was maintained for a few hours. This might be regarded as an obvious indication of leakage. The difficulty in interpreting this behaviour arose from the uncertainty concerning the oxygen diffusivity in the test sample. Considering a disc specimen, 0.28cm in thickness and 10 $cm^2$ in diffusion area, the current ($I_d$) equivalent to the amount of oxygen diffused per second through the specimen would be 0.2, 0.9 and 1.7 μA at the assumed diffusivities ($D_i$) $10^{-8}$, $5x10^{-8}$ and $10^{-7}$ $cm^2$/sec respectively (see equation 5.6). If the diffusivity was greater than $5x10^{-8}$, the end current $I_e$ (0.38 μA) at $t_d$=0 (see figure 5.5) could thus not be stable since the consumed amount of oxygen was less than the diffused. It will be shown later that the diffusivity in 0.65 w/c OPC paste is greater than $10^{-7}$ $cm^2$/sec.

Because it is important to ensure that no unwanted oxygen migrates into the cathode compartment in such an arrangement of the test system, an experiment was conducted as follows. A thick disc of 0.65 w/c OPC paste of 1 cm in thickness was used. Both compartments were initially bubbled with nitrogen for three days before the

anode compartment was $O_2$-saturated and the cathode compartment closed. Cathodic polarization at -0.4 volt Vs SCE for twenty minutes was then carried out at several diffusion time periods, $t_d$. The currents recorded at the end of polarization are 0.52, 0.40, 0.49 and 3.4 μA respectively at the diffusion time $t_d$=0, 1.2, 4.1 and 11.8 days (at $t_d$=1.2 days there was a temperature drop during the measurement due to a fault of the water-bath used). Little variation of the end current was observed for the first four days, which can be explained only by the fact that no steady-state diffusion had been established. In comparison with the end current shown in figure 5.6 for the thinner specimen, the end currents obtained in this experiment are generally smaller for a comparable diffusion time, which should be interpreted as an obvious effect of the sample thickness on the flux.

5.3.1.3 The diffusion cell

The anode compartments used to determine the diffusivity of oxygen were those used in the preliminary work. It is suggested by efficiency equation 5.5 that, to improve the effectiveness of oxygen reduction, decreasing the volume of the cathode compartment would be an alternative to increasing the surface area of the cathode. It is clear that a maximum efficiency can be achieved if the cathode compartment is made as small as possible, provided that steady-state conditions of $O_2$ diffusion are not violated,

and that convenient stirring of the solution is possible. Although the cathode compartment used was similar to that shown in figure 5.3, it was constructed to have a volume of about 35 ml. The platinum cathode was cut from a foil and had a roughly estimated surface area 20 $cm^2$. It was initially cleaned in boiling aqua regia for ten minutes and washed with deionised water. The preparation of the cathode was completed by polarizing at -1.2 volts Vs SCE in saturated $Ca(OH)_2$ solution overnight. Two such cells were used in the experimental study.

The stirring system was similar to that described earlier. The external stirrer consisted of a magnet driven by a small motor connected to a d.c generator, and was isolated by fixing in a plastic cylinder. The actual rotation speed of the follower in the compartment was around 250 rpm which is smaller than that employed in the preliminary work. Nevertheless, it was observed experimentally that further increase of the rotation speed only resulted in a slight increase of current.

### 5.3.2 Diffusion of oxygen

#### 5.3.2.1 Experimental set-up

Specimens of OPC and OPC/20%PFA pastes of w/c 0.35, 0.5 and 0.6 were prepared in a similar way as described in paragraph 3.3.1.1, chapter 3. The discrepancies in the preparation procedures among individual specimens will be noted in the discussion, section 5.3. The pastes were

cured in air-tight PVC moulds for two weeks and then in saturated $Ca(OH)_2$ solution at 22°C. Discs of the pastes, 0.2 to 0.4 cm in thickness, were cut one month before a diffusion experiment started. The discs were again immersed in saturated $Ca(OH)_2$ solution. This was intended to ensure that the pores in the samples were water-saturated, as diffusion of oxygen in air-filled pores would be much faster than in water-filled pores.

After the sample disc was mounted in the diffusion cell, the anode compartment was filled with saturated $Ca(OH)_2$ solution and bubbled through with oxygen. The cathode compartment was filled with de-aerated $Ca(OH)_2$ solution which had been purged, in a de-aeration cell, with nitrogen for about one day. The use of de-aerated solution was found later to be unnecessary, as it will be shown in paragraph 5.3.2.3 that it is possible with such a diffusion cell to consume electrochemically all the oxygen in the air-saturated solution contained in the cathode compartment. Care was taken to ensure that no gas bubbles were present in the cathode compartment, as even a small volume of the gas phase may contain a comparatively high quantity of oxygen in a vapour-solution system so that accuracy of the measurements may be affected.

The cell was finally placed into a water-bath controlled at 25°C. After the experiment was finished, the diffusion area (ca. 10 $cm^2$) of the disc was measured from the marks

left by the grease on the gasket. The cathode was washed with deionised water, 0.01 M nitric acid and acetone, then placed in deionised water ready for the next experiment.

5.3.2.2 Electrochemical measurements

It was noticed that it took four to seven days for diffusion of oxygen to reach a steady state. Cathodic polarization at -0.600 volt Vs SCE for 6000 seconds was carried out every one or two days during the period of non-steady state diffusion, but the current and charge passed were generally not recorded simply for the purpose of saving computer disks. The Model 350 Corrosion Measurement System was used for samples 1 to 6. A Multistat System supplied by Thompson Electrochem Ltd, which consists of potentiostats, a CCU and a BBC Master computer, was used for the rest of the samples. The current was measured every second with the programmed measurement range 0.3 to 1538 μA, and the charge passed was integrated numerically through the computer programme.

Diffused oxygen was then determined at diffusion-time intervals normally between 1 and 4 days. These intervals were purposely chosen to be different from each other for each sample, intending to check whether the consumption of oxygen was complete enough or not. A constant ratio of the charge passed to the diffusion-time interval would indicate a reasonably complete consumption of the diffused oxygen.

All of the cathodic polarizations were carried out by holding the potential at -0.600 volt Vs SCE for a certain length of time. The polarization time in the range from 6000 to 10000 seconds was chosen such that the residual current was nearly the same for each run of polarization. The differences in the residual current varied less than 2 μA. Therefore a reasonable reference zero concentration of oxygen in the cathode compartment was attained after each polarization. The residual currents recorded, $I_e$, were less than approximately three times the flux current $I_d$ which has been defined in equation 5.6 as the equivalence of the quantity diffused per second, suggesting that a reasonably complete consumption of the diffused oxygen was obtained (see paragraph 5.3.2.3 for further discussion). Examples of the current-time curves are given in figure 5.7.

During steady state of diffusion, the charge passed (Q) or the accumulative charge ($Q_t$) should be proportional to the time interval ($t_i$) or the total time ($t_d$) of the diffusion. Both the ratios $Q/t_i$ and $Q_t/t_d$ can be used to calculate the flux by Faraday's law. This work used the latter ($Q_t/t_d$). The experiment was stopped if the calculated ratio, $Q/t_i$, varied little for four to six consecutive measurements. The calculation procedures are as follows. Table 5.2 shows the recorded end current $I_e$ and the charge passed for eight consecutive measurements obtained from sample 18. The time corresponding to the

second measurement listed in the table was assumed as the reference zero point for the calculation of the total diffusion time and the accumulative charge. The $Q_t$ was then plotted against $t_d$ as shown in figure 5.8, and the slope was used to calculate the diffusivity by equation 5.9.

Correlation coefficients of the linear $Q_t$-$t_d$ relationship were found all to be above 0.99. The intercept at the reference point of zero diffusion time is an indication of whether or not a stable reference zero concentration after each polarization was controlled, which is the main reason for the use of $Q_t/t_d$ in the calculation of the flux. In order to compare the diffusion rates in different types of paste, the products, $LQ_t$, are plotted in figures 5.9 and 5.10 against the diffusion time, $t_d$, for some selected samples, where L is the thickness of the sample disc.

5.3.2.3 Oxygen solubility in saturated $Ca(OH)_2$ solution

To calculate the diffusivity of oxygen, it is necessary to know its concentration in the anode compartment, i.e. its solubility in saturated $Ca(OH)_2$ solution. The solubility at 25°C was determined as follows. Solution of $Ca(OH)_2$ was initially bubbled with $O_2$ for five hours. The aerator cell containing the solution was positioned in the water-bath. The gas was first passed through a spiral glass tube which was also placed in the water-bath.

Table 5.2 Calculation of the flux current $Q/t_i$ or $Q_t/t_d$

(Sample No. 18)

| No. | tp | $I_e$ (μA) | Q (coul) | $t_i$ (days) | $Q/t_i$ | $t_d$ | $Q_t$ |
|---|---|---|---|---|---|---|---|
| 1 | 9 | 2.0 | 0.166 | | | | |
| 2 | 6 | 1.8 | 0.066 | 1.08 | 0.061 | (0) | (0) |
| 3 | 9 | 1.7 | 0.145 | 4.00 | 0.036 | 4.00 | 0.145 |
| 4 | 9 | 1.8 | 0.139 | 4.01 | 0.035 | 8.01 | 0.284 |
| 5 | 10 | 2.0 | 0.171 | 4.93 | 0.035 | 12.93 | 0.455 |
| 6 | 8 | 2.0 | 0.091 | 2.19 | 0.042 | 15.12 | 0.546 |
| 7 | 8 | 2.5 | 0.136 | 3.76 | 0.036 | 18.88 | 0.682 |
| 8 | 6 | 2.6 | 0.084 | 2.00 | 0.042 | 20.88 | 0.766 |

*: tp -- Polarization time (x1000 seconds)

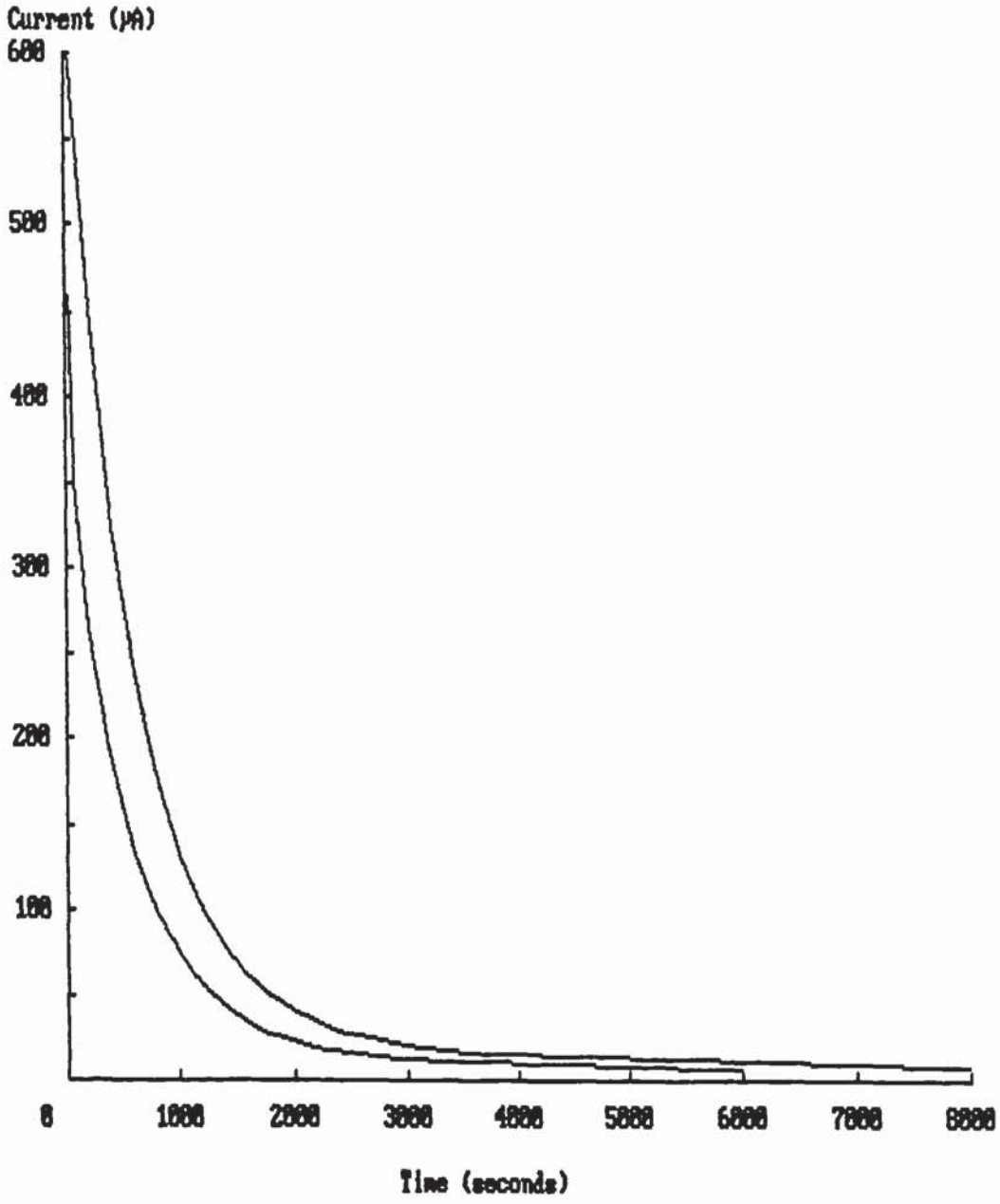


Figure 5.7 Decay of the cathodic current with polarization time

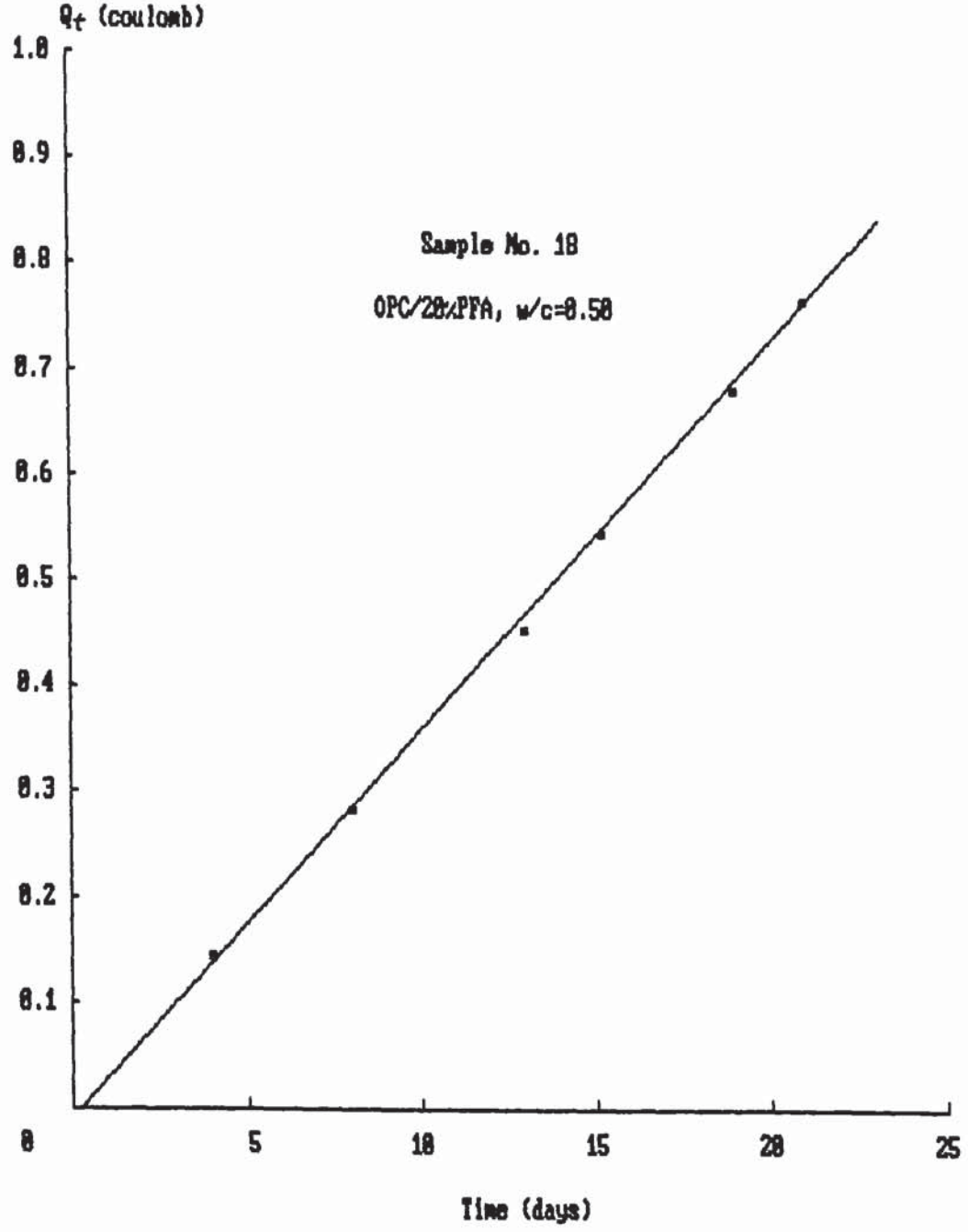


Figure 5.8 Linear relationship between the charge passed and the total diffusion time

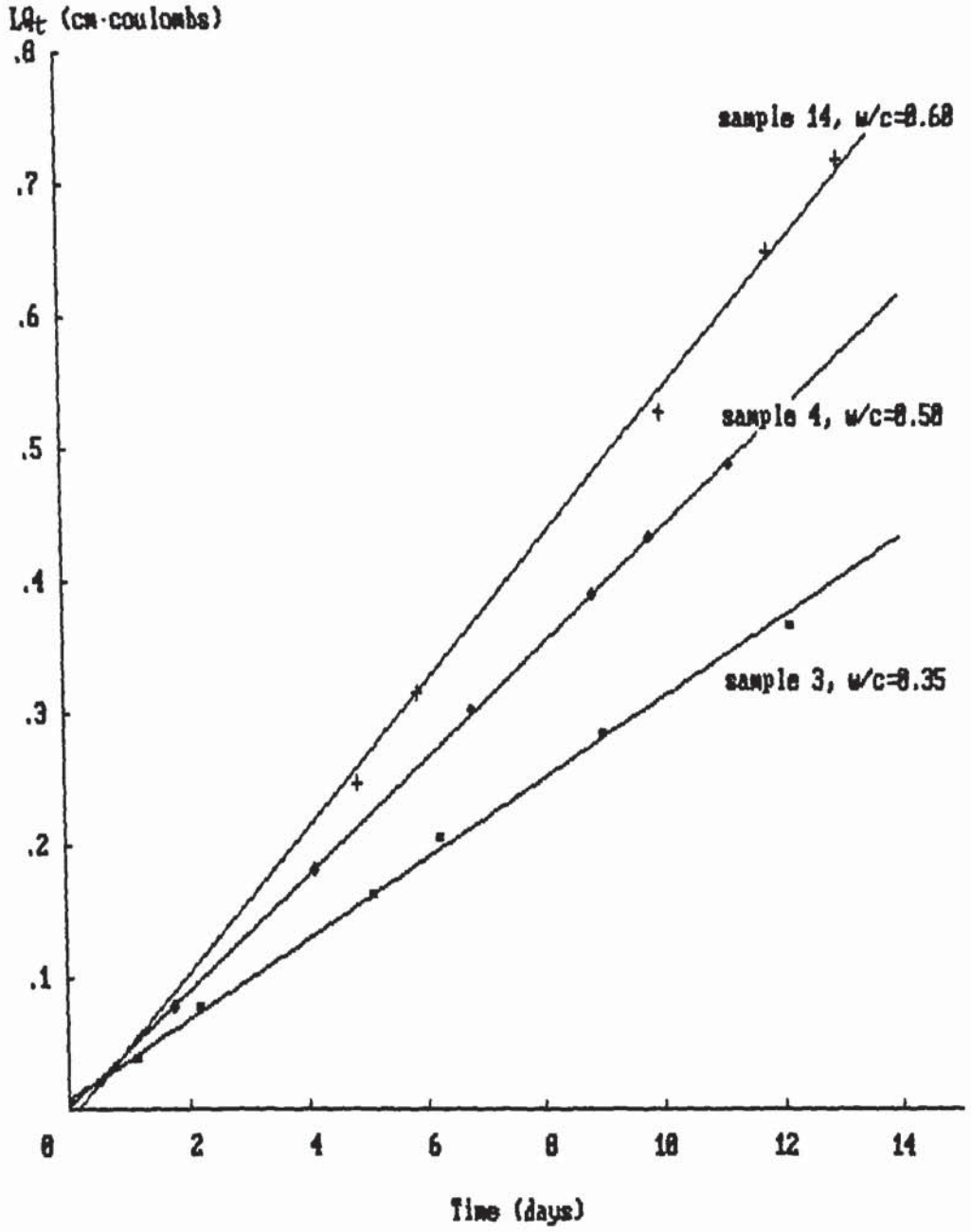


Figure 5.9 Examples of the $LQ_t - t_d$ curves for the OPC specimens of w/c ratios 0.35, 0.50 and 0.60

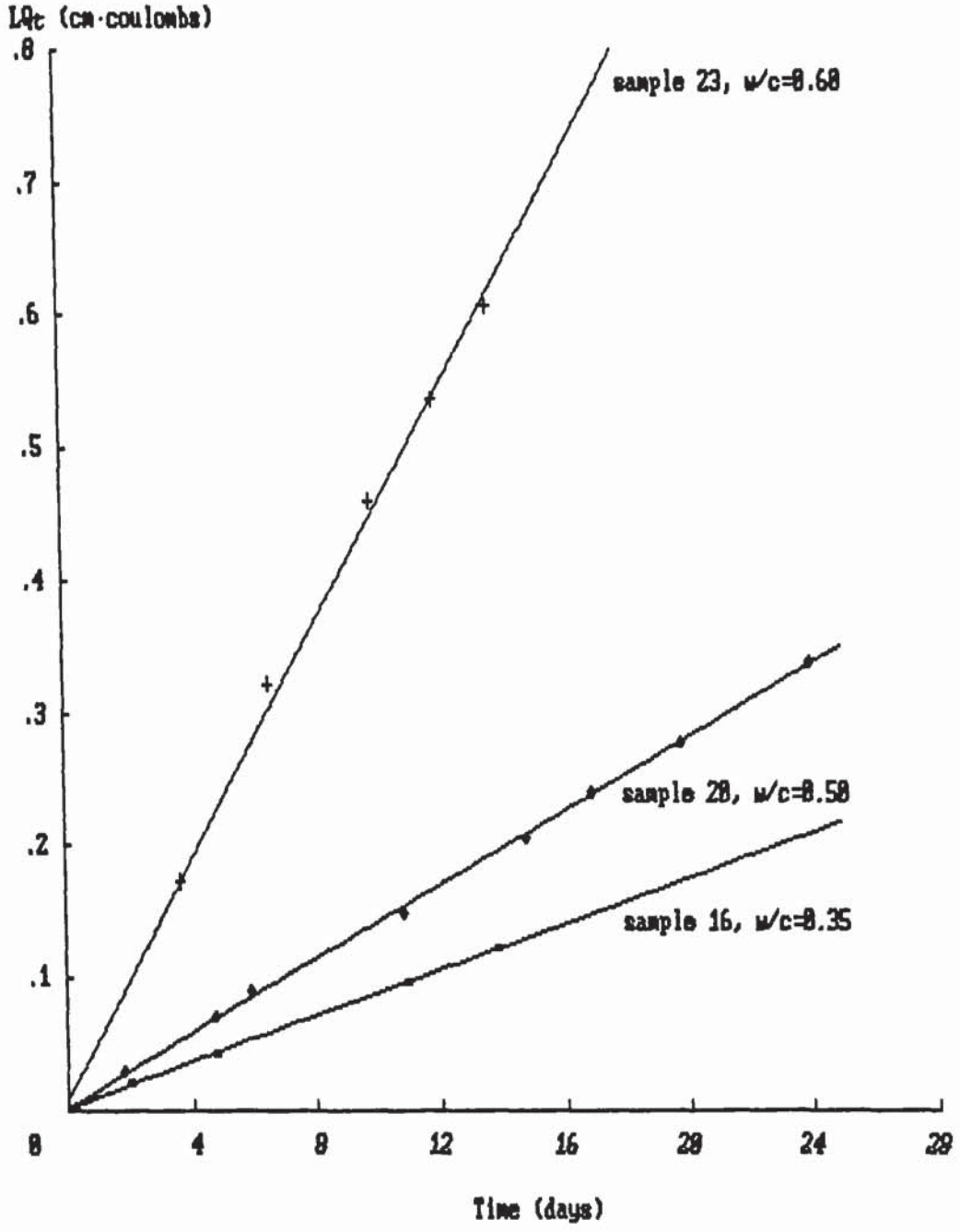


Figure 5.10 Examples of the $LQ_t - t_d$ curves for the OPC/20%PFA specimens of w/c ratios 0.35, 0.50 AND 0.60

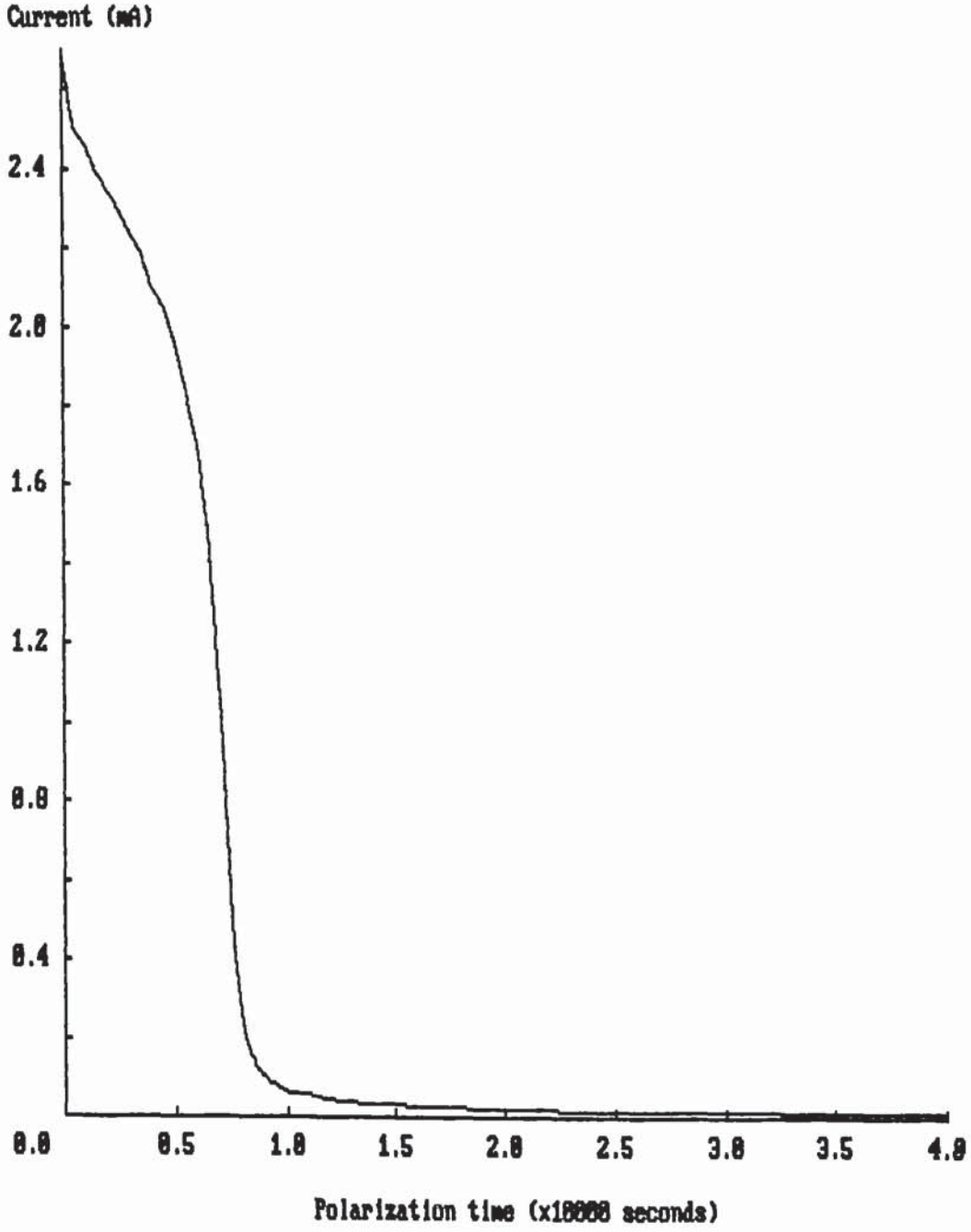


Figure 5.11 Current-time curve obtained from the measurement of oxygen solubility in $Ca(OH)_2$ solution

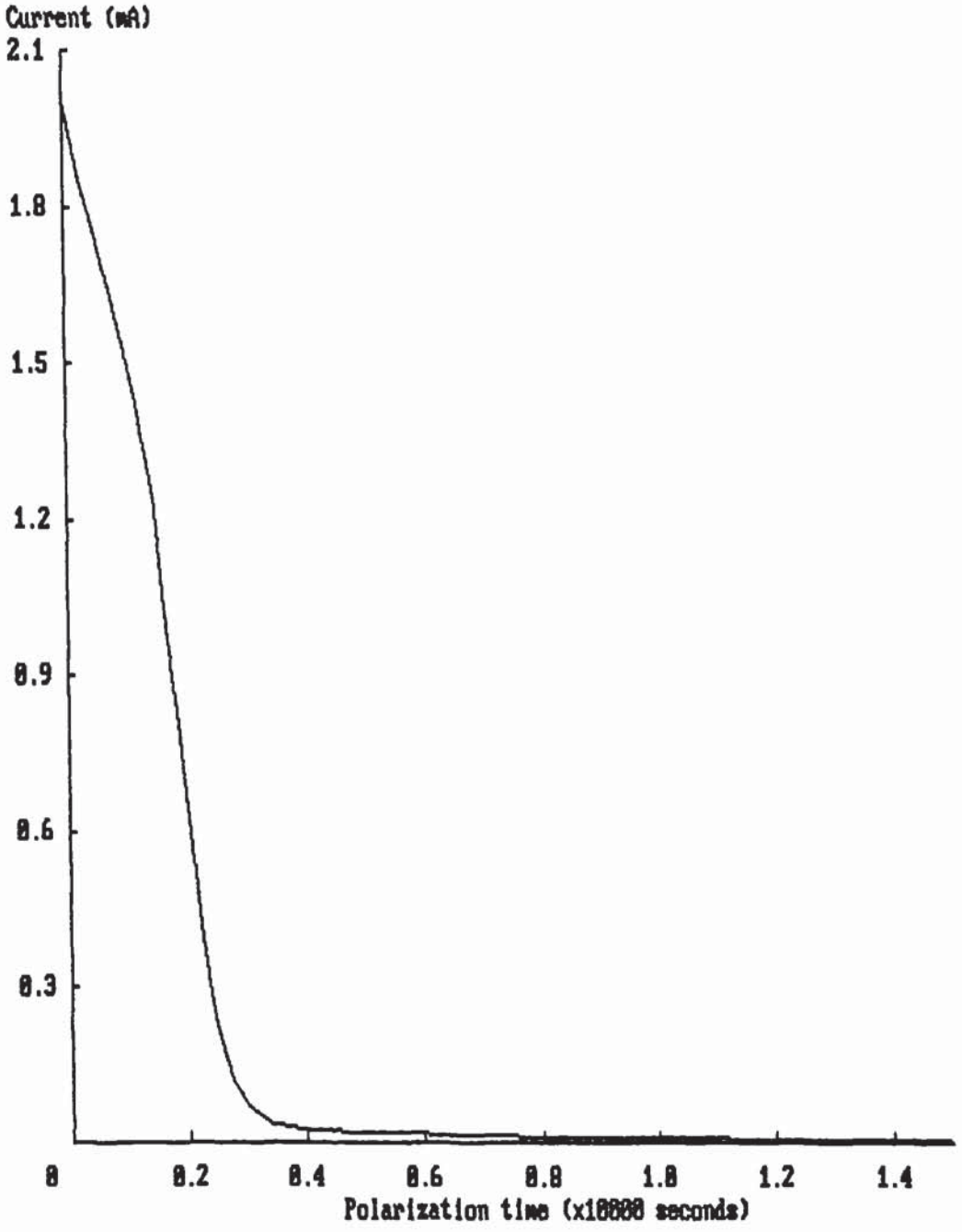


Figure 5.12 Current-time curve obtained when the cathode compartment contained initially air-saturated $Ca(OH)_2$ solution

The procedures to set up the cell were similar to those used for diffusion measurements. The cathode compartment was filled with the prepared solution, while the anode compartment contained air-saturated solution. The solubility was determined by polarizing the cathode at -0.600 volt for 11.1 hours. The two measurement ranges of the current, 0.3 to 1500 μA and 1500 μA to 1 A, were obtained through a computer programme. The current-time curve recorded is shown in figure 5.11. The charge passed was integrated to be 16.125 coulombs. The actual volume of the solution in the cathode compartment was 32.25 ml obtained by weighing.

The calculated solubility would be $1.25 \times 10^{-3}$ M. Compared with the value, $1.23 \times 10^{-3}$ M[107], in water at 1 atmosphere from the total of the partial pressures of oxygen and water vapour, the experimentally determined result is only 1.6% higher. In agreement with the results obtained by Gjorv et al[106] and Newton[105] using some other methods, oxygen has almost the same solubility in $Ca(OH)_2$ solution as in water at least at the temperature concerned (25°C). However, the solubility in water may considered to be more appropriate for the calculation of the diffusivity, as the pressure at which the solution was made to fill the cathode compartment was slightly higher than 1 atmosphere.

Figure 5.11 indicates that approximately 12000 seconds of polarization were required to consume the dissolved oxygen

and to enable the measurement of the solubility. Therefore, some justifications should be given for the much shorter polarization time, normally between 6000 and 10000 seconds, chosen for a diffusion measurement. Figure 5.12 gives the current-time curve recorded for a measurement of the amount of the oxygen in air-saturated $Ca(OH)_2$ solution at room temperature. The experimental procedures were similar to those described for the measurement of solubility in oxygen-saturated solution.

It can been seen from figure 5.12 that the oxygen contained in the air-saturated solution was virtually consumed within 6000 seconds, which justifies the polarization time chosen for the diffusion measurement. As the initial oxygen concentration in the cathode compartment became lower, shorter time of polarization was required for a virtually complete consumption, which has been explained in section 5.3.1.2 concerning the current-concentration relationship revealed in figure 5.6. However, the time required is still much longer than those listed in table 5.1, suggesting specific considerations concerning the effectiveness of oxygen reduction should be made with regard to the design of such diffusion cells.

### 5.3.2.4 Oxygen diffusivity

The intrinsic diffusivity, $D_i$, was calculated from Fick's first law and Faraday's law:

$$D_i = L(Q_t/t_d)/(4FAC_O) \qquad \ldots\ldots (5.9)$$

where L is the disc thickness, $Q_t/t_d$ (mA) is the slope determined from the $Q_t$-$t_d$ curve, A is the diffusion area of the sample, $C_0$ is the solubility ($1.23 \times 10^{-3}$ M), and $C_0/L$ is the assumed concentration gradient. The results are listed in tables 5.3-4. Since the curing ages of the specimens were not standardized, the ages are also noted.

### 5.3.3 Diffusion of Chloride

After an experiment for oxygen diffusion had been completed, the test disc was demounted and used for the measurement of chloride diffusivity. One exception was the 0.5 w/c OPC paste; where different samples were used for oxygen and chloride diffusion. Chloride diffusion experiment was carried out at 25°C in the same way as described in subsection 3.3.1, chapter 3. The high concentration side of the cell contained 1.0 M NaCl solution with calcium hydroxide suspension, while the low concentration side contained initially saturated calcium hydroxide solution. Chloride concentration on the low concentration side of the cell was determined as described in chapter 2. An example of the concentration-time curve is shown in figure 5.13. The chloride diffusivities were calculated as explained in chapter 4 are shown in tables 5.3-4.

**Table 5.3** Oxygen and chloride diffusivities in hydrated OPC pastes

| w/c | No. | Age (month) | $D_i[O_2]$ ($10^{-8}$) | $D_i[Cl^-]$ ($\times 10^{-8}$) | $\frac{D_i[O_2]}{D_i[Cl^-]}$ |
|---|---|---|---|---|---|
| 0.35 | 1 | 10 | 8.81 | 1.07 | 8.2 |
| | 2 | 10 | 8.94 | 0.90 | 9.9 |
| | 3 | 10 | 7.17 | —— | —— |
| (average) | | | 8.31 | 0.99 | 8.4 |
| 0.50 | 4 | 3 | 10.35 | | |
| | 5 | 3 | 11.19 | | |
| | 6 | 3 | 10.90 | | |
| | 7 | 3 | | 4.70 | |
| | 8 | 3 | | 5.48 | |
| | 9 | 3 | | 5.81 | |
| | 10 | 3 | | 5.84 | |
| (average) | | | 10.81 | 5.46 | 2.0 |
| 0.60 | 11 | 4 | 13.36 | 9.13 | 1.5 |
| | 12 | 4 | 12.81 | 6.62 | 1.9 |
| | 13 | 4 | 9.19 | 6.49 | 1.4 |
| | 14 | 4 | 13.00 | 6.86 | 1.9 |
| (average) | | | 12.09 | 7.28 | 1.7 |

**Table 5.4** Oxygen and chloride diffusivities in hydrated OPC/20%PFA pastes

| w/c | No. | Age (month) | $D_i[O_2]$ ($10^{-8}$) | $D_i[Cl^-]$ ($\times 10^{-8}$) | $\frac{D_i[O_2]}{D_i[Cl^-]}$ |
|---|---|---|---|---|---|
| 0.35 | 15 | 2.5 | 5.69 | 0.39 | 14.7 |
| | 16 | 4 | 2.05 | 0.55 | 3.7 |
| | 17 | 4 | 4.10 | 0.42 | 9.8 |
| (average) | | | 3.95 | 0.45 | 8.8 |
| 0.50 | 18 | 7 | 2.93 | 0.64 | 4.6 |
| | 19 | 7 | 3.87 | 0.87 | 4.4 |
| | 20 | 8 | 3.29 | 0.76 | 4.3 |
| | 21 | 8 | 8.12* | —— | —— |
| (average) | | | 3.36 | 0.76 | 4.4 |
| 0.60 | 22 | 6 | 10.56 | 3.38 | 3.1 |
| | 23 | 6 | 10.47 | 2.90 | 3.6 |
| | 24 | 7 | 10.13 | 3.32 | 3.1 |
| (average) | | | 10.39 | 3.20 | 3.2 |

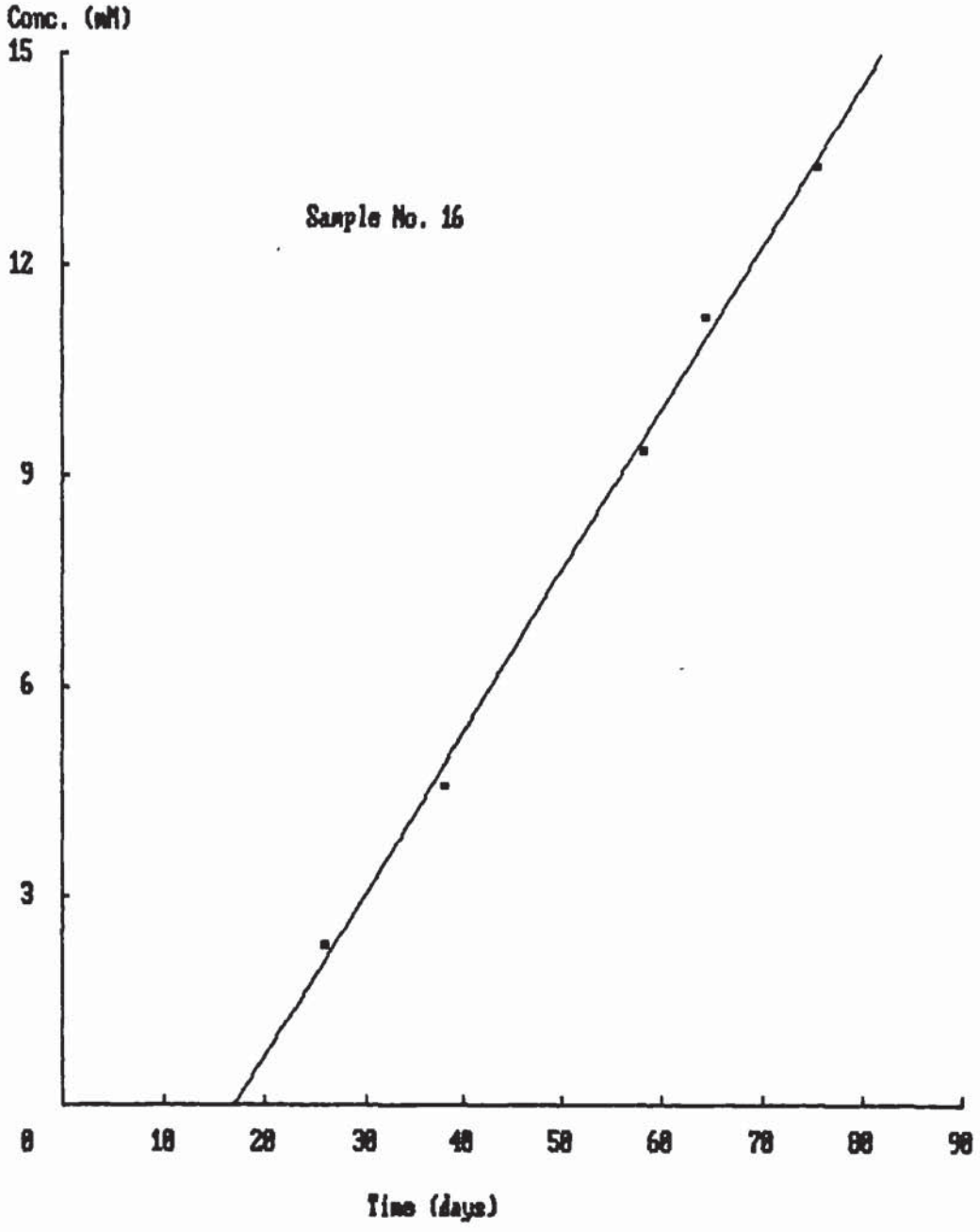


Figure 5.13 Rise of chloride concentration in the compartment 2 of the ionic diffusion cell

## 5.4 Discussion

It has been noted in subsection 5.3.1 that some difficulties associated with the effectiveness of reducing electro-chemically the diffused oxygen were encountered during the development of the technique. Before the reliability of the cell used to obtain the results shown in tables 5.3-4 was to be tested, it was thought that it might be increasingly difficult to consume the accumulated oxygen if the diffusion rate was getting higher. The cement slurry was vibrated for up to approximately 15 minutes in order to produce denser specimens than those used for the diffusion of quaternary ammonium ions. The samples were prepared in such ways, except for the 0.5 w/c OPC samples which were made in the same way as described in subsection 3.3.1.1, chapter 1.

It can been seen from tables 5.3 and 5.4 that chloride diffusivity decreased for both the OPC and OPC/20%PFA pastes as w/c ratio decreased. Comparing the chloride diffusivities obtained for the two types of binder prepared at the same w/c ratio, chloride diffused about 2 to 4 times faster in the OPC pastes than in the OPC/20%PFA pastes. One exception was observed with the 0.5 w/c pastes, where the OPC samples had about 8 times faster diffusion rates. This may be due to fact mentioned earlier that the 0.5 w/c OPC samples were prepared in a different way.

Tables 5.3 and 5.4 indicate that oxygen diffused generally slower as w/c ratio decreased. The oxygen diffusivities obtained for the 0.35 w/c PFA paste (samples 15 to 17) exhibit the greatest variation with individual specimen. By contrast to the 0.5 w/c PFA paste (samples 18 to 20), samples 15 and 17 showed higher oxygen diffusion rates, which may have been caused by the difference in their curing ages. Nevertheless, the chloride diffusivities obtained for samples 15 to 17 are reasonably close. As an experiment for chloride diffusion was carried out after that for oxygen diffusion using the same disc sample had been finished, there are some differences between the actual sample ages for the two types of diffusion experiment. It took about four months to complete one chloride diffusion experiment using the specimens of low diffusivity such as samples 15 to 17, while only less than one month was required for one oxygen diffusion experiment. With such a difference in the actual ages, it is probably unrealistic to compare the diffusivities of oxygen and chloride for samples 15 to 17. However, it is still apparent from tables 5.3 and 5.4 that oxygen diffused faster in the OPC pastes than in the PFA of the same w/c ratios.

It seems reasonable to assume that the interfacial layer between the bulk solution in a compartment of the diffusion cell and the specimen surface can yield only a small difference in concentrations of the two phases. Thus

the concentration gradients for the two species, which is related to the flux by Fick's first law, have been correctly calculated by dividing the concentration difference in the two compartments by the disc thickness. If both oxygen and chloride diffusion in hydrated cement pastes were controlled by the same factors, they would have diffused at similar relative rates as they do in water. It is seen from tables 5.3 and 5.4 that oxygen diffused evidently faster in both types of paste than chloride ions did in terms of the diffusivity.

The ratios of oxygen to chloride diffusivities, are also shown in tables 5.3 and 5.4. The ratio varies approximately from 1.2 to 8, depending mainly on the w/c ratio. They seem to decrease with the increase of w/c ratio, clearly for the OPC paste as w/c ratio increases from 0.35 to 0.5, and for the 20%PFA as w/c ratio increases from 0.5 to 0.6. As explained before, the ratios calculated for the 0.35 w/c PFA paste may be not reliable, but the real values would be expected not to be less than those found for the 0.5 w/c PFA paste.

The ratio of oxygen to chloride diffusivities, calculated from their average diffusivities, is plotted in figure 5.14 against the chloride diffusivity. It can be seen from this figure that the average ratio appears to decrease with the increase of chloride diffusivity. The solid line given in the figure is not intended to represent precisely the actual relationship, as it does not show any

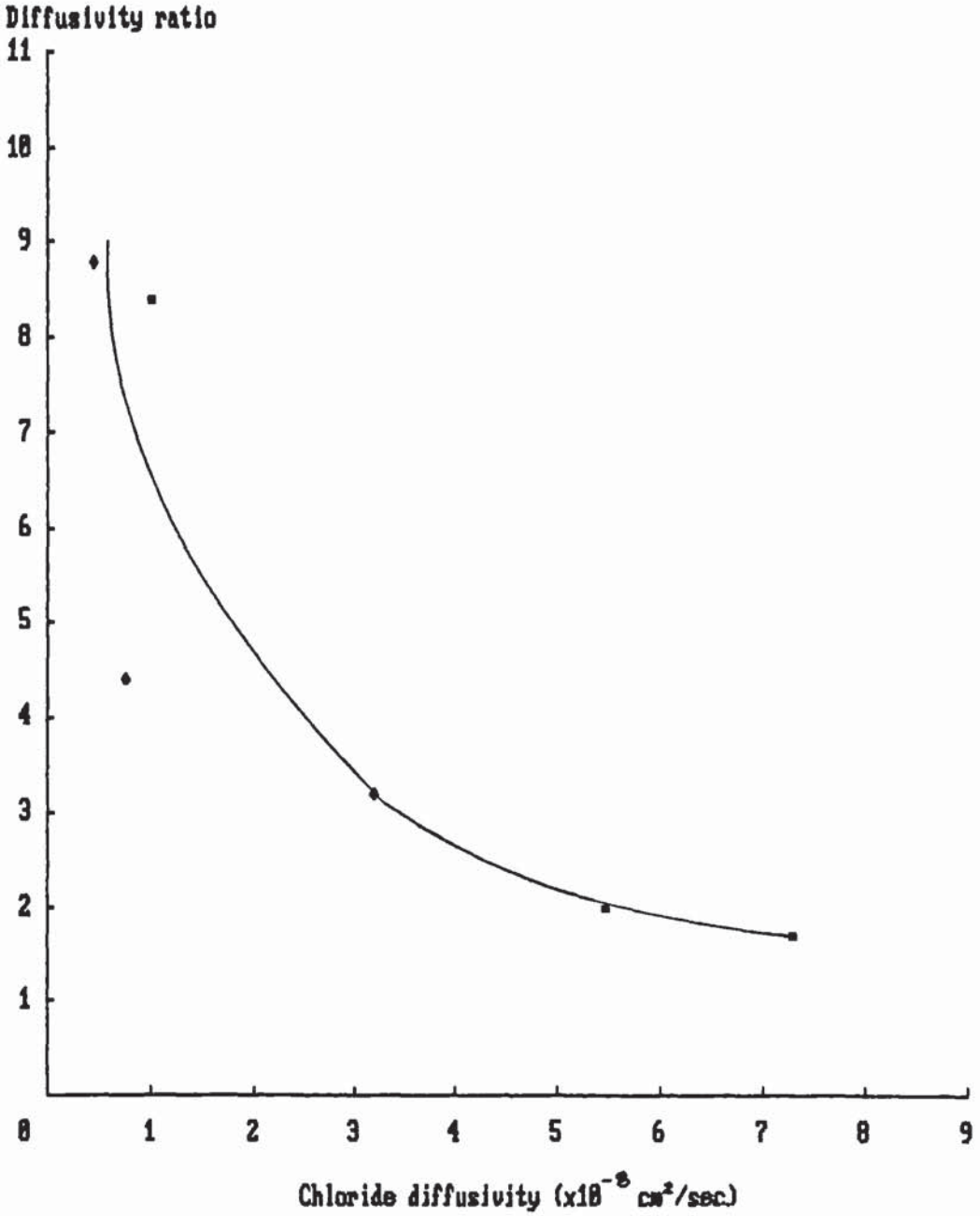


Figure 5.14 Decrease of the oxygen to chloride diffusivity ratio with the increase of chloride diffusivity

difference in the diffusion behaviours in the OPC and OPC/20%PFA pastes. Nevertheless, there is not enough evidence, because of the limited number of samples used, to show quantitatively any definite difference in this relationship between the two types of paste.

The above comparisons of the diffusivities of chloride and oxygen suggest that the rate-controlling factors of diffusion in both types of paste are not all the same for chloride as an anion and oxygen as a neutral molecule. Figure 5.14 indicates that if the w/c ratio increases from 0.6 further to be above certain values, the difference in oxygen and chloride diffusivities may become either stable or insignificant. However, the ratio of oxygen to chloride diffusivities can be as much as 4 to 8 for some dense pastes, namely the OPC paste of w/c 0.35 and the OPC/20%PFA pastes of w/c 0.35 and 0.50. This implies that there could be some fundamental differences in the mechanisms of chloride and oxygen diffusion, particularly in the dense pastes.

It can be seen that the diffusion of chloride appears to be retarded compared with the diffusion of oxygen. This could lead to two possible conclusions. In one, the retarded diffusion of chloride is caused directly by the surface charge effect, while in the other, there is a greater effective diffusion area for oxygen. The latter is actually saying that chloride and oxygen do not share all

of their diffusion paths and that oxygen can diffuse through more pores. However, as the two species diffuse at similar rates in dilute solutions, they should also have similar sizes in hydrated states. For chloride to have a smaller effective diffusion area, it must be repelled from some pores that contribute to the diffusion of oxygen. The separation of diffusion paths could be achieved only through the electrical field existing at the pore/solution interface which presumably repels chloride ions. Therefore, a smaller diffusion area for chloride compared with oxygen, if it exists, is primarily due to the effect of surface charge on chloride diffusion.

Although this work can not suggest any surface charge effect on oxygen diffusion, the relative degree of the surface charge effect on chloride diffusion can be estimated from the differences in oxygen and chloride diffusivities or diffusibilities. Therefore, surface charge plays a dominant part in determining the chloride diffusion rates in the dense pastes that showed relatively large ratios, varying approximately from four to eight, of oxygen to chloride diffusivities. The decrease of the oxygen to chloride diffusivity ratio with increase of w/c ratio also supports the suggestion made in the previous chapter that the surface charge of the micro and gel pores can affect ionic diffusion rates. Smaller oxygen to chloride diffusivity ratios observed for the 0.65 w/c pastes compared with dense pastes can be explained by the

relatively small fractions of micro and gel pores contributing to both oxygen and chloride diffusion in the 0.65 w/c pastes.

## 5.5 Conclusions

(1). Both oxygen and chloride diffused faster as the w/c ratio increased.

(2). In comparison with the diffusion kinetics in water, oxygen diffuses relatively faster than chloride in the OPC and OPC/20%PFA pastes.

(3). The ratio of oxygen to chloride diffusivities appears to decrease with the increase of chloride diffusivity or of w/c ratio for the OPC and OPC/20%PFA pastes. The relatively large values of the ratio for most of the dense pastes suggest that a surface charge effect tends to dominate chloride diffusion in dense pastes.

(4). The OPC/20%PFA paste showed lower values of oxygen and chloride diffusivities than the OPC paste of same w/c ratio. However, the results obtained in this study are insufficient to conclude any definite difference in the diffusion mechanisms in the two types of paste.

# CHAPTER 6 MODELLING OF IONIC DIFFUSION

## 6.1 Introduction

To describe ionic diffusion processes in cementitious materials in terms of the concentration distribution with time and distance or depth, it is necessary to consider two important aspects:

(1). Kinetics of diffusion, which determines the flux from the driving forces.

(2). Chemical reactions between the migrating ions and the cement-matrix.

Based on the mass balance in a bulk volume of hydrated cement paste, the mathematical expression for the relationship between the kinetics and the reactions is derived in appendix 2 for an individual ion diffusing unidirectionally:

$$C_t(x,t) + S_t(x,t)/W = -J_x(x,t)/\epsilon \quad \ldots\ldots (6.1)$$

where C is the concentration, S is the amount of the ions combined into the solid phases of the cement-matrix, J is the flux per bulk section area of the paste, W is the content of the pore solution in which diffusion occurs, and $\epsilon$ is the volume fraction of the W and expressed on bulk volume of the paste.

Non-steady state diffusion in hydrated OPC pastes was studied in this work based on the above mass balance equation with the aid of computer-modelling. The experimental data used for the modelling were obtained by

Sergi[64] whose experiments are described in next subsection.

Fick's first law has been commonly employed to describe diffusion in hydrated cement pastes and concrete[17-24]. However, it has been shown in section 1.1, chapter 1, that Fick's first law does not explicitly consider the effects of ionic interactions on diffusion in electrolytes. Ionic diffusion in hydrated cement pastes is a multi-component process. It is likely that diffusion of one ion can affect diffusion of the other ions. In order to show some characteristics of a multi-component diffusion process, diffusion in dilute aqueous electrolytes will be considered in subsection 6.1.2. As mentioned in chapter 1, the Nernst-Planck equation 1.2 can describe the diffusion flux in dilute electrolytes very accurately. In subsection 6.1.2, comparisons between the concentration profiles predicted by Fick's first law and the Nernst-Planck equation will be made with some examples, and the implication for the description of ionic diffusion in hydrated cement pastes will be discussed in subsection 6.1.3 and section 6.8.

### 6.1.1 Diffusion in hydrated cement pastes

An obvious way of studying non-steady state diffusion is by exposing only one flat surface of a uniform test sample to a solution usually maintained at a constant composition with time. The distributions of the investigated ionic

species at increasing depth are determined at a certain length of diffusion time. Non-steady diffusion experiments were made as long ago as 1952 by Spinks et al[108]. Their cylindrical specimens, with sides coated with paraffin wax but ends left bare, were exposed to several salt solutions. After diffusion had proceeded for a certain time, the profiles of concentration against penetration depth for several ions were determined by radioactive tracer measurements. They showed that the concentration distributions can be interpolated by the mathematical solutions of Fick's second law. This enabled them to calculate the effective diffusivities.

Non-steady state diffusion technique has been extensively employed by a number of researchers[109-113] to study the mechanisms of chloride penetration into hydrated cement pastes and concrete, These studies showed that the total and free chloride penetration profiles for a particular diffusion time can be, in general, well approximated by Fick's second law.

Diffusion experiments were carried out by Sergi[64] at Aston University using cylindrical 0.5 w/c OPC specimens, 4.9 cm in diameter. The specimens were prepared in a similar way as described in paragraph 3.3.1.1, chapter 3. Three types of experiment were carried out at the controlled temperature of either 22 or 25 °C.

One experiment involved measuring the chloride ingress in

a hydrated OPC paste cured for 3 months. The specimens were trimmed to give a length of approximately 6.65 cm, and sealed with paraffin wax as done by Spinks et al[108]. They were, in groups of 12, placed horizontally into a sealed container filled with 5 litres of 1M NaCl solution saturated with calcium hydroxide. After 100 days' exposure, one set of specimens were sliced at a 0.7cm interval of depth. A second set were first cut at a depth of 0.35 cm followed by a series of slices at 0.7 cm intervals. Slices of the same depth were grouped together, and the pore solutions were extracted by a pore-expression device. The hydroxyl and chloride concentrations of the solution were finally analyzed. A third set of specimens were cut in the manner described to produce samples for evaporable water and total chloride analysis. Assuming that chloride was distributed uniformly in the evaporable water at the concentration determined from the extracted pore solution, the bound chloride contents based on weight of the unhydrated cement were calculated. Both free and total chloride contents were found to be reasonably well approximated by Fick's second law. This experiment is referred to in this chapter as the "NaCl ingress" test, and the data obtained are shown in table 6.1.

In another experiment, well characterised OPC paste specimens with NaCl addition and a curing period of one year were, in groups of 12, exposed to 5 litres of deionised water. The water was then refreshed occasionally

so that its pH was not allowed to rise above 12. The ionic concentrations in the external solution were determined during a diffusion period of 150 days. It was found that the total amount of the leached ions increased linearly with the square root of time, with almost zero intercept at zero value of time for sodium and potassium but not for chloride and hydroxyl ions. The ionic profiles at 165 days were also determined. It was shown by the measurements of pore size distribution that dissolution of some hydrate phases during diffusion occurred near the exposed surface, approximately within 0.35 cm from the surface. This experiment is referred to in this chapter as the "diffusion-out" test, and the experimental data are given in tables 6.2 and 6.3.

With the experimental arrangements described above, ionic diffusion was initiated by the difference in compositions of the bulk and pore solutions. Joining a chloride and sodium rich OPC paste cylinder to a chloride-free one by a thin layer of fresh OPC slurry, Sergi[64] obtained the concentration profiles within the two cylinders at the diffusion time of 225 days. The specimens had a curing age of 3 months. Sodium ions appeared to diffuse according to Fick's second law, while diffusion of hydroxyl and chloride ions was complicated by their interactions with the cement matrix. This experiment is referred to in this chapter as the "diffusion-within" test, and the experimental data for chloride and sodium are summarised

**Table 6.1** Profiles obtained from the "NaCl-ingress" test

| depth x (cm) | $C[Cl^-]$ (M) | $C[OH^-]$ (M) | We (%) | Tot. $Cl^-$ (mmol/g) |
|---|---|---|---|---|
| 0.000 | 1.0 | | | |
| 0.175 | 0.991* | 0.104 | 39.03 | 0.660 |
| 0.350 | 0.838 | 0.112 | 32.12 | 0.599 |
| 0.700 | 0.670 | 0.134 | 30.18 | 0.438* |
| 1.050 | 0.572 | 0.171 | 30.94 | 0.424 |
| 1.400 | 0.366 | 0.219 | 29.32 | 0.345 |
| 1.750 | 0.292 | 0.257 | 30.46 | 0.182* |
| 2.100 | 0.135 | 0.274 | 29.89 | 0.199 |
| 2.450 | 0.059 | 0.319 | 29.84 | 0.108* |
| 2.800 | 0.039 | 0.335 | 33.04 | 0.078 |
| 3.150 | 0.024 | 0.351 | 28.63 | 0.017* |
| 3.500 | 0.014 | 0.364 | 29.90 | 0.031 |
| 3.850 | 0.015 | 0.355 | 27.53 | 0.002* |
| 4.200 | 0.007 | 0.375 | 28.57 | 0.004* |
| 4.550 | 0.002 | 0.388 | 27.25 | 0.002* |
| 4.900 | 0.001 | 0.384 | 28.89 | 0.004* |
| (average) | | | 29.7 | |

*: not considered in calculations
average Wn=18.9%

**Table 6.2** Profiles obtained from the "diffusion-out" test

| x (cm) | C[$Na^+$] (M) | C[$K^+$] (M) | C[$Cl^-$] (M) | C[$OH^-$] (M) | We (%) | Tot.[$Cl^-$] (mmol/g) |
|---|---|---|---|---|---|---|
| 0.000 | | | | | | 0.033 |
| 0.175 | 0.058 | 0.018 | 0.014 | 0.075 | 39.69 | 0.150 |
| 0.350 | 0.122 | 0.035 | 0.032 | 0.136 | 38.36 | 0.161 |
| 0.700 | 0.248 | 0.073 | 0.067 | 0.246 | 36.38 | 0.189 |
| 1.050 | 0.356* | 0.104 | 0.102 | 0.326 | 34.88 | 0.211 |
| 1.400 | 0.394 | 0.120 | 0.119 | 0.351 | 35.67 | 0.212 |
| 1.750 | 0.469 | 0.140 | 0.157 | 0.409 | 35.59 | 0.228 |
| 2.100 | 0.496 | 0.164 | 0.168 | 0.444 | 35.20 | 0.230 |
| 2.450 | 0.551 | 0.177 | 0.192 | 0.463 | 34.31 | 0.232 |
| 2.800 | 0.550 | 0.188 | 0.191 | 0.480 | 35.80 | 0.235 |
| 3.150 | 0.599 | 0.201 | 0.215 | 0.514 | 35.32 | 0.247 |
| 3.500 | 0.592 | 0.211 | 0.210 | 0.516 | 35.04 | 0.238 |
| 3.850 | 0.589* | 0.203* | 0.215 | 0.527 | 34.77 | 0.253 |
| 4.200 | 0.629 | 0.226 | 0.228 | 0.535 | 35.65 | 0.249 |
| 4.550 | 0.626 | 0.221 | 0.232 | 0.531 | 35.29 | 0.256 |
| 4.900 | 0.636 | 0.232 | 0.230 | 0.539 | 35.08 | 0.252 |
| 5.250 | 0.648 | 0.229 | 0.241 | 0.534 | 35.81 | 0.249 |
| 5.600 | 0.643 | 0.241 | 0.231 | 0.543 | 35.52 | 0.243 |
| 5.950 | 0.659 | 0.238 | 0.247 | 0.542 | 35.66 | 0.250 |
| (Av.) | | | | | 35.78 | |

*: not considered in calculations
average Wn=19.64%

Table 6.3 Accumulative concentrations in the external solution ("diffusion-out" test)

| $t_p$ (days) | $[Na^+]$ (mM) | $[K^+]$ (mM) | $[Cl^-]$ (mM) | $[OH^-]$ (mM) |
|---|---|---|---|---|
| 5 | 2.60 | 1.39 | 0.69 | 10.60 |
| 6 | 2.87 | 1.40 | 0.79 | 11.25 |
| 7 | 3.44 | 1.65 | 0.82 | 12.15 |
| 8 | 3.64 | 1.76 | 0.89 | 14.15 |
| 11 | 4.23 | 2.08 | 1.05 | 17.30 |
| 12 | 4.42 | 2.14 | 1.10 | 18.13 |
| 13 | 4.59 | 2.23 | 1.17 | 19.05 |
| 18 | 5.08 | 2.41 | 1.40 | 22.17 |
| 20 | 5.35 | 2.53 | 1.49 | 24.75 |
| 22 | 5.61 | 2.64 | 1.57 | 26.22 |
| 29 | 6.42 | 3.01 | 1.82 | 29.97 |
| 43 | 7.87 | 3.67 | 2.25 | 37.45 |
| 53 | 8.82 | 4.07 | 2.53 | 42.90 |
| 61 | 9.42 | 4.38 | 2.74 | 45.33 |
| 77 | 10.70 | 4.98 | 3.16 | 52.16 |
| 95 | 11.92 | 5.55 | 3.51 | 58.36 |
| 105 | 12.65 | 5.87 | 3.71 | 62.49 |
| 112 | 13.08 | 6.08 | 3.85 | 64.09 |
| 132 | 14.26 | 6.63 | 4.18 | 69.69 |
| 150 | 15.27 | 7.08 | 4.44 | 74.54 |

**Table 6.4(a)** Profiles at x<0 obtained from the "diffusion-within" test

| depth x (cm) | C[$Na^+$] (M) | C[$Cl^-$] (M) | We (%) | Tot. $Cl^-$ (mmol/g) |
|---|---|---|---|---|
| -0.350 | 0.906 | 0.562 | 26.60* | 0.326 |
| -0.700 | 1.140 | 0.688 | | 0.443 |
| -1.050 | 1.250 | 0.777 | 30.43 | 0.364 |
| -1.400 | 1.343 | 0.855 | | 0.404 |
| -1.750 | 1.345 | 0.900 | 32.07 | 0.436 |
| -2.100 | 1.375 | 0.920 | | 0.453 |
| -2.450 | 1.438 | 0.954 | 31.63 | 0.458 |
| -2.800 | 1.435 | 0.992 | | 0.451 |
| -3.150 | 1.375 | 0.980 | 32.03 | 0.433 |
| -3.500 | 1.435 | 0.998 | | 0.507 |
| -3.850 | 1.375 | 0.991 | 31.55 | 0.452 |
| -4.200 | 1.405 | 0.986 | | 0.491 |
| -4.550 | 1.475 | 1.010 | 31.89 | 0.473 |
| -4.900 | 1.435 | 1.001 | | 0.465 |
| -5.250 | 1.410 | 1.002 | 33.06* | 0.503 |
| -5.600 | 1.405 | 1.005 | | 0.513 |
| -5.950 | 1.438 | | | |
| (average) | | | 31.6 | |

*: not considered in calculations
average Wn=19.9%

**Table 6.4**(b) Profiles at x>0 obtained from the "diffusion-within" test

| depth x (cm) | C[$Na^+$] (M) | C[$Cl^-$] (M) | We (%) | Tot. $Cl^-$ (mmol/g) |
|---|---|---|---|---|
| 0.350 | 0.570 | 0.185* | 25.61 | 0.172* |
| 0.700 | 0.433 | 0.115 | | 0.113 |
| 1.050 | 0.328 | 0.037 | 26.13 | 0.073 |
| 1.400 | 0.270 | 0.022 | | 0.024 |
| 1.750 | 0.205 | 0.004 | 16.15 | 0.015 |
| 2.100 | 0.171 | 0.001 | | 0.010* |
| 2.450 | 0.143 | 0.001 | 26.19 | 0.003* |
| 2.800 | 0.135 | 0.001 | | 0.003* |
| 3.150 | 0.105 | 0.001 | 25.45 | 0.002* |
| 3.500 | 0.120 | 0.001 | | |
| 3.850 | 0.105 | 0.002 | 25.42 | |
| 4.200 | 0.120 | 0.001 | | |
| 4.550 | 0.114 | 0.003 | 24.51* | |
| 4.900 | 0.120 | 0.001 | | |
| 5.250 | 0.114 | 0.003 | | |
| 5.600 | 0.120 | 0.001 | | |
| 5.950 | 0.111 | 0.002 | | |
| (average) | | | 26.0 | |

*: no considered in calculations
average Wn=20.8%

in table 6.4.

### 6.1.2 Effects of electrostatic interactions on diffusion in aqueous dilute electrolytes

#### 6.1.2.1 The electrostatic interactions

It has been shown in section 1.2, chapter 1, that the Nernst-Planck equation:

$$J = -D_O[C_x(x,t) + zeCE_x(x,t)/(kT)] \quad \ldots\ldots (6.2)$$

can be used to describe the flux by a characteristic value, the absolute diffusivity $D_O$, where C is the concentration, and E is the electrical potential. This equation can describe diffusion of each ion accurately[6,10-13], provided the electrolyte is very dilute.

As mentioned in chapter 1, an internal electrical field can be automatically created to maintain the charge balance if the diffusing ions in an electrolyte have different absolute mobilities. The charge balance can be expressed by

$$\Sigma(zC)=0 \quad \ldots\ldots (6.3a)$$

$$\Sigma(zJ)=0 \quad \ldots\ldots (6.3b)$$

By combining the above two equations with the Nernst-Planck equation 6.2, the gradient of the electrical potential can be obtained[11]:

$$eE_x(x,t)/(kT) = -\Sigma[zD_OC_x(x,t)]/\Sigma[z^2D_OC_x(x,t)] \ldots\ldots (6.4)$$

The flux for each ion can be obtained by incorporating

equation 6.4 into the Nernst-Planck equation. Therefore, it can be seen that the flux for one ion can be dependent on its concentration. The diffusion rate for one ion can also be affected by the concentrations and charges of the other ions. As Fick's first law has been commonly employed and was considered in this work to describe diffusion in hydrated cement pastes. it will be compared with the Nernst-Planck equation in the following two paragraphs.

6.1.2.2 Diffusion in 1-1 electrolytes

The Fickian diffusivity defined by Fick's first law can be derived from the Nernst-Planck equation to be[6,11,15]

$$D_+=D_-= 2D_{O+}D_{O-}/(D_{O+} + D_{O-}) \quad \ldots\ldots (6.5)$$

for a single 1-1 electrolyte, where the (subscript) minus and plus signs are for the anion and cation respectively. This shows that both the cation and the anion can be exactly described by Fick's first law.

As can be seen from the above equation, it is the slow ion, normally the cation, that dominates the overall diffusion rate[6]. To show this, the following four ions will be considered as examples, and their absolute diffusivities ($\times 10^{-5}$ $cm^2/sec$) at infinite dilutions (see table 1.1) can be be used:

$Na^+$: 1.33, $(C_5H_{11})_4N^+$: 0.465

$Cl^-$: 2.03, $OH^-$: 5.30

The Fickian diffusivities calculated from equation 6.5 for their solutions are shown in table 6.5. Compared with the

Table 6.5 Diffusivities in dilute 1-1 electrolytes

| Solution | D ($\times 10^{-5}$ $cm^2/sec$) |
|---|---|
| NaCl | 1.61 |
| NaOH | 2.13 |
| $(C_5H_{11})_4NCl$ | 0.76 |
| $(C_5H_{11})_4NOH$ | 0.85 |

absolute diffusivity, the Fickian diffusivity in the solution is smaller for anions but greater for cations. In the $(C_5H_{11})_4NOH$ solution, the Fickian diffusivity for the hydroxyl ion is only about one-sixth of the absolute diffusivity, suggesting that the $OH^-$ ion diffusion rate is greatly affected by the slow cation, although the $(C_5H_{11})_4N^+$ ion diffuses twice faster than it does at infinite dilutions.

6.1.2.3 Diffusion in mixed electrolytes

The electrostatic interactions between ions in a mixed electrolytes are much more complex than those in a single electrolyte[12]. To show the complexity of the electrostatic interactions and more importantly, to see if Fick's first law with a constant diffusivity can be practically used to describe diffusion in mixed electrolytes, three examples concerning diffusion in mixed electrolytes were considered and are described below.

Diffusion in mixed electrolytes associated with the four

ions mentioned in the previous paragraph were modelled with the following calculation steps:

(1). The ions involved were supposed to diffuse into or out of an initially homogeneous solution contained in a tube of length 6.3 cm.

(2) The ionic concentration at the opening (x=0) of the tube, i.e. the "surface concentration", was kept constant.

(3). The Nernst-Planck equation 6.2 was used to calculate numerically the concentration profiles at the diffusion time of 0.6 day. The absolute diffusivities shown in the previous paragraph were used for the calculation.

(4). The concentration data obtained as described above were then used to obtain the best-fitted Fickian diffusivities (D's) by interpolating them with Fick's second law[8]

$$C_t(x,t) = DC_{xx}(x,t) \qquad \ldots\ldots (6.6)$$

The final calculation step will be described in section 6.4. The concentration profile calculated by Fick's second law with the diffusivity (D) obtained from the final step is thus the best approximation to the theoretical profile obtained with the third step. It was noted that the Fickian diffusivities obtained can vary with the diffusion time assumed for the calculation. However, this variation is not significant for all the three examples considered if the assumed value of diffusion time is not too high.

The first example is the diffusion in a $Na^+$-$Cl^-$-$OH^-$ solution. The surface and initial concentrations assumed are shown in table 6.6. The diffusivities obtained from Fick's second law are also included in this table.

The concentration profiles calculated by the Nernst-Planck equation are plotted in figure 6.1 as squares, while those by Fick's second law are shown as solid lines. It can be seen from figure 6.1 that the concentration profiles of all the three ions can be well interpolated by Fick's second law. The Fickian diffusivity obtained for each ion is very close to its absolute diffusivity, suggesting that the electrostatic interactions between the ions do not affect the overall diffusion rate strongly. However, some effects of the interactions can be seen from the chloride and hydroxyl concentration profiles at a certain distance away from the surface, as the diffusion of the two ions is through an "ion-exchange" process.

The second example shown in figure 6.2 and table 6.7 is the diffusion in a $(C_5H_{11})_4N^+$-$Cl^-$-$OH^-$ solution. The assumed surface and initial concentrations are the same as those for the first example, except that sodium is replaced by $(C_5H_{11})_4N^+$. The $(C_5H_{11})_4N^+$ concentration profile calculated from the Nernst-Planck equation can also be accurately approximated by Fick's second law with the diffusivity $0.63 \times 10^{-5}$ $cm^2/sec$. As this value is greater than the absolute diffusivity $0.47 \times 10^{-5}$ $cm^2/sec$,

**Table 6.6** Diffusivities calculated at assumed values of surface and initial concentrations in the $Na^+$-$Cl^-$-$OH^-$ solution (example 1)

| IONS | $C_s$ (M) | $C_i$ (M) | D ($\times 10^{-5}$ $cm^2$/sec) |
|---|---|---|---|
| $Na^+$ | 0.023 | 0.010 | 1.26 |
| $Cl^-$ | 0.020 | 0.000 | 2.09 |
| $OH^-$ | 0.003 | **0.010** | 4.57 |

**Table 6.7** Diffusivities calculated at assumed values of $C_s$ and $C_i$ in the $(C_5H_{11})_4N^+$-$Cl^-$-$OH^-$ solution (example 2)

| IONS | $C_s$ (M) | $C_i$ (M) | D ($\times 10^{-5}$ $cm^2$/sec) |
|---|---|---|---|
| $N(C_5H_{11})_4^+$ | 0.023 | 0.010 | 0.63 |
| $Cl^-$ | 0.020 | 0.000 | 1.65 |
| $OH^-$ | 0.003 | **0.010** | 5.25 |

**Table 6.8** Diffusivities calculated at assumed values of $C_s$ and $C_i$ in the $(C_5H_{11})_4N^+$-$Cl^-$-$OH^-$ solution (example 3)

| IONS | $C_s$ (M) | $C_i$ (M) | D ($\times 10^{-5}$ $cm^2$/sec) |
|---|---|---|---|
| $N(C_5H_{11})_4^+$ | 0.020 | 0.002 | 0.79 |
| $Cl^-$ | 0.010 | 0.000 | 0.83 |
| $OH^-$ | 0.010 | 0.002 | 0.75 |

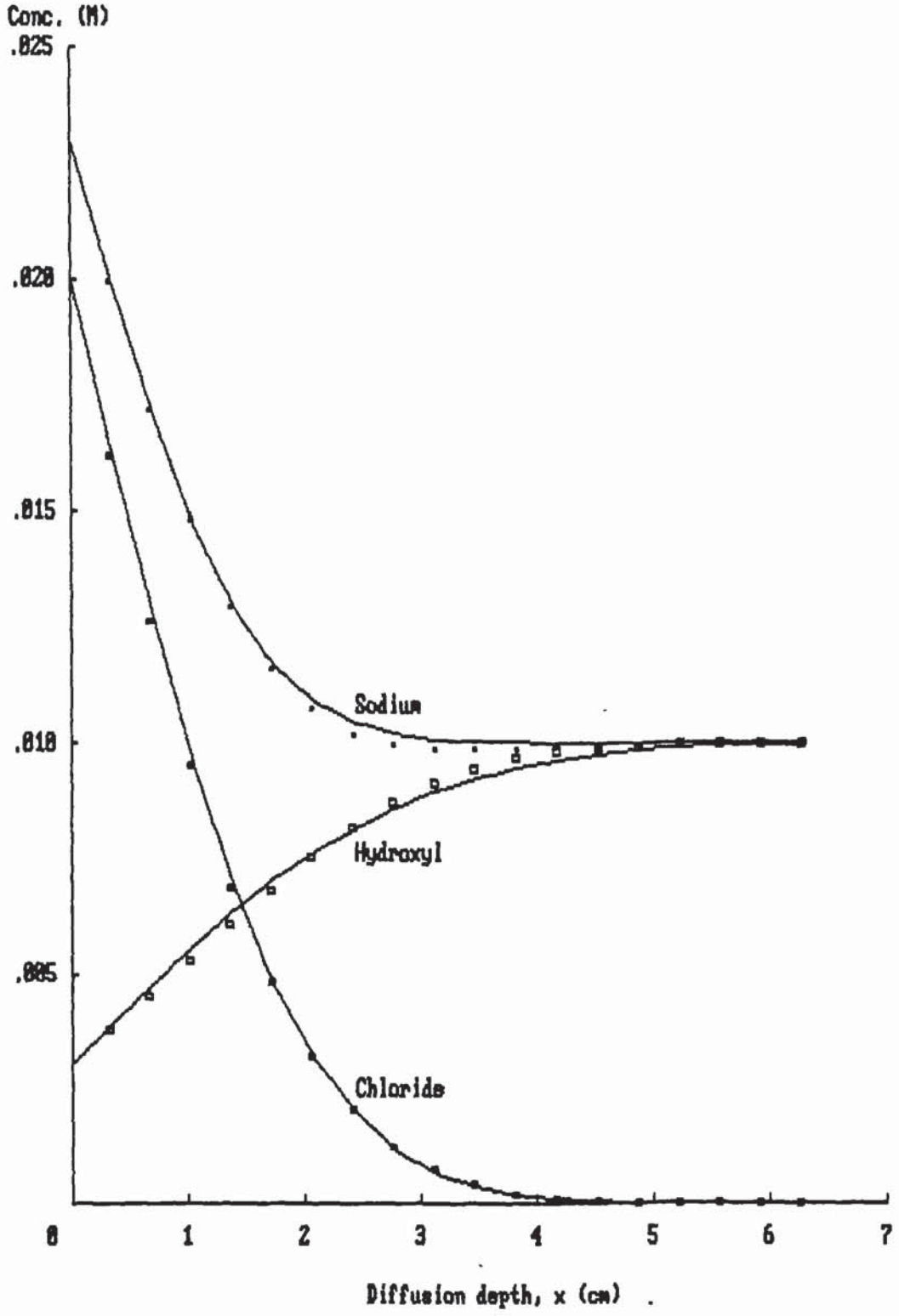


Figure 6.1 Concentration profiles at 0.6 days for NaOH and NaCl diffusion (example 1)

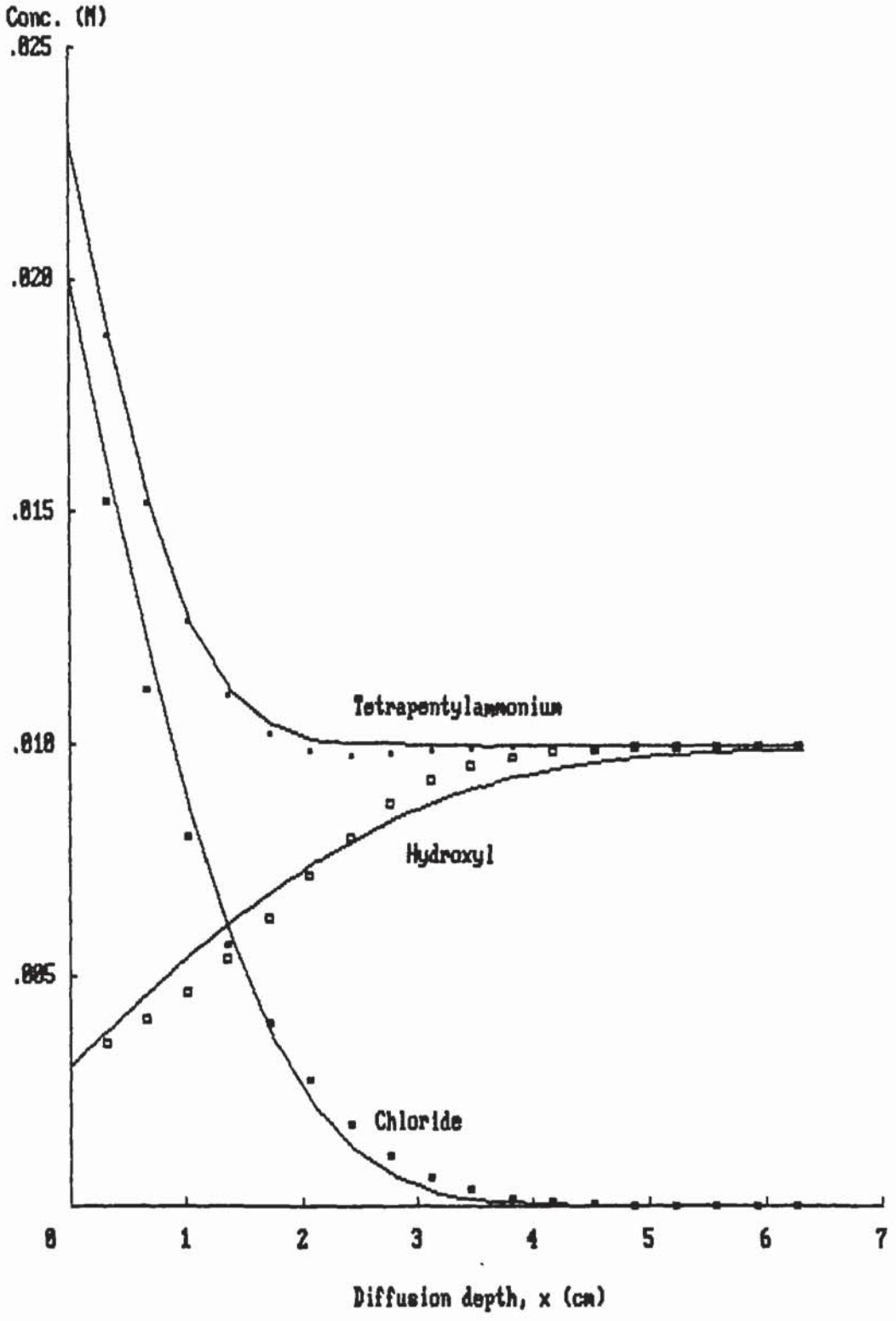


Figure 6.2 Concentration profiles at 0.6 days for $(C_5H_{11})_4NOH$ and $(C_5H_{11})_4NCl$ diffusion (example 2)

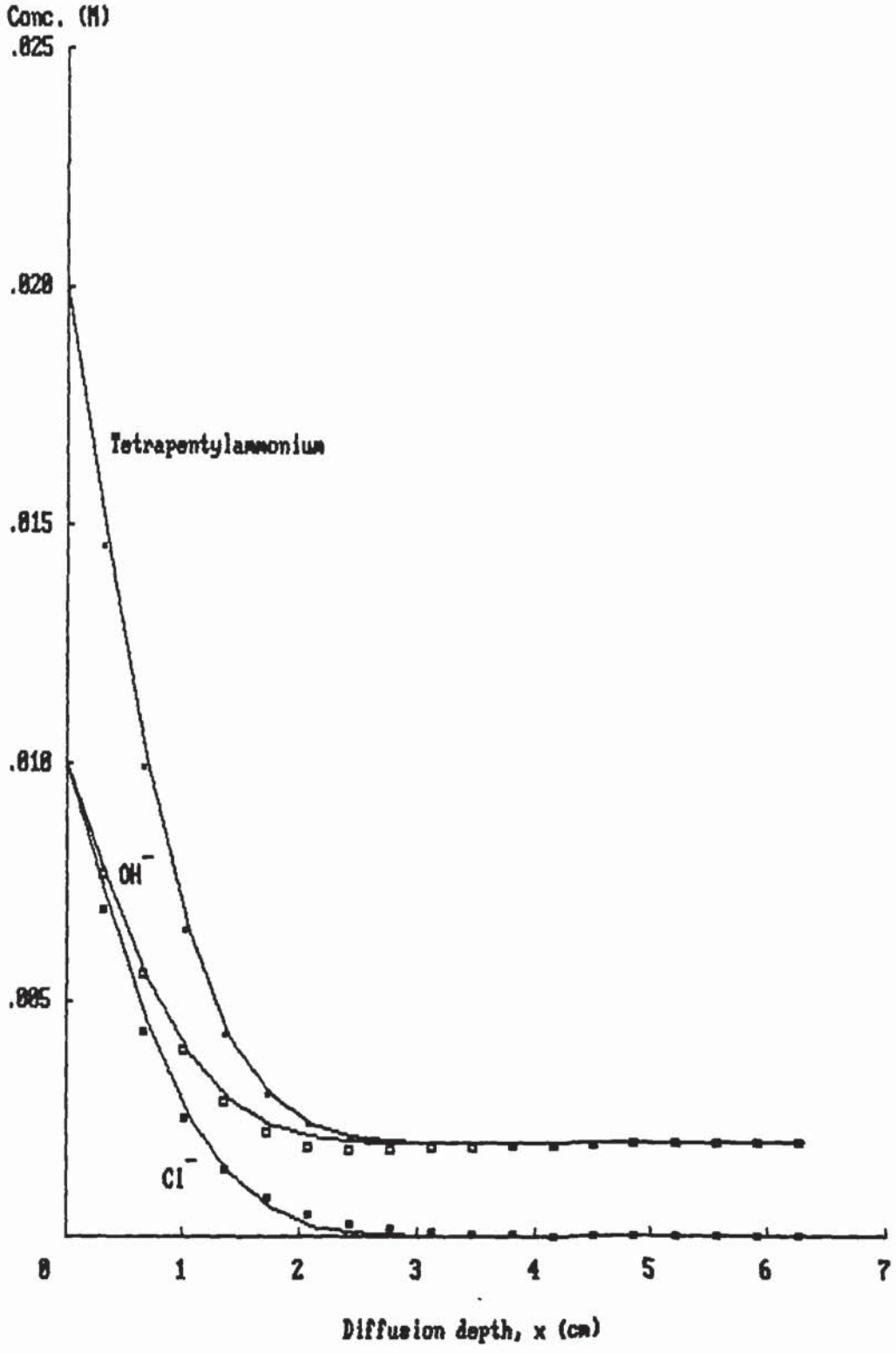


Figure 6.3 Concentration profiles at 0.6 days for $(C_5H_{11})_4NOH$ and $(C_5H_{11})_4NCl$ diffusion (example 3)

$(C_5H_{11})_4N^+$ diffusion is therefore accelerated through the electrostatic interactions. The interpolation by Fick's second law appears to be reasonably good for chloride, but not good for hydroxyl ions.

By comparing the hydroxyl concentrations shown in figure 6.2 for the second example with those in figure 6.1 for the first example, it can be seen that hydroxyl ions appear to diffuse faster near the surface in the second system. With regard to the Fickian diffusion behaviours represented by the solid lines in figure 6.2 for chloride and hydroxyl ions, hydroxyl ion diffuses obviously faster near the surface than it does at certain distances away from the surface, while the opposite is shown for chloride.

The final example demonstrates a very strong effect of the electrical field created on the diffusion of chloride and hydroxyl ions in another $(C_5H_{11})_4N^+$-$Cl^-$-$OH^-$ solution (see table 6.8). The concentration profiles are shown in figure 6.3. It can be seen from this figure that Fick's second law can describe quite accurately the concentration distributions of all the three ions. However, all the ions appear to diffuse at approximately the same rates in terms of their Fickian diffusivities obtained. In comparison with the results obtained for the first two examples, diffusion of hydroxyl and chloride ions is thus retarded considerably by the slow cation in the final example system.

### 6.1.3 Scope of study

The "thin-disc" method described in chapter 3 has been widely employed normally to study diffusion of individual ions[17-24]. Fick's first law has been used to characterize the flux obtained experimentally by the intrinsic Fickian diffusivity. It has been shown in the previous subsection that Fick's laws with appropriate Fickian diffusivities can describe quite accurately the diffusion of all the ions involved in the systems considered for the examples shown in figures 6.1 and 6.3. However, they can not describe the diffusion of chloride and hydroxyl ions as accurately as that of the $(C_5H_{11})_4N^+$ ions for the example shown in figure 6.2. To model and predict the diffusion processes in cement-based materials, it is therefore important to know diffusion of which ion can be approximately described by Fick's first law with a constant diffusivity.

As suggested by the mass balance equation 6.1, diffusion can be affected by the ionic binding. The binding behaviours for each ion, particularly for chloride, are considered in the next section. Numerical analyses applied to the experimental data obtained by Sergi whose diffusion experiments have been described previously were carried out to examine the diffusion behaviours of individual ions. The approaches used are similar to those described in the previous subsection, more specifically, to obtain a best-fitted Fickian diffusivity for a particular

concentration profile. The concentration profile computed with this diffusivity is thus the best fit to the experimental data. Goodness of the fit could reveal the actual diffusion kinetics and thus provide the basis for general modelling and prediction. The results are presented in sections 6.5 to 6.7. In each of these sections, one type of ion is considered, and a summary of the results is given for a particular diffusion experiment. Based on the comparative studies of diffusion behaviours for sodium, potassium, chloride and hydroxyl ions, a model concerning the prediction of diffusion processes in hydrated OPC pastes is presented and discussed in section 6.8.

## 6.2 Ionic Binding

### 6.2.1 Sodium and potassium

It is common knowledge that sodium and potassium ions are released from cement minerals into the pore fluid during the early stage of cement hydration. It is suggested in the literature[114,115] that during the later stages of cement hydration this process may almost stop or even be reversed, depending on the type of binder and the chemical environments.

Diamond[114] showed that the concentrations of sodium and potassium ions in the pore solution of OPC pastes can reach steady values after a few days' hydration. Page and

Vennesland[115] found that there is no obvious increase of sodium and potassium concentrations in the pore solution of the OPC paste cured from 8 to 12 weeks, but for the OPC paste blended with microsilica there are continuous reductions of the concentrations in the pore solution from 1 up to 12 weeks.

Experimental studies[116,117] seem to indicate that the C-S-H gel with a low C/S molar ratio is able to incorporate alkalis, in particular potassium ions. Partial removal of alkali ions from the pore solution would also occur as a result of some chemical processes, for example, alkali-silica reaction[118]. As this chapter is concerned mainly with diffusion in relatively mature OPC paste in experimentally controlled chemical environments, further adsorption or desorption of the two ions during diffusion was assumed to be negligible, which will be justified in section 6.5.

### 6.2.2 Chloride

By studying the kinetics of chloride penetration into a hydrated OPC paste exposed to a chloride solution, Traetteberg[109] observed the formation of chloro-aluminate, i.e. Friedel's salt. The author believed that this product was formed by transformation of ettringite accompanied by precipitation of calcium sulphate.

Studies[110,111,119] carried out by some other researchers

confirmed the reactions between chloride ions and the aluminate phase in the cement-matrix, but suggested that Friedel's salt is not formed at the expense of aluminate hydrates, but only by reaction with anhydrous $C_3A$. This reaction has an idealized form

$$3C_3A + 2Cl^- + 10H_2O + Ca(OH)_2 \rightarrow 3C_3A.CaCl_2.10H_2O + 2OH^-$$

Binding of chloride is probably accompanied by the release of hydroxyl ions[120], as indicated by the above equation. It is also possible that the accompanying release of sulphate ions may occur[121], since this reaction has not been sufficiently understood to eliminate the possible effect of sulphate ions on chloride-binding. It is thus likely that bound chloride is determined not only by chloride concentration, but also by the concentration of hydroxyl or sulphate ions in the pore solution.

In order to see the effect of ionic binding on diffusion, the mass balance equation 6.1 suggests that it is necessary to know the change of the binding rate with free chloride or time. Pereira and Hegedus[122] showed by experimental studies that binding of chloride during diffusion can be treated as an instantaneous reaction characterized by the Langmuir isotherm of adsorption. Page and Sergi[39] also used Langmuir's adsorption theory in the preliminary modelling of chloride diffusion.

According to Langmuir's theory, the amount of the equilibrium chemi-sorption is related to the bulk

concentration C by[123]

$$s=K_1C/(1+K_2C) \quad \ldots\ldots \quad (6.7a)$$

or

$$K_1C/s=1+K_2C \quad \ldots\ldots \quad (6.7b)$$

where $K_1$ and $K_2$ in appropriate units are constant, and s is expressed as a function of the concentration C only. Chloride-binding was assumed in this work to be a very fast process compared with diffusion, and the above relationship between C and s was used.

Page[124] at Aston University carried out statistical analysis to a large quantity of data obtained from several types of concrete made from OPC. For a small amount of the total chloride added, most of the chloride is in combined form, whilst for a large amount of total chloride, the relationship between the total and free chloride contents is linear. It appears there is a gradual saturation of binding sites as total chloride increases. Such a behaviour is in qualitative agreement with the Langmuir adsorption isotherm.

Tutti[125] reported that bound chloride was approximately proportional to chloride concentration in the pore solution. However, an assumed linear relationship between the C and s, obtained by a regression analysis, often gives a finite value of s at C=0. Langmuir's equation 6.7 was therefore used in the present work. The bound chloride was calculated from the contents of the total chloride and average evaporable water determined experimentally. If Langmuir's equation 6.7 is applicable, the curve

constructed by plotting C/s against C should be a straight line with a C/s-intercept above zero, and the parameters $K_1$ and $K_2$ can be obtained from the curve.

The ratios of the chloride concentration in the pore solution to the bound chloride, obtained from the "NaCl ingress" test, are plotted in figure 6.4(a) against the concentration. Figure 6.4 suggests that Langmuir's equation 6.7 can be used to describe the bound chloride approximately. The bound chloride contents obtained from the "diffusion-within" test are plotted against the concentration in figure 6.5 where the solid line shows the approximation by Langmuir's equation 6.7. The adsorption parameters K's obtained from figures 6.5 to 6.7 will be given in section 6.6. The bound and free chloride contents obtained from the "diffusion-out" test are plotted against the diffusion depth in Figure 6.6, which appears to show that the bound chloride did not change much with depth, despite the fact that there was an obvious increase of chloride concentration with depth.

### 6.2.3 Hydroxyl ions

As mentioned earlier, hydroxyl and sulphate concentrations have been considered to be able to affect the bound chloride contents. Adsorption or desorption of calcium ions can also be involved during diffusion. Since calcium and sulphate ions are minor components in the pore solution, their adsorptions were not considered in the

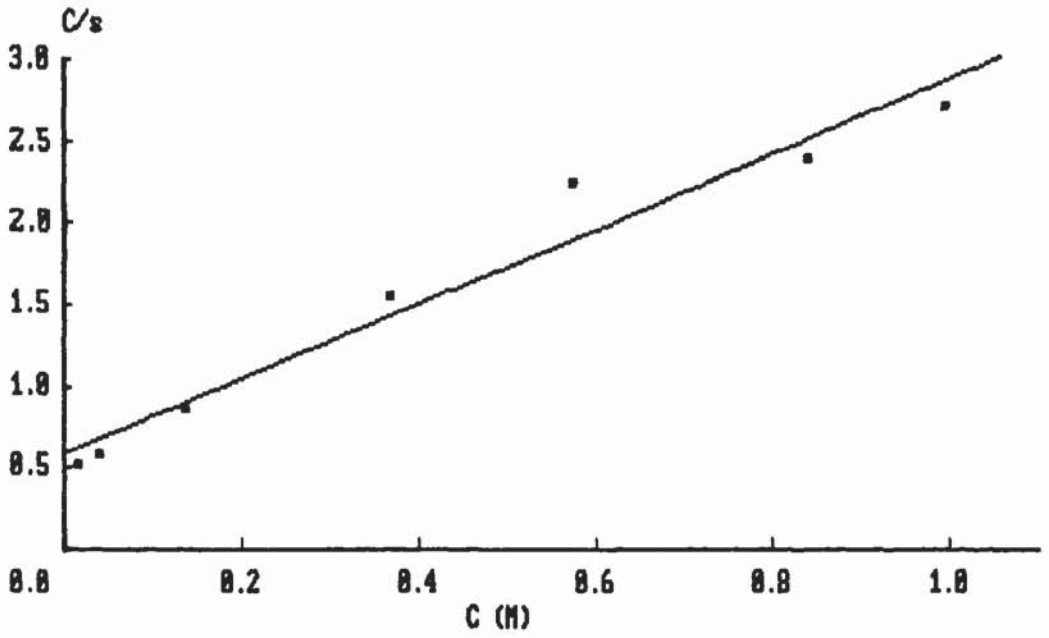


(a) The C/s-C curve

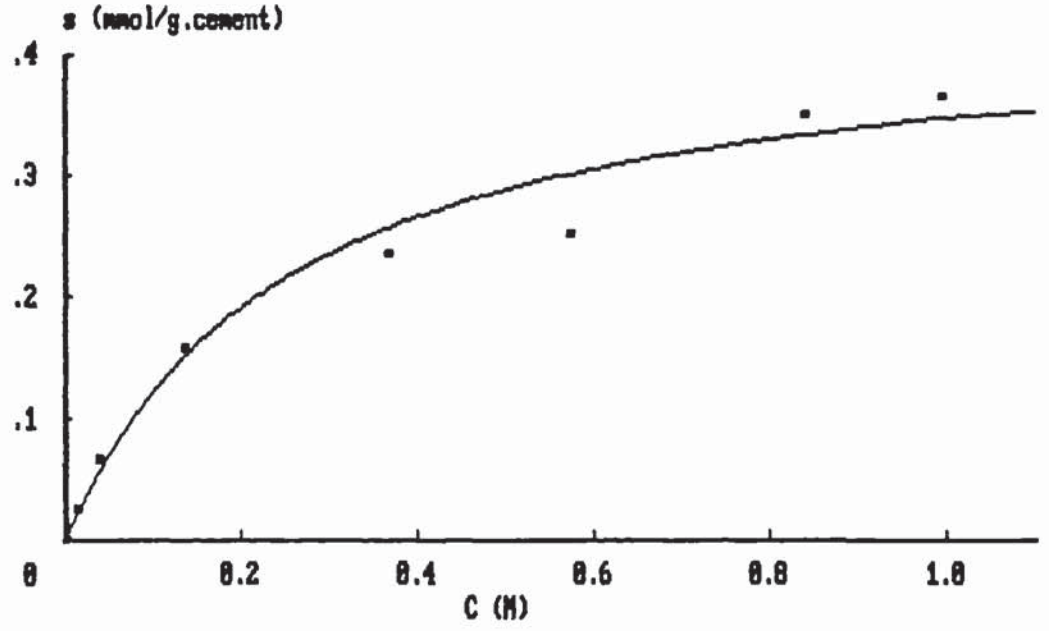


(b) The s-C curve

Figure 6.4 Approximation of bound chloride by Langmuir's adsorption theory ('Nacl-ingress' test)

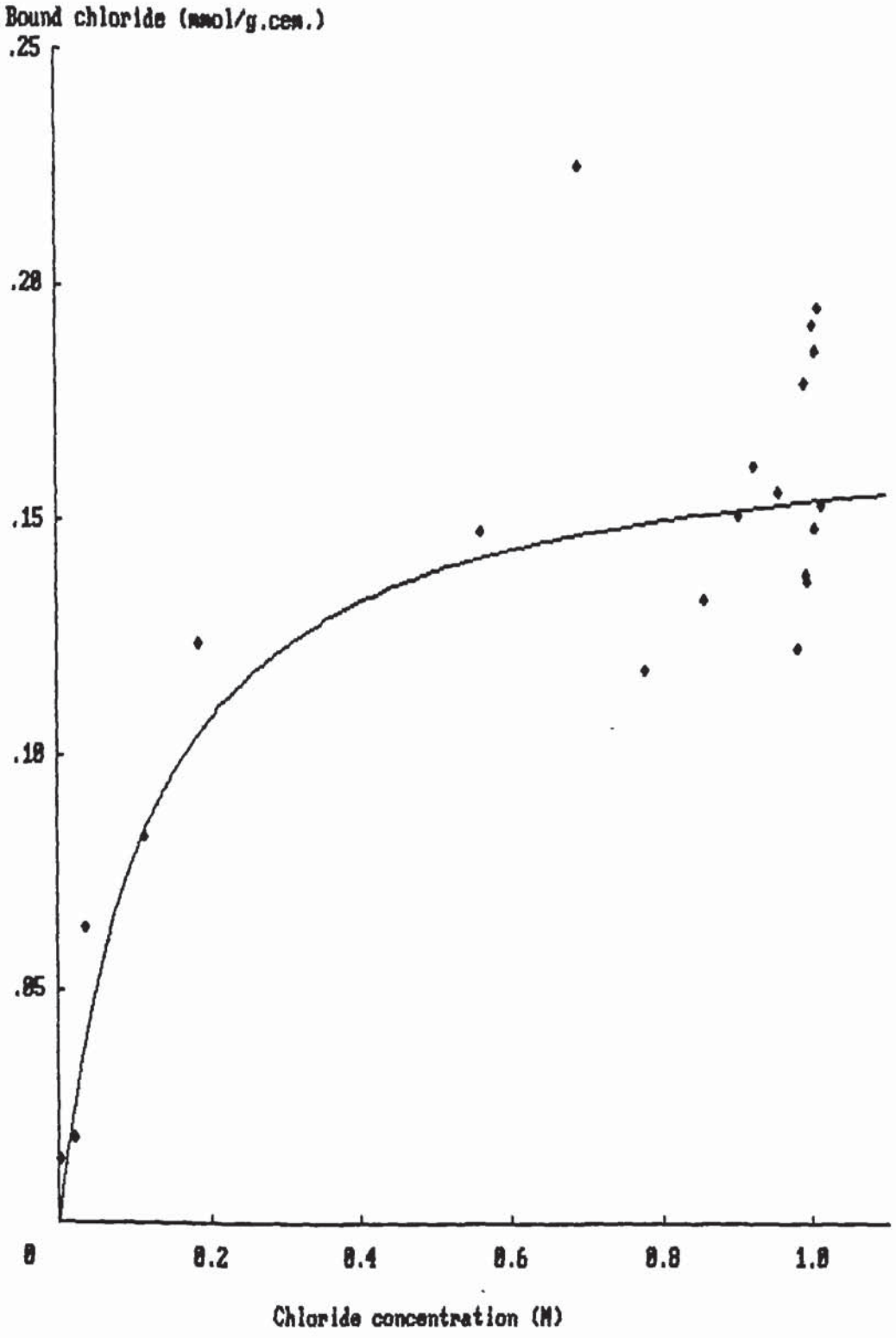


Figure 6.5 Variation of the bound chloride contents with the chloride concentration from the 'diffusion-out' test

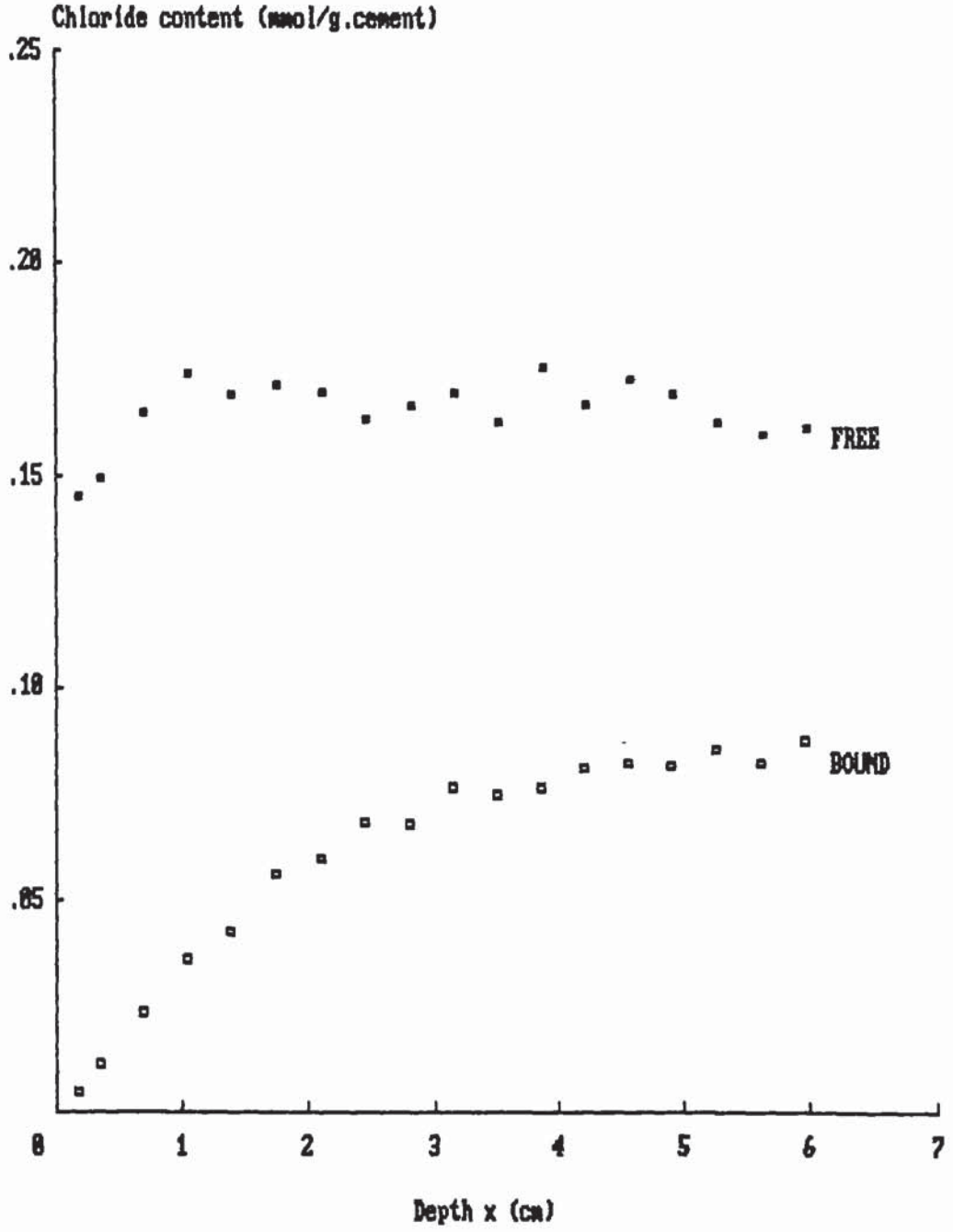


Figure 6.6 Bound and free chloride profiles obtained from the 'diffusion-out' test

present work. It is the desorption rate of bound hydroxyl ions that was assumed to balance the binding rate of chloride.

### 6.3 Diffusion Equations

After the binding of an ion during its diffusion has been approximated, the next step for the characterization of a concentration profile is to set up the flux equation. If Fick's first law (equation 1.1 or 3.1) and Langmuir's equation 6.7(a) are considered, the concentration as a function of the distance and time can be derived from the mass balance equation 6.1 to be

$$C_t(x,t)[W + K_1/(1+K_2C)^2]/W = DC_{xx}(x,t) \quad \ldots\ldots (6.8)$$

for diffusion in an essentially uniform specimen. If there is no adsorption or desorption during diffusion, i.e. $K_1=0$, the above equation is simply Fick's second law shown by equation 6.6.

If $K_2=0$ and $K_1\neq 0$, it is the case where the adsorbed amount, s, is proportional to the concentration, C, so

$$C_t(x,t)=[D/(1+K_1)]C_{xx}(x,t) \quad \ldots\ldots (6.9a)$$

The effective diffusivity ($D_e$) is defined here according to

$$C_t(x,t)=D_eC_{xx}(x,t), \text{ at } K_1\neq 0 \quad \ldots\ldots (6.9b)$$

for any value of $K_2$. At $K_2=0$, the value of $D_e$ is thus reduced by $K_1$ times from the Fickian diffusivity (D). Equation 6.9(a) was used, for example, by Tutti[125], to calculate chloride diffusivity (D) with a value of $K_1$

obtained by statistical analysis.

When there is adsorption during diffusion, the effective diffusivity ($D_e$) obtained by interpolating a concentration profile with equation 6.9(b) is therefore not the Fickian diffusivity. It differs from the Fickian diffusivity (D) in that it is not related to the flux in the way as defined by Fick's first law.

Fick's second law and equations 6.8 and 6.9 were used in this work to describe the diffusion of sodium, potassium and chloride ions. As the desorption rate of hydroxyl ions was assumed to be the same as the binding rate of chloride, the hydroxyl ions concentration distribution, C(x,t), obtained from Fick's first law is:

$$C_t(x,t) = DC_{xx}(x,t) + K_1C[Cl]_t(x,t)/\{W(1+K_2C[Cl])^2\} \quad \ldots\ldots (6.10)$$

where C[Cl] is the chloride concentration.

## 6.4 Numerical Methods

Two types of numerical calculation were used in this work. In one, such a diffusivity is to be found that the concentration profile calculated with it from one of the equations shown in the previous section is a best fit to the experimental data. This was involved mainly in the work presented in sections 6.5 to 6.7. In the other type of calculation, the concentration profiles are computed with certain assumed values of diffusivity and diffusion

time, which were used in the work shown in section 6.7. The finite difference method[126-129] was used in the numerical calculations.

One particular characteristic of all the diffusion equations shown in the previous section is that the concentration can be treated as a function of the distance x and the product of the diffusivity and diffusion time, Dt or $D_e t$. The concentrations at a certain interval of the diffusion depth were calculated numerically at a chosen step of the product, Dt or $D_e$, until the square sum of the differences in the concentrations between the numerically computed and the experimentally obtained reached a minimum at a value of the product which was noted. This is the "least-square" criterion[130]. The diffusivity was then obtained by dividing the noted product of Dt or $D_e t$ by the known diffusion time.

For a diffusion presumed to obey Fick's second law, the surface ($C_s$) and initial ($C_i$) concentrations can also be found together with the diffusivity by combining the numerical calculations with linear regression. The concentration profile obtained with the calculated $C_s$ and $C_i$ can be much better fitted to the experimental data than those calculated with any other assumed values of $C_s$ and $C_i$. However, such procedures were used only when there were uncertainties about the actual surface or initial concentrations.

The average concentration in a group of the equidistant discs cut at 0.7 or 0.35 cm intervals from the diffusion specimens, as experimentally determined by Sergi[64], was assumed to correspond to the concentration at the central depth of the discs. This concentration therefore does not necessarily represent the actual concentration at the depth x. Nevertheless, such a representation of experimental data was found numerically to be acceptable for the cutting intervals considered in this work. In addition, to minimize the sensitivity of the calculated diffusivity or the interpolated concentration profiles to certain points of the experimental data, these points were disregarded in the numerical fitting procedures and are noted in tables 6.1 to 6.4.

Values of concentrations, calculated numerically using a certain diffusion equation with the best-fitted diffusivity, are listed in appendices 3 to 5 for the "diffusion-out", "diffusion-within" and "NaCl-ingress" tests respectively.

## 6.5 Diffusion of Sodium and Potassium

### 6.5.1 Diffusing out of the OPC paste

The sodium and potassium concentration profiles obtained from the "diffusion-out" test at the diffusion time of 165 days were first interpolated by Fick's second law, and the

**Table 6.9** Results obtained from the "diffusion-out" test

| IONS | $C_s$ (M) | $C_i$ (M) | D-value ($\times 10^{-7}$) | Equation (No.) used for the calculations |
|---|---|---|---|---|
| $Na^+$ | 0.025 | 0.638 | 1.00 | 6.6 |
| $K^+$ | 0.009 | 0.236 | 1.61 | 6.6 |
| $Cl^-$ | 0.000 | 0.236 | 1.35 | 6.8 ($K_1$=0) |
| $OH^-$ | 0.054 | 0.534 | 0.84 | 6.6 |
| (*) | 0.132 | 0.540 | 1.15 | 6.6 |
| *: results obtained when the concentration data at x=0.175 and 0.350 were not considered | | | | |

results are summarised in table 6.9.

The surface concentrations, obtained as explained in the previous section, may be regarded as the averages over the time during which the external solution was not refreshed. The concentration profiles calculated by Fick's second law with the diffusivities obtained are shown in figure 6.7 as the solid lines. As suggested in figure 6.7, Fick's second law characterizes sodium and potassium diffusion.

To see if the diffusivities obtained are related to the flux by Fick's first law, the accumulative concentrations of sodium and potassium ions in the external solution can be compared with those expected from Fick's laws. The accumulative concentrations determined experimentally, c,

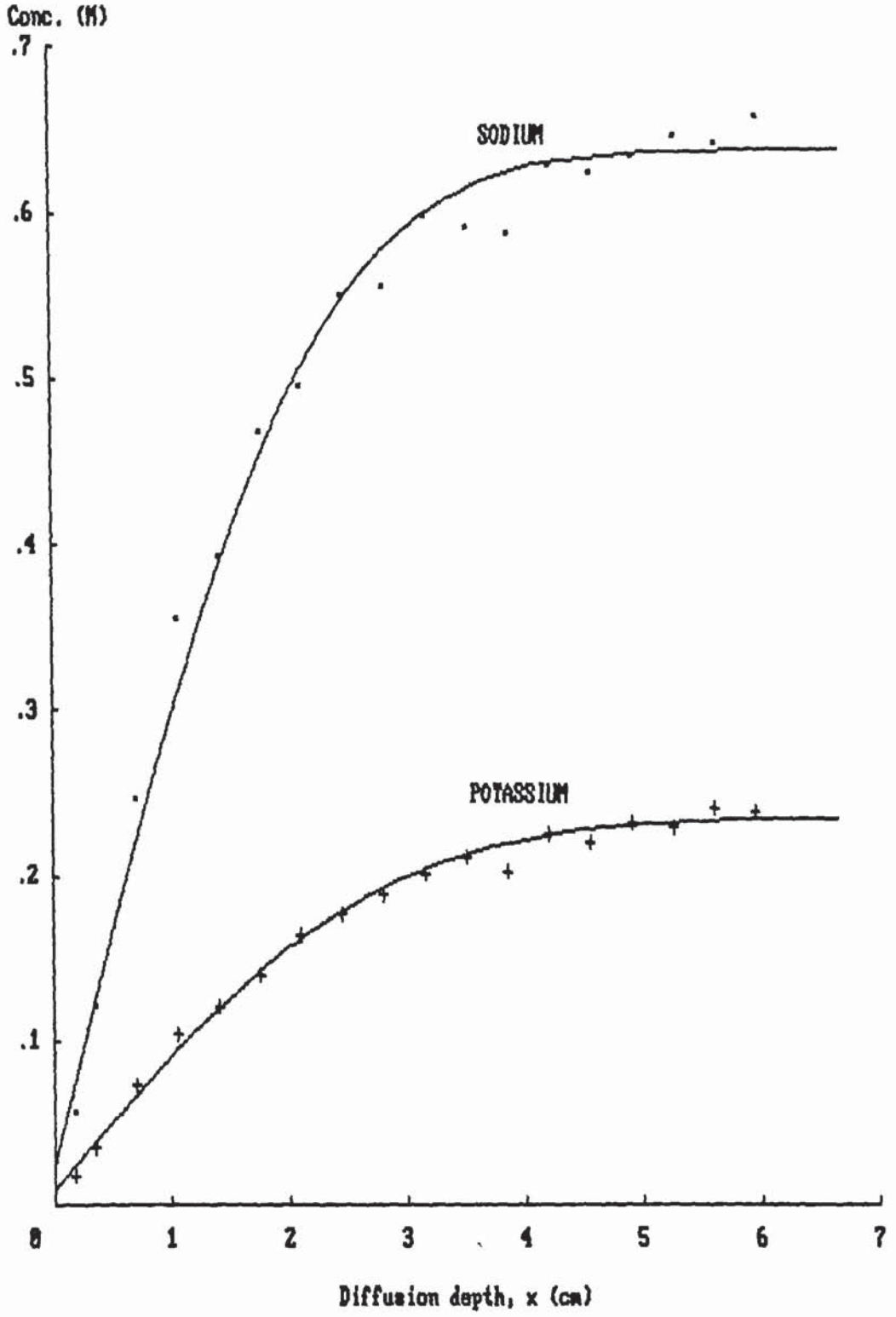


Figure 6.7 Sodium and potassium concentration profiles at 165 days obtained from the 'diffusion-out' test

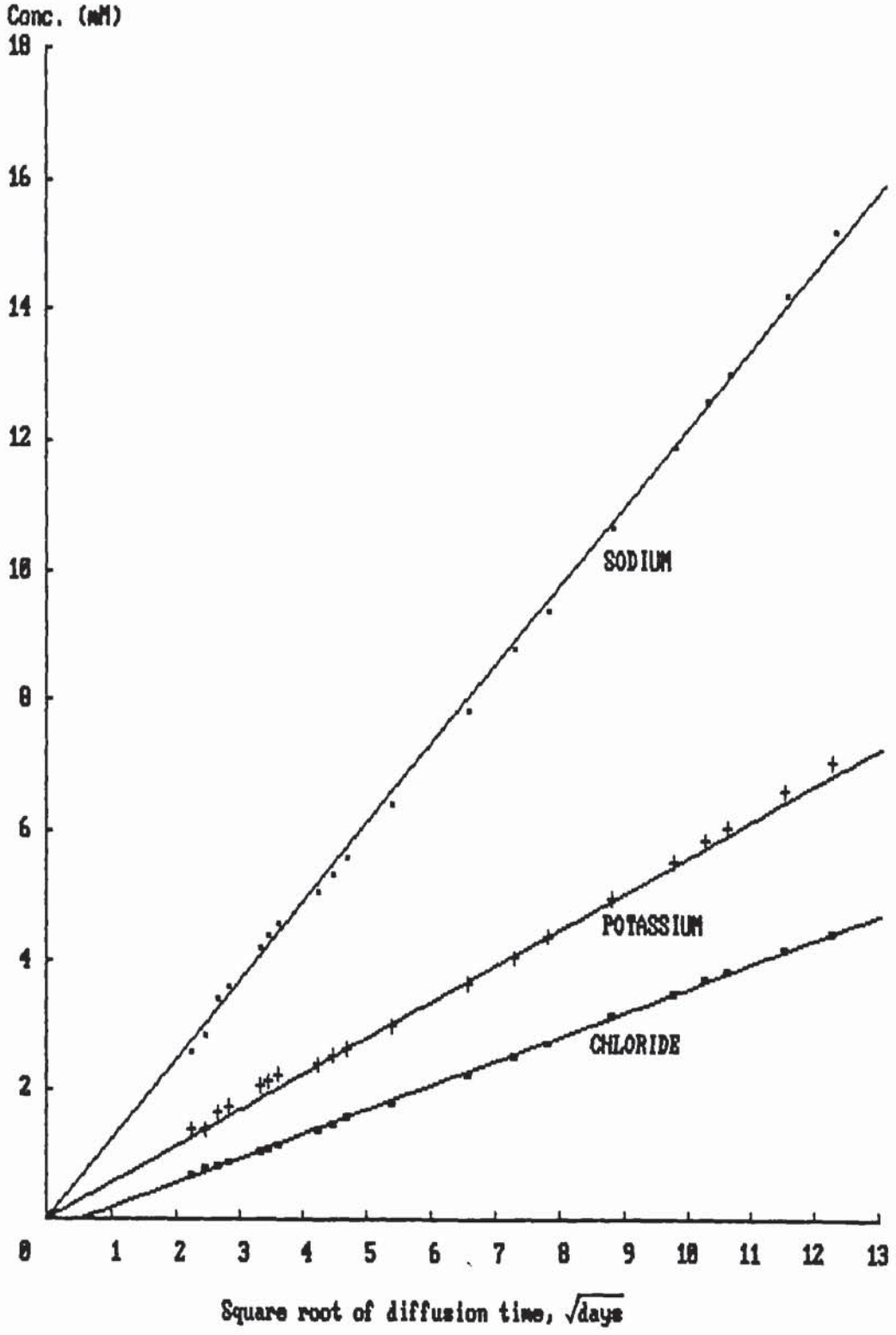


Figure 6.8 Rise of sodium, potassium and chloride concentrations in the external solution

are plotted in figure 6.8 against the square root of time. It can been seen for this figure that the curves obtained for the two ions almost pass through the origin, and the relationships obtained from regression analysis are:

$$\text{Na:}\quad c=1.229[t/(24\times3600)]^{1/2} \quad \text{(mM)} \quad \ldots\ldots \quad (6.11a)$$

$$\text{K:}\quad c=0.573[t/(24\times3600)]^{1/2} \quad \text{(mM)} \quad \ldots\ldots \quad (6.11b)$$

Generally speaking, the behaviour that the leached amount increases linearly with the square root of time has been observed for most diffusion systems even when the diffusivity is found not to be a constant, provided that the diffusion is semi-infinite and has proceeded for above a certain period of time[8]. However, if D is not a constant, or the diffusion is complicated by non-linear desorption or adsorption, this relationship would not hold for a small period of time, and the concentration intercept at t=0 is normally not zero[8].

If the amount of the ions combined to the solid phases is linearly related to the concentration in the pore solution by

$$s=S_0 + KC \quad \ldots\ldots \quad (6.12)$$

where $S_0$ and K in appropriate units are constants for either sodium or potassium, the total amount of ions leached out of the pore solution for a semi-infinite diffusion specimen is[8]

$$M=2(C_i-C_s)[(1+K)Dt/\pi]^{1/2} \quad \text{(mmol)} \quad \ldots\ldots \quad (6.13)$$

where M is the amount leached per $cm^2$ pore solution, and

the diffusivity used in the above equation, D, is related to the flux by Fick's first law.

The concentration profiles shown in figure 6.7 indicate that the specimens behaved almost as semi-infinite bodies at the diffusion time of 165 days. According to equation 6.13, the rise of the accumulative concentration (c) in the 5 litre external solution in contact with 12 specimens is

$$c=12\times18.86/5\times2\epsilon(C_i-C_s)[(1+K)Dt/\pi)^{1/2} \text{ (mM)} \ldots\ldots \text{(6.14)}$$

where 18.86 is the section area for each specimen, and $\epsilon$ is the volume or area fraction of the pore solution in which diffusion occurred.

By comparing the above equation with the relationships (equation 6.11) found experimentally, the volume fraction of the pore solution is approximately 0.42 for both sodium and potassium diffusion if the diffusivities obtained numerically (see table 6.9) are assumed to be Fickian. The value of $\epsilon$, estimated from the water contents based on the paper by Powers[45] (see appendix 6), is also 0.42. This suggests that there may be no significant desorption of the two ions during the diffusion and that the diffusivities obtained are probably Fickian. Therefore, the quantity of ions lost from the pore solution appears to have been balanced by that gained in the external solution for both sodium and potassium diffusion throughout all the diffusion time.

In summary, Fick's laws probably characterize sodium and potassium diffusion, because:

(1). The concentration data shown in figure 6.7 were found to be well approximated by Fick's second law.

(2). There were reasonable mass balances between the quantity of ions lost from the pore solution and that gained in the external solution, indicating that no significant desorption occurred during the diffusion.

(3). The accumulative concentrations of the two ions in the external solution increased proportionally with the square root of time.

### 6.5.2 Diffusing within the OPC paste

In this experiment carried out by Sergi[64], two half specimens of unequal initial concentrations of sodium ions were joined together. The sodium concentrations determined at the diffusion time 225 days are shown in figure 6.9. The interface is here assumed to be at $x=0$. The half specimens of higher concentrations are in the left half plane, $x<0$; while the other half specimens are in the right half plane $x>0$.

This type of experiment is of great value in showing experimentally whether or not a particular diffusing ion is partially removed from, or released into the pore solution that can be extracted by the pore-expression technique. If the amount of the sodium ions lost in the pore solution of the left half specimens was completely

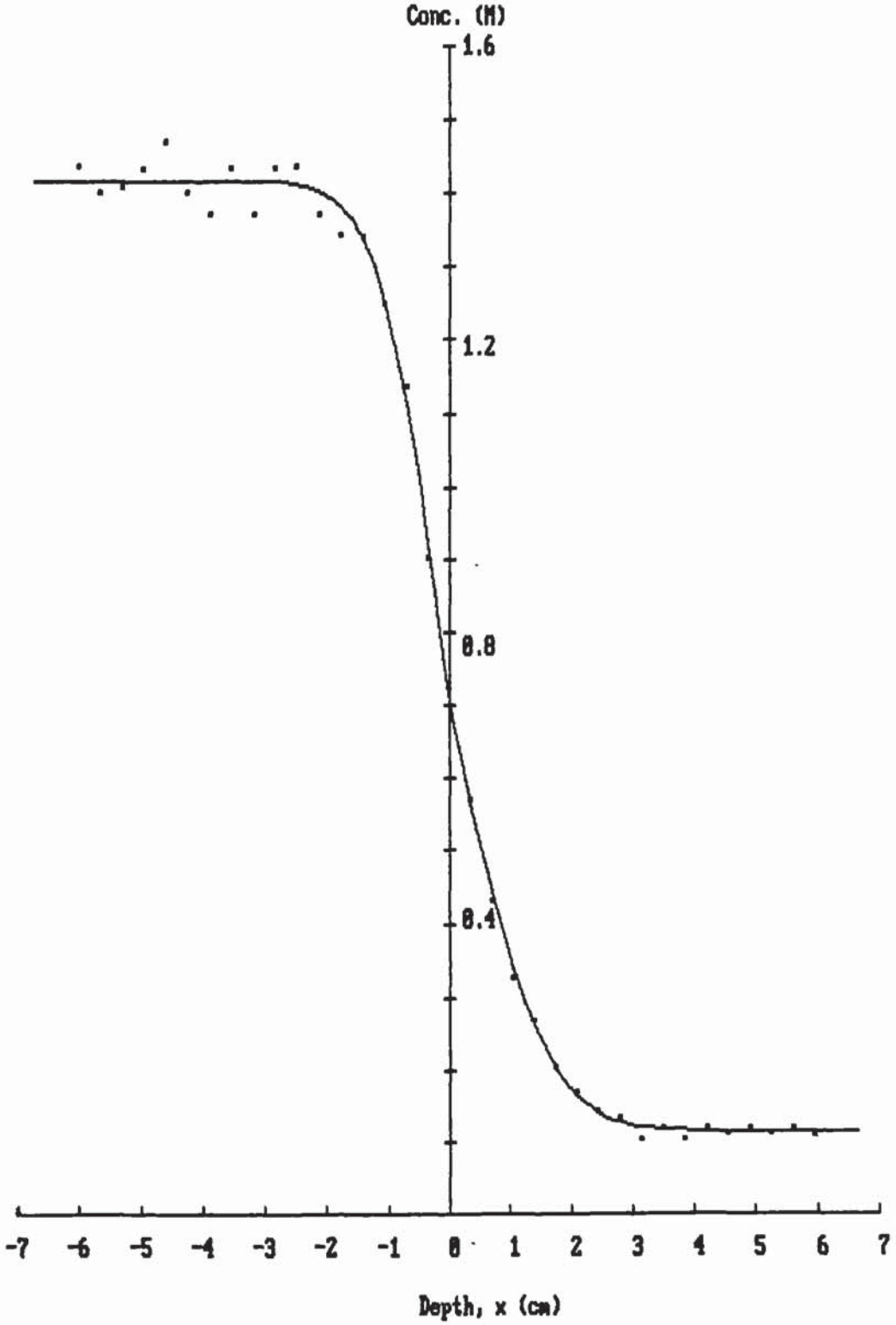


Figure 6.9 Sodium concentration profile at 225 days obtained from the 'diffusion-within' test

balanced by that gained in the pore solution of the other half specimens, it should be reasonable to assume there was no significant adsorption or desorption occurring during the period of diffusion.

As there was a difference in the evaporable water contents, $W_1$=31.6% and $W_2$=25.6% for the left and right half pastes respectively, there should have been a difference in their effective diffusion areas. Therefore, the conditions of mass balance described above could not be checked directly. The approaches were to assume, at first, that the mass balance existed, so the diffusivities determined from Fick's second law can be used to describe the continuity in flux at the interface, x=0:

$$\epsilon_1 D_1 C_{x-}(x,t)=\epsilon_2 D_2 C_{x+}(x,t) \qquad \ldots\ldots (6.15)$$

where the subscripts 1 and 2 represent the left and right sides of the half specimens respectively.

Because the two half pastes behaved as semi-infinite bodies, a Fickian diffusion process should have the following characteristics[8]:

(1). Except at t=0, the concentration at the interface should always be a constant

$$C(0,t)=C_{i2} + [C_{i1}-C_{i2}]/(1+v_2/v_1) \qquad \ldots\ldots (6.16)$$

(2). Diffusion on one side can be regarded as being independent of the diffusion on the other side.

(3). If Fick's second law and the above two characteristicsis are used for the calculation of concentration profile, the continuity in the flux at x=0, expressed by

equation 6.15, is automatically satisfied.

Numerical calculations were made to obtain the interface and initial concentrations and the diffusivities for each half specimen. The results are summarised in table 6.10. The concentration profiles computed are shown in in figure 6.9 as the solid lines. It can be seen from figure 6.9 that the initial concentrations obtained are in good agreement with what can be estimated from the experimental data. The values of the interface concentration obtained for each half paste are very close, so it was considered not necessary to perform an overall fitting to reduce the small discrepancies in the mass balance.

**Table 6.10** Results obtained from the "diffusion-within" test

| IONS | $C_i$ (M) | C(0,0) (M) | D-value ($\times 10^{-8}$) | Equation No. used for the calculations |
|---|---|---|---|---|
| $Na^+$ ($x \leq 0$) | 1.417 | 0.699 | 1.97 | 6.6 |
| ($x \geq 0$) | 0.115 | 0.692 | 3.83 | 6.6 |
| $Cl^-$ ($x \leq 0$) | 1.000* | 0.404 | 3.93 | 6.8, 6.18 |
| ($x \geq 0$) | 0.000* | 0.404 | 3.93 | 6.8, 6.18 |
| ($x \leq 0$) | 0.998 | 0.459 | 4.38 | 6.6 |
| *: values estimated from the experimental data | | | | |

As the concentrations in the right half specimens would have been determined more accurately, presumably because less tedious diluting of the extracted pore solution was required for the concentration measurements, the C(0,0) obtained for this half specimens may be considered to be closer to the actual interface concentration. The ratio, $\epsilon_2/\epsilon_1$, calculated from equation 6.16, was found to be 0.90. The left half specimens thus had a greater diffusion area. This result is in qualitative agreement with the difference in the evaporable water contents ($W_1$=31.6% and $W_2$=25.6%), although it is impossible to show whether there is a definite quantitative agreement.

The left half specimens were prepared with an addition of 2% chloride by weight of cement. If the added sodium was not adsorbed into the solid phases of the cement-matrix, the minimum sodium concentration in the extracted pore solution would expected to have been: 0.02/35.5/0.316*1000 =1.78 M. The value expected is higher than that measured experimentally (ca. 1.417 M), indicating that some sodium ions were adsorbed in the left half specimens. This suggests that the adsorbed sodium may not be significantly released further into the pore solution, otherwise because of the desorption in the left half specimens, the computed ratio, $v_2/v_1$, should have been much lower than 0.9. Therefore, the actual difference in the effective diffusion areas may be close to the calculated, $v_2/v_1$=0.9 (see appendix 6 for a rough estimation of the ratio).

To sum up, Fick's laws characterize the sodium diffusion, as indicated by the following findings:

(1). The concentration data shown in figure 6.9 are well approximated by Fick's laws.

(2). The calculation procedures treating the diffusion in one half specimens as being independent of the diffusion in the other half gave nearly the same values of the interface concentration.

(3). It appears that there was a reasonable mass balance between the sodium ions lost in the pore solution of the left half specimens and those gained in the other half specimens.

## 6.6 Diffusion of Chloride

### 6.6.1 Diffusing into the OPC paste

This is the experiment in which the OPC paste specimens were exposed to a 1M NaCl solution for 100 days. Equation 6.8 was first used to obtain the Fickian diffusivity with the assumed parameters:

$C_s$=1 M, $C_i$=0 M, $K_1$=1.71, $K_2$=3.93, W=29.7% ..... (6.17a)

where the adsorption parameter K's were obtained as explained in subsection 6.2.3. The diffusivity obtained is

$$D=4.407\times10^{-7}\ cm^2/sec \qquad \ldots\ldots (6.17b)$$

The fitted concentrations are shown in figure 6.10 as the solid line. Figure 6.10 shows that a reasonably good overall-fit of the concentration profile calculated from

equation 6.8 to the experimental data is achieved.

As Fick's second law has been widely used in practice to describe chloride diffusion, the effective diffusivity defined in equation 6.9(b), $D_e$, obtained with the surface and initial concentrations 1 and 0 M respectively is

$$D_e = 1.400 \times 10^{-7} \text{ cm}^2/\text{sec} \quad \ldots\ldots \text{(6.17c)}$$

The concentration profile calculated from Fick's second law with this diffusivity is shown in figure 6.10 as the dotted line. Although the fit is not as good as that achieved with the D, it is still good enough to show that the effective diffusivity can be used practically to describe the chloride concentration distribution.

It can be therefore concluded that both the Fickian and effective diffusivities can be used to characterize chloride diffusion by equations 6.8 and 6.9 respectively, at least for the case considered.

### 6.6.2 Diffusing within the OPC paste

It was found by computations based on equation 6.8 that, similarly to the case of sodium diffusion described in subsection 6.5.2, chloride diffusion in one half of the two specimens can be treated mathematically as being independent of the diffusion in the other half. The interface concentration was also found to be a constant. However, it is determined by the effective diffusion area ratio ($v_2/v_1$), diffusivities and the adsorption parameters

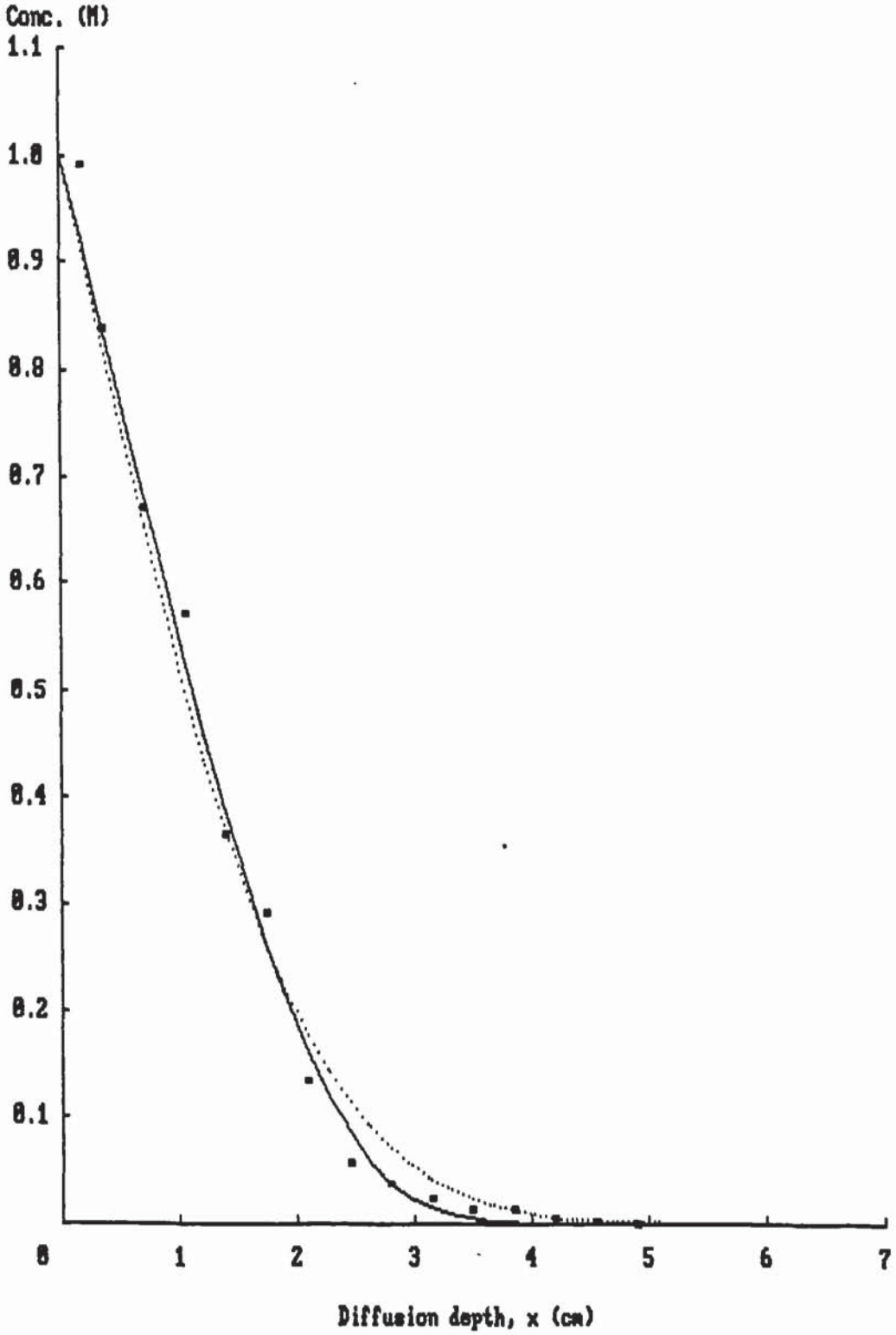


Figure 6.10 Chloride concentration profile at 100 days obtained from the 'NaCl-ingress' test

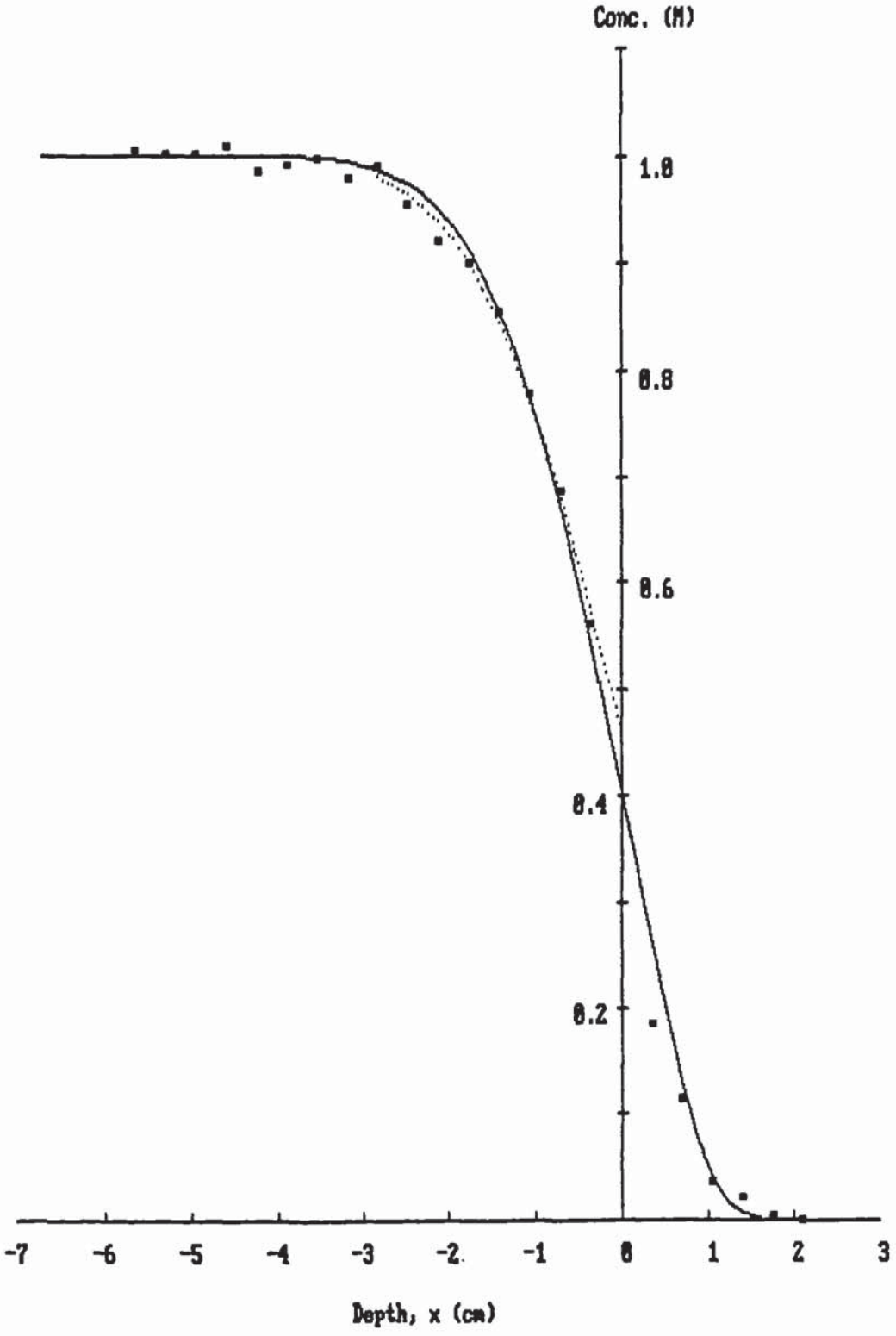


Figure 6.11 Chloride Concentration profile at 225 days obtained from the 'diffusion-within' test

K's, as equation 6.8 is non-linear with no analytical solution.

Although there is some scatter of the bound chloride in relation to the chloride concentration in the pore solution, The approximation of the bound chloride by the Langmuir adsorption isotherm, which has been shown in figure 6.5 was still considered. The calculations based on equation 6.8 were made by assuming that chloride had the the same diffusivities in both of the half specimens. The other assumptions are:

$$K_1=1.43, \qquad K_2=8.27 \qquad \ldots\ldots \text{(6.18a)}$$

$$C_{i1}=1.0\ M, \qquad C_{i2}=0.0\ M \qquad \ldots\ldots \text{(6.18b)}$$

$$v_2/v_1=0.9 \qquad \ldots\ldots \text{(6.18c)}$$

$$\epsilon_1 C_{x-}(x,t)=\epsilon_2 C_{x+}(x,t), \quad x=0 \qquad \ldots\ldots \text{(6.18d)}$$

where the subscripts 1 and 2 in equations 6.18(b) to 6.18(c) are for the left and right half specimens respectively. The concentration at x=0.35 cm was disregarded in the calculation, as it appears to conflict with the flux continuity expressed by equation 6.18(d).

The results obtained are shown in table 6.10. The concentration profile calculated, which is shown in figure 6.11 as the solid line, appears to interpolate the experimental data reasonably well. It was found that better fit could be achieved if the two half specimens were assumed to have different diffusivities. However, as the adsorption parameters $K_1$ and $K_2$ could not quantify the

bound chloride accurately, attention was not drawn to any possible difference in the diffusivities.

It appears that the desorption of the bound chloride in the left half specimens is negligible, presumably because saturation of the binding sites was achieved. If Fick's first law with a constant diffusivity characterizes the diffusion in the left half specimens, the concentration profile in this half should thus be very close to that determined by Fick's second law. The dotted line in figure 6.11 represents the concentrations calculated from Fick's second law, and the results are also shown in table 6.10. Compared with the solid line, the dashed line is indeed much better-fitted to the experimental data.

To sum up,

(1). Although the bound chloride could not be quantified accurately, it was still possible to use equation 6.8 to obtain a reasonably good fit of the calculated concentration profile to the experimental data.

(2). Fick's first law with a constant diffusivity probably characterizes the chloride diffusion, as revealed by the fact that Fick's second law gives a good approximation of the concentration profile when the bound-chloride desorption is negligible.

### 6.6.3 Diffusing out of the OPC paste

As shown in figure 6.6, it seems that bound chloride determined from the "diffusion-out" test did not change much with the depth. No desorption or adsorption of chloride during diffusion was assumed, and the results obtained from the numerical calculations are included in table 6.9. The computed concentration profile is shown in figure 6.12. A very good fit to the concentration data was obtained.

As for the diffusion of sodium and potassium ions, a consideration concerning the mass balance between the amount of the chloride lost in the pore solution and that gained in the external solution can give some information on the effective area and diffusion kinetics. Figure 6.8 shows that the accumulative concentration of chloride in the external solution increased linearly with the square root of time, but with a negative concentration intercept at t=0:

$$c = -0.1946 + 0.3792[t/(24\times3600)]^{1/2} \quad \ldots\ldots \quad (6.19)$$

The amount of chloride gained in the external solution at 165 days was estimated to be 1.95 mmol per specimen cylinder, while that lost from the pore solution was calculated, as explained in subsection 6.5.1, to be about $6.97\epsilon$ mmol per specimen cylinder at the assumed surface and initial concentrations 0.000 and 0.236 M respectively. The value of $\epsilon$ would thus be: 1.95/6.97=0.28, which is in

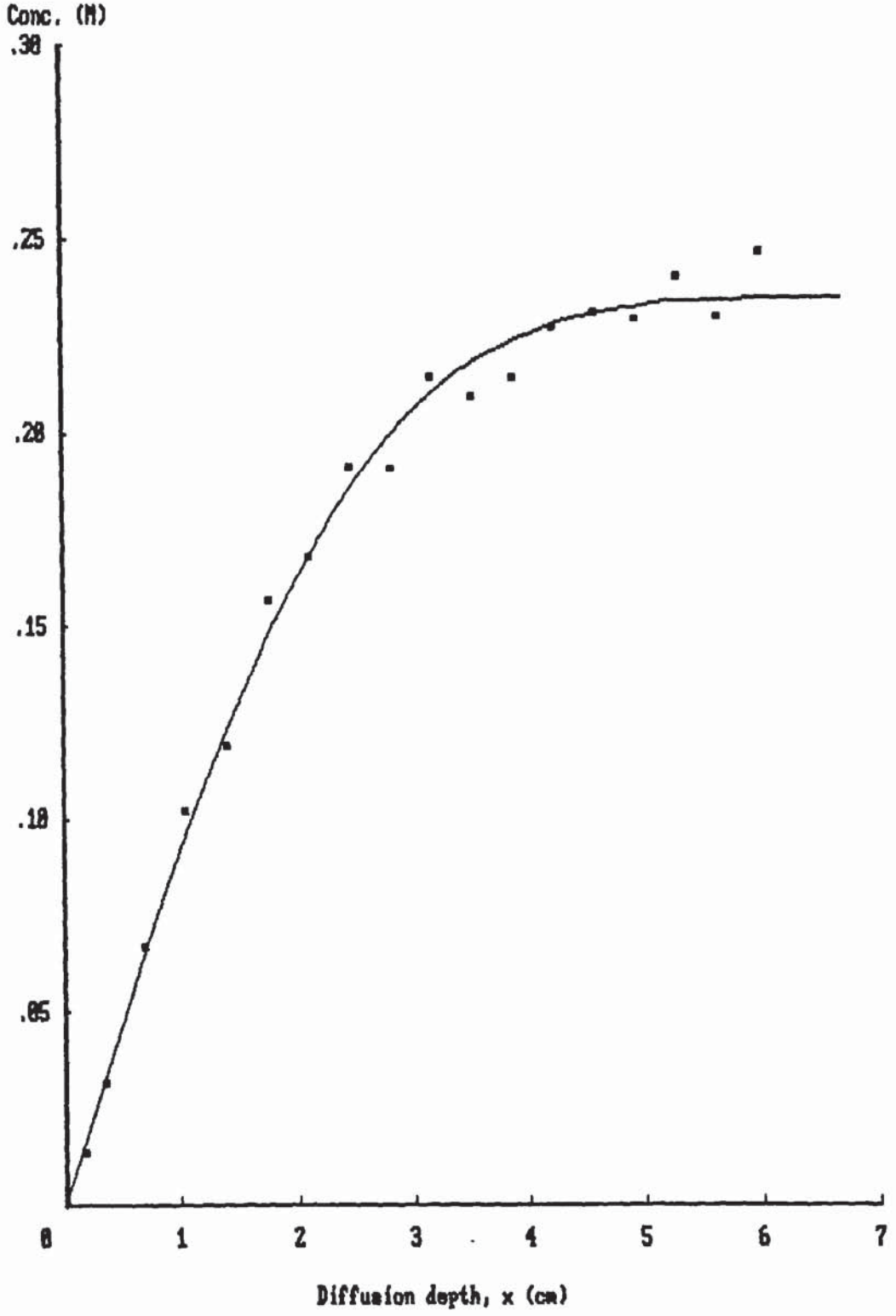


Figure 6.12 Chloride concentration profiles at 165 days obtained from the 'diffusion-out' test

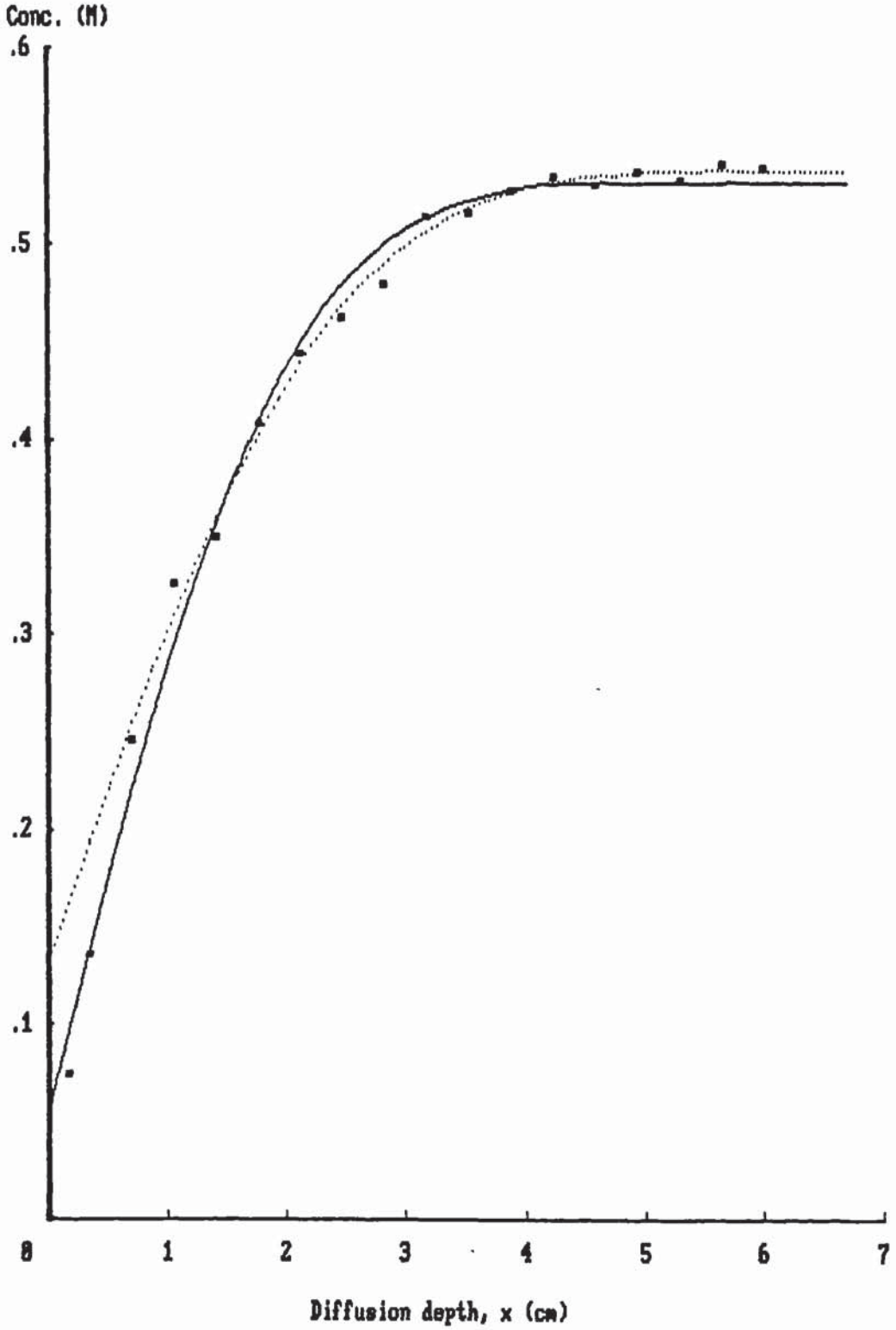


Figure 6.13 Hydroxyl concentration profile at 165 obtained from the 'diffusion-out' test

obvious contradiction with that (0.42) estimated from sodium and potassium diffusion.

It can be therefore concluded from the above calculations that:

(1). The chloride concentration profile was found to be well interpolated by Fick's second law.

(2). The rise of chloride concentration in the external solution is, however, not in exact agreement with what would be expected from Fick's second law.

(3). The effective diffusion area estimated from the chloride diffusion with the calculated initial concentration 0.236 M is in contradiction with that obtained from sodium and potassium diffusion (see section 6.8 for explanations).

## 6.7 Diffusion of Hydroxyl Ion

### 6.7.1 Diffusing out of the OPC paste

The hydroxyl concentration data shown in figure 6.13 were obtained by Sergi[64] from the experiment in which all the major ions were leaching out of the OPC paste in constant contact with an external solution of pH value below 12. Fick's second law was used to interpolate all the points of the concentration data, and the results are given in table 6.9. The calculated profile is shown in figure 6.13 as the solid line. As hydroxyl ions were found to be produced by dissolution of the cement hydrates near the

exposed surface, the effective diffusivity obtained may not show the diffusion kinetics.

The dissolution of the cement hydrates might be expected to have occurred in the following ways. Near the surface in contact with the low pH solution, dissolution took place continuously, and equation 6.1 should be used in general; whereas at the depths far away from the surface, there was no hydrate dissolution and hydroxyl desorption, and the concentration profile was thus determined by Fick's second law. Therefore, there would be a depth, X, which was a moving boundary of the dissolution front.

Diffusion in the region x>X could thus be assumed to be characterized by Fick's second law, but with the imagined "surface" concentration ($a+C_i$) that was determined by both the diffusivities and the desorption kinetics in the two regions[8]. For a semi-infinite diffusion in x>X with the diffusivity D, the concentration would be[8]:

$$C(x,t)=C_i + [(a+C_i)-C_i]\mathrm{erfc}[x/(4Dt)^{1/2}] \quad \ldots\ldots \quad (6.20)$$

where a is constant. One implication of this equation is that the dissolution front should increase linearly with the square root of time if dissolution of the cement hydrates occurs at a certain critical $OH^-$ concentration.

The fit to the experimental data exclusive of the first two points at x<0.7, obtained from equation 6.20, is shown in fig 6.13 as the dotted line, and the results are listed in table 6.9. Extrapolation of the dotted line to the

depth x< 0.7 cm gives concentrations that are higher than those experimentally obtained. As the dissolution of the hydrates may be considered to occur at a pH value close to 12, the above interpretation of the data should have given a "surface concentration" of value below, say, 0.04 M.

Therefore, it seems difficult to explain the diffusion behaviour of hydroxyl ions by Fick's laws, although the concentration profile determined experimentally is approximately interpolated by Fick's second law. It can also be seen from table 6.9 that for this particular experiment hydroxyl ions diffused slower than chloride and potassium ions in terms of the diffusivities obtained.

### 6.7.2 $OH^-$ Counter-diffusion due to NaCl ingress

As desorption rate of bound hydroxyl ions was assumed to balance the binding rate of chloride, equation 6.10 was used to describe the counter-diffusion of hydroxyl ions observed from the "NaCl ingress" test. The hydroxyl concentration data are presented in figure 6.14.

For the sake of simplicity in the calculations, the surface concentration of hydroxyl ions was assumed to have remained at a constant value of 0.1 M. Figure 6.14 gives three profiles calculated at the hydroxyl diffusivities $2.5 \times 4.407 \times 10^{-7}$, $3.5 \times 4.407 \times 10^{-7}$ and $4.5 \times 4.407 \times 10^{-7}$ $cm^2/sec$ respectively, where the value $4.407 \times 10^{-7}$ is the chloride diffusivity shown in equation 6.17(b).

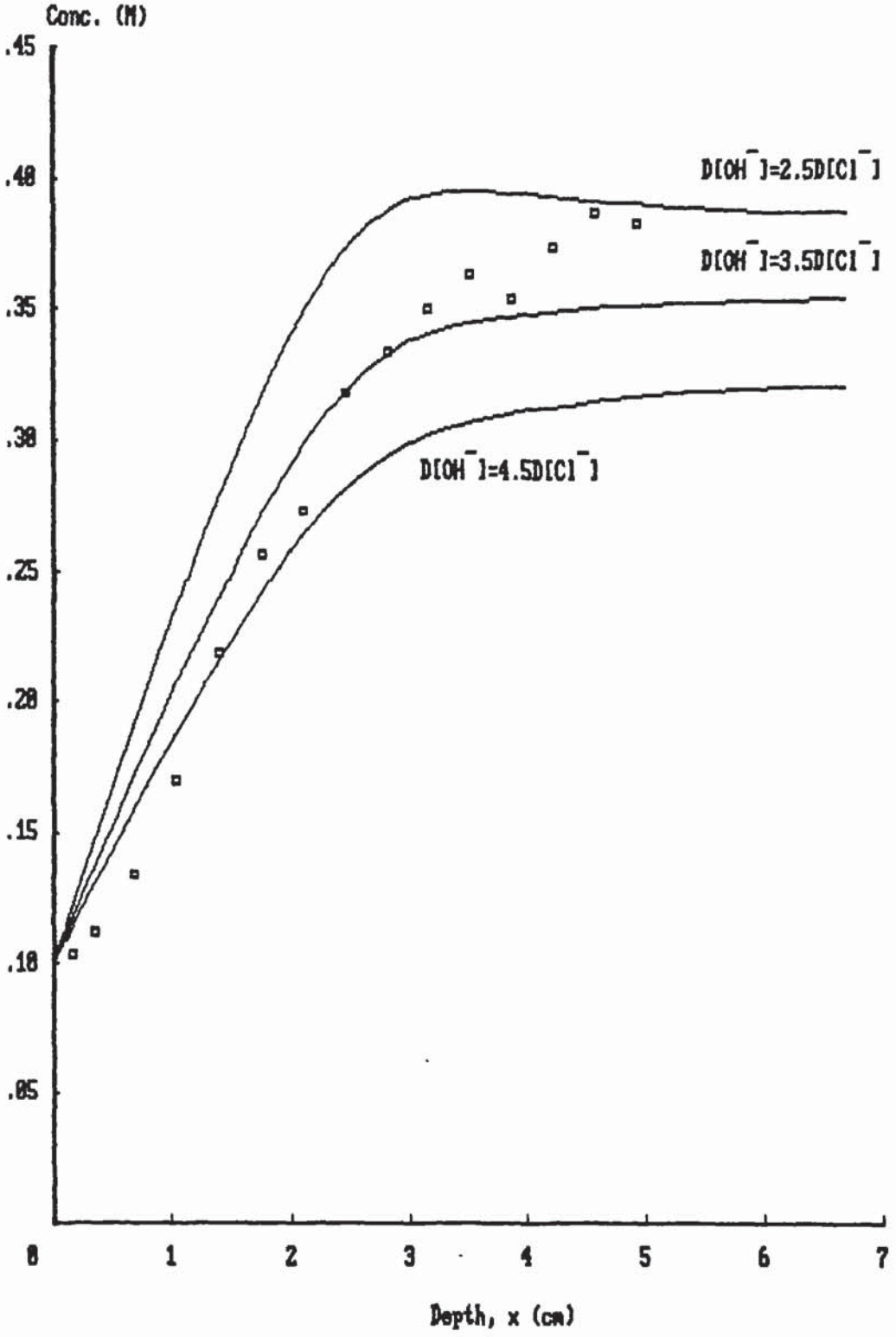


Figure 6.14 Hydroxyl concentration profile at 100 days obtained from the 'NaCl-ingress' test

It can be seen from figure 6.14 that all of the three profiles computed deviate considerably from the experimental data. Therefore, equation 6.10 cannot describe diffusion of hydroxyl ions. However, It can still be seen from figure 6.14 that hydroxyl ions evidently diffused a few times faster than chloride ions.

## 6.8 Modelling and Prediction

Based on the diffusion behaviours known from the previous sections, the following model may be used to characterize and to predict ionic diffusion in hydrated OPC pastes:

(1). Sodium and potassium ions diffuse according to Fick's first and second laws. Their adsorption or desorption during diffusion can be assumed to be insignificant.

(2). Chloride diffusion can be modelled through two approaches:

(a). A Fickian diffusivity is used in equation 6.8, which is based on Fick's first law and Langmuir's theory of adsorption, to predict the concentration profiles; while the bound chloride is obtained from Langmuir's adsorption equation 6.7.

(b). An effective diffusivity is used to predict the concentration profiles based on the mathematical solutions of Fick's second law; while the bound chloride is also obtained from Langmuir's adsorption

equation 6.7.

(3). As sulphate and calcium ions are minor components in the pore solutions, their diffusion can be either neglected or assumed to follow Fick's second law with certain effective diffusivities.

(4). Diffusion of hydroxyl ions is such that it simply maintains the electroneutrality in the pore solution.

The preliminary model proposed by Page and Sergi[39] is essentially the same as the above described, except that chloride diffusion was modelled by the second approach using an effective diffusivity.

As already concluded in section 6.5, when adsorption or desorption of sodium and potassium ions is insignificant, the concentration profiles determined by Fick's laws always give good approximations to the experimental data. Diffusion of the two cations appears to be much simpler than the diffusion of anions. For the purpose of prediction, the two ions can be treated as simply following Fick's laws.

As shown in subsections 6.6.1 and 6.6.2, equation 6.8, which is based on the Langmuir isotherm of adsorption and Fick's first law, can be used to characterize the distributions of free chloride and thus total or bound chloride. The effective diffusivity, $D_e$, determined from the profiles of either free or total chloride, has been

widely used as a parameter for the characterization and prediction of chloride ingress in hydrated cement pastes and concrete. It has also been shown in subsection 6.6.1 that a concentration profile described by Fick's second law with an appropriate effective diffusivity can also approximate the experimental data reasonably well.

It is mentioned in section 6.3 that the effective diffusivity obtained when there is binding of chloride during diffusion does not describe the flux by Fick's first law. Nevertheless, it is a parameter simpler and more convenient to use for the purpose of the prediction of chloride ingress in concrete. It would thus be of interest to compare the concentration profiles predicted with the effective $D_e$ and Fickian (D) diffusivities determined from the "NaCl-ingress" experiment. Here $D_e$ and D are $1.400 \times 10^{-7}$ and $4.407 \times 10^{-7}$ $cm^2/sec$ respectively (see equation 6.17).

Figure 6.15 gives the concentration profiles predicted at 30, 50 and 300 days at a surface concentration 1M and a zero initial concentration. The dotted line is the result calculated from Fick's second law with the $D_e$ while the solid line is calculated from equation 6.8 with the D. It can be seen that the main difference in the profiles occurs in the depths of low concentration. At 300 days, the profile predicted with effective diffusivity ($D_e$) suggests that the paste would not behave as a semi-

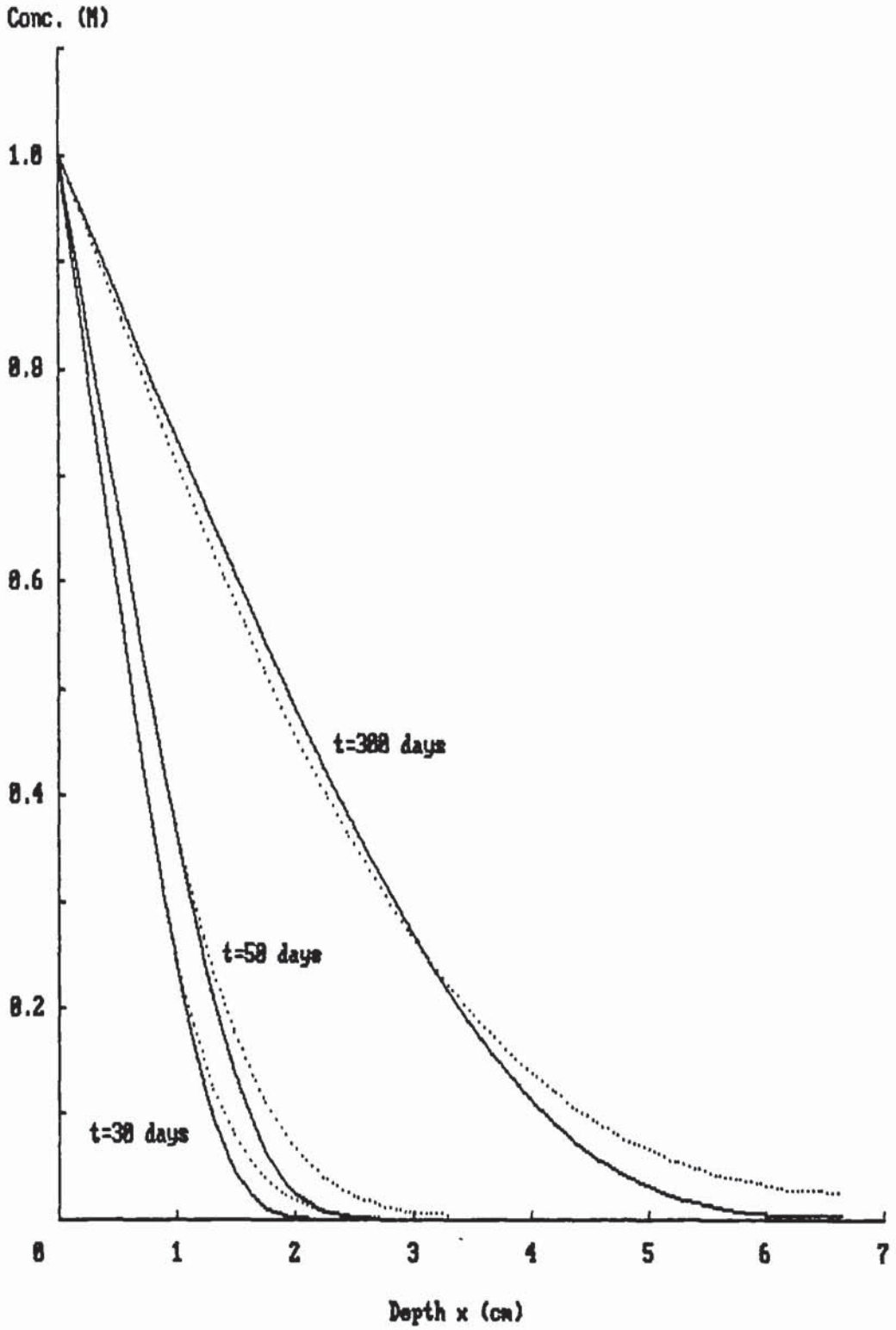


Figure 6.15 Predicted chloride concentration profiles for the 'NaCl-ingress' test

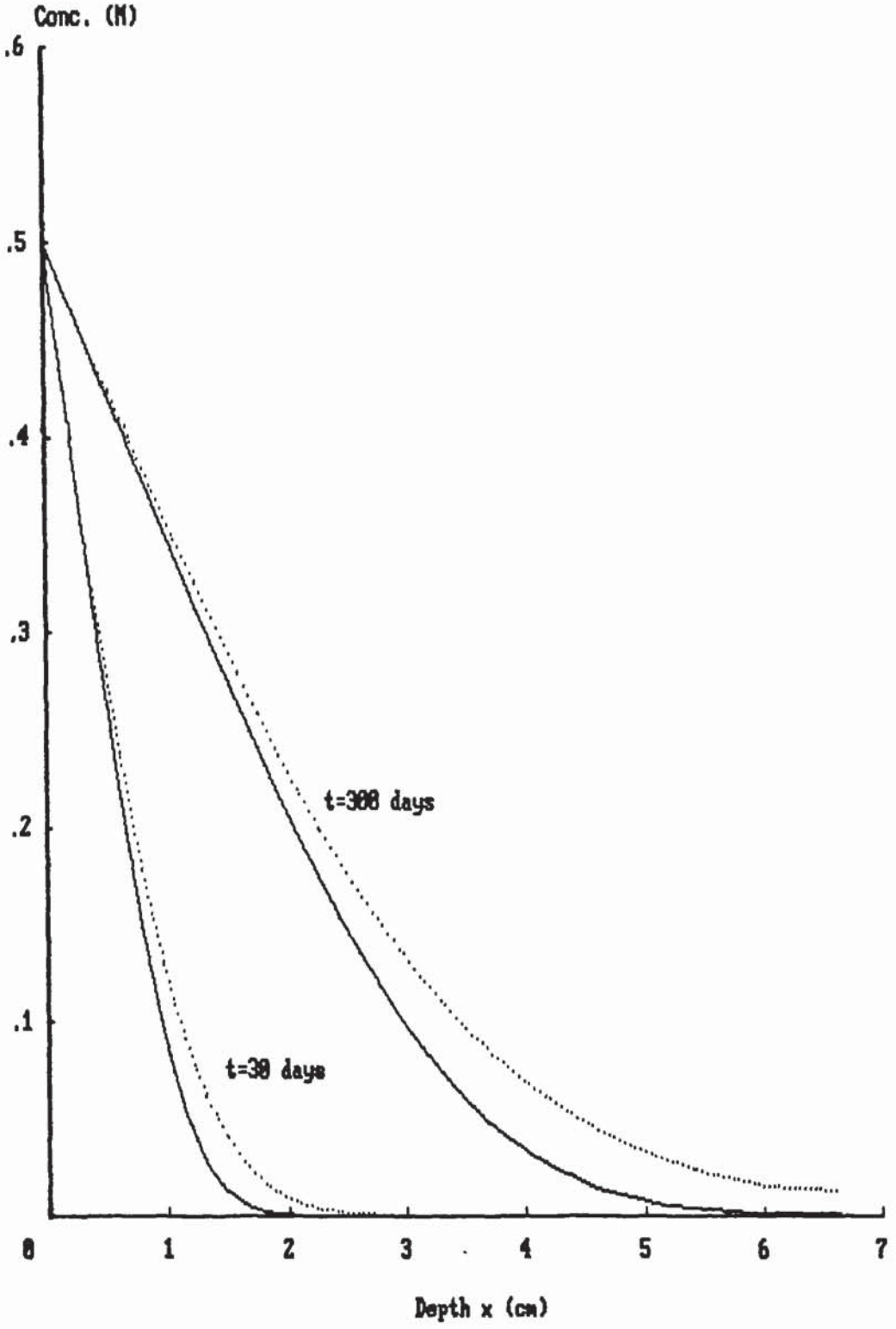


Figure 6.16 Predicted chloride penetration profiles with a surface concentration 0.5 M

infinite diffusion medium. The predictions from Fick's second law with the effective diffusivity ($D_e$) thus tend to overestimate the penetration depth.

If the kinetics of chloride diffusion and binding are assumed to be quite independent of the presence of other ions, chloride diffusion may be considered as more closely characterized by the Fickian diffusivity D. Figure 6.16 shows the concentration profiles predicted at 30 and 300 days if a surface concentration 0.5 M is assumed, where the solid lines are the results from equation 6.8 with the D and the dotted lines, from Fick's second law with the $D_e$. It can been seen that the concentrations calculated with the effective diffusivity ($D_e$) are greater than those obtained with the D.

Because sulphate and calcium ions are minor components in the pore solutions of hydrated OPC pastes, it is practical to neglect their diffusion, so they can be assumed to have constant concentrations within the paste. Alternatively, their diffusion can be modelled by Fick's second law with appropriate effective diffusivities.

Hydroxyl diffusion seems to be much less predictable than the diffusion of sodium, potassium and chloride, as suggested by the fact that hydroxyl concentration profile shown in figure 6.14 from the "NaCl-ingress" experiment cannot be approximately characterized by Fick's first law with a constant diffusivity. As diffusion of the other

ions has been modelled in acceptable ways, hydroxyl concentrations can be practically calculated from the requirement of charge balance. However, treating hydroxyl ion as a charge-balancing species is obviously empirical.

The hydroxyl concentration profile obtained from the "NaCl-ingress" test was fitted based on the following assumptions:

(1). The chloride profile is that obtained with the Fickian diffusivity and shown in figure 6.10 by the solid line.

(2). Sodium ions had a zero surface concentration, a 0.115M initial concentration which is suggested by the data obtained from the "diffusion-within" test, and a diffusivity $1.205 \times 10^{-7}$ $cm^2/sec$.

(3). Potassium ions had a 0.100M surface concentration, a 0.265M initial concentration and a diffusivity $2.410 \times 10^{-7}$ $cm^2/sec$.

(4). The concentrations of the minor-component ions such as sulphate and calcium were zero

The sodium and potassium diffusivities were chosen such that their ratio is similar to that suggested by the diffusivities obtained from the "diffusion-out" test. Figure 6.17 shows the concentration profiles for sodium, potassium and hydroxyl ions. It can be seen that a reasonably good fit to hydroxyl concentration profile is achieved.

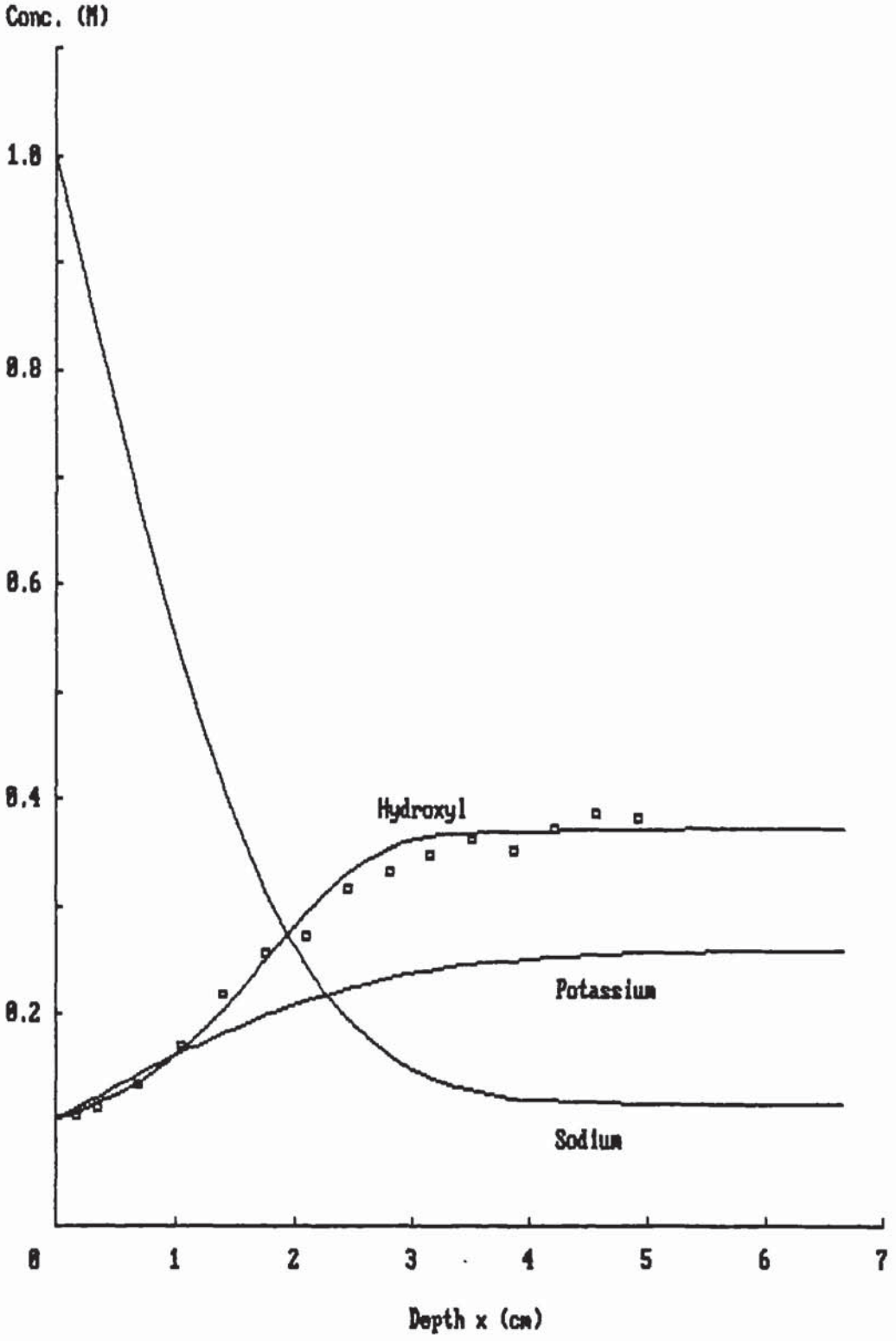


Figure 6.17 Hydroxyl, potassium and sodium concentration profiles at 100 days according to the model for the 'NaCl-ingress' test

Although it is difficult to make a kinetic explanation of the model, the diffusion behaviours observed experimentally appear to be associated with some characteristics of a multi-component electrolyte diffusion system. The examples presented in paragraph 6.1.2.3 and in figures 6.1 to 6.3 concerning ionic diffusion in mixed dilute electrolytes have shown that Fick's laws tend to approximate the concentration profiles of cations better than those of anions. This is probably because cations are less mobile than the anions in terms of the absolute diffusivity, so the cations may control the overall diffusion rates and their overall diffusion deviates from Fickian behaviour comparably less than that of the faster anions, particularly hydroxyl ion. It has been shown in subsection 6.7.2 that hydroxyl ion appears to be the fastest diffusing species in the OPC paste.

It appears that the hydroxyl profiles in the two diffusion systems associated with figures 6.14 and 6.2 have certain similarities. The concentrations shown by the square dots in both figures are considered here as the actual values, while those shown by the solid lines represent the diffusion behaviour expected from Fickian processes. Compared with the behaviour expected from the Fickian diffusion, hydroxyl ions diffuse faster near the surface than they do at certain distances away from the surface, which is much more obvious than that shown in figure 6.1 for a diffusion system of smaller differences in the

diffusivities.

As far as the overall diffusion is concerned, sodium and potassium ions in the "NaCl-ingress" experiment can be assumed to be one cation, as they have similar values of diffusivity. Therefore, with regard to the way in which the diffusion occurs, the three diffusion processes shown in figures 6.1, 6.2 and 6.14 are similar in that a cation and the chloride diffuse into the medium while hydroxyl ions diffuse out of the medium. In either of the cases shown in figures 6.2 and 6.14, the cation appears to have a few times smaller diffusivity than the chloride. The similarity in hydroxyl diffusion behaviours in these two systems may suggest that the cation tends to affects hydroxyl diffusion in hydrated cement pastes.

As mentioned in subsection 6.1.2 and chapter 1, the Nernst-Planck equation is applicable only to diffusion in dilute electrolytes. However, this equation may be used to assess qualitatively the effect of ionic electrostatic interactions on the rates of the overall diffusion process[6]. To show the possibility that the rates of ionic diffusion in the OPC paste could be affected the electrostatic interactions, the Nernst-Planck equation was used to model the fluxes in the "NaCl-ingress" test. The ionic system was assumed to be composed of $Na^+$, $Cl^-$ and $OH^-$ ions. Table 6.11 gives the assumed values of $C_s$, $C_i$ and the absolute diffusivity ($D_o$) for the three ions. Values of the adsorption parameter K's and the W shown in

**Table 6.11** Assumed values of $C_s$, $C_i$ and $D_0$ for the calculation of the concentration profiles using the the Nernst-Plank equation

| IONS | $C_s$ (M) | $C_i$ (M) | D ($\times 10^{-7}$ $cm^2/sec$) |
|---|---|---|---|
| $Na^+$ | 1.080 | 0.375 | 0.7 |
| $Cl^-$ | 1.000 | 0.000 | 5.2 |
| $OH^-$ | 0.080 | 0.375 | 13.6 |

equation 6.17(a) were used.

The accordingly computed concentration profiles at the diffusion time of 100 days are presented in figure 6.18. The square dots in this figure represent the concentrations determined experimentally by Sergi[64]. Values of $Na^+$ concentration shown as the smallest dots are the sum of $Cl^-$ and $OH^-$ concentrations. It can be seen from figure 6.18 that it may be possible to explain qualitatively the diffusion behaviours of all the three ions based on the Nernst-Planck equation and Langmuir's theory of adsorption. However, there has been no experimental proof to support the applicability of the Nernst-Planck equation to the description of ionic diffusion in hydrated cement pastes. Furthermore, the absolute diffusivities used for the above modelling are ambiguous with regard to the difficulties in determining them experimentally. Therefore, this approach may not be

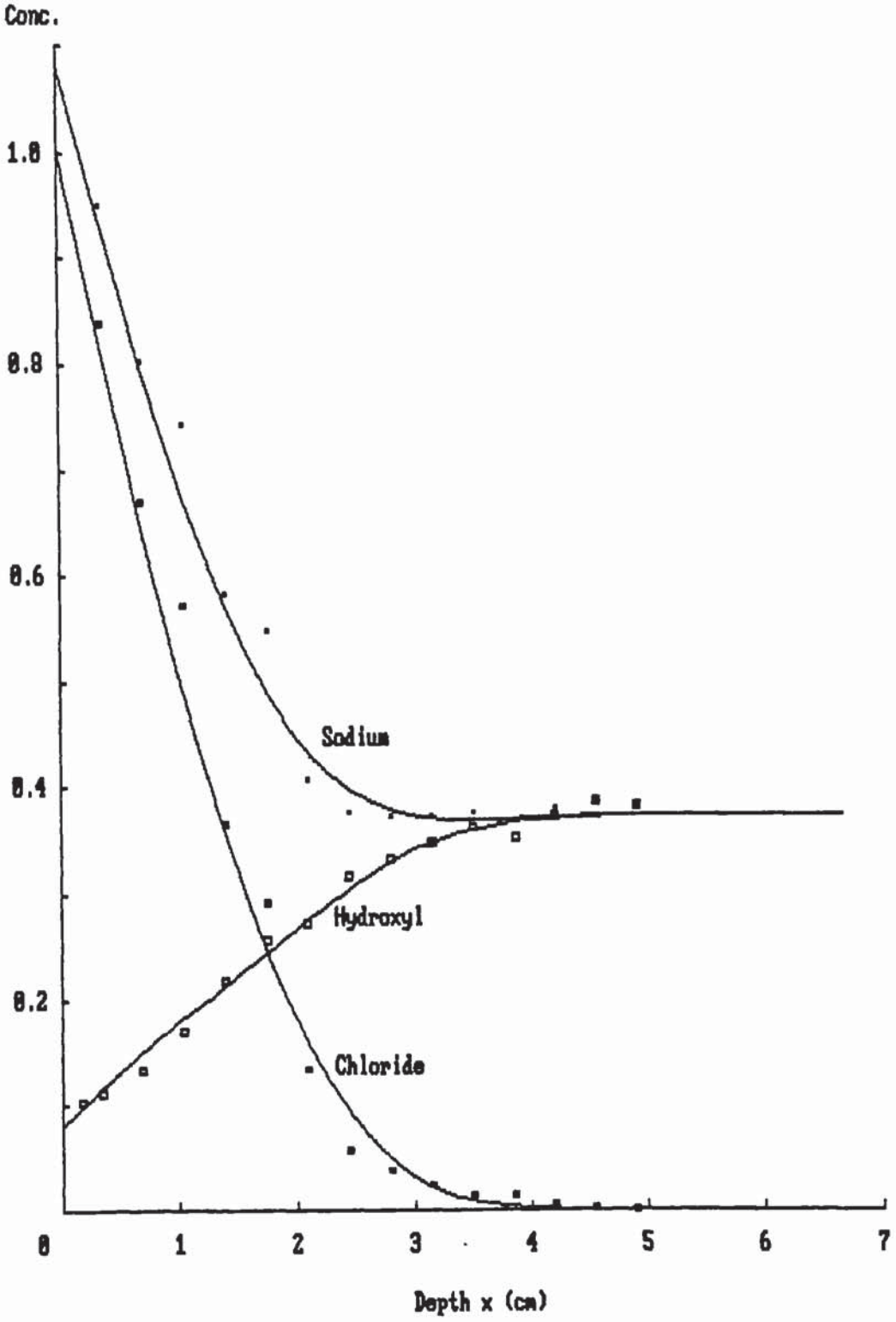


Figure 6.18 Sodium, chloride and hydroxyl concentration profiles calculated with the Nernst-Planck equation

considered as an alternative method to model and to predict ionic diffusion in hydrated cement pastes. Nevertheless, the illustrations involving the Planck-Nernst equation for the characterization of diffusion processes, which is shown here and in section 6.1.2, may reveal the importance of the effect of electrostatic interactions between ions in hydrated OPC paste on the diffusion rates. Further work may be considered with this regard.

It is quite difficult to interpret the anion diffusion behaviours observed from the "diffusion-out" test. Although the chloride concentration profile can be well interpolated by Fick's second law, the rise of concentration in the external solution can not be explained with regard to the mass balance between the quantities of ions lost from the pore solution and that gained in the external solution. As suggested by Sergi[64], this may be associated with the complex natures of chloride and hydroxyl binding involved during diffusion. The actual initial concentration for chloride diffusion may have been much lower than that obtained by the numerical analysis presented in subsection 6.6.3, which was suggested by Sergi who also determined the initial ionic concentrations with parallel specimens.

As can be seen from table 6.9, hydroxyl ion diffused slower than chloride and potassium in terms of the effective diffusivities obtained for the "diffusion-out"

test, which appears to contradict to the suggestion made earlier that hydroxyl ion can be considered as the fastest diffusing species. The difficulties in interpreting this arise from the uncertainties concerning the actual initial concentrations for hydroxyl and chloride diffusion. Nevertheless, as shown in table 6.9, chloride and potassium ions were found by the numerical calculations to have similar diffusivities and initial concentrations. If this is to be accepted, two ions can be treated as one neutral species diffusing out of the paste. The ionic diffusion system can be thus simplified by assuming it to have been composed only of sodium, hydroxyl and the minor-component ions, which suggests that sodium and hydroxyl ions would have similar diffusivities because of the requirement of electroneutrality. Therefore, although hydroxyl ion is more mobile than the other ions, it does not necessarily have a obviously greater Fickian diffusivity than the other ions in a mixed electrolyte, which has been shown in paragraph 6.1.2.3 for the third example system considered. (see table 6.8 and figure 6.3).

## 6.9 Conclusions

(1). Diffusion of sodium and potassium in mature OPC paste obeys Fick's first and second laws to a good approximation.

(2). Fick's first law probably characterizes chloride

diffusion. Bound chloride can be described by Langmuir's adsorption isotherm. A combination of Fick's first law and Langmuir's adsorption theory can be used to model and to predict chloride diffusion.

(3). Fick's second law can be used to describe chloride diffusion with an appropriate effective diffusivity.

(4). Hydroxyl diffusion appears to deviate from a Fickian diffusion behaviour. However, hydroxyl ion can be practically treated as a charge-balancing species for the purpose of predicting its diffusion in mature OPC paste.

(4). Ionic diffusion in hydrated cement pastes shows some characteristics of a multi-component process. The electro-static interactions between ions may be able to affect diffusion particularly of hydroxyl ion.

# CHAPTER 7 GENERAL CONCLUSIONS AND RECOMMENDATIONS FOR FURTHER WORK

The aim of the present work, as mentioned in the introductory chapter, was to contribute to the understanding of the mechanisms of diffusion in hydrated cement pastes and to aid the prediction of ionic diffusion in concrete structures. Attempts were made to study the role of the pore structure and surface charge in determining ionic or molecular diffusion rates in hydrated OPC and PFA pastes. Work was also carried out to model the diffusion process in hydrated OPC pastes, intending to provide a general basis for the prediction of ionic penetration into concrete structures.

## 7.1 GENERAL CONCLUSIONS

### 7.1.1 Effect of pore structure

Work was carried out to study the pore structure effect on diffusion by means of experimental determinations of the diffusivities of quaternary ammonium ions and oxygen. The diffusibility has been considered in chapter 3 as a relative measure of the restriction of the hydrated cement pastes to diffusion with respect to different diffusing ions, whilst the diffusivities of a particular species are compared with respect to different cement pastes.

It has been mentioned in chapter 3 that quaternary

ammonium ions diffuse through the continuous capillary pores, so that the diffusion kinetics of these ions are closely related to the capillary pore structures. Two aspects of the capillary pore structure have been considered: the size distributions and the tortuosity or interconnection.

The diffusibility was found to be strongly associated with the sizes of the diffusing ions. As the ionic size increases, the diffusibility generally decreases. The speed of the reduction in diffusibility with the increase of ionic radius was found to be mainly a function of w/c ratio. The OPC and PFA pastes of w/c ratio 0.65 showed significantly higher diffusibilities than the pastes of lower w/c ratio for a particular quaternary ammonium ion. As mentioned in chapter 3, this is associated with the relatively coarse size distributions and large volumes of the capillaries in the pastes of w/c ratio 0.65.

The 0.5 w/c OPC paste was found to show a relatively sharp reduction of the diffusibility as the sizes of the diffusing ions increased from 4.9 to 5.3 Å. The continuous capillary pores contributing to the diffusion of ions with sizes smaller than 5.3 Å thus appear to interconnect most of the macropores. Decreasing the w/c ratio from 0.5 to 0.35 for the OPC paste yielded a continuous and considerable drop in the relative diffusion rate or diffusibility. Although the continuous capillary pores in the w/c ratio 0.35 are likely to be smaller than those in

the 0.5 w/c paste, their sizes may distribute more uniformly with respect to their volumes.

Figure 3.4 shows that the $(C_5H_{11})_4N^+$ ions diffuse at similar rates in the OPC pastes of w/c 0.35 and 0.5, while the smaller quaternary ammonium ions can have different diffusibilities. This suggests that the continuous capillary pores contributing to the diffusion fluxes of the quaternary ammonium ions smaller than $(C_5H_{11})_4N^+$ may be very important in determining the mechanisms of diffusion in the dense OPC pastes. However, it is difficult to estimate the sizes of these continuous micropores based on the results obtained.

In comparison with the diffusion behaviours of the quaternary ammonium ions in dense OPC pastes, the diffusibilities for the PFA pastes of the same w/c ratio were found to be smaller but less strongly influenced by the size of the diffusing ion. Moreover, oxygen has been shown in chapter 5 to diffuse slower in the PFA paste than the OPC paste of the same w/c ratio. It can been seen from tables 5.3 and 5.4 that oxygen diffusivities are a few times smaller in the PFA pastes of w/c ratios 0.35 and 0.5 than in the dense OPC pastes, whereas they are slightly greater in the coarser PFA paste than in the coarser OPC paste.

Therefore, it appears that the pore structure of the PFA paste differs from that of the OPC paste of the same w/c

ratio. If the difference in oxygen diffusivities for the two types of paste of the same w/c ratio is not caused by the different strengths of the viscous force in the pore solution, the PFA pastes, particularly the dense PFA pastes, should have much finer or more discontinuous pore structures than the OPC pastes.

### 7.1.2 Effects of surface charge on ionic diffusion

It was found that the magnitude of the zeta potential of hydrated cement pastes is small. It would be therefore difficult, based on the determinations of the zeta potential, to make suggestions concerning the effect of surface charge on ionic diffusion. This is because, even if the zeta potentials had been measured accurately, they would be likely not to change significantly with the types of bulk solution and cement paste employed for the measurements. However, small zeta potentials do not necessarily mean small values of surface charge in hydrated cement pastes. Some oxides have been shown to have very high values of titratable surface charge, but the zeta potentials have been found to be small in different solutions[48]. It has been mentioned in chapter 4 that the zeta potential is the potential at the so-called shear plane, so it is not the surface potential.

Increasing the ionic strength in the bulk solution would cause a considerably faster drop of the potential with distance from the surface[90]. The pore solutions of

hydrated cement pastes are normally concentrated so the variation of the potential would occur within only a short distance at the pore/solution interfaces (see chapter 4). Therefore, it is the potential distributions in the gel and micro pores, and the collisions between the diffusing ions and the pore walls that can affect ionic diffusion rates. Furthermore, there should be close links between the effects of pore structure and surface charge. The sizes, volume fraction and continuity or tortuosity of the micro and gel pores can determine the degree to which the surface charge can affect ionic diffusion.

The ratios of the oxygen to chloride diffusivities have been considered in chapter 5 to be a relative indication of the surface charge effect on chloride diffusion. The ratio, as shown in figure 5.14, was found to be as high as four to eight for most dense OPC and OPC/20%PFA pastes, whereas it is approximately one for bulk dilute solutions. This suggests that compared with the pure pore-structure effect, the surface charge effect dominates and retards chloride diffusion in these dense pastes.

It can be seen from table 5.3 that the ratio of the oxygen diffusivity in the 0.35 w/c OPC paste to that in the 0.50 w/c OPC paste is 1.3, whereas the ratio of the corresponding chloride diffusivities is much higher, approximately 5. If the oxygen diffusivities are considered to represent the pure pore-structure effect,

the denser pore structure in the 0.35 paste enables the surface charge to play a greater role in decreasing chloride diffusion rates.

Although the pore structure of the 0.65 w/c OPC paste can be expected to be much coarser than those of the OPC pastes of w/c ratios 0.5 and 0.35, the surface charge in the 0.65 w/c paste appears to be able to decrease the relative diffusion rates of the quaternary ammonium ions smaller than $(C_5H_{11})_4N^+$, as indicated by the increase of the diffusibility with the increase of the ionic radius from 4.9 to 5.3 A. The surface charge in relatively coarse pastes can also play a certain part in affecting ionic diffusion rate. This is consistent with the results obtained from oxygen diffusion experiments. Tables 5.3 and 5.4 show that the oxygen to chloride diffusivity ratios for the OPC and OPC/20PFA% pastes of w/c ratio 0.6 are about 1.7 and 3.2 respectively. It may thus be expected that the ratio would decrease if the w/c ratio is increased further to be above 0.6, as a result of the decrease of the surface charge effect on chloride diffusion.

### 7.1.3 Description of ionic diffusion processes in hydrated cement pastes

The work presented in chapter 6 is mainly focused on the characterization of concentration profiles in terms of Fick's laws and of the ionic binding behaviours. Diffusion

of sodium, potassium, chloride and hydroxyl ions have been studied.

Sodium and potassium were found to diffuse in mature OPC pastes according to Fick's laws. By comparing with the ionic diffusion behaviours in mixed dilute electrolytes, they were considered to be able to dominate the overall diffusion rates and to affect the diffusion kinetics of the anions.

Chloride was also shown to diffuse according to Fick's first law. By using Langmuir's adsorption theory to approximate the bound chloride contents in relation to the free chloride, the concentration profiles of free chloride can be characterized based on the mass balance equation 6.1. Furthermore, Fick's second law with an appropriate effective diffusivity was found to interpolate the free chloride profile very well.

The approaches to treat hydroxyl diffusion as being independent of the presence of the other ions were found to be inadequate in characterizing the hydroxyl profile. However, it has been shown in chapter 6 that the diffusion behaviour of hydroxyl ion in the OPC paste appears to be associated with certain characteristics of its diffusion in mixed electrolytes. Further work is needed to clarify the extent to which diffusion of sodium and potassium can affect the diffusion of chloride and hydroxyl ions, because the latter has much importance in affecting

aspects of concrete durability such as reinforcement corrosion.

## 7.2 Recommendations for Further Work

It has been suggested in chapters 1 and 5 that both the pore structure and the viscosity of the pore solution can affect diffusion rates, and the two types of effect can be separated to some degree by determining the activation energies of oxygen diffusion. Work can be carried out to determine the oxygen diffusivities by varying the temperature, w/c ratio and type of binder. The difference between the viscosities of the pore solutions of different pastes can be qualitatively evaluated from the activation energies for oxygen diffusion. This could yield better understanding of the differences in the pore structures of different pastes.

It can be seen from the experimental studies carried out in this work and by other workers[17,18] that compared with diffusion of oxygen, ionic diffusion is retarded, whereas compared with diffusion of anions, diffusion of cations is retarded. The difference in diffusion behaviours between cations and anions is probably associated with the effect of surface charge. Compared with certain anions, cations may have more frequent collisions with the pore walls. Furthermore, because of the negative surface charge in micro and gel pores, cation distributions may be more compressed near the pore

surfaces than those of certain anions, so they tend to have lower activity or diffusivity, which has been speculated in chapter 4. However, it was impossible to show in this work the exact nature of the causes for the slower cation diffusion. Further work is needed for the elucidation of the difference in diffusion behaviours between cations and anions.

It has been shown in chapter 6 that the electrostatic interactions between the diffusing ions may exist and affect the overall ionic diffusion kinetics in hydrated cement pastes. Although the quantitative nature of the interactions may be very different from what can be seen from the Nernst-Planck equation 1.2 for the transport in dilute bulk solutions, it is possible to obtain some qualitative information about the interactions using the approaches involving computer-modelling of non-steady state diffusion. This may be important with regard to the possibility that the diffusivities obtained from the concentration profiles in a particular diffusion system are determined by many factors such as initial and surface concentrations. A certain value of diffusivity can give an accurate prediction of the diffusion process in a particular concrete structure, whereas it may not for other systems.

Chloride-binding can affect diffusion of hydroxyl and chloride. Further work can be carried out to study the

factors that determine bound chloride contents. The effects of hydroxyl and free chloride concentrations on bound chloride can be examined. These factors can be studied through experimental determinations of the chloride, hydroxyl and sulphate profiles in a non-steady state diffusion. Some other theories of adsorption, besides the Langmuir isotherm, may be considered to quantify the bound chloride contents more precisely.

Diffusion in hydrated blended cement pastes may be quite different from that in OPC paste. Sodium and potassium have been shown to have much lower values of diffusivity than chloride for PFA and BFS blended pastes[21,22]. It is possible that the cation can dominate the diffusion of anions, which may complicate the prediction of chloride penetration into certain concrete structures. Diffusion in blended cement pastes can thus be studied in further work using the approaches described in chapter 6.

## REFERENCES


1 KAY E.A., FOOKES P.G., POLLOCK D.J.
"Deterioration related to chloride ingress", Concrete, 15(11), 22-28 (1981).

2 HAUSMAN D.M.
"Steel corrosion in concrete", Materials Protection, 6(11), 19-23 (1967).

3 ATKINSON A., NICKERSON A.K.
"Diffusion and sorption of Cs, Sr and I in water-saturated cement", U.K. Automatic Energy Authority, Harwell, Report AERE R12124 (1986).

4 ATKINSON A., NICKERSON A.K.
"The diffusion of ions through water-saturated cement", J. of Materials Science, 19, 3068-3078 (1984).

5 KUMAR A., KOMARNENI S., ROY D.M.
"Diffusion of $Cs^+$ and $Cl^-$ through sealing materials", Cem. Concr. Res., 17(1), 153-160 (1987).

6 CUSSLER E.L.
"Multicomponent Diffusion", Elsevier Scientific Company, Amsterdam (1976).

7 CUSSLER E.L.
"Diffusion, Mass Transfer in Fluid System", Cambridge University Press (1984).

8 CRANK J.
Mathematics of Diffusion", 2nd edition, Clarendon Press, Oxford (1975).

9 BURNEL M.E., BREUER M.M.
"Diffusion near the lower consolute temperature point", in "Diffusion Process" (J.N. Sherwood, A.V. Chadwick, W.M. Muir and F.L. Swinton eds), Vol. 1, pp. 119-127, Gordon and Breach, London (1971).

10 SCHULTZ S.G.
"Basic Principles of Membrane Transport", Cambridge University Press, Cambridge (1980).

11 IBI N
"Fundamentals of transport phenomena in electrolytic systems", in "Comprehensive Treatise of Electrochemistry", Vol. 6, "Electrodics: Transport" (E. Yeager, J.O'M. Bockris, B.E. Conway and S. Sarangapani eds), pp. 1-64, Plenum Press, New York and London (1983).

12 HELFFERICH F.
"Ion Exchange", McGraw-Hill, New York (1962).

13 LAKSHMINARAYANAIAH N.
"Transport Phenomena in Membranes", Academic Press, New York (1969).

14 ROBINSON R.A., STOKES R.H.
"Electrolyte Solutions", 2nd edition, Butterworths, London (1959).

15 LAWRENCE C.D.
"Chloride ingress into concretes", paper prepared for september meeting British Ceramic Society in Aberdeen, October 1989.

16 SMEDLEY S.I.

"The Interpretation of Ionic Conductivity in Liquid", Plenum Press, New York (1980).

17 KONDO R., SATAKE M., USHIYAMA H.

"Diffusion of various ions in hardened portland cement", 28th General Meeting of Cement Association of Japan, pp. 41-43, Tokyo (1974).

18 ROY D.M., KUMAR A., RHODES J.P.

"Diffusion of chloride and cesium ions in portland cement pastes and mortars containing blast furnace slag and fly ash", Proc. 2nd International Conference on Fly Ash, Silica Fume, Slag and Natural Pozzolans in Concrete, Vol. 2, pp. 1423-1444, Madrid, Spain (1986).

19 BAKKER R.F.M., THOMASSEN W.J.M.

"The influence of the type of cement on the diffusion of ions", Concrete Research Foundation of the Dutch Cement Industries (June 1977).

20 BYFORS K.

"Influence of silica fume and flyash on chloride diffusion and pH values in cement paste", Cem. Concr. Res., 17(1), 115-130 (1987).

21 UCHIKAWA H., UCHIDA S., OGAWA K.

"Influence of character of blending component on the diffusion of $Na^+$ and $Cl^-$ ions in hardened blended cement paste", Proc. 8th International Congress on the Chemistry of Cement, Vol. IV, pp. 251-256, Rio de Janeiro, Brasil (Sept. 1986).

22 PAGE C.L., SHORT N.R., TARRAS A EL.
"Diffusion of chloride ions in hardened cement pastes", Cem. Concr. Res., 11(3), 395-406 (1981).

23 LAMBERT P., PAGE C.L., SHORT N.R.
"Diffusion of chloride ions in hardened cement pastes containing pure cement minerals", British Ceramic Society, Proc., The chemistry of chemically related properties of cement" (F.P. Glasser ed.), No. 35, pp. 267-276 (Sept. 1984).

24 GOTO S., ROY D.M.
"Diffusion of ions through hardened cement pastes", Cem. Concr. Res., 11(5), 751-757 (1981).

25 PARSONS R.
"Handbook of Electrochemical Constants", p. 79, Butterworths, London (1959).

26 PAGE C.L.
"An overview of current research", Proc. 2nd International Conference on Deterioration and Repair of Reinforced Concrete in the Arabian Gulf, Vol. II, pp. 167-171, Bahrain (1987).

27 KUMAR A.
"Diffusion and Pore Structure Studies in Cementitious Materials", Ph.D. Thesis, Pennsylvania State University (1985).

28 SHIGERU K., TAKAGI T., GOTO S., DAIMON M.
"Diffusion of ions through hardened pastes of various cements", CAJ Review, pp. 75-77 (1983).

29 TAKAGI T., GOTO S., DAIMON M.
"Diffusion of $I^-$ ion through hardened cement paste", Review of the 38th General Meeting of Cement Association of Japan, pp. 72-75 (May 1984).

30 GOTO S., DAIMON M.
"Ion diffusion in cement paste", Proc. 8th International Congress on the Chemistry of Cement, Vol. VI, pp. 405-409, Rio de Janeiro, Brasil (Sept. 1986).

31 UCHIKAWA H., UCHIDA S., OGAWA K.
"Diffusion of alkali ions in hardened cement paste containing slags or fly ash", Review of the 38th General Meeting of Cement Association of Japan, Vol. 14, pp. 56-59 (1984).

32 UCHIKAWA H.
"Effect of blending components on hydration and structure formation", Proc. 8th International Congress on the Chemistry of Cement, Vol. I, pp. 249-280, Rio de Janeiro, Brasil (Sept. 1986).

33 FELDMAN R.F.
"Pore structure, permeability and diffusivity as related to durability", Proc. 8th International Congress on the Chemistry of Cement, Vol. I, pp. 336-356, Rio de Janeiro, Brasil (Sept. 1986).

34 PANTELI F.
"The Pore System and Engineering Properties of Hardened Cement Pastes", PH.D. thesis, Aston University (1988).

35 ANDERSON P.J.

"The effect of superplasticizers and air-entraining agents on the zeta potential of cement particles", Cem. Concr. Res., 16(6), 931-940 (1986).

36 DAIMON M., ROY D.M.
"Rheological properties of cement mixes: II, zeta potential and preliminary viscosity studies", Cem. Concr. Res., 9(1), 103-110 (1979).

37 SUZUKI K., NICKIKAWA T., KATO K., HAYASHI H., ITO S.
"Approach by zeta-potential measurement on the surface change of hydrating $C_3S$", Cem. Concr. Res., 11(5/6), 759-764 (1981).

38 SORENSON B., MAAHN E.
"Penetration rate of chloride in marine concrete structures", Nordic Concrete Research, Vol. 1, 24.1-24.18 (1982).

39 SERGI G., PAGE C.L.
"Pore solution chemistry and ionic diffusion in hydrated cements", 22nd Concrete Society Materials Research Seminar, University of Birmingham (July 1988).

40 LONGUET P., BURGLEN P., ZELLWER A.
"Phase liquid du ciment hydrate", Materiaux de Construction et Travaux Publics, 676, 35-41 (1973).

41 SILSBEE J., MAEK R.I.A., ROY D.M.
"Composition of pore fluids extracted from slag cement pastes", Proc. 8th International Congress on the Chemistry of Cement, Vol. IV, pp. 263-269, Rio de

Janeiro, Brasil (Sept. 1986).

42 VOGEL A.T.
"Vogel's Textbook of Quantitative Inorganic Analysis", 4th edition, Longmans, London, pp. 754-755 (1978).

43 CROMPTON T.R.
"Determination of Organic Substances in Water", Vol. 1, Chichester Wiley-Interscience Pub., pp. 247-249 (1985).

44 THOMAS L.C., CHAMBERLIN G.J.
"Colorimetric Chemical Analytical Methods", 9th edition, The Tintometer Ltd Pub., Salisbury, England, pp. 24-26 (1980).

45 POWERS T.C.
"Physical properties of cement paste", Proc. 4th International Symposium on the Chemistry of Cement, Vol. 2, pp. 577-613, Washington (1960).

46 TAYLOR H.F.W
"Bound water in cement paste and its significance for pore solution compositions", Proc. Mat. Res. Soc. Symp., Vol. 85, pp. 47-54, Materials Research Society (1987).

47 BRITISH STANDARD 4550: PART 2: SECTION 13.2
"Loss-on-ignition" (1970).

48 HUNTER R.J.
"Zeta Potential in Colloid Science, Principles and Applications", Academic Press, London (1981).

49 OVERBEEK J.Th.G.

"Electrokinetic Phenomena", in "Colloid Science" (H.R. Kruyt ed), Vol. 1, pp. 194-244, Elsevier, Amsterdam and London (1952).

50 BRIGGS D.R.
"The determination of the zeta-potential on cellulose - a method", J. Phys. Chem., 32, 641-675 (1928).

51 RUTGERS A.J.
"Streaming potentials and surface conductance. Part I-(B), streaming effects and surface conduction", Trans. Faraday Soc., 36, 69-80 (1940).

52 SHAW D.J.
"Introduction to Colloid and Surface Chemistry", 3rd edition, Butterworths, London (1980).

53 HUNTER R.J., ALEXANDER A.E.
"Some notes on the measurement of electrokinetic potentials", J. Colloid Sci., 17(8), 781-788 (1962).

54 MARDIN M., PAPIRET E., SCHULTZ J.
"An electrokinetic study of the interactions between glass fibers and aqueous solutions of calcium", J. Colloid Sci. 88(1), 204-213 (1982).

55 LAUFFER M.A., GORTNER R.A.
"Electrokinetics. XX. Interfacial energy and the molecular structure of organic compounds VI", J. Phys. Chem., 42, 641-656 (1938).

56 HORN J.M. Jr., ONODA G.Y. Jr.
"Streaming potential and noncreeping flow in porous beds", J. Colloid Sci., 61(2), 272-278 (1976).

57 HAZEL J.F., SCHNABLE G.L.
"Streaming potential measurements and the adhension of phosphors on cathode ray screen", J. Electrochem. Soc., 100(2), 65-71 (1953).

58 ROBINSON McD., PASK J.A., FUERSTENAU D.W.
"Surface charge of alumina and magnesia in aqueous media", J. Amer. Ceram. Soc., 47(10), 516-520 (1964).

59 SOMASUNDARAN P., KULKARNI R.D.
"A new streaming potential appratus and study of temperature effect using it", J. Colloid and Interface Sci., 45(3), 591-600 (1973).

60 MIDGLEY M.G., ILLSTON J.M.
"Some comments on the microstructure of hardened cement pastes", Cem. Concr. Res., 13(2), 197-206 (1983).

61 WINSLOW D.N.
"The validity of high pressure mercury intrusion porosimetry", J. Colloid and Interface Sci., 67, 42-47 (1978)

62 DIAMOND S.
"A critical comparison of mercury porosimetry and capillary condensation pore size distributions of portland cement pastes", Cem. Concr. Res., 1(5), 531-545 (1971).

63 BUENFELD N.R., NEWMAN J.B.
"Examination of three methods for studying ion diffusion in cement pastes, mortars and concrete", Materials and Structures, 20, 3-10 (1987).

64 SERGI G.
"Corrosion of Steel in Concrete: Cement Matrix Variables", PH.D. thesis, Aston University (1986).

65 DIAMOND S., DOLCH W.L.
"General log-normal distribution of pore sizes in hydrated cement paste", J. Colloid and Interface Sci., 38(1), 234-244 (1972).

66 FELDMAN R.F., SEREDA P.J.
"A new model for hydrated portland cement and its practical implications", Eng. J. Canada, 53, 53-59 (1970).

67 RAMACHANDRAN V.S., FELDMAN R.F., BEAUDOIN J.J.
"Concrete Science, Treatise on Current Research", Heyden Pub., London (1981).

68 KALOUSEK G.C.
Discussion on "Simplified method for determination of apparent surface area of concrete products", Proc. Amer. Concr. Inst., 51(4), 448 (1955).

69 SOROKA I.
"Portland Cement Paste and Concrete", The Macmillan Press Ltd, London and Basingstoke (1979).

70 DAIMON M., ABO-EL-ENEIN S.A., HOSAKA G., GOTO S., KONDO, R.
"Pore structure of calcium silicate hydrate in hydrated tricalcium silicate", J. Amer. Ceram. Soc., 60, 110-114 (1977).

71 BRUNAUER S., SKALNY J., ODLER I.

"Pore structure and properties of materials", Proc. RILEM/IUPAC Int. Symp., Pore structure and properties of materials, Prague C3-26 (1973).

72 POWERS T.C.
"Structure and physical properties of hardened cement paste", J. Amer. Ceram. Soc., 41(1), 1-6 (1958).

73 POWERS T.C., COPELAND L.E., HAYES J.C., MANN H.M.
"Permeability of portland cement paste", Proc. Amer. Concr. Res. Inst., 51(3), 285-298 (1954).

74 PARROTT L.J., PATEL R.G., KILLOH D.C., JENNINGS H.M.
"Effect of age on diffusion in hydrated alite cement", J. Amer. Ceram. Soc., 67(4), 233-237 (1984).

75 KUMAR A., ROY D.M.
"Diffusion and pore structure in portland cement pastes blended with low calcium fly ash", Mat. Res. Soc. Symp., 85, Materials Research Society (1986).

76 FELDMAN R.F.
"Pore structure damage in blended cements caused by mercury intrusion", J. Amer. Ceram. Soc. 67(1), 30-33 (1984)

77 FELDMAN R.F.
"Significance of porosity measurements on blended cement performance", Proc. 1st Int. Conf. on the use of flyash, silica fume, slag and other mineral by-products in concrete, Montebello Que., Canada, SP 79, Vol. 1, pp. 415-434 (1983).

78 MARSH B.K., DAY R.L.
"Some difficulties in assessment of pore structure of

high performance blended cement pastes", Materials Research Society Symp. Proc., "Very high strength cement-based materials", 42(1), pp. 113-122 (1985).

79 LEA F.M.
"The Chemistry of Cement and Concrete", 3rd edition, pp. 270-279, Pub: Edward Arnold (1970).

80 LI S., ROY D.M.
"Investigation of relations between porosity, pore structure and $Cl^-$ diffusion of fly ash and blended cement pastes", Cem. Concr. Res., 16, 749-759 (1986).

81 OTTEWILL R.H.
"Chemistry of colloidal silicates and cement", Phil. Trans. R. Soc., A310, 67-78 (1983).

82 CHAPMAN D.L.
"A contribution to the theory of electrocapillarity", Phil. Mag. 25, 475 (1913).

83 NAGELE E., NEY P.
A discussion on of the paper "approach by zeta-potential measurement on the surface change of hydrating $C_3S$", Cem. Concr. Res., 12(4), 535-536 (1982)

84 NAGELE E.
"The zeta potential of cement, III: the non-equilibrium double layer on cement", Cem. Concr. Res., 17(4), 573-580 (1986).

85 NAGELE E.
"The zeta potential of cement, II: effect of pH-

value", Cem. Concr. Res., 16(6), 853-863 (1986).

86 NAGELE E.

"The zeta-potential of cement", Cem. Concr. Res., 15(3), 453-462 (1985).

87 STEIN H.G.

"Surface Charges on calcium silicates and calcium silicate hydrates", J. Colloid and Interface Sci., 28(2), 203-213 (1968).

88 SPIERINGS G. A.C.M., STEIN H.N.

"The coagulation of $Ca_3Al_2(OH)_{12}$ in aqueous electrolyte solutions", Colloid and polymer Sci., 257, 171-177 (1979).

89 WITTMANN F.H., HOLLENZ C.

"On the significance of electroosmosis in hardened cement paste", Cem. Concr. Res., 4(3), 389-398 (1974).

90 DUKHIN S.S.

"Development of notations as to the mechanism of electrokinetic phenomena and the structure of the colloid micelle", in "Surface and Colloid science" (E. Matijevic ed), Vol. 7, pp. 1-48, John Wiley & Sons, New York (1974).

91 BOLT G.H.

"Surface interaction between soil solid phase and the soil solution", in "Soil Chemistry, A. Basic Elements" (G.H. Bolt and M.G.M Bruggenwert eds), Elsevier Scientific Publishing Company, pp. 43-53, Amsterdam (1978).

92 VERWEY E.J.W., OVERBEEK J.Th.G.
"Theory of Stability of Lyophobic Colloids", Elsevier, Amsterdam (1948).

93 OVERBEEK J.Th.G.
"The interaction between colloidal particles", in "Colloid Science" (H.R. Kruyt ed), Vol. 1, pp. 245-277, Elsevier, Amsterdam and London (1952).

94 STEVENS C.F.
"Changing views of ion permeation", in "Ion Permeation Through Membrane" (C.F. Stevens and R.W. Tsien eds), Vol. 3, pp. 1-4, Raven Press (1979).

95 PAGE C.L., LAMBERT P.
"Kinetics of oxygen diffusion in hardened cement pastes", J. of Materials Science, 22, 942-946 (1987).

96 LINGANE J.J.
"Controlled potential electroanalysis", in "Coulometry in Analytical Chemistry" (G.W.C Milner and G. Phillips eds), pp. 172-186, Pergmon Press Ltd, Oxford (1967)

97 LINGANE J.J.
"Electroanalytical Chemistry", pp. 227-229, Interscience Publishers, New York (1958).

98 HOARE J.P.
"The Electrochemistry of Oxygen", Interscience Publishers (1968)

99 LAITINEN H.A., KOLTHOFF I.M.
"Voltammetry with stationary microelectrodes of

platinum wire", J. Phys. Chem. 45, 1061-1079 (1941).

100 LAITINEN H.A., KOLTHOFF I.M.
"Voltammetric determinations and amperometric titrations with a rotating micro-electrode of platinum wire", J. Phys. Chem. 45, 1079-1083 (1941).

101 LINGANE J.J.
"Coulometric analysis", J. Amer. Chem. Soc., 67, 1916-1922 (1945).

102 MaCNEVIE W.M., BAKER B.B.
"Primary coulometric determination of iron(II) and arsenic(III). New method of current summation", in "Coulometry in Analytical Chemistry" (G.W.C Milner and G. Phillips eds), pp. 148-158, Pergmon Press Ltd, Oxford (1967)

103 VETTER K.J
"Electrochemical Kinetics", pp. 188-198, Academic Press, New York and London (1967).

104 NERNST W., MERRIAM E.S.
"Zur Theorie des Reststroms", Z. Physik. Chem. 53, 235-243 (1905).

105 NEWTON C.J.
"The Effect of Concrete Coatings on Pipelines Corrosion", D.Phil. Thesis, Oxford University (1988).

106 GJORV O.E., VENNESLAND O.,EL-BUSAIDY A.H.S.
"Diffusion of dissolved oxygen through concrete", Corrosion 76, NACE, Houston, Paper No. 17, March 17.

107 DEAN J.A.
"Lange's Handbook of Electrochemistry", 13th edition,

p. 10, McGraw-Hill, New York (1985).

108 SPINKS J.W.T., BALDWIN H.W., THORVALDSON T.
"Tracer studies of diffusion in set portland cement", Canadian J. of Technology, 30, 20-28 (1952).

109 TRAETTEBERG A.
"The mechanism of chloride penetration in concrete", Report by Cement and Concrete Research Institute, Trondhein, Norway, STF65, A77070 (1977).

110 MIDGLEY H.G., ILLSTON J.M.
"Effect of chloride penetration on the properties of hardened cement pastes", Proc. 7th International Congress on the chemistry of cement, Vol. III, pp. 101-103 Paris (1980).

111 MIDGLEY M.G., ILLSTON J.M.
"The penetration of chloride into hardened cement paste", Cem. Concr. Res., 14, 546-558 (1984).

112 OST B., MONFORE G.E.
"Penetration of chloride ions into concrete", J. of the PCA Research and Development Laboratories, 8(1), 46-52 (1966).

113 GJORV O.E., VENNESLAND O.
"Diffusion of chloride ions from seawater into concrete", Cem. Concr. Res., 9(2), 229-238 (1979).

114 DIAMOND S.
in "Alkalis In concrete, Research and Practice" (G.M. Idorn and Steen Rostam eds), pp. 155-166, Danish concrete Association, Copenhagen (1983).

115 PAGE C.L., VENNESLAND O.
"Pore solution composition and chloride binding capacity of silica-fume cement pastes". Material Structures (RILEM), 16(91), 19-25 (1983).

116 RAYMENT P.L.
"The effect of pulverized-fuel ash on the C/S molar ratio and alkali content of calcium hydrates in cement", Cem. Concr. Res., 12, 133-140 (1982).

117 GLASSER F.P., MARR J.
"The alkali binding potential of OPC and blended cements", II Cemento, 82, 85-94 (1985).

118 HOBBS D.W.
"Alkali-Silica Reaction in Concrete", Thomas Telford, London (1988).

119 MEHTA P.K.
"Effect of cement composition on corrosion of reinforcing steel in concrete", in "Chloride Corrosion of Steel in Concrete", ASTM STP 629, D.E. Tonini and S.W. Dean eds, pp. 12-19, American Society for Testing and Materials (1977)

120 TRITTHART J.
"Chloride binding in cement, II: the influence of the hydroxide concentration in the pore solution of hardened cement paste on chloride binding", Cem. Concr. Res., 19(5), 683-691 (1989).

121 ROY D.M.
"Mechanisms of cement paste degradation due to chemical and physical factors", Proc. 8th Inter-

national Congress on the Chemistry of Cement, Vol. I, pp. 362-380, Rio de Janeiro, Brasil (Sept. 1986).

122 PEREIRA C.J., HEGEDUS L.L.
"Diffusion and reaction of chloride ions in porous concrete", European Federation of Chemical Engineering, EFCE Publication Series No. 37, ISCRE 8, The 8th International Symposium on Chemical Reaction Engineering.

123 GLASSTONE S.
"Textbook of Physical Chemistry", 2nd edition, pp. 1198-1208, Macmillian and Co. limited, London (1960)

124 PAGE C.L., LAMBERT P., VASSIE P.
"Investigations of reinforcement corrosion: I. The pore electrolyte phase in chloride contaminated concrete" (in press)

125 TUTTI K.
"Corrosion of steel in concrete", Swedish Cement and Concrete Research Institute, S-100, 44-CBI Forskning Research No. 4.28, Stockholm (1982).

126 AMES W.F.
"Numerical Methods for Partial Differential Equations", 2nd edition, Academic Press, New York (1977).

127 MITCHELL A.R., GRIFFITHS D.F.
"The Finite Difference Method in Partial Differential Equations", John Wiley & Sons Ltd (1980).

128 SMITH G.D.

"Numerical Solutions of Partial Differential Equations, Finite Difference Methods", 2nd edition, Clarendon Press, Oxford (1978).

129 NA T.Y.

"Computational Methods in Engineering Boundary Value Problems", Academic Press, New York (1979).

130 HAYS W.L

"Statistics", 3rd edition, 329, Holt, Rinehart and Winston (1981)

## Appendix 1 Intrinsic diffusivities of quaternary ammonium ions ($\times 10^{-10}$ $cm^2/sec$)

| paste | $N(C_2H_5)_4^+$ | $N(C_3H_7)_4^+$ | $N(C_4H_9)_4^+$ | $N(C_5H_{11})_4^+$ |
|---|---|---|---|---|
| 0.35 w/c | 28.0 | | 6.40 | 0.47 |
| OPC | 30.0 | | 5.10 | 1.60 |
| | 21.8 | | | 1.49 |
| 0.50 w/c | 21.7 | 20.4 | 19.6 | 0.89 |
| OPC | 14.2 | 25.7 | 5.1 | 0.98 |
| | 29.7 | 9.6 | 13.9 | 1.11 |
| | 31.7 | 15.9 | 6.6 | 0.89 |
| 0.65 w/c | 991 | 450 | 395 | 536 |
| OPC | 790 | 488 | 217 | 459 |
| | 763 | 340 | 302 | 400 |
| 0.35 w/c | | 3.60 | 3.05 | 0.77 |
| OPC/40%PFA | | 9.00 | 2.53 | 0.81 |
| | | | 1.63 | 0.48 |
| 0.50 w/c | 8.82 | 10.7 | 2.60 | 3.07 |
| OPC/40%PFA | 22.3 | 7.25 | 4.06 | 1.95 |
| | 12.7 | 5.67 | 8.80 | 1.26 |
| 0.65 w/c | 420 | 435 | 303 | 236 |
| OPC/40%PFA | 496 | 376 | 337 | 233 |
| | 565 | 384 | 181 | 167 |
| 0.65 w/c | 738 | 424 | 353 | 205 |
| OPC/20%PFA | 702 | 590 | 244 | 219 |
| | 730 | 434 | 292 | 152 |

## Appendix 2 Derivation of mass balance equation 6.1

To derive the relationship between the concentration, flux and ionic binding, the mass balance in a volume unit of the bulk cement paste will be considered. This volume unit is assumed to have a bulk diffusion area of 1 $cm^3$ and a length $2\delta x$ cm, as shown schematically below.

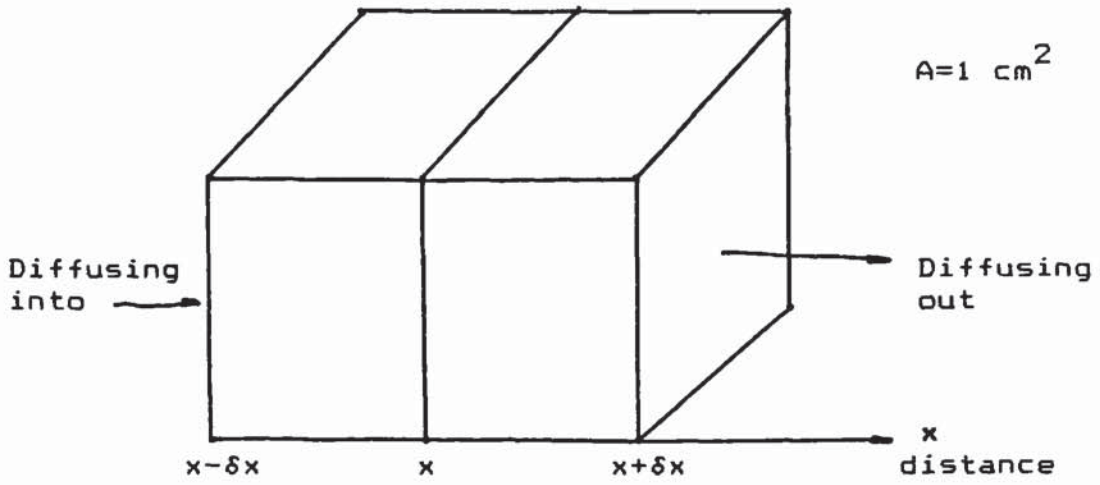


The mass balance suggests that the difference in the quantities of ions diffused into and out of the volume unit should yield an equivalent change in the quantities of ions present within the unit. The quantity of ions diffused into the unit is

$$W_{in} = J(x,t) - \delta x J_x(x,t) \qquad \text{(mmol/sec)}$$

where J is the flux in mmol per 1 $cm^2$ area of the bulk cement paste. The quantity of ions diffused out of the unit is

$$W_{out} = J(x,t) + \delta x J_x(x,t) \qquad \text{(mmol/sec)}$$

The change in the quantity of ions present in the pore solution of the paste is

$$W_{solution} = 2\epsilon\delta x S_t(x,t) \qquad (mmol/sec)$$

The change in the quantity of ions combined into the solid phase of the cement-matrix is

$$W_{solid} = (2\epsilon\delta x d/W) S_t(x,t) \qquad (mmol/sec)$$

where d in $g/cm^3$ is the specific density of the pore solution in which diffusion occurs.

The mass balance can thus be expressed by

$$W_{out} - W_{in} = W_{solution} + W_{solid}$$

or

$$-2\delta x J_x(x,t) = 2\epsilon\delta x [C_t(x,t) + (d/W) S_t(x,t)$$

Assuming that the pore solution has a specific density of 1 $g/cm^3$, the above equation can be written as

$$C_t(x,t) + S_t(x,t)/W = -J_x(x,t)/\epsilon$$

which is the same as equation 6.1.

## Appendix 3 Computed concentration profiles of sodium, potassium, chloride and hydroxyl ions for the "diffusion-out" test

| x (cm) | $Na^+$ (mM) | $K^+$ (mM) | $Cl^-$ (mM) | $OH^-$ (mM) * | $OH^-$ (mM) # |
|---|---|---|---|---|---|
| 0.000 | 25.4 | 9.3 | 0.3 | 54.3 | 131.5 |
| 0.175 | 75.9 | 24.1 | 17.0 | 97.5 | 163.0 |
| 0.350 | 125.8 | 38.7 | 33.6 | 140.1 | 194.1 |
| 0.525 | 174.7 | 53.1 | 50.0 | 181.6 | 224.7 |
| 0.700 | 222.1 | 67.2 | 65.9 | 221.6 | 254.4 |
| 0.875 | 267.4 | 81.0 | 81.4 | 259.6 | 283.1 |
| 1.050 | 310.4 | 94.3 | 96.3 | 295.2 | 310.4 |
| 1.225 | 350.8 | 107.1 | 110.4 | 328.2 | 336.3 |
| 1.400 | 388.2 | 119.4 | 123.8 | 358.4 | 360.5 |
| 1.575 | 422.6 | 130.9 | 136.4 | 385.7 | 383.0 |
| 1.750 | 453.8 | 141.9 | 148.1 | 410.0 | 403.6 |
| 1.925 | 481.8 | 152.1 | 159.0 | 431.3 | 422.5 |
| 2.100 | 506.8 | 161.6 | 168.9 | 449.9 | 439.5 |
| 2.275 | 528.7 | 170.3 | 177.9 | 465.8 | 454.7 |
| 2.450 | 547.8 | 178.4 | 186.0 | 479.3 | 468.1 |
| 2.625 | 564.2 | 185.7 | 193.3 | 490.6 | 479.9 |
| 2.800 | 578.2 | 192.3 | 199.8 | 499.9 | 490.2 |
| 2.975 | 590.0 | 198.3 | 205.5 | 507.5 | 499.0 |
| 3.150 | 599.9 | 203.6 | 210.5 | 513.6 | 506.6 |
| 3.325 | 608.0 | 208.4 | 214.8 | 518.5 | 513.0 |
| 3.500 | 614.6 | 212.5 | 218.5 | 522.3 | 518.3 |
| 3.675 | 620.0 | 216.2 | 221.7 | 525.2 | 522.8 |
| 3.850 | 624.3 | 219.3 | 224.4 | 527.5 | 526.4 |
| 4.025 | 627.6 | 222.1 | 226.6 | 529.2 | 529.4 |
| 4.200 | 630.3 | 224.4 | 228.5 | 530.4 | 531.8 |
| 4.375 | 632.3 | 226.4 | 230.0 | 531.4 | 533.7 |
| 4.550 | 633.9 | 228.1 | 231.3 | 532.1 | 535.2 |
| 4.725 | 635.1 | 229.6 | 232.4 | 532.5 | 536.4 |
| 4.900 | 636.0 | 230.8 | 233.2 | 532.9 | 537.3 |
| 5.075 | 636.6 | 231.7 | 233.9 | 533.1 | 538.1 |
| 5.250 | 637.1 | 232.5 | 234.4 | 533.3 | 538.6 |
| 5.425 | 637.5 | 233.2 | 234.8 | 533.4 | 539.0 |
| 5.600 | 637.7 | 233.7 | 235.1 | 533.5 | 539.3 |
| 5.775 | 637.9 | 234.1 | 235.4 | 533.5 | 539.5 |
| 5.950 | 638.0 | 234.5 | 235.6 | 533.6 | 539.7 |
| 6.125 | 638.1 | 234.7 | 235.7 | 533.6 | 539.8 |
| 6.300 | 638.1 | 234.9 | 235.8 | 533.6 | 539.9 |
| 6.475 | 638.2 | 234.9 | 235.8 | 533.6 | 539.9 |
| 6.650 | 638.2 | 235.0 | 235.9 | 533.6 | 539.9 |

* and #: data corresponding to the solid and dotted lines in figure 6.13 respectively

## Appendix 4 Computed concentration profiles of sodium and chloride ions for the "diffusion-within" test

| \|x\| (cm) | x ≤ 0 | | | x ≥ 0 | |
|---|---|---|---|---|---|
| | $Na^+$ (mM) | $Cl^-$ (mM) * | # | $Na^+$ | $Cl^-$ * |
| 0.000 | 699.1 | 403.8 | 459.0 | 691.6 | 403.8 |
| 0.175 | 812.4 | 473.5 | 516.4 | 626.0 | 329.5 |
| 0.350 | 921.4 | 541.6 | 572.8 | 561.7 | 257.3 |
| 0.525 | 1022.0 | 606.7 | 627.1 | 500.0 | 189.4 |
| 0.700 | 1111.4 | 667.5 | 678.7 | 441.9 | 128.6 |
| 0.875 | 1187.7 | 723.2 | 726.7 | 388.5 | 78.1 |
| 1.050 | 1250.3 | 773.1 | 770.5 | 340.2 | 40.9 |
| 1.225 | 1299.7 | 817.0 | 810.0 | 297.4 | 18.2 |
| 1.400 | 1337.1 | 854.8 | 844.7 | 260.4 | 7.1 |
| 1.575 | 1364.3 | 886.7 | 874.9 | 229.0 | 2.4 |
| 1.750 | 1383.4 | 913.0 | 900.5 | 202.8 | 0.8 |
| 1.925 | 1396.2 | 934.4 | 922.0 | 181.5 | 0.2 |
| 2.100 | 1404.5 | 951.3 | 939.6 | 164.5 | 0.1 |
| 2.275 | 1409.7 | 964.5 | 953.8 | 151.2 | 0.0 |
| 2.450 | 1412.8 | 974.6 | 965.1 | 140.9 | 0.0 |
| 2.625 | 1414.5 | 982.1 | 973.9 | 133.3 | 0.0 |
| 2.800 | 1415.5 | 987.6 | 980.6 | 127.6 | |
| 2.975 | 1416.0 | 991.6 | 985.6 | 123.6 | |
| 3.150 | 1416.3 | 994.4 | 989.4 | 120.7 | |
| 3.325 | 1416.4 | 996.3 | 992.1 | 118.7 | |
| 3.500 | 1416.5 | 997.6 | 994.0 | 117.3 | |
| 3.675 | 1416.5 | 998.5 | 995.3 | 116.4 | |
| 3.850 | 1416.5 | 999.1 | 996.2 | 115.9 | |
| 4.025 | 1416.5 | 999.4 | 996.9 | 115.5 | |
| 4.200 | 1416.5 | 999.7 | 997.3 | 115.3 | |
| 4.375 | 1416.5 | 999.8 | 997.5 | 115.1 | |
| 4.550 | 1416.5 | 999.9 | 997.7 | 115.0 | |
| 4.725 | 1416.5 | 999.9 | 997.8 | 115.0 | |
| 4.900 | 1416.5 | 1000.0 | 997.9 | 115.0 | |
| 5.075 | 1416.5 | 1000.0 | 997.9 | 114.9 | |
| 5.250 | 1416.5 | 1000.0 | 998.0 | 114.9 | |
| 5.425 | 1416.5 | 1000.0 | 998.0 | 114.9 | |
| 5.600 | 1416.5 | 1000.0 | 998.0 | 114.9 | |
| 5.775 | 1416.5 | 1000.0 | 998.0 | 114.9 | |
| 5.950 | 1416.5 | 1000.0 | 998.0 | 114.9 | |
| 6.125 | 1416.5 | 1000.0 | 998.0 | 114.9 | |
| 6.300 | 1416.5 | 1000.0 | 998.0 | 114.9 | |
| 6.475 | 1416.5 | 1000.0 | 998.0 | 114.9 | |
| 6.650 | 1416.5 | 1000.0 | 998.0 | 114.9 | |

* and #: data corresponding to the solid and dotted lines in figure 6.11 respectively

## Appendix 5 Computed concentration profiles for the "NaCl-ingress" test

5(a). Sodium, potassium, chloride and hydroxyl profiles according to the model

| x (cm) | $Na^+$ (mM) | $K^+$ (mM) | $OH^-$ (mM) | $Cl^-$ (mM) * | $Cl^-$ (mM) # |
|---|---|---|---|---|---|
| 0.000 | 1000 | 100 | 100 | 1000.0 | 1000.0 |
| 0.175 | 915 | 111 | 107 | 918.6 | 910.5 |
| 0.350 | 831 | 122 | 115 | 837.6 | 822.2 |
| 0.525 | 749 | 132 | 124 | 757.5 | 736.0 |
| 0.700 | 671 | 143 | 135 | 678.7 | 653.0 |
| 0.875 | 597 | 153 | 149 | 601.6 | 574.1 |
| 1.050 | 529 | 163 | 165 | 526.9 | 500.1 |
| 1.225 | 466 | 172 | 183 | 455.0 | 431.4 |
| 1.400 | 409 | 181 | 204 | 386.6 | 368.6 |
| 1.575 | 359 | 190 | 226 | 322.3 | 311.8 |
| 1.750 | 315 | 197 | 250 | 262.7 | 261.1 |
| 1.925 | 277 | 205 | 273 | 208.6 | 216.3 |
| 2.100 | 244 | 211 | 295 | 160.7 | 177.4 |
| 2.275 | 217 | 218 | 315 | 119.6 | 144.0 |
| 2.450 | 195 | 223 | 332 | 85.7 | 115.6 |
| 2.625 | 176 | 228 | 345 | 59.0 | 91.8 |
| 2.800 | 162 | 233 | 355 | 39.0 | 72.1 |
| 2.975 | 150 | 237 | 362 | 24.8 | 56.1 |
| 3.150 | 141 | 240 | 366 | 15.3 | 43.1 |
| 3.325 | 134 | 243 | 368 | 9.1 | 32.7 |
| 3.500 | 129 | 246 | 370 | 5.2 | 24.6 |
| 3.675 | 125 | 248 | 370 | 2.9 | 18.3 |
| 3.850 | 122 | 250 | 371 | 1.6 | 13.4 |
| 4.025 | 120 | 252 | 371 | 0.9 | 9.7 |
| 4.200 | 118 | 254 | 371 | 0.5 | 7.0 |
| 4.375 | 117 | 255 | 372 | 0.2 | 5.0 |
| 4.550 | 116 | 256 | 372 | 0.1 | 3.5 |
| 4.725 | 116 | 257 | 373 | 0.1 | 2.4 |
| 4.900 | 116 | 257 | 373 | 0.0 | 1.7 |
| 5.075 | 115 | 258 | 373 | 0.0 | 1.1 |
| 5.250 | 115 | 258 | 374 | 0.0 | 0.7 |
| 5.425 | 115 | 259 | 374 | 0.0 | 0.5 |
| 5.600 | 115 | 259 | 374 | 0.0 | 0.3 |
| 5.775 | 115 | 259 | 374 | 0.0 | 0.2 |
| 5.950 | 115 | 259 | 374 | 0.0 | 0.2 |
| 6.125 | 115 | 259 | 375 | 0.0 | 0.1 |
| 6.300 | 115 | 260 | 375 | 0.0 | 0.1 |
| 6.475 | 115 | 260 | 375 | 0.0 | 0.0 |
| 6.650 | 115 | 260 | 375 | 0.0 | 0.0 |

* and #: data corresponding to the solid and dotted lines in figure 6.10 respectively

5(b) Sodium, chloride and hydroxyl profiles calculated by the Nernst-Planck equation.

| x (cm) | $Na^+$ (mM) | $Cl^-$ (mM) | $OH^-$ (mM) | x (cm) | $Na^+$ (mM) | $Cl^-$ (mM) | $OH^-$ (mM) |
|---|---|---|---|---|---|---|---|
| 0.000 | 1080 | 1000 | 80 | 0.175 | 1006 | 907 | 99 |
| 0.350 | 933 | 816 | 117 | 0.525 | 862 | 728 | 134 |
| 0.700 | 794 | 643 | 151 | 0.875 | 730 | 563 | 167 |
| 1.050 | 671 | 489 | 183 | 1.225 | 618 | 419 | 198 |
| 1.400 | 570 | 356 | 214 | 1.575 | 527 | 298 | 229 |
| 1.750 | 491 | 247 | 244 | 1.925 | 460 | 200 | 260 |
| 2.100 | 435 | 160 | 275 | 2.275 | 415 | 124 | 290 |
| 2.450 | 399 | 94 | 305 | 2.625 | 388 | 70 | 318 |
| 2.800 | 380 | 50 | 331 | 2.975 | 375 | 34 | 341 |
| 3.150 | 372 | 23 | 349 | 3.325 | 371 | 15 | 356 |
| 3.500 | 371 | 9 | 361 | 3.675 | 371 | 6 | 365 |
| 3.850 | 372 | 3 | 368 | 4.025 | 372 | 2 | 370 |
| 4.200 | 373 | 1 | 372 | 4.375 | 373 | 1 | 373 |
| 4.550 | 374 | 0 | 373 | 4.725 | 374 | 0 | 374 |
| 4.900 | 374 | 0 | 374 | 5.075 | 375 | 0 | 375 |
| 5.250 | 375 | 0 | 375 | 5.425 | 375 | 0 | 375 |
| 5.600 | 375 | 0 | 375 | 5.775 | 375 | 0 | 375 |
| 5.950 | 375 | 0 | 375 | 6.125 | 375 | 0 | 375 |
| 6.300 | 375 | 0 | 375 | 6.475 | 375 | 0 | 375 |
| 6.650 | 375 | 0 | 375 | | | | |

## Appendix 6 Estimation of the diffusion area (Є) from evaporable and non-evaporable water contents

According to Powers[45], one gramme dry cement may be assumed to produce the following volume components after hydration:

1. Original volume of the cement, i.e. the specific volume of cement, which is 0.32 $cm^3/g$ for a typical OPC cement.
2. Expanded spaces of the solid phase beyond the original volume of cement due to the hydration, which was assumed to be 0.82Wn by Powers.
3. Spaces occupied by the evaporable water (W°) when the paste is fully saturated with water. The evaporable water was assumed by Powers to have a specific volume 0.99 $cm^3/g$.

If diffusion occurs through the evaporable water phase, the volume fraction of the pore solution, Є, is:

$$Є = 0.99We/(0.32 + 0.82Wn + 0.99W°)$$

The specimens used for "diffusion-out" test had evaporable and non-evaporable water contents of 19.64% (Wn) and 35.78% (We or W°) per gramme unhydrated cement respectively. The value of Є can be calculated from the above equation to be 0.42.

The specimens used for the "diffusion-within" test was not water-saturated. However, as shown by Powers, the total water content of a fully water-saturated cement paste is

approximately 5% bigger than the w/c ratio used during the mixing. Therefore, the value of $\epsilon$ for the specimens can be roughly estimated to be:

$$\epsilon = 0.99We/[0.32 + 0.82Wn + 0.99(We+5\%)]$$

The water contents, Wn and We, were 19.9% and 31.6% for the chloride-rich half specimens respectively, and 20.8% and 26.6% for the other half specimens respectively. The volume fractions of the evaporable water, denoted in chapter 6 as $\epsilon_1$ and $\epsilon_2$, can be estimated from the above equation to be 0.37 and 0.33 respectively. The ratio $\epsilon_2/\epsilon_1$ is thus 0.89, which is very close to the value (0.9) calculated in subsection 6.5.2, chapter 6.